

# **SINGLE BUBBLE BEHAVIOUR STUDY IN A FLOTATION COLUMN**

**Abbas Sam**

Department of Mining and Metallurgical Engineering  
McGill University  
Montreal, Canada.

A thesis submitted to the Faculty of Graduate Studies and Research  
in partial fulfillment of the requirements for the degree of  
Doctor of Philosophy.

© Abbas Sam, 1995

*In the name of God,  
the Compassionate, the merciful*

*To my parents, my wife and  
my children,  
Mohammad, Shima and Reyhaneh*

**ABSTRACT**

The axial velocity profiles (local velocity versus time or position) of single bubbles in the absence and presence of flotation reagents such as frother were measured in a water-jacketed transparent Plexiglas square ( $10 \times 10$  cm) column over a distance of 400 cm. The test liquid temperature was maintained uniform and constant at  $30^\circ\text{C}$  by water circulation in the jacket. Single bubbles, covering a size range of interest in flotation, were studied. A bubble generation frequency was selected such that velocity was independent of frequency. To follow the bubble during its rise, a video camera supported on a track and capable of moving vertically at adjustable speeds was employed.

In the absence of flotation reagents, the profiles showed two stages: first the velocity increased rapidly to reach a maximum value and then decreased continuously. In all cases these two stages were observed in the profiles (even in distilled water) but, the profile shape, particularly the slope of the second stage was variable presumably reflecting differences in water quality.

In the presence of frother (Dowfroth 250, MIBC and pine oil), a third stage was reached, a constant (terminal) velocity. The first two stages were dependent on frother concentration and type but, the third stage was only a function of frother type. In these cases, the bubble velocity profile characteristics (maximum velocity, time to reach terminal velocity (or adsorption time), and the terminal velocity) were evaluated.

The effect of frother on bubble size, shape and path during its rise and the effect of methanol, xanthate, pH and temperature on velocity profiles were also investigated.

The observations are qualitatively explained in terms of time-dependent adsorption of surfactants, either present as contaminants in tap and distilled water or deliberately added in the case of frother. An empirical model for estimation of adsorption time for moving bubbles is introduced.

## RÉSUMÉ

Dans une colonne de flottation carrée ( $10 \times 10$  cm) à chemise d'eau faite de plexiglas transparent, on a mesuré, sur une distance de 400 cm, les profils de vitesse axiale (vitesse locale versus temps ou position) de bulles simples avec ou sans la présence de réactifs de flottation tel le moussant. En circulant de l'eau dans la chemise, la température du liquide à l'intérieur de la colonne fut maintenue à une température constante de  $30^{\circ}\text{C}$ . On a étudié des bulles simples ayant des diamètres d'intérêt pour la flottation. Une fréquence de génération des bulles fut choisie afin que la vitesse soit indépendante de la fréquence. Pour suivre la bulle lors de son ascension, on a utilisé une caméra vidéo montée sur rail et pouvant se déplacer verticalement à des vitesses variables.

En l'absence de moussant, les profils illustrent deux étapes: dans une première étape la vitesse augmente rapidement jusqu'à atteindre une valeur maximale puis décroît continuellement sur la distance de 4 mètres. Pour tous les cas ces deux étapes se retrouvent sur les profils (même avec de l'eau distillée). Toutefois, la forme du profil et particulièrement la pente de la deuxième partie varie présumément en réaction à la différence de qualité de l'eau.

En présence de moussant (Dowfroth 250, MIBC et huile de pin) on a atteint une troisième étape, une vitesse (terminale) constante. Les deux premières étapes étant dépendantes de la concentration et du type de moussant mais la troisième étape variant seulement selon le type de moussant. Dans ce dernier cas, les caractéristiques du profil de vitesse (vitesse maximale, temps d'adsorption et vitesse terminale) furent évaluées.

On a aussi examiné l'effet du moussant sur la dimension des bulles, la forme et le tracé lors de l'ascension ainsi que l'effet du méthanol, du xanthate, du pH et de la température sur les profils de vitesse.

Les observations sont expliquées de façon qualitative en terme d'adsorption de surfacteurs en fonction du temps, que ces surfacteurs soient présents en tant que contaminant dans l'eau du robinet ou l'eau distillée, ou délibérément ajoutés dans le cas des moussants.

## ACKNOWLEDGEMENTS

Grateful acknowledgement is hereby made for the helpful contributions of the many whose names do not appear on the title page. I am especially indebted to:

My parents and my wife, for their continuous sacrifice, constant support, encouragement and patience.

My supervisor, Prof. J.A. Finch, for his excellent leadership, constant enthusiasm, encouragement, expert guidance, advice and helpful discussions and suggestions during my Ph.D. study and for his patience throughout the preparation of this thesis.

Dr. C.O. Gomez, for his help in experimental work, useful discussions, encouragement and advice throughout this project.

I gratefully acknowledge Prof. M.E. Weber for his helpful suggestions; my colleague Dr. Shen for sharing his knowledge on data-acquisition programs; Prof. Z. Xu, for his friendship and useful discussions; Prof. A.R. Laplante and Dr. S.R. Rao for helpful discussions; Mr. M. Leroux, Mr. M. Knoepfel, Mr. E. Chnyrenkov and Mr. J. Boka for their friendship and help in experimental work and all my fellow colleagues, past and present, associated with McGill's Mineral Processing Group.

I would like to thank INCO, and Natural Sciences and Engineering Research Council of Canada through the INCO-NSERC Chair in Mineral Processing, held by Prof. J.A. Finch for funding.

Last, but not the least, the author wishes to thank the Ministry of Culture and Higher Education of Iran for making his post-graduate studies possible.

**TABLE OF CONTENTS**

ABSTRACT .....	i
RÉSUMÉ .....	ii
ACKNOWLEDGEMENTS .....	iii
TABLE OF CONTENTS .....	iv
NOMENCLATURE.....	x
LIST OF FIGURES .....	xv
LIST OF TABLES .....	xxi
LIST OF APPENDIXES .....	xxiii
<b>CHAPTER 1 INTRODUCTION .....</b>	<b>1</b>
1.1 Column Flotation Characteristics .....	3
1.2 Bubble-Liquid Systems .....	6
1.3 Objectives of the Present Work .....	6
1.4 Structure of Thesis .....	8
<b>CHAPTER 2 FUNDAMENTAL CONSIDERATIONS .....</b>	<b>10</b>
2.1 Particle Collection Efficiency .....	10
2.1.1 Bubble-Particle Collision .....	11
- Collision Time .....	17
- Sliding Time .....	17
- Contact Time .....	17
- Induction Time .....	18
2.1.2 Bubble-Particle Attachment .....	18
2.2 Flotation Reagents .....	19

---

2.2.1 Collectors .....	19
2.2.2 Frother .....	24
2.2.3 Regulators .....	26
- pH Modifiers .....	26
- Activators .....	26
- Depressants .....	27
2.3 Fluid Flow Around a Sphere .....	27
2.3.1 Streamline, Flow Pattern .....	28
2.3.2 Stream Function, Velocity Distribution .....	29
- Stokes Flow .....	30
- Intermediate Flow .....	31
- Potential Flow .....	33
2.3.3 Pressure Distribution .....	34
2.4 Forces Acting on a Single Fluid Particle in Motion .....	36
2.4.1 Navier-Stokes Equation .....	37
2.4.2 Surface Tension Force .....	38
2.4.3 Force Ratios (Dimensionless Groups) .....	39
2.4.4 Buoyancy Force .....	41
2.4.5 Drag Force .....	42
2.5 Wake Phenomena .....	45
2.6 Bubble Internal Circulation .....	49
2.7 Bubble Behaviour .....	51
2.7.1 Bubble Size .....	52
- Bubble Formation and Bubble Size at the Orifice ....	52
- Effect of Hydrodynamic Pressure on Bubble Size ...	54
2.7.2 Bubble Shape .....	58
2.7.3 Bubble Rise Path .....	61

---

2.7.4 Bubble Rise Velocity .....	62
2.8 Mechanism and Effects of Surfactant Adsorption .....	64
2.8.1 Time-Dependent Surfactant Adsorption .....	65
2.8.2 Uniform Surface Tension .....	66
2.8.3 Non-Uniform Surface Tension .....	69
- Marangoni Effect .....	69
- Effect on Bubble Internal Circulation .....	69
- Temperature Effect .....	73
2.8.4 Surface Tension and Surface Viscosity Gradients .....	75
2.8.5 Interaction Between Surfactant and Water Molecules ...	76
2.9 Theories and Models of Bubble Velocity .....	76
2.9.1 Single Particle Motion in the Absence of Resistance ....	76
2.9.2 Single Solid Particle Motion in a Viscous Fluid .....	77
2.9.3 Single Fluid Particle in Motion .....	85
- Stokes' Law .....	85
- Hadamard-Rybczynski Equation .....	87
- Boussinesq Equation .....	90
- Levich Equation .....	91
- Moore's Theory .....	92
- Mendelson's Theory .....	94
- Zhou et al., Model .....	96
- Typical Bubble $C_D$ - $R_e$ and $U_T$ - $d_e$ Curves .....	97
2.9.4 Bubble Swarms (Drift Flux Model) .....	100
2.10 Interaction Between Bubbles .....	102
2.11 Wall Effects .....	103

---

<b>CHAPTER 3 BUBBLE SIZE AND ESTIMATION TECHNIQUES .....</b>	<b>105</b>
3.1 Optical Techniques .....	105
3.1.1 Optical Fiber Probes .....	105
- Single Fiber Probe .....	105
- Multi-Fiber Probes .....	106
- Optical Detectors Using Capillary Tube .....	107
3.1.2 Laser Beam Techniques .....	107
3.1.3 Photographic Techniques .....	110
3.1.4 X-Ray Photography Technique .....	111
3.2 Electroresistivity Techniques .....	111
3.2.1 One Element Probe .....	111
3.2.2 Two-Element Probe .....	112
3.2.3 Multi-Element Probe .....	113
3.3 Ultrasonic Techniques .....	114
3.3.1 Resonant Scattering Method .....	114
3.3.2 Second Harmonic Method .....	115
3.3.3 Double Frequency Technique .....	115
3.4 Discussion .....	117
<b>CHAPTER 4 EXPERIMENTAL EQUIPMENT AND PROCEDURES .</b>	<b>119</b>
4.1 Column Set-up .....	119
4.2 Temperature Control .....	119
4.3 Gas Line .....	124
4.4 Camera Moving Device .....	125
4.5 Procedures .....	125

---

<b>CHAPTER 5 RESULTS .....</b>	<b>129</b>
5.1 Bubble Size, Shape, and Path .....	129
5.1.1 Effect of Bubble Generation Frequency .....	129
5.1.2 Test Liquid Properties .....	129
5.1.3 Bubble Size and Shape .....	133
5.1.4 Bubble Rise Path .....	136
5.2 Axial Bubble Velocity Profiles .....	137
5.2.1 In the Absence of Surfactant .....	137
5.2.2 In the Presence of Frother .....	140
5.2.3 Effect of Methanol .....	155
5.2.4 Effect of Collector .....	157
5.2.5 Effect of pH .....	158
5.2.6 Effect of Temperature .....	159
<b>CHAPTER 6 GENERAL DISCUSSION .....</b>	<b>160</b>
6.1 Bubble Size, Shape and Path .....	160
6.2 Axial Bubble Velocity Profile .....	161
6.2.1 Stage 1, Maximum Velocity .....	161
6.2.2 Stage 2, Adsorption Time .....	162
- Model of Adsorption Time Based on Diffusion .....	163
- Model of Adsorption Time Considering Surface Tension Gradient .....	167
- Empirical Model for Prediction of Adsorption Time for Moving Bubbles .....	172
6.2.3 Stage 3, Terminal Velocity .....	181
6.3 Significance to Flotation .....	186

---

**CHAPTER 7 CONCLUSIONS AND SUGGESTIONS FOR  
FUTURE WORK ..... 189**

    7.1 Conclusions ..... 189

    7.2 Claims for Original Research ..... 193

    7.3 Suggestions for Future Work ..... 194

REFERENCES ..... 195

APPENDIXES ..... 209

## NOMENCLATURE

$a, a$	Sphere radius, cm
$A$	Particle projected area, $\text{cm}^2$ , bubble surface area, $\text{cm}^2$ (Eq. 6.18)
$A_a$	Bubble projected area, $\text{cm}^2$ (Eq. 6.16)
$A_r$	Archimedes number (Eq. 2.98)
$b$	Bubble major axis, cm (Eq. 2.61)
$Bo$	Bond number
$C$	Surface dilational viscosity/ $1.5 d_p$ (Eq. 2.115), frother concentration
$C_b$	$C/A$ , mole/ $\text{cm}^2$ (Eq. 6.18)
$C_B$	Bulk concentration, mole/ $\text{cm}^3$ (Eq. 6.11)
$C_c$	Contamination factor (Eq. 2.126)
$C_D$	Drag coefficient (Eq. 2.59)
$C_t$	$C \times V_a$ , moles (Eq. 6.17)
$D_d$	Diffusion coefficient, $\text{cm}^2/\text{s}$ (Eq. 6.1)
$D$	Column diameter, cm (Section 2.11)
$d_b$	Bubble diameter, cm
$d_e$	Bubble volume-equivalent diameter, cm
$d_p$	Particle diameter, cm
$E_A$	Attachment efficiency
$E_C$	Collision efficiency
$E_{cg}$	Collision efficiency by gravitation (Eq. 2.14)
$E_{ci}$	Collision Efficiency by interception (Eq. 2.14)
$E_{co}$	Collision efficiency (Eq. 2.14)
$E_K$	Collection efficiency
$E_o$	Eötvös number
$f$	Bubble oscillation frequency, $\text{s}^{-1}$
$F_B$	Buoyancy force (Eq. 2.58)

---

$F_D$	Drag force (Eq. 2.59)
$Fr$	Froude number
$F_w$	Gravitational force (2.77)
$g$	Gravitational acceleration, $981\text{cm/s}^2$
$G$	Dimensionless parameter (Eqs. 2.9 and 2.10)
$G(x), H(x)$	Moore's functions (Eq. 2.122)
$h$	Bubble minor axis, cm (Eq. 2.61)
$h_a$	Adsorption height, cm (Eq. 6.15)
$h_l$	Liquid height over the particle (Eq. 2.64)
$j_g$	Superficial gas velocity, cm/s (Eq. 2.132)
$j_l$	Superficial liquid velocity, cm/s (Eq. 2.132)
$K$	$\mu_p / \mu_l$ (Eqs. 2.72 and 2.103)
$K_a$	Dimensionless number ( $C_b/\Gamma$ ) (Eq. 6.19)
$K'$	Velocity ratio, $U_T / (U_T)_{\text{Stokes}}$ (Eq. 2.112)
$K''$	Coefficient (Eq. 2.9)
$K_1$	$U_c / U_{if}$ (Eqs. 2.134-2.139)
$K_2$	$d_c / D$ (Eqs. 2.134-2.139)
$K_m$	Mass transfer coefficient, cm/s (Eq. 6.11)
$Ly$	Lyashchenko number (Eq. 2.98)
$m$	Coefficient (Eq. 2.133)
$Mo$	Morton number
$N$	mole/cm <sup>3</sup> (Table 6.3)
$n$	Number of gas moles (Eq. 2.68)
$n_1$	Coefficient (Eq. 2.12)
$P$	Pressure, $\text{dyne/cm}^2 \approx 10^{-3} \text{ cm H}_2\text{O}$
$P(r, \theta)$	Pressure distribution (Eq. 2.99)
$P_0$	Uniform freestream pressure (Eq. 2.44), absolute hydrostatic pressure (Eq. 2.64)

---

$P_{\text{atm}}$	Atmospheric pressure (Eq. 2.64)
$P_{\text{B}}$	Pressure at bubble sides (Eq. 2.45)
$P_{\text{c}}$	Gas pressure inside the capillary tube (Eq. 2.66)
$P_{\text{i}}$	Gas pressure inside the bubble (Eq. 2.66)
$P_{\text{op}}$	Constant (Eq. 2.106)
$P_{\text{p}}$	Pressure for the inner fluid particle (Eq. 2.104)
$P_{\text{s}}$	Pressure at bubble stagnation point (Eq. 2.45)
$R$	Universal gas constant, erg/mole $^{\circ}$ K (Eq. 2.68)
$r_0$	Orifice radius (Eq. 2.62)
$R_1, R_2$	Principal radii of the bubble surface (Eq. 2.67)
$r_{\text{b}}$	Bubble radius, cm
$r_{\text{c}}$	Collision radius, cm
$Re, Re_{\text{b}}$	Reynolds number
$r_{\text{p}}$	Particle radius, cm
$R_{\text{v}}$	Visual bubble radius, cm (Eq. 2.126)
$S$	Slope of $\sigma$ -C curve (Eq. 6.10)
$Sr$	Strouhal number (Section 2.7.3)
$St$	Stokes' number (Eq. 2.13)
$t$	Time, s
$T$	Temperature, $^{\circ}$ K (Eq. 2.68)
$t_{\text{a}}$	Surfactant adsorption time, s (Eq. 6.21)
$Ta$	Tadaki number
$t_{\text{c}}$	Collision time, s
$t_{\text{con}}$	Contact time, s
$t_{\text{d}}$	Adsorption time for a stationary bubble, s (Eq. 6.1)
$t_{\text{f}}$	Film drainage time, s
$t_{\text{i}}$	Induction time, s
$t_{\text{s}}$	Sliding time, s; characteristic adsorption time, s (Eq. 6.11)

$t_{\text{TPC}}$	Three-phase contact time, s
$U_{\theta}$	Velocity in $\theta$ direction
$U_0$	Fluid velocity far from the sphere, cm/s (Eq. 2.25)
$U_b$	Bubble velocity, cm/s
$U_B$	Stream velocity at bubble sides, cm/s
$U_c$	Bubble velocity in a column, cm/s (Section 2.11)
$U_{\text{if}}$	Bubble velocity in a liquid of infinite dimensions, cm/s (Section 2.11)
$U_{\text{in}}$	Initial velocity (Section 2.9.1)
$U_p$	Particle velocity
$U_p^*$	$U_p/U_b$ (Eq. 2.16)
$U_r$	Velocity in $r$ direction
$U_{\text{re}}$	Velocity of the bubble relative to solid particle (Eqs. 2.9 and 2.10)
$U_s$	Slip velocity, cm/s (Eq. 2.132)
$U_S$	Stream velocity at bubble stagnation point, cm/s
$U_T$	Terminal velocity, cm/s
$V, V_b$	Bubble volume, $\text{cm}^3$ (Eq. 2.60)
$V_a$	$h_a \times A_a$ , $\text{cm}^3$ (Eq. 6.16)
$V_w$	Wake volume, $\text{cm}^3$ (Eq. 2.60)
$We$	Weber number
$W_{\text{S/A}}$	Work of adhesion (Eq. 2.21)
$x$	$1 + r_p/r_b$ (Eq. 2.5), $b/h$ (Eq. 2.123)
$Y$	Bubble oscillation amplitude, cm

### Greek Symbols

$(\Delta p)_{\text{i-o}}$	Pressure difference between inside and outside of a bubble (Eq. 2.71)
$\alpha$	Constant (Eq. 2.98)
$\alpha'$	Surface tension gradient (Eq. 2.74)

---

$\beta$	Constant (Eq. 2.98)
$\Gamma$	Adsorption density, mole/cm <sup>2</sup> (Eq. 6.2)
$\Delta\rho$	Density difference, $\rho_l - \rho_g$
$\Delta p$	Pressure difference (Eq. 2.57)
$\Delta y$	Height difference (Eq. 2.45)
$\epsilon_g$	Gas holdup (Eq. 2.132)
$\theta, r$	Angular and radial coordinates, respectively
$\theta$	Contact angle (Eq. 2.20)
$\theta_c$	Angle of closest approach for fluid streamlines (Eq. 2.18)
$\lambda'$	Constant (Eq. 2.74)
$\mu$	Viscosity, g/cm.s
$\mu_l$	Liquid viscosity, g/cm.s
$\rho$	Density, g/cm <sup>3</sup>
$\rho_g$	Gas density, g/cm <sup>3</sup>
$\rho_l$	Liquid density, g/cm <sup>3</sup>
$\rho_p$	Particle density, g/cm <sup>3</sup>
$\sigma$	Surface tension, dyne/cm
$\Sigma F$	Sum of forces acting on a particle in motion (Eq. 2.47)
$\sigma_{S/A}$	Solid-air interfacial surface tension, dyne/cm (Eq. 2.20)
$\sigma_{S/W}$	Solid-water interfacial surface tension, dyne/cm (Eq. 2.20)
$\sigma_{W/A}$	Water-air interfacial surface tension, dyne/cm (Eq. 2.20)
$\tau(r, \theta)$	Shear stress (Eq. 2.99)
$\tau_0$	Tangential force (Eq. 2.72)
$\psi$	Stream Function for the outer fluid particle (Eq. 2.103)
$\psi(r, \theta)$	Stream Function
$\psi_p$	Stream Function for the inner fluid particle (Eq. 2.104)
$\nabla^2 U$	Laplacian of velocity (Eq. 2.48)
$\nabla P$	Pressure gradient (Eq. 2.48)

## LIST OF FIGURES

Figure 1.1:	General mineral processing activities .....	2
Figure 1.2:	Schematic of flotation column .....	5
Figure 1.3:	Relevance of the study (shaded) to flotation .....	7
Figure 2.1:	Illustration of the trajectory of a particle moving past a bubble in streamline flow .....	12
Figure 2.2:	Contact angle between bubble and particle in an aqueous medium .....	20
Figure 2.3:	Classification of collectors (after Glembotskii et al., 1972) ...	22
Figure 2.4:	Comparison of Stokes flow and potential flow past a sphere (White, 1991) .....	28
Figure 2.5:	Drag coefficients of smooth, axially symmetric bodies (Massey, 1983) .....	44
Figure 2.6:	Circulation region (wake) behind a sphere at various Reynolds numbers, $Re$ (Vennard and Street, 1975) .....	46
Figure 2.7:	Flow around submerged bodies (Foust, 1980): (a) streamlined shape-no separation, (b) nonstreamlined shape-separation of the boundary layer ....	47
Figure 2.8:	Schematic description of internal and external flow patterns (Clift et al., 1978): (a) a small liquid drop with negligible distortion, (b) a large, skirted drop .....	50
Figure 2.9:	General parameters which determine single bubble behaviour .....	51
Figure 2.10:	Shape regimes for bubbles and drops in unhindered gravitational motion through liquids (Clift et al., 1978) .....	60

Figure 2.11: Terminal velocity of air bubbles in water reported by several investigators (Clift et al., 1978) .....	63
Figure 2.12: Velocity of air bubbles ascending in the aqueous solutions of SDS (Okazaki, 1964): (1) distilled water, (2) $1.0 \times 10^{-6}$ molar SDS, (3) $1.2 \times 10^{-5}$ molar SDS, (4) $1.0 \times 10^{-4}$ molar SDS, (5) $1.0 \times 10^{-3}$ molar SDS, (6) rigid sphere in distilled water ..	67
Figure 2.13: Effect of surface tension on bubble rise velocity (Zhou et al., 1991): (1) surface tension: 72 dyne/cm, (2) surface tension: 50 dyne/cm .....	68
Figure 2.14: The distribution of adsorbed surface active solute on the surface of a rising drop (or bubble) (Linton, 1957) .....	71
Figure 2.15: The internal circulation of moving drops showing the direction of relative flow (Linton, 1957): (a) full circulation, (b) part circulation, (c) stagnant .....	71
Figure 2.16: Schematic representation of experimental arrangement (Young et al., 1959) .....	74
Figure 2.17: Drag coefficient versus Re for various empirical formulas (Concha and Almendra, 1979): (1) Schiller and Naumann, (2) Rubey, (3) Dallavalle (1943), (4) Dallavalle (1948), (5) Lapple, (6) Torobin, (7) Olson, (●) standard drag curve by Lapple and Shepherd (1940) .....	83
Figure 2.18: Drag coefficient versus Re: (line) Concha and Almendra (1979), (●) standard drag curve (Lapple and Shepherd, 1940) .....	83

Figure 2.19: Terminal velocities of spheres in air and water at 20 °C (Clift et al., 1978) .....	84
Figure 2.20: Typical curve and regions of the terminal velocity of bubbles (Mendelson, 1967) .....	95
Figure 2.21: Drag coefficient as a function of Re for water drops in air and air bubbles in water, compared with standard drag curve (Clift et al., 1978) .....	98
Figure 2.22: Theoretical and experimental data and models for terminal velocity of air bubbles in water .....	99
Figure 3.1: Single-fiber probes (Ishida and Tanaka, 1982) .....	106
Figure 3.2: Comparison between probe C and D (Ishida and Tanaka, 1982) .....	106
Figure 3.3: Schematic diagram of bubble-sizing apparatus (Randall et al., 1989) .....	108
Figure 3.4: Laser beam method (Meernik, 1988) .....	108
Figure 3.5: Three dimensional laser-beam system (Sung and Burgess, 1987) .....	109
Figure 3.6: Typical pulse sequence (Sung and Burgess, 1987) .....	109
Figure 3.7: Scheme of the sensor probe, one-element (Otero et al., 1991) .....	112
Figure 3.8: Two-element probe (Castillejos, 1986) .....	113
Figure 3.9: Configuration of Doppler blood-flow transducer (Nishi, 1972) .....	114
Figure 3.10: Second harmonic technique device (Miller, 1981) .....	116
Figure 3.11: The double frequency technique (Chapelon, 1985) .....	116
Figure 3.12: Laser plane technique (plan view) .....	118

Figure 4.1:	Schematic of the column set-up and water temperature control device .....	120
Figure 4.2:	Calibration diagram of thermistor no. 1 for Channel no. 1 (as an example) .....	121
Figure 4.3:	Water (in the column) and room temperature at three locations as a function of time (no temperature control) .....	122
Figure 4.4:	Temperature in the column at three locations as a function of time with temperature control at 30 °C. The system gave a constant and uniform temperature .....	123
Figure 4.5:	Schematic of the gas line and the bubble generation frequency control device .....	124
Figure 4.6:	Schematic of arrangement for video camera to follow the bubble motion .....	126
Figure 4.7:	Bubble position in consecutive frames (1/30 s): distance moved is measured on measuring tape (0.6 mm), therefore local velocity is 18 cm/s .....	128
Figure 5.1:	The effect of bubble generation frequency on velocity in tap water at locations: (a): $\approx$ 20 cm above the orifice, (b): $\approx$ 400 cm above the orifice .....	130
Figure 5.2:	Relationship between surface tension of solutions and concentration (a: ppm, b: mole/l) of the three types of frother at 30 °C .....	132
Figure 5.3:	Inside diameter of the glass capillary tube (SEM micrograph) .....	133

Figure 5.4:	Bubble shape in tap water under different conditions and at different positions:	
	5.4A- Bubble shape in tap water only:	
	(a) 20 cm above the orifice; (b) at top (4m),	
	5.4B- Bubble shape in presence of 30 ppm Dowfroth 250:	
	(c) 20 cm above the orifice; (d) at top (4m). Note, $d_e = 2.7$ mm	135
Figure 5.5:	Bubble velocity profiles in the same tap water for different bubble sizes (April 94)	138
Figure 5.6:	Bubble velocity profiles in distilled water and tap water on different dates ( $d_e = 1.5$ mm)	139
Figure 5.7:	Bubble velocity profiles ( $d_e = 0.9$ mm, frother = Dowfroth 250)	140
Figure 5.8:	Bubble velocity profiles ( $d_e = 1.5$ mm, frother = Dowfroth 250)	141
Figure 5.9:	Bubble velocity profiles ( $d_e = 2.2$ mm, frother = Dowfroth 250)	142
Figure 5.10:	Bubble velocity profiles ( $d_e = 2.7$ mm, frother = Dowfroth 250)	143
Figure 5.11:	Bubble velocity profiles ( $d_e = 0.9$ mm, frother = pine oil)	144
Figure 5.12:	Bubble velocity profiles ( $d_e = 1.5$ mm, frother = pine oil)	145
Figure 5.13:	Bubble velocity profiles ( $d_e = 2.2$ mm, frother = pine oil)	146
Figure 5.14:	Bubble velocity profiles ( $d_e = 2.7$ mm, frother = pine oil)	147
Figure 5.15:	Bubble velocity profiles ( $d_e = 0.9$ mm, frother = MIBC)	148
Figure 5.16:	Bubble velocity profiles ( $d_e = 1.5$ mm, frother = MIBC)	149
Figure 5.17:	Bubble velocity profiles ( $d_e = 2.2$ mm, frother = MIBC)	150
Figure 5.18:	Bubble velocity profiles ( $d_e = 2.7$ mm, frother = MIBC)	151

Figure 5.19: Bubble velocity profile characteristics .....	153
Figure 5.20: First stage of bubble velocity profile ( $d_c = 1.5$ mm) .....	153
Figure 5.21: Bubble velocity profiles ( $d_c = 1.5$ mm) in presence of methanol .....	156
Figure 5.22: Bubble velocity profiles ( $d_c = 1.5$ mm) in presence of collector (potassium ethyl xanthate) .....	157
Figure 5.23: Bubble velocity profiles ( $d_c = 1.5$ mm) in presence of modifiers (pH = 10) .....	158
Figure 5.24: Bubble velocity profiles ( $d_c = 1.5$ mm, frother = Dowfroth 250) at 20 and 40 °C .....	159
Figure 6.1: Comparison between the present and published data for pure water .....	162
Figure 6.2: Relationship between adsorption density at gas-liquid interface (a: ppm, b: mole/l) and frother concentration at 30 °C using Gibbs equation .....	165
Figure 6.3: Adsorption distance ( $h_a$ ) for a moving bubble .....	173
Figure 6.4: $K_a$ as a function of $d_c$ for various frothers; a: Dowfroth 250, b: pine oil, c: MIBC .....	176
Figure 6.5: Adsorption time vs frother concentration for various $d_c$ ; a: Dowfroth 250, b: pine oil, c: MIBC (in log-log form) .....	180
Figure 6.6a: Comparison between the present data on terminal velocity for bubbles in presence of frother and published data for bubbles in contaminated water and solid particles in water .....	183
Figure 6.6b: Figure 6.6a continued .....	184
Figure 6.7: Terminal velocity of bubbles in presence of frothers .....	185

## LIST OF TABLES

Table 2.1:	Classification of polar minerals (Wills, 1988; Crozier, 1992) .....	20
Table 2.2:	Common flotation collectors .....	23
Table 2.3:	Common flotation frothers .....	25
Table 2.4:	Moore's functions for distorted bubbles (Harper, 1972) .....	93
Table 5.1:	Frother specifications .....	131
Table 5.2a:	Bubble size measured about 20 and 400 cm above the orifice in tap water and predicted from Tate's Law .....	134
Table 5.2b:	The equivalent measured results in the presence of Dowfroth 250 (30 ppm) .....	134
Table 5.3:	Bubble oscillation amplitude and frequency (bubble rise path) in the absence and presence of frother (Dowfroth 250, 30 ppm) about 20 cm and 400 cm above the orifice .....	136
Table 5.4:	The maximum velocity of bubbles in tap water .....	139
Table 5.5:	Adsorption time (time to reach terminal velocity) for different bubble sizes and frother types at various concentrations .....	154
Table 5.6:	The effect of frother type on terminal velocity (cm/s) .....	155
Table 6.1:	Adsorption time (Eq. 6.1) for various frothers at different concentrations .....	166
Table 6.2:	The predicted adsorption time, $t_s$ (Eq. 6.14) for frothers at various concentrations .....	171
Table 6.3:	The numbers $N$ , $\Gamma$ and $C_b$ ( $d_c = 1.5$ mm) .....	174
Table 6.4:	The coefficients for Eq. 6.20 .....	175
Table 6.5:	Measured and predicted adsorption time .....	178

---

Table 6.6:	The measured (here) and calculated (Zhou et al., 1992) bubble average velocity over a distance of 90 cm from the orifice ( $d_o = 1.5$ mm) .....	181
Table 6.7:	Coefficients for Eq. 6.22 .....	185
Table 6.8:	Comparison of bubble size estimation from drift flux model .....	187

**LIST OF APPENDIXES**

Appendix 1: Computer data acquisition program ..... 209  
Appendix 2: Calculation of the diffusion coefficient ..... 219

**CHAPTER 1****INTRODUCTION**

Today, virtually no mineral as mined is suitable for use as a final product; rather it requires preparation and separation by physical and chemical methods (Kelly and Spottiswood, 1989). The physical methods collectively form the discipline of mineral processing. The essence of mineral processing is to reduce the bulk of the ore and to separate the valuable minerals from each other and from waste (gangue) minerals. Such processing increases the contained value of the ore to allow economic transportation and subsequent metal extraction (Wills, 1988; Claridge et al., 1989). Typical mineral processing unit operations are shown schematically in Fig. 1.1.

Froth flotation, or simply flotation, was patented in 1906 (Wills, 1988). It is now used worldwide and is the most versatile and selective mineral processing technique. Over the years, many investigators have developed and described applications of the flotation processes (Rickard and Ralston, 1917; Wark, 1934, 39; Sutherland, 1948; Gaudin, 1957; Fuerstenau, 1962, 76; Glembotskii et al., 1963; Klassen and Mokrousov, 1963; Tyurnikova and Noumov, 1981; Leja, 1982; King, 1982; Ives, 1984; Schulze, 1984; Kelly and Spottiswood, 1989; Laskowski, 1989; Matis and Mavros, 1991; Crozier, 1992).

The reasons flotation is such a common method of beneficiation include: relatively low cost compared to many other processes; the wide range of minerals to which flotation may be applied and the efficiency of separation which can usually be achieved (Claridge et al., 1989). Flotation can be used to achieve specific separation from low-grade and multi-mineral ores and ores that require fine grinding for adequate liberation (Kelly and Spottiswood, 1982; Crozier, 1992).

Flotation performance is controlled by the properties of the air (bubbles), liquid, solids and chemical reagents (collectors, frothers, regulators) in the system. In addition

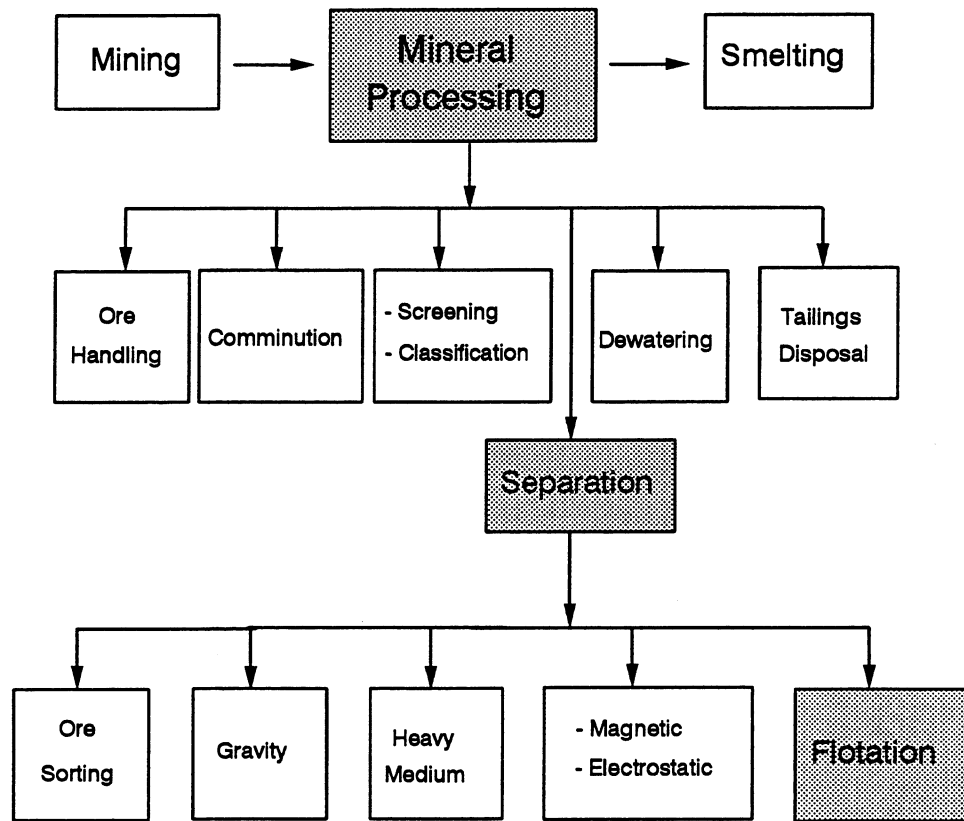


Figure 1.1: General mineral processing activities.

to chemical reagent control, the overall process of selective separation by flotation depends on many other factors, such as: the hydrodynamics of solid-in-water slurries, the kinetics of chemical reactions and physical processes such as wetting and the attachment of solid/gas phases (Leja, 1982).

Most minerals are naturally hydrophilic (i.e., are unfloatable). The surface of hydrophilic minerals can be changed to hydrophobic (floatable) by the use of chemical reagents (collectors). Frothers are required to provide a reasonably stable bubble dispersion and a stable froth above the pulp. Regulators (including pH modifiers) are used to activate or depress mineral attachment to air-bubbles. In general, the concept of flotation is to recover hydrophobic particles by attachment to bubbles, with subsequent transport of these particles to the pulp surface (Schulze, 1984; Wills, 1988; Laskowski, 1993).

### 1.1. COLUMN FLOTATION CHARACTERISTICS

Flotation machines with a columnar geometry have been tried since 1910 (Gahl, 1917). The modern era of "column flotation" followed the patents in the early 1960s by Boutin and Tremblay (Canadian patents 680,576 and 694,547). Early descriptions of the column and testwork were given by Wheeler (1966) and Boutin and Wheeler (1967). The first significant installation was in 1980, at Noranda's Les Mines Gaspé. During the past few years, there has been a rapid growth in practice related to column design, construction, operation, gas injection and control (Dobby and Finch, 1986b). Over the same period, this field has witnessed much research and development interest worldwide and applications are expanding to new areas, for example, de-inking of recycle paper. It has also given rise to several derivative devices such as: the Jameson cell, the Pneumatic cell, the Contact cell, the Centrifloat, the Packed column and the microbubble column (Harris, 1976; Yang, 1988; Jameson, 1988; Jameson and Manlapig, 1991; Finch, 1995). Recently, at McGill University, a new generation of flotation cell based on

bubble formation by cavitation has been initiated under the supervision of Profs. Z. Xu and J.A. Finch.

Flotation columns have been employed to treat a variety of ores, including those of iron, copper, molybdenum, fluorite and coal. The column is attractive for treating fine particles (Xu and Finch, 1988; Szatkowski and Freyberger, 1988) as it can often upgrade in fewer stages compared with mechanical cells (Dobby and Finch, 1986b).

Flotation columns differ radically from conventional mechanical flotation units both in design and operating philosophy (Yianatos et al., 1986). Commercial units are typically 5-15m in height and 0.5 m to 3.0m in diameter (Xu, 1991). The cross-section may be square or circular. From an operational point of view, two main zones can be identified: a collection (bubbling) zone, where feed enters, and a cleaning (froth) zone (Fig. 1.2). Wash water is added into the froth to clean the froth of particles entrained in the water crossing with the bubbles from the collection zone. The tailings withdrawal at the bottom of the column is controlled at a rate slightly greater than the feed flowrate (called a positive bias) (Finch and Dobby, 1990). The bubble generators (spargers) in flotation columns, located at the bottom, produce small bubbles at controllable sizes without mechanical agitation. In general, the flotation column is distinguished from a mechanical flotation machine by: the bubble generation system, the lack of mechanical agitation, the use of wash water and the geometry (e.g., height, diameter ratio).

At McGill University, the study and development of flotation columns were started in 1981. Some of the results of these studies appeared in the monograph "Column Flotation" authored by Finch and Dobby (1990). Several theses have also been produced (Dobby, 1984; Yu, 1985; Xu, 1990; Mecklenburg, 1991; Uribe-Salas, 1991; Banisi, 1994 and Shen, 1994).

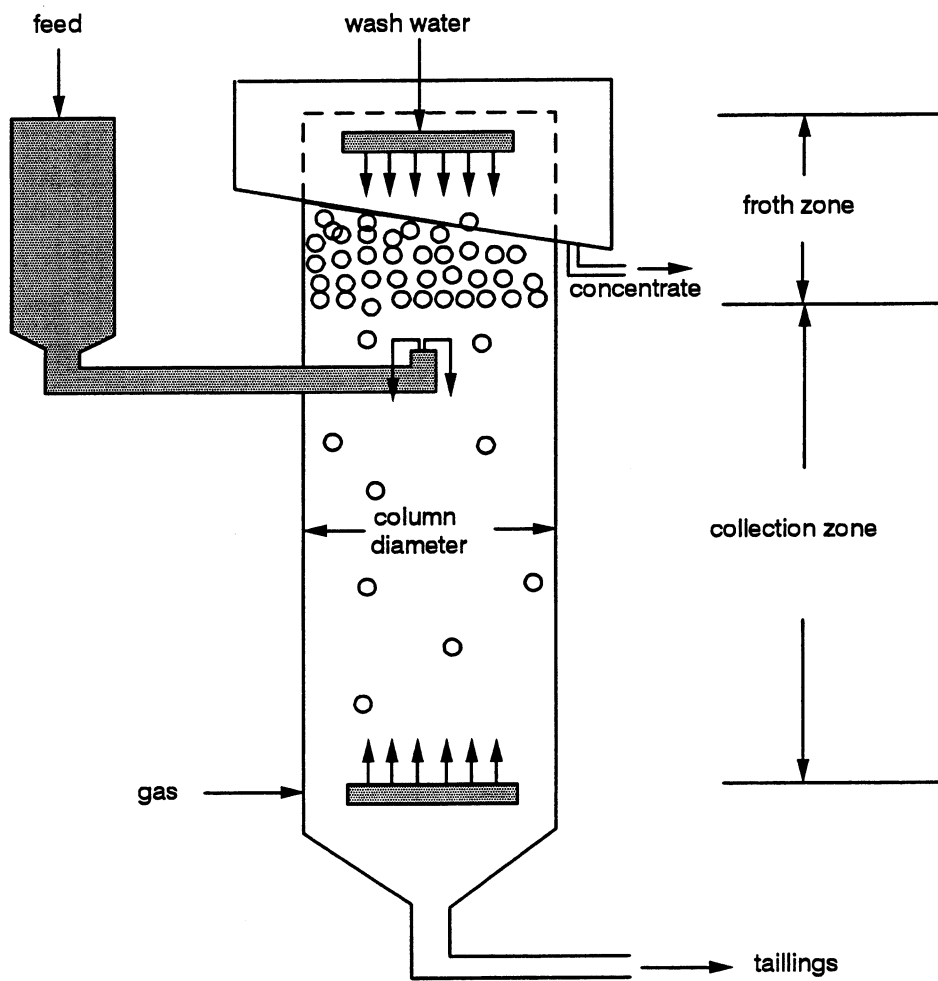


Figure 1.2: Schematic of flotation column.

## 1.2. Bubble-Liquid Systems

Bubble-separation techniques are applied in many processes encountered in chemical and metallurgical engineering. For example, operations involving fermentation, flotation, purification, fluidization, adsorption, cavitation, boiling heat transfer, and vacuum degassing all generally involve the motion of gas bubbles in liquids (Davidson and Harrison, 1971; Grace, 1973). Understanding of the systems needs research into the bubble formation, bubble motion, bubble surface chemistry, bubble coalescence and breakup, bubble distribution, adsorption-desorption, mass transfer, etc (Davies and Rideal, 1961; Bhaga, 1976; Leja, 1982; Li, 1992).

In flotation, bubbles obviously play a key role. Before the interactions involving bubbles in a bubble swarm can be understood, it is necessary to understand the behaviour of single bubbles (Fuerstenau and Wayman, 1958; Grace et al., 1976; Anfruns and Kitchener, 1977; Jameson, 1993). Because of the larger height of a flotation column compared with mechanical flotation cells, bubble motion and the effect of chemical surfactants over this height may play a role in the flotation performance. Also, fundamental particle/bubble collision/attachment models usually include bubble behaviour but little basic work has actually been performed on systems relevant to flotation.

## 1.3. Objectives of the Present Work

The present investigation considers fundamental aspects of the properties of single bubbles, such as size, shape, path and velocity, during their rise in a column in the presence and absence of flotation reagents such as frothers. The relevancy of this study to flotation is illustrated in Fig. 1.3.

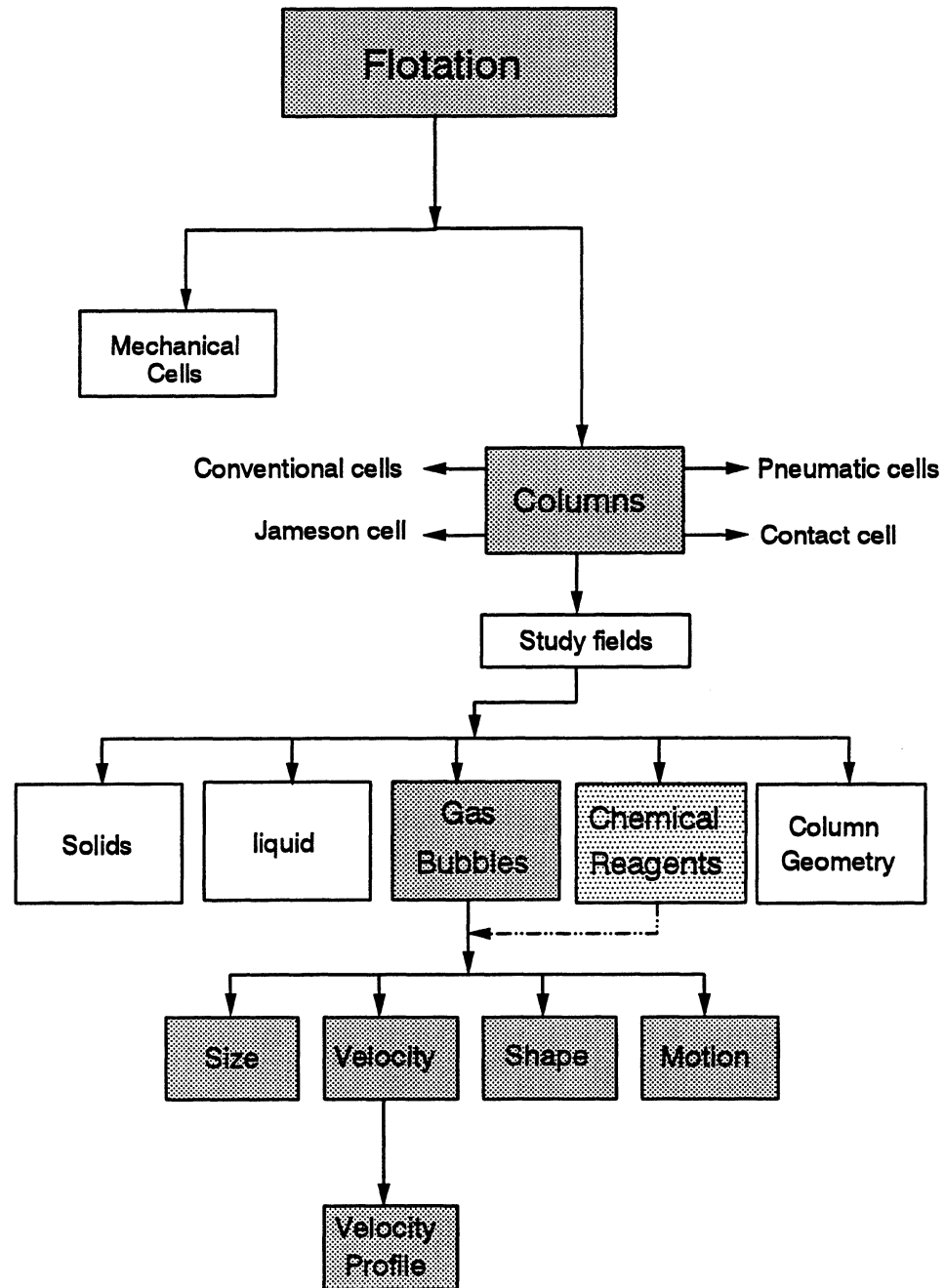


Figure 1.3: Relevance of the study (shaded) to flotation.

#### 1.4. Structure of Thesis

This thesis consists of 7 chapters. In Chapter 1, column flotation is introduced along with some of the important machines and operating characteristics. The objectives of the thesis and the structure of the thesis are also presented.

Chapter 2 describes the fundamental considerations and includes:

- a- Effect of bubble size on particle collection efficiency.
- b- Chemical reagents used in flotation and their applications.
- c- Hydrodynamics of bubble-water system.
- d- Forces acting on a single bubble.
- e- Bubble behaviour.
- f- Mechanism and effects of surfactant adsorption.
- g- A review on theories and models of bubble velocity.
- h- Bubble swarms (drift flux model)
- i- Interaction between bubbles.
- j- Wall effects.

Chapter 3 reviews bubble size and velocity estimation techniques.

Chapter 4 describes the experimental set-up and techniques. The column set-up, the temperature control, the gas line, the camera moving device and the experimental procedures are discussed.

Chapter 5 presents the results including bubble generation frequency, test liquid properties, bubble size, shape, path, and velocity as a function of height. The effect of flotation surfactants, pH and temperature on bubble velocity profile (local velocity versus

height or time) is described. The measured bubble maximum velocity, terminal velocity and surfactant adsorption time are introduced.

Chapter 6 interprets the results. A comparison between the present and published data is introduced. An empirical model to estimate adsorption time for moving bubbles is presented.

Finally, Chapter 7 concludes the work, and gives the claims for original research and suggestions for future work.

## CHAPTER 2

### FUNDAMENTAL CONSIDERATIONS

#### 2.1. Particle Collection Efficiency

The aim of flotation is to mineralize air bubbles with target minerals (particle collection) and levitate them to form a froth product while leaving the non-target particles in the pulp. The mineralization of air bubbles involves a complex physical-chemical process. Derjaguin and Dukhin (1961) established a theory of flotation of small and medium-size particles. They considered the interaction between particles and bubbles and the forces acting on the bubble in a flotation system. In this section, those physical aspects of the particle collection mechanism which are related to bubble size are described.

An air bubble must be able to attach to a particle, and lift it to the froth zone. The air bubbles can only adhere to hydrophobic particles. Some minerals are naturally hydrophobic but most are hydrophilic. After treatment with various reagents, differences in mineral surface properties become apparent in the particles' ability to attach to gas bubbles. The mechanism has been studied by many investigators (Glembotskii et al., 1963; Flint and Howarth, 1971; Reay and Ratcliff, 1973, 75; Anfruns and Kitchener, 1976, 77; Ahmed and Jameson, 1985; Jiang and Holtham, 1986; Dobby and Finch, 1986, 87; Szatkowski and Freyberger, 1988; Schulze et al., 1989; Schulze, 1989; Yoon and Luttrell, 1989; Ahmed and Jameson, 1989; Laskowski, 1989; Finch and Dobby, 1990, Vinogradova, 1994).

Schulze (1989) summarized the collection mechanism as:

- a. Approach of a particle to a bubble in the field of flow.

- b. Formation of a thin liquid film between the particle and the bubble and its rupture with the formation of a dynamic three-phase contact (TPC).
- c. Stabilization of bubble/particle aggregates against external stress in the flotation machine.
- d. Transport of the bubble/particle aggregate to the froth layer.

Particle collection is considered to occur by particle-bubble collision followed by the particle sliding over the bubble during which attachment (due to the hydrophobic nature of the mineral surface) may occur. The flotation rate is limited by the particle-bubble collision and subsequent attachment probabilities (Dobby and Finch, 1987; Ahmed et al., 1989).

In the absence of significant detachment, the collection efficiency is defined by

$$E_K = E_C \times E_A \quad (2.1)$$

where  $E_K$ ,  $E_C$  and  $E_A$  are the collection, collision and attachment efficiencies, respectively.

### 2.1.1. Bubble-Particle Collision

In flotation, particles and bubbles are generally moving in opposite directions. One of the major factors that affects the probability of bubble/particle collision is the fluid flow pattern around the moving bubbles. Because the stream function that describes the flow pattern, is a function of bubble size, the collision efficiency varies with different stream functions. The fluid pattern around the bubble varies with the Reynolds number

of the bubble ( $Re_b$  or generally  $Re$ ). With increasing bubble diameter ( $d_b$ ), the bubble terminal velocity ( $U_b$  or  $U_T$ ), and hence  $Re$ , increase.  $Re$  is given by

$$Re = \frac{U_b d_b \rho_l}{\mu_l} \quad (2.2)$$

where  $\rho_l$  and  $\mu_l$  are liquid density and viscosity, respectively.

Yoon and Luttrell (1989) gave a general model for particle collision efficiency ( $E_c$ ) based on the stream functions ( $\psi$ ) for different flow conditions,

$$E_c = \frac{2 \psi}{U_b r_b^2} \quad (2.3)$$

where  $r_b$  is bubble radius. The trajectory of a particle is considered to be determined by the streamline which passes through its center. Assuming that the streamlines come closest to the bubble at its equator, a grazing streamline is defined as the one passing through the center of a particle (radius  $r_p$ ) at the equator and the collision radius ( $r_c$ ) at an infinite distance from the bubble (Fig. 2.1).

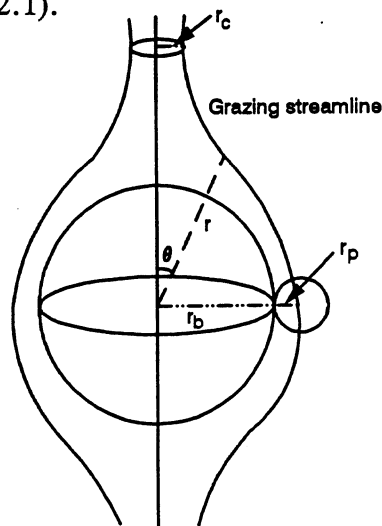


Figure 2.1: Illustration of the trajectory of a particle moving past a bubble in streamline flow.

The collision radius can be obtained by

$$r_c^2 = \frac{2 \Psi}{U_b} \quad (2.4)$$

According to Yoon and Luttrell (1989), the collision efficiency can be determined by:

a) for Stokes flow conditions ( $0 \leq \text{Re} \leq 1$ )

$$E_c = \sin^2 \theta \left( x^2 - \frac{3}{2} x + \frac{1}{2x} \right) \quad (2.5)$$

In case of grazing at the bubble equator,  $r = r_p + r_b$ ,  $x = 1 + r_p / r_b$ , and  $\theta = 90^\circ$ , the collision efficiency becomes

$$E_c = \frac{3}{2} \left( \frac{r_p}{r_b} \right)^2 \quad (2.6)$$

b) for intermediate flow conditions ( $1 < \text{Re} < 100$ )

$$E_c = \left( \frac{3}{2} + \frac{4 \text{Re}^{0.72}}{15} \right) \left( \frac{r_p}{r_b} \right)^2 \quad (2.7)$$

c) for potential flow conditions ( $Re > 100$ )

$$E_c = 3 \left( \frac{r_p}{r_b} \right) \quad (2.8)$$

The efficiency of collision is defined as the fraction of particles in the path of a bubble that actually collide with it (Jiang and Holtham, 1986). According to the Flint and Howarth (1971) approach, particle behaviour can be characterized by two dimensionless parameters

$$K'' = \frac{\rho_p (d_p)^2 U_{re}}{9 \mu_l d_b} \quad (2.9)$$

and

$$G = \frac{(\rho_p - \rho_l) (d_p)^2 g}{18 \mu_l U_{re}} \quad (2.10)$$

where  $U_{re}$  is velocity of the bubble relative to the particle,  $g$  is acceleration due to gravity and  $\rho_p$  is particle density.

For coarse particles ( $K'' > 1.0$ ), collision efficiency depends strongly on the inertial force of the particle. For fine particles ( $K'' < 0.1$ ) it depends strongly on the parameter  $G$ . When the inertial forces are negligible, the collision efficiency for both Stokes flow and potential flow is given by

$$E_c = \frac{G}{1 + G} \quad (2.11)$$

For particles less than 20  $\mu\text{m}$  in diameter and bubble size less than 100  $\mu\text{m}$ , the collision efficiency (ignoring the inertial force) is obtained from

$$E_c \propto \left( \frac{d_p}{d_b} \right)^{n_1} \quad (2.12)$$

where  $n_1$  equals 2.05 and 1.90 for particles of relative density 2.5 and 1.0, respectively (Reay and Ratcliffe, 1973).

The Stokes number (St), which represents a ratio of inertial to drag forces, is useful for determining the tendency of a particle to adjust to changes in fluid flow (Yoon and Luttrell, 1989) and is given by

$$St = \frac{1}{9} \frac{\rho_p}{\rho_l} \left( \frac{d_p}{d_b} \right)^2 Re \quad (2.13)$$

Based on equations of particle motion, Weber and Paddock (1983) derived a model for  $St = 0$  and low particle inertia for determination of collision efficiency ( $E_{co}$ ), which is the sum of gravitational ( $E_{cg}$ ) and interceptional collision ( $E_{ci}$ ) (Finch and Dobby, 1990):

$$E_{co} = E_{cg} + E_{ci} \quad St = 0 \quad (2.14)$$

$E_{ci}$  is given by (Weber and Paddock, 1983)

$$E_{ci} = \frac{1.5}{1 + U_p} \left( \frac{d_p}{d_b} \right)^2 \left( 1 + \frac{(3/16) Re}{1 + 0.249 Re^{0.56}} \right) \quad (2.15)$$

where  $U_p$  is particle velocity.

For  $0 < Re \leq 300$ ,  $E_{cg}$  is given by (Reay and Ratcliff, 1973)

$$E_{cg} = \frac{U_p^*}{(1 + U_p^*)} \left( 1 + \frac{d_p}{d_b} \right)^2 \sin^2 \theta_c \quad (2.16)$$

where  $U_p^*$  is the terminal particle velocity divided by bubble velocity, that is given by (also see Nguyen-Van et al., 1994)

$$U_p^* = \frac{g (\rho_p - \rho_l) d_p^2}{18 \mu_l} \quad (2.17)$$

and  $\theta_c$  is the angle of closest approach for fluid streamlines, given by

$$\theta_c = 78.1 - 7.37 \log Re \quad (2.18)$$

In the general case, the collision efficiency for  $St > 0.1$  can be obtained by (Dobby and Finch, 1990)

$$E_c = E_{co} (1.63 Re^{0.06} St^{0.54} U_p^{-0.16}) \quad St > 0.1 \quad (2.19)$$

### *Collision time*

After collision with the particle, deformation occurs on the surface of the bubble. The motion of the particle on the surface of the bubble due to bubble deformation and elasticity of the bubble is similar to the motion of a spring (Schulze et al., 1989) if we assume the colliding particle trajectory is normal to the deformed bubble surface (in the radial direction). Deformation and motion of the bubble surface continues until the energy of the bubble becomes zero and at this time the velocity of the particle in the radial direction of the bubble is zero. The particle will continue to slide over the bubble surface (due to gravitational forces and streamlines) unless attachment occurs. The time from collision to the onset of particle sliding is called the "collision time,  $t_c$ ". Collision time can be estimated from the equation of harmonic oscillation of the colliding particle normal to the deformed bubble surface (Schulze, 1989).

### *Sliding time*

The particle slides over the surface of the bubble unless attachment occurs. The sliding time ( $t_s$ ) can be determined by the velocity of the liquid flowing past the rising bubble and the size of the bubble (Dobby and Finch, 1986; Yoon and Luttrell, 1989).

### *Contact time*

Contact time ( $t_{con}$ ) is the total time after the first collision and before attachment ( $t_{con} = t_c + t_s$ ).

### *Induction time*

During the contact time period, the thin liquid film formed between the bubble and the particle must drain and rupture, giving rise to a three-phase contact (TPC) which is sufficiently large to stabilize the bubble/particle aggregate (Schulze, 1989; Yoon and Luttrell, 1989). Induction time ( $t_i$ ) is the sum of the film drainage time,  $t_f$  and TPC expansion time,  $t_{TPC}$  ( $t_i = t_f + t_{TPC}$ ).

#### **2.1.2. Bubble-Particle Attachment**

As a bubble rises through the pulp it encounters particles. Those particles that are hydrophobic enough attach to the bubble. Bubble/particle attachment ( $E_A$ ) will occur when  $t_{con} \geq t_i$ . Generally  $E_A$  is a function of bubble/particle size and induction time (Dobby and Finch, 1986b; Yoon and Luttrell, 1989).

After attachment occurs, the bubble/particle aggregate rises to reach the pulp-froth interface; other bubbles arriving behind the bubble/particle aggregate in question push it into the froth zone. The liquid between bubbles consists of non-target minerals which can be rejected by use of wash water.

Recently, the attachment of hydrophobic particles to bubbles on collision has been investigated theoretically by Vinogradova (1994). According to his approach, hydrophobicity is related to the slippage of liquid over a solid surface and to the size of the critical rupture thickness of the interlayer at water between bubble and particle. The result is the velocity of particle approach to the bubble increases with particle surface hydrophobicity.

## 2.2. Flotation Reagents

Reagents are organic and inorganic chemicals that are added to flotation circuits to control the separation between mineral types. The selection of a suite of reagents for effective processing of a particular ore by flotation requires a considerable knowledge of surface properties and solution chemistry and generally requires extensive trial-and-error experimentation (Crozier, 1992). Flotation reagents are typically classified under three headings: collectors, frothers and regulators (or modifiers).

### 2.2.1. Collectors

The hydrophobicity of a mineral surface is defined by the degree of reaction of surface species with water molecules. These surface species are broadly classified into non-polar and polar types. With non-polar species, there is little interaction with water molecules, i.e. they are hydrophobic (Wills, 1988; Ives, 1984). Some minerals, such as graphite, sulphur, molybdenite, diamond, talc and coal are non-polar and naturally hydrophobic. Species with strong covalent or ionic bonding are polar. The reaction of the polar species with water molecules is strong, i.e. they are hydrophilic. Table 2.1 shows a list of minerals in groups of increasing polarity, divided into classes dependent on the magnitude of the polarity, which increases from groups 1 to 5. The minerals in group 1 are all sulphides, which are weakly polar. In general, the degree of polarity increases from sulphide, through sulphates, to carbonates, phosphates, etc., then to oxides-hydroxides, and finally, silicates and quartz.

In order for a solid particle (mineral) to be floated, a gas phase must replace a liquid phase at the solid surface. The condition for this can be described by wetting models: Young (1805), Harkins (1952) and Zisman (1964). The tensile forces tending to separate a mineral and a bubble (Fig. 2.2) lead to the development of an angle (contact angle,  $\theta$ ) between the mineral surface and the bubble surface.

Table 2.1: Classification of polar minerals (Wills, 1988; Crozier, 1992).

Group 1	Group 2	Group 3	Group 4	Group 5
Galena, [PbS]	Barite, [BaSO <sub>4</sub> ]	Malachite, [Cu <sub>2</sub> CO <sub>3</sub> (OH) <sub>2</sub> ]	Hematite, [Fe <sub>2</sub> O <sub>3</sub> ]	Zircon, [ZrSiO <sub>4</sub> ]
Chalcopyrite, [CuFeS <sub>2</sub> ]	Anhydrite, [CaSO <sub>4</sub> ]	Azurite, [2CuCO <sub>3</sub> .Cu(OH) <sub>2</sub> ]	Geothite, [FeO(OH)]	Hemimorphite, [Zn <sub>4</sub> Si <sub>2</sub> O <sub>7</sub> (OH) <sub>2</sub> .2H <sub>2</sub> O]
Covellite, [CuS]	Gypsum, [CaSO <sub>4</sub> .2H <sub>2</sub> O]	Chrysocolla, [CuSiO <sub>3</sub> .2H <sub>2</sub> O]	Chromite, [FeCr <sub>2</sub> O <sub>4</sub> ]	Beryl, [Be <sub>3</sub> Al <sub>2</sub> Si <sub>6</sub> O <sub>18</sub> ]
Bornite, [Cu <sub>3</sub> FeS <sub>4</sub> ]	Anglesite, [PbSO <sub>4</sub> ]	Wulfenite, [PbMoO <sub>4</sub> ]	Pyrolusite, [MnO <sub>2</sub> ]	Garnet, [Ca <sub>3</sub> Al <sub>2</sub> (SiO <sub>4</sub> ) <sub>3</sub> ]
Chalcocite, [Cu <sub>2</sub> S]		Cerrusite, [PbCO <sub>3</sub> ]	Borax, [Na <sub>2</sub> B <sub>4</sub> O <sub>7</sub> ]	Quartz, [SiO <sub>2</sub> ]
Energite, [Cu <sub>3</sub> (As,Sb)S <sub>4</sub> ]		Flourite, [CaF <sub>2</sub> ]	Wolframite, [(Fe,Mn)WO <sub>4</sub> ]	
Argentite, [Ag <sub>2</sub> S]		Witherite, [BaCO <sub>3</sub> ]	Columbite, [(Fe,Mn)(Nb,Ta) <sub>2</sub> O <sub>6</sub> ]	
Millerite, [NiS]		Magnesite, [MgCO <sub>3</sub> ]	Tantalite, [FeTa <sub>2</sub> O <sub>6</sub> ]	
Cobaltite, [CoAsS]		Dolomite, [CaMg(CO <sub>3</sub> ) <sub>2</sub> ]	Rutile, [TiO <sub>2</sub> ]	
Arsenopyrite, [FeAsS]		Apatite, [Ca <sub>5</sub> (F,Cl)(PO <sub>4</sub> ) <sub>3</sub> ]	Cassiterite, [SnO <sub>2</sub> ]	
Pyrite, [FeS <sub>2</sub> ]		Scheelite, [CaWO <sub>4</sub> ]		
Pyrrhotite, [Fe <sub>7</sub> S <sub>8</sub> ]		Smithsonite, [Zn silicata clay]		
Sphalerite, [ZnS]		Rhodochrosite, [MnCO <sub>3</sub> ]		
Stibnite, [Sb <sub>2</sub> S <sub>3</sub> ]		Siderite, [FeCO <sub>3</sub> ]		
Orpiment, [As <sub>2</sub> S <sub>3</sub> ]		Monazite, [(Ce,La,Di)PO <sub>4</sub> ]		
Pentlandite, [(Fe,Ni) <sub>9</sub> S <sub>8</sub> ]				
Realgar, [AsS]				
Cinnabar, [HgS]				
Albandite, [MnS]				
Native [Au, Ag, Pt, Cu]				

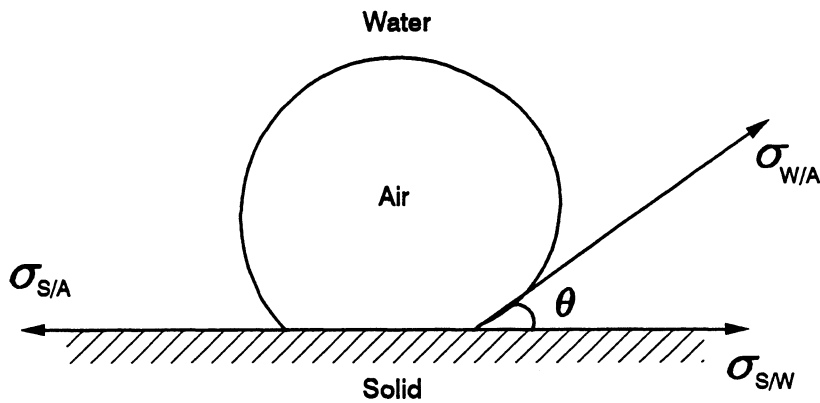


Figure 2.2: Contact angle between bubble and particle in an aqueous medium.

Based on the Young model, the relationship between these forces at equilibrium can be derived as:

$$\sigma_{S/A} = \sigma_{S/W} + \sigma_{W/A} \cos \theta \quad (2.20)$$

where  $\sigma_{S/A}$ ,  $\sigma_{S/W}$  and  $\sigma_{W/A}$  are the surface energies (interfacial surface tension) between solid-air, solid-water and water-air, respectively. The force is required to break the mineral-bubble interface is called the "work of adhesion,  $W_{S/A}$ ", and is equal to the work required to separate the solid-air interface and produce separate air-water and solid-water interfaces (Wills, 1988), that is

$$W_{S/A} = \sigma_{W/A} + \sigma_{S/W} - \sigma_{S/A} \quad (2.21)$$

and from Eq. 2.20, gives

$$W_{S/A} = \sigma_{W/A} (1 - \cos \theta) \quad (2.22)$$

As this equation shows, with increasing contact angle, the work of adhesion between mineral and bubble increases. Values of contact angle between  $0^\circ$  and  $180^\circ$  provide an indication of the degree of the hydrophobic (literally "water fearing") character of the surface. The hydrophobicity of a mineral therefore increases with contact angle and thus often correlates with increased floatability. The contact angle between a hydrophilic (water-loving) mineral surface and bubble surface is low, therefore, it is not naturally floatable. There are no known solids that exhibit a contact angle more than  $108^\circ$  which is the value obtained with Teflon (Fuerstenau, 1984). The naturally hydrophobic minerals exhibit contact angles less than  $108^\circ$ .

Most minerals have hydrophilic species on the surface and must acquire their hydrophobic character by the adsorption of surfactants. In order to change the surface to hydrophobic, surfactants known as collectors are added (Leja, 1982). By adsorption of collector molecules or ions on the mineral surface, the balance can switch from hydrophilic to hydrophobic to such an extent that attachment of the particle to the bubble occurs on contact (Claridge et al., 1989).

Collectors are heterogeneous compounds that contain an active inorganic group coupled with a hydrocarbon chain (R). The inorganic (polar) group adsorbs on the mineral surface, while the hydrocarbon chain (non-polar), provides hydrophobicity to the mineral surface after collector adsorption (King, 1982). Different collectors can be used with respect to the mineral type, Fig. 2.3 and Table 2.2 show collectors classification and common flotation collectors, respectively.

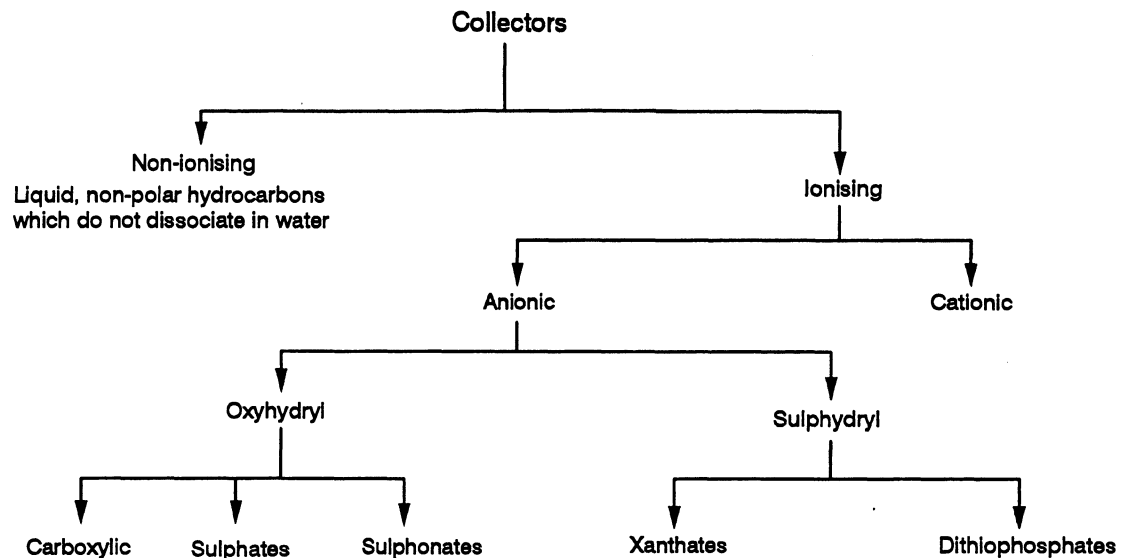


Figure 2.3: Classification of collectors (after Glembotskii et al., 1972).

Table 2.2: Common flotation collectors.

Anionic	Cationic
Alkyl Mercaptan $R-SH$	primary Amine
Alkyl Dithiocarbonate (Xanthate) $R-O-C \begin{matrix} \diagup S \\ \diagdown S^- Na^+ (K^+) \end{matrix}$	$\begin{matrix} R & & H \\ & \diagdown & / \\ & N & \\ & / & \diagdown \\ H & & H^+ Cl^- \end{matrix}$
Dialkyl Disulfide (Dixanthogen) $R-O-C \begin{matrix} \diagup S \\ \diagdown S \end{matrix} - S - \begin{matrix} S \\ \diagdown C-O-R' \end{matrix}$	Quaternary Amine
Xanthogen Formates $R-O-C \begin{matrix} \diagup S \\ \diagdown S \end{matrix} - S - \begin{matrix} O \\ \parallel \\ C-O-R' \end{matrix}$	$\begin{matrix} R'' & & R''' \\ & \diagdown & / \\ & N & \\ & / & \diagdown \\ R' & & R^+ Cl^- \end{matrix}$
Dialkyl Thionocarbamate $R-O-C \begin{matrix} \parallel S \\ \diagdown N \end{matrix} \begin{matrix} H \\ \diagup \\ R' \end{matrix}$	
Dialkyl Dithiophosphate $R-O \begin{matrix} \diagdown \\ \diagup \end{matrix} P \begin{matrix} \diagup S \\ \diagdown S^- Na^+ \end{matrix}$	
Dialkyl Dithiocarbamate $R' \begin{matrix} \diagdown \\ \diagup \end{matrix} N-C \begin{matrix} \diagup S \\ \diagdown S^- Na^+ \end{matrix}$	
Carboxylate (Fatty Acid) $R-C \begin{matrix} \parallel O \\ \diagdown O^- H^+ \end{matrix}$	
Alkyl Sulphate $R-O-S \begin{matrix} \parallel O \\ \diagdown OH \\ \parallel O \end{matrix}$	

### 2.2.2. Frothers

The hydrophobic particles must attach to bubbles and be transported to the froth zone. For this, a swarm of stable and small (to provide high specific surface area and collision efficiency) bubbles is required. In absolutely pure liquids, the formation of such a swarm is difficult and the presence of a surface active agent (frother) is necessary (King, 1982). Frother molecules, by adsorbing at the air-water interface, minimize coalescence and preserve small bubbles (Agrawal and Wasan, 1979).

Frothers are chemically similar to ionic collectors. When a frother is added to water the surface tension of the solution decreases as a result of the heteropolar nature of the molecules. The frother molecules are arranged at the interface such that the hydrophilic (polar) group is situated in the water phase and the hydrophobic (non-polar) hydrocarbon chain in the air phase (King, 1982; Wills, 1988). The most effective frothers include in their structure particular chemical groups, such as hydroxyl (-OH), carbonyl (-CO), carboxyl (-COOH) and amino groups (-NH<sub>2</sub>). The alcohols (-OH) are the most widely used, since they have practically no collector properties, and in this respect are preferable to other frothers (Wills, 1988). Table 2.3 summarizes the frother types and their chemical structures.

Frothers are known to reduce the induction time and hence make the flotation process more kinetically favourable. Good flotation frothers have branched hydrocarbon radicals and form loosely packed gaseous films at the liquid/gas interface. The HLB (hydrophile-lipophile balance) values of the most effective frothers are close to 6 (Laskowski, 1993). This allows frothers to co-operate actively with the adsorbed collector at the moment of particle-to-bubble attachment. Increasing molecular weight at roughly the same HLB values makes frothers more powerful (Laskowski, 1993).

There is interaction between frother and water and also between frother and collector molecules (Davies and Rideal, 1961; Leja, 1982; Crozier 1992; Urry, 1995). These surface complexes can be due to hydrogen bonds between molecules. In general,

the interaction strength is related to the structure of frother and collector molecules.

**Table 2.3: Common flotation frothers.**

Polypropylene Glycol Ether (Dowfroths)	$\text{CH}_3 - (\text{O} - \text{C}_3\text{H}_6)_n - \text{OH}$
Methyl Isobutyl Carbinol (MIBC)	$\begin{array}{ccccccc} \text{CH}_3 & - & \text{CH} & - & \text{CH}_2 & - & \text{CH} & - & \text{CH}_3 \\ & &   & & & &   & & \\ & & \text{CH}_3 & & & & \text{OH} & & \end{array}$
Terpineol (Pine Oil)	$\begin{array}{c} \text{CH}_2 - \text{C} = \text{CH}_2 - \text{CH}_2 - \text{CH}_2 - \text{CH} - \text{C} - \text{OH} \\ \quad   \\ \quad \text{CH}_3 \\ \quad   \\ \quad \text{CH}_3 \end{array}$
Xylenol (Cresylic Acid) $(\text{CH}_3\text{C}_6\text{H}_4\text{OH})$	

### 2.2.3. Regulators

Regulators can be classified as pH modifiers, activators and depressants:

#### *pH Modifiers*

Pulp alkalinity plays a very important role in flotation, and in practice, selectivity in complex separations is dependent on a delicate balance between reagent concentrations and pH (Wills, 1988, Leja, 1982). Alkalinity can be controlled by the addition of lime (CaO), soda ash (Na<sub>2</sub>CO<sub>3</sub>), caustic soda (NaOH) or acids such as H<sub>2</sub>SO<sub>4</sub> and HCl.

#### *Activators*

These are chemicals that are used to permit flotation of a mineral that is difficult or impossible to float with only the use of a collector and a frother (Crozier, 1992). The classical example is the use of copper sulphate to activate sphalerite. Copper deposits on the surface as it is more electro-negative than zinc. The resulting "copper sulphide" deposit on the sphalerite surface reacts readily with collector (e.g., xanthate) to form insoluble copper xanthate, which renders the sphalerite surface hydrophobic. Sphalerite is not floated satisfactorily by a xanthate collector alone as zinc-xanthate is relatively soluble in water, and consequently does not provide a stable hydrophobic film on the mineral (Wills, 1988; Kelly and Spottiswood, 1989). In general, activation is a method to increase the selectivity of minerals. The common activators are: copper sulphate, lead nitrate and sodium sulphide, the latter also being known as a "sulphidizing" reagent.

### *Depressants*

These assist in the separation of minerals when the floatability of two or more minerals is too similar for a particular collector to effect a separation (Crozier, 1992). Cyanides are widely used in the selective flotation of lead-copper-zinc and copper-zinc ores as depressants for sphalerite, pyrite and certain copper sulphides (Wills, 1988). The common depressants are: sodium cyanide, sodium hydrosulphide, zinc sulphate, sodium sulphide and starches.

### **2.3. Fluid Flow Around a Sphere**

Fluid flow around the bubble controls bubble motion. Fluid flow about bodies (e.g., solid particles, liquid drops, air bubbles) has been discussed by many investigators (Stokes, 1851; Eskinazi, 1968; Wallis, 1969; Davidson and Harrison, 1971; Binder, 1973; Clift, 1978; Potter and Foss, 1982; Yoon and Luttrell, 1989; Fan and Tsuchiya, 1990; White, 1991; Pnueli and Gutfinger, 1992). Mathematical analysis is generally possible only if certain simplifying assumptions are made. Simplification is often obtained by assuming that the properties of the fluid do not vary with time at a given point in space of the fluid (steady flow). In steady state motion, the partial derivatives of the properties with respect to time are zero. The imposition of the solid boundary is of geometrical importance; that is, it serves the purpose of guiding the flow according to its geometry. Considering two-dimensional motion implies that there exists complete symmetry with respect to one axis. In other words, the conditions of flow are the same all around a circle normal to the axis of symmetry and with the center on the axis of symmetry. This condition is often referred to as the condition of axisymmetry.

Since the velocity and pressure distribution around a bubble play a significant role in defining bubble motion, the purpose of this section is to consider these factors.

2.3.1. Streamline, Flow Pattern

A streamline is an artificial line drawn in the fluid in such a manner that the tangent at every point on this line gives the direction of the fluid velocity at that point. In general, streamlines constitute the outline of the fluid layers in motion.

A flow pattern is determined by a group of streamlines around the object in motion. Figure 2.4 shows the coordinate system and flow pattern relative to stationary and moving spheres for different flow conditions (White, 1991).

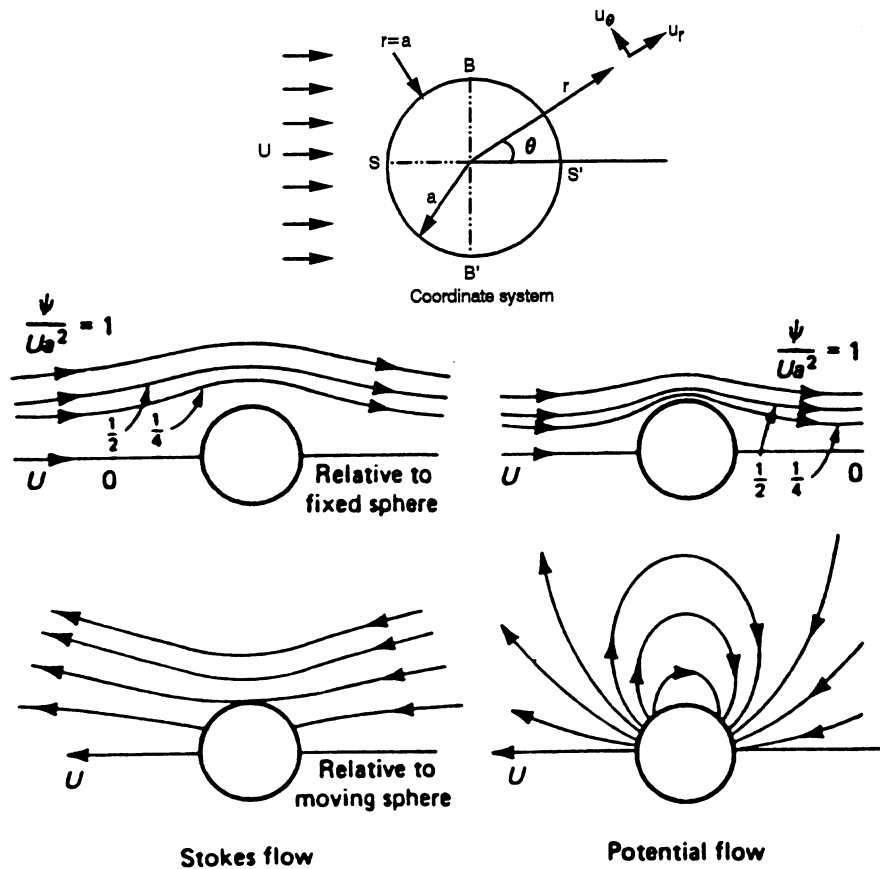


Figure 2.4: Comparison of Stokes flow and potential flow past a sphere (White, 1991).

### 2.3.2. Stream Function, Velocity Distribution

The stream function is a mathematical function representing the geometry of the stream surface at a given time. In two dimension flow, the stream function, (in spherical coordinates),  $\psi(r,\theta)$  is the rate of mass flow per unit density and per unit depth.

From knowledge of the stream function of a given flow field, the velocity distribution around the object can be determined. In axisymmetric spherical coordinates, the stream velocities ( $U_r$  and  $U_\theta$ ) can be obtained by

$$U_r = \frac{1}{r^2 \sin \theta} \times \frac{\partial \psi}{\partial \theta} \quad (2.23)$$

and

$$U_\theta = - \frac{1}{r \sin \theta} \times \frac{\partial \psi}{\partial r} \quad (2.24)$$

where  $\theta$  and  $r$  are the angular and radial coordinates, respectively.

Most problems in fluid flow (e.g., flow patterns around a sphere, Fig. 2.4) are defined based on the dimensionless Reynolds number, which is the ratio of inertia and viscous forces. Here, the Stokes, intermediate and potential fluid flow conditions are considered.

*Stokes Flow*

When the viscous shear effects are sufficiently large, a Stokes flow exists; for this type of flow the acceleration (inertia force) is negligible. Such a condition exists if the Reynolds number is small. In Stokes flow, the Reynolds number is strictly valid only when it is much less than unity but agrees with experiment up to  $\approx 1$  (White, 1991). For Stokes flow, the velocity distribution is described by the Stokes stream function (Stokes, 1851) which can be expressed mathematically as:

- *fluid in motion, sphere at rest*

$$\psi = U_0 \sin^2 \theta \left( \frac{a^3}{4r} - \frac{3ra}{4} + \frac{r^2}{2} \right) \quad (2.25)$$

where,  $U_0$  is the fluid velocity far from the sphere or sphere velocity in a stagnant fluid and  $a$  is the sphere radius.

$$U_r = U_0 \cos \theta \left( 1 + \frac{a^3}{2r^3} - \frac{3a}{2r} \right) \quad (2.26)$$

$$U_\theta = U_0 \sin \theta \left( -1 + \frac{a^3}{4r^3} + \frac{3a}{4r} \right) \quad (2.27)$$

- *fluid at rest, sphere in motion*

$$\psi = U_0 \sin^2 \theta \left( \frac{a^3}{4r} - \frac{3ra}{4} \right) \quad (2.28)$$

$$U_r = U_0 \cos \theta \left( -\frac{a^3}{2r^3} + \frac{3a}{2r} \right) \quad (2.29)$$

$$U_\theta = U_0 \sin \theta \left( \frac{a^3}{4r^3} + \frac{3a}{4r} \right) \quad (2.30)$$

### *Intermediate Flow*

Yoon and Luttrell (1989) developed the stream function for intermediate flow conditions ( $0 < Re < 100$ ), by combining the Stokes and potential flow equations which can be expressed by:

- *fluid in motion, sphere at rest*

$$\psi = U_0 \sin^2 \theta \left[ \frac{r^2}{2} - \frac{3ra}{4} + \frac{a^3}{4r} + \frac{Re^{0.72}}{15} \left( \frac{a^4}{r^2} - \frac{a^3}{r} + ra - a^2 \right) \right] \quad (2.31)$$

$$U_r = U_0 \cos \theta \left[ 1 - \frac{3a}{2r} + \frac{a^3}{2r^3} + \frac{Re^{0.72}}{15} \left( \frac{2a^4}{r^4} - \frac{2a^3}{r^3} + \frac{2a}{r} - \frac{2a^2}{r^2} \right) \right] \quad (2.32)$$

$$U_\theta = U_0 \sin \theta \left[ -1 + \frac{3a}{4r} + \frac{a^3}{4r^3} - \frac{Re^{0.72}}{15} \left( -\frac{2a^4}{r^4} + \frac{a^3}{r^3} + \frac{a}{r} \right) \right] \quad (2.33)$$

- fluid at rest, sphere in motion

$$\psi = U_0 \sin^2 \theta \left[ -\frac{3ra}{4} + \frac{a^3}{4r} + \frac{Re^{0.72}}{15} \left( \frac{a^4}{r^2} - \frac{a^3}{r} + ra - a^2 \right) \right] \quad (2.34)$$

$$U_r = U_0 \cos \theta \left[ \frac{3a}{2r} - \frac{a^3}{2r^3} - \frac{Re^{0.72}}{15} \left( \frac{2a^4}{r^4} - \frac{2a^3}{r^3} + \frac{2a}{r} - \frac{2a^2}{r^2} \right) \right] \quad (2.35)$$

$$U_\theta = U_0 \sin \theta \left[ \frac{3a}{4r} + \frac{a^3}{4r^3} - \frac{Re^{0.72}}{15} \left( -\frac{2a^4}{r^4} + \frac{a^3}{r^3} + \frac{a}{r} \right) \right] \quad (2.36)$$

In the intermediate fluid flow equations, as the Reynolds number approaches zero, they are reduced to the equations for Stokes flow.

*Potential Flow*

In situations where the effect of internal friction (viscosity) is small ( $Re > 100$ ), the flow is called potential flow. This condition, although not real, helps to determine certain aspects of the flow that are not affected by frictional resistance. Therefore, in this case the flow is said to slip over the boundary (Eskinazi, 1968; White, 1991):

- *fluid in motion, sphere at rest*

$$\psi = U_0 \sin^2 \theta \left( \frac{r^2}{2} - \frac{a^3}{2r} \right) \quad (2.37)$$

$$U_r = U_0 \cos \theta \left( -1 + \frac{a^3}{r^3} \right) \quad (2.38)$$

$$U_\theta = U_0 \sin \theta \left( -1 - \frac{a^3}{2r^3} \right) \quad (2.39)$$

- *fluid at rest, sphere in motion*

$$\psi = U_0 \sin^2 \theta \left( -\frac{a^3}{2r} \right) \quad (2.40)$$

$$U_r = U_0 \cos \theta \left( \frac{a^3}{r^3} \right) \quad (2.41)$$

$$U_\theta = U_0 \sin \theta \left( - \frac{a^3}{2 r^3} \right) \quad (2.42)$$

As the above equations show, for Stokes and intermediate flow conditions, the stream velocity related to a fixed or moving sphere on the sphere surface ( $r=a$ ) is equal to zero.

For potential flow conditions, the relative stream velocity is zero when  $r=a$  and  $\theta=0^\circ$  or  $180^\circ$  (Fig. 2.4) but it has a value at the other points on the surface. The points on the surface where the stream velocity vanishes are called stagnation points (S and S'). In general, in this case, the relative stream velocity from the front stagnation point, ( $\theta=180^\circ$ ,  $U_s=0$ ) to the side ( $\theta=90^\circ$ ,  $U_B=U_{\max}$ ) increases, that is,  $U_s < U_B$ .

While  $r > a$ , in both small and high Reynolds number cases, the velocity from the front of the sphere to the sides also increases. When  $r \rightarrow \infty$ , velocity is equal to  $U_0$  for a fixed sphere and is zero for a moving sphere.

### 2.3.3. Pressure Distribution

A sphere in motion is subjected not only to the ambient hydrostatic pressure, but also to the dynamic pressure acting on its surface determined by the particular flow field around the sphere (Fan and Tsuchiya, 1990).

When the Reynolds number is small (inertia force is negligible), with  $U_r$  and  $U_\theta$  known, the pressure around the sphere can be found by integrating the momentum relation (White, 1991), which is defined by

$$\nabla P \approx \mu_l \nabla^2 U \quad (2.43)$$

and the result is

$$P = P_0 - \frac{3 \mu_l a U_0}{2 r^2} \times \cos \theta \quad (2.44)$$

where  $P$  is the pressure at any point about the sphere,  $P_0$  is the uniform freestream pressure and  $\mu_l$  is liquid viscosity. As this equation shows, the pressure from the front stagnation point ( $P_s$ ) to the side ( $P_B$ ) decreases; that is,  $P_s > P_B = P_0$ .

For a frictionless ( $\mu=0$ ) fluid, the dynamic pressure at any point around the sphere can be obtained based on the Bernoulli equation (Binder, 1973; Potter and Foss, 1982) which is applicable along a streamline in steady flow between two points. The Bernoulli equation for stagnation and side points can be written as

$$P_s = P_B + \frac{1}{2} \rho_l (U_B^2 - U_s^2) + \rho_l g (\Delta y) \quad (2.45)$$

where  $\rho_l$  is liquid density,  $g$  is acceleration due to gravity and  $\Delta y$  is the vertical height between two points. In potential flow, where  $U_s$  is zero and if we assume  $\Delta y$  is negligible then the dynamic pressure at the stagnation point can be obtained from

$$P_S = P_B + \frac{\rho_l U_B^2}{2} \quad (2.46)$$

which shows the pressure from front stagnation point to the sides increases, that is,  $P_S > P_B$ .

In general, the full dynamic pressure of the flow appears as an inward push against the upstream bubble surface. When the Reynolds number is small (e.g., very small bubble in motion in water), the bubble velocity due to the buoyancy force is also small. In fact, the right term in Eq. 2.44 can be assumed negligible. In other words, the pressure on the surface when the Reynolds number is small is almost uniform and constant and equal to  $P_0$  (or hydrostatic pressure). As the sphere size and consequently the velocity and  $Re$  increase, the liquid, due to its incompressible nature, must accelerate to maintain the flow; hence, the pressure of the flow decreases from the front stagnation point to the sides.

#### 2.4. Forces Acting on a Single Fluid Particle in Motion

Fluid particle motion is controlled by forces acting on the particle. The fundamental physical laws for particle motion in a fluid are based on Newton's second law. According to this law: "when a mass  $m$  is moved from rest to a given velocity, or when the direction of its velocity  $U$  is changed, it can be verified that the force  $F$  necessary to perform this change is proportional to the rate of change of momentum  $mU$ ". For systems, where the mass remains constant, we have,

$$\Sigma F = m \frac{dU}{dt} \quad (2.47)$$

where,  $\Sigma F$  is the total forces acting on the particle,  $m$  is particle mass and  $dU/dt$  is the particle acceleration. For a particle in motion,  $m dU/dt$  is called "inertia force".

#### 2.4.1. Navier-Stokes Equation

Newton's second law has been applied to determine the forces acting on the infinitesimal element of an incompressible Newtonian fluid (constant density,  $\rho$  and dynamic viscosity,  $\mu$ ) in motion, which is illustrated by momentum "Navier-Stokes equation"

$$\rho g - \nabla P + \mu \nabla^2 U = \rho \frac{dU}{dt} \quad (2.48)$$

where, all terms (forces) are expressed per unit volume of fluid element and from left to right represent the gravitational, dynamic pressure, viscous and inertia forces.

For a frictionless fluid ( $\mu=0$ ), from Euler's equation of motion (Binder, 1973) in steady flow ( $dU/dt=0$ ), the pressure field can be determined based on Bernoulli's equation when the velocity distribution is known.

The influence of the internal friction or dynamic viscosity ( $\mu$ ) in fluids demonstrates itself only when the fluid is undergoing a frictional or shearing motion. In fact, this character is defined as the property of a fluid to resist the rate at which deformation takes place when the fluid is acted upon by tangential shear forces. In Newtonian fluids the ratio of shear stress to rate of shear strain, which represents the value of viscosity, is constant. Since the viscous force is dependent on the velocity field, both pressure and velocity fields are unknown. In general, the Navier-Stokes equation can not be applied directly to determine the motion.

### 2.4.2. Surface Tension Force

The Navier-Stokes equation is a general force balance for a fluid in motion. When an interface is involved (e.g., bubble-water interface), the phenomenon of interfacial (or surface) tension has to be taken into account. The interface behaves in a way similar to a thin stressed membrane under tension (Eskinazi, 1968). From a molecular point of view, the difference in behaviour of the interface compared to the bulk can be explained by the fact that, at the interface, the cohesive forces between the molecules on one side of the interface are different from those on the other side of the interface. The surface tension of a water-air interface can be readily changed by surface active agents, i.e., agents whose molecules preferentially accumulate (adsorb) at the interface rather than remain in the bulk water. In the presence of surface active agents (or surfactants) the surface tension may decrease measurably with time after formation of fresh water-air interface as in generating a bubble (so-called dynamic surface tension), (Finch, 1971, 73; Finch and Smith, 1972; Kulkarni and Somasundaran, 1975; Leja, 1982). In general, the time required to reach equilibrium is dependent on the surfactant type and concentration. For instance, adsorption time of short-chain alcohols is less than those with long-chain molecules (Leja, 1982).

The equilibrium surface tension of a liquid-air interface depends on the quantity of surfactant molecules adsorbed at the interface; for example, the surface tension of the water-air interface decreases with increasing frother concentration in solution (Leja, 1982). Above a certain concentration of surfactant, the surface tension becomes constant. Instead of adsorption at the interface, the surfactant species added to the solution in excess are utilized in forming colloidal aggregates within the bulk of solution. Such aggregates are known as micelles and the concentration as the critical micelle concentration, CMC.

The surface tension-concentration behaviour of the solutions is described by the Gibbs adsorption equation (Leja, 1982). However, the Gibbs equation applies only to the range of concentrations below the CMC.

### 2.4.3. Force Ratios (Dimensionless Groups)

Dimensional analysis is a mathematical tool useful for checking equations and units, determining a convenient arrangement of variables of a physical relation, and planning systematic experiments (Binder, 1973). Dimensional analysis is not a means for solving problems explicitly but is a powerful method for establishing groupings of pertinent variables that are likely to appear if an analytical solution is at all possible. In dimensional analysis, the implication is that, since physical laws express natural phenomena, they are independent of the units of the dimensions used. Thus one can say that in the formulation of such laws it must be possible to express them in dimensionless form.

Dimensionless numbers (e.g., ratios of forces) arise from dynamic similarity (Massey, 1983). If two systems are dynamically similar then the magnitude of forces at similarly located points in each system are in a fixed ratio. In fluid flow, the streamline pattern for one body must also be similar to the streamline pattern for another body which is geometrically similar. The velocity direction at a certain point in one flow must be the same as the velocity direction in the other flow. The velocity direction at any point in the field of flow is determined by the ratio of forces acting on a fluid particle at that point. When the ratio of forces acting on a fluid particle in one flow is the same as the ratio of the forces acting at a corresponding point in the other flow, then, mechanical similarity is realized (Binder, 1973). In general, the flow depends not on one ratio of forces, but on two or possibly three ratios.

Below, a set of convenient dimensionless groups which are available in the literature for bubble motion analysis, are given:

$$Re \text{ (Reynolds No.)} = \frac{\text{inertia force } [\rho U^2 L^2]}{\text{viscous force } [\mu UL]} = \frac{\rho_l U_b d_e}{\mu_l} \quad (2.49)$$

$$We \text{ (Weber No.)} = \frac{\text{inertia force } [\rho U^2 L^2]}{\text{surface tension force } [\sigma L]} = \frac{\rho_l U_b^2 d_e}{\sigma} \quad (2.50)$$

$$Eo \text{ (Eotvos No.)} = \frac{\text{gravity force } [\rho g L^3]}{\text{surface tension force } [\sigma L]} = \frac{g \rho_l d_e^2}{\sigma} \quad (2.51)$$

$$Fr \text{ (Froude No.)} = \frac{\text{inertia force } [\rho U^2 L^2]}{\text{gravity force } [\rho g L^3]} = \frac{U_b^2}{d_e g} \quad (2.52)$$

$$Bo \text{ (Bond No.)} = Eo^{1/2} = d_e \left( \frac{g \rho_l}{\sigma} \right)^{1/2} \quad (2.53)$$

$$Mo \text{ (Morton No.)} = \frac{g \mu_l^4}{\rho_l \sigma^3} \quad (2.54)$$

$$Ta \text{ (Tadaki No.)} = g^{1/4} \left( \frac{\rho_l}{\sigma} \right)^{3/4} d_e U_b \quad (2.55)$$

where,  $U_b$ ,  $\sigma$  and  $d_e$  are bubble velocity, liquid surface tension in contact with air, and bubble diameter (for a volume-equivalent sphere), respectively. One relationship among these numbers is (Fan and Tsuchiya, 1990):

$$Ta \approx Re \, Mo^{1/4} = \left( \frac{We^3}{Fr} \right)^{1/4} = (Eo^3 Fr^2)^{1/4} \quad (2.56)$$

Pressure difference between the stagnation point and the freestream pressure ( $P_s - P_0$ ) is equal to  $\rho_l U_0^2/2$  which is called dynamic or velocity pressure (Binder, 1973). The pressure difference between any point on the particle surface and  $P_0$  (or  $\Delta P$ ) divided by the dynamic pressure represents the pressure coefficient:

$$\text{Pressure Coefficient} = \frac{\Delta P}{\rho_l U_b^2 / 2} \quad (2.57)$$

#### 2.4.4. Buoyancy Force

In general, the motion of a particle through a viscous fluid (starting from rest) is subjected to three forces: the weight (gravitational force), the buoyancy force and the resistance (drag) force. In bubble motion analysis, it is usually assumed that the air density is negligible, and therefore, that the gravitational force is negligible.

A particle immersed in a liquid seems to have less weight than when immersed in air, and a particle whose average density is less than that of the liquid floats in that fluid. Archimedes' principle states that "when a body is immersed in a fluid, the fluid exerts an upward force on the body equal to the weight of the fluid which is displaced by the body" (Sears et al., 1977). The direction of the buoyancy force for both falling and rising particles in a liquid is upward. The buoyancy force for a bubble in motion  $F_B$ , is determined by

$$F_B = - \frac{\pi d_e^3 \rho_l g}{6} \quad (2.58)$$

#### 2.4.5. Drag Force

The resultant of the forces acting to resist motion of a particle in a liquid is called the "drag force"; it assumes a downward direction in the case of bubble motion. The Reynolds number which represents the ratio of inertia and viscous forces, can become very small if the fluid is very viscous, if the particle velocity is very low or if the particle dimensions are very small. A high Reynolds number, however, should not imply that the effect of viscosity on drag is negligible. A fluid may have a very low viscosity but this can still have an appreciable effect, directly and indirectly, on the flow (Binder, 1973). In fact, the assumption of frictionless fluids (especially for liquids) is hardly ever realistic.

If a particle is in motion relative to a fluid, a skin (viscous or shear) drag will exist between the particle surface and the fluid. This drag comes from the friction of the fluid on the particle surface and appears as the viscous force in the Navier-Stokes equation. In the case of the frictionless fluid assumption, the skin drag is negligible.

In addition to skin drag, significant frictional losses occur because of acceleration and deceleration of the fluid past the particle. Because a low-energy flow separates to the rear of a particle in motion, the pressure there is smaller than that in nonseparated flow region. This difference in pressure, multiplied by the particle projected area, yields a drag force which is called pressure or form (i.e. shape) drag (Foust et al., 1980; Massey, 1983). Viscosity effects can change the flow pattern, so as to cause eddies, and thus can influence the pressure distribution.

From dimensional reasoning, the total drag,  $F_D$ , can be made dimensionless by dividing it by a characteristic pressure of the flow,  $\rho_l U_b^2/2$  the dynamic or velocity pressure (which has the same dimension as the particle kinetic energy,  $mU_b^2/2$  per unit volume), and a characteristic area ( $A$ ) of the particle (projected area normal to the stream). This dimensionless quantity is called the "drag coefficient  $C_D$ ". In general, the total drag force as a function of the drag coefficient can be obtained by

$$F_D = C_D \times \frac{\rho_l U_b^2}{2} \times A \quad (2.59)$$

The drag coefficient is dependent on the particle shape. For instance, a streamlined particle can be defined as one with a minimum pressure drag. Dynamic similarity and dimensional analysis show that the drag coefficient is also a function of the Reynolds number (Eskinazi, 1968; Binder, 1973; John and Haberman, 1988). Normally, the drag coefficient is presented as a plot against the Reynolds number for different particle shapes (e.g., Fig. 2.5) (Massey, 1983).

As the general drag force equation indicates, the drag force increases with increasing particle velocity, particle projected area and  $C_D$ . The drag coefficient is inversely proportional to the Reynolds number and also is a function of the particle shape and particle surface nature (e.g., roughness). For example, for two spheres, one small

and one large (with the same surface nature), the  $C_D$  for the larger sphere is less than for the other one (Fig. 2.5). Indeed, the drag coefficient is not only related to the physical properties of the two phases (solid particle and fluid medium), but also is strongly dependent on the fluid flow pattern around the particle surface.

Wake phenomena behind the particle in motion results in a difference in pressure between the front and the rear of the particle. This phenomena is discussed next.

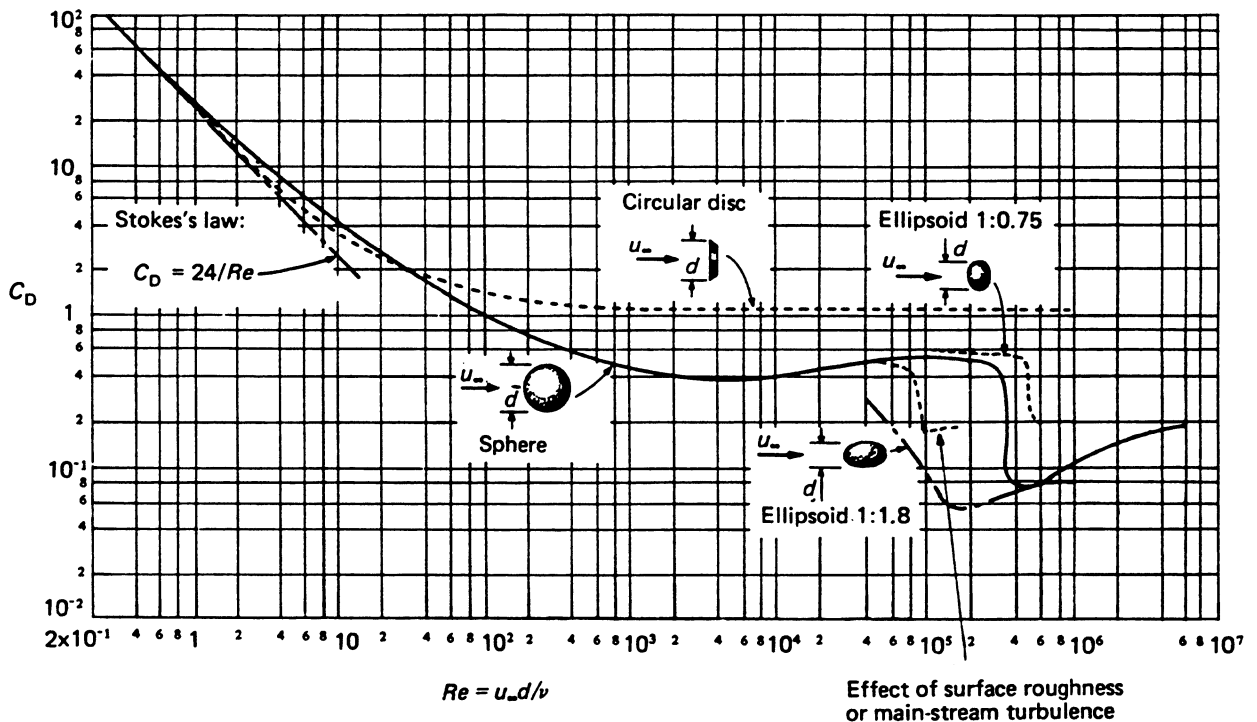


Figure 2.5: Drag coefficients of smooth, axially symmetric bodies (Massey, 1983).

### 2.5. Wake Phenomena

It is known that the rise characteristics of bubbles in liquid, such as shape, rise velocity and oscillations are closely related to the bubble wake behaviour (Tsuchiya and Fan, 1988).

In case of low relative velocity between a particle and a fluid, the flow just outside the particle closely follows the particle surface. In other words, at sufficiently small Reynolds number, the contour of the particle forms part of a streamline known as the dividing streamline. As the Reynolds number and consequently the pressure difference on the surface increase, at a certain Reynolds number, the flow starts to separate from the particle surface. This critical Reynolds number is dependent on the particle shape, particle surface nature and the turbulence intensity in the surrounding medium. In general, this critical Reynolds number is about 20 (Fan and Tsuchiya, 1990). At relatively low Reynolds number, the flow separates from the surface sooner than at higher Reynolds numbers. A wake does not exist when  $Re \ll 1$ . Figure 2.6 shows the flow pattern about a sphere and the wake behind the sphere at different Reynolds numbers (Vennard and Street, 1975).

As the Reynolds number increases from the critical value, the separated streamlines branch off from the particle contour and create a closed region behind the particle called the "wake or circulation region". The flow separation refers to the detachment of a thin layer called the "boundary layer". The fluid outside the boundary layer is subjected to acceleration opposite the leading face of the particle and to a deceleration (as the fluid returns to the normal freestream pattern) downstream of the particle. Figure 2.7 shows the flow pattern and the wake phenomena for streamlined and non-streamlined shapes. The wake structure is dependent upon several factors including: the geometry and shape of the particle, the nature of the particle surface, the size of the particle, the relative motion between the particle and the surrounding medium, and the physical properties of the particle and surrounding medium.

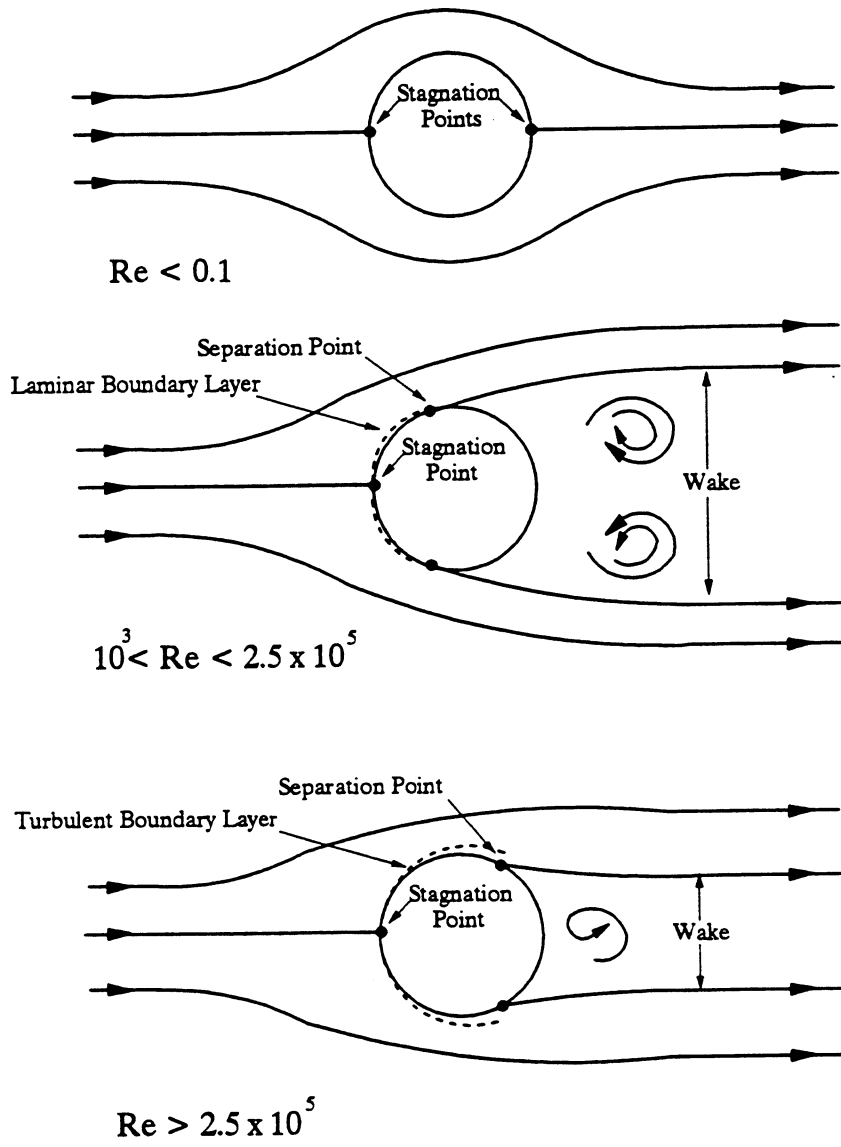


Figure 2.6: Circulation region (wake) behind a sphere at various Reynolds numbers,  $Re$  (Vennard and Street, 1975).

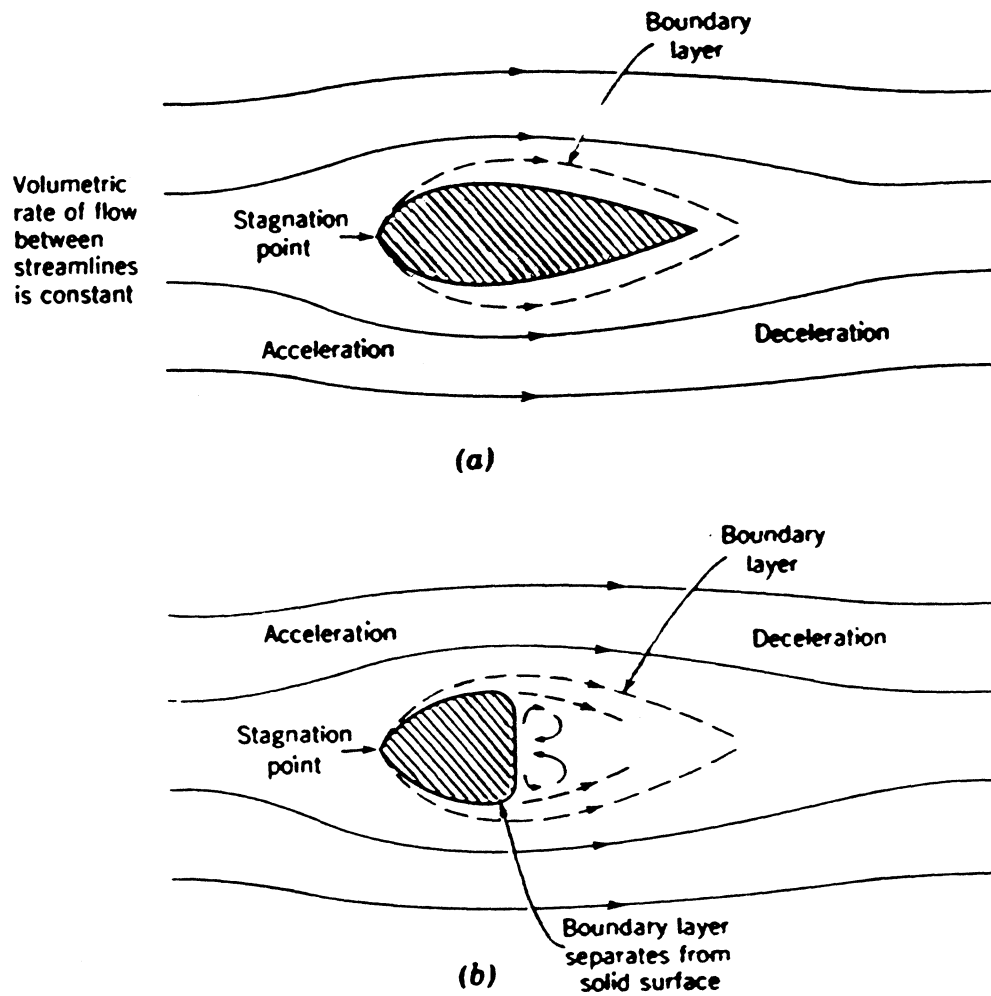


Figure 2.7: Flow around submerged bodies (Foust, 1980);

(a) streamlined shape-no separation,

(b) nonstreamlined shape-separation of the boundary layer.

Bhaga (1976), Clift et al. (1978), Bhaga and Weber (1980, 81), Weber and Bhaga (1982), Tsuchiya and Fan (1988), Kreischer et al. (1990) and Fan and Tsuchiya (1990) among others have investigated bubble wake phenomena. They discussed the bubble wake structure and geometry (e.g., wake length and volume), circulation flow pattern in the bubble wake and bubble wake instability for different bubble sizes and shapes or, generally, for different Reynolds numbers.

Circulation, which forms a vortex in the wake (Fig. 2.7), is due to the difference in magnitude of the pressure between the inner side (wake side) and outer side of the wake. This difference comes from the fact that the inner pressure is lower than the outer pressure. In general, the flow pattern behind the bubble is characterized by an axisymmetric circulation whose direction is upward along the wake central axis and downward along the separated streams.

The wake structure for bubbles is known to be different from that for solid particles, due to bubble oscillation or rocking under the influence of asymmetric vortex shedding. The energy associated with the wake-shedding process for gas bubbles can be exchanged between the bubble and the surrounding medium, while all the shedding energy for a solid particle is confined to the surrounding fluid (Tsuchiya et al., 1989). Wake instability sets in as the Reynolds number exceeds a certain critical value: for large bubbles in viscous media, the critical  $Re$  for wake shedding is approximately 100; for small bubbles in low viscosity media, the critical  $Re$  depends on the medium purity, being approximately 200 for contaminated systems (Fan and Tsuchiya, 1990).

The wake volume is a function of the Reynolds number. In the other words, the ratio of the wake volume ( $V_w$ ) to the bubble volume ( $V$ ) increases with increasing Reynolds number (Bhaga and Weber, 1981). For example, for  $Re$  between 3 and 110, this ratio is

$$\frac{V_w}{V} = 0.037 Re^{1.4} \quad (2.60)$$

## 2.6. Bubble Internal Circulation

The movement (circulation) inside fluid particles (drops and bubbles) has been studied on several occasions (Hadamard-Rybczynski, 1911; Garner and Hammerton, 1954; Linton and Sutherland, 1957; Griffith, 1962; Lochiel, 1965, Clift et al., 1978). The internal circulation is a property of fluid particles in motion. This phenomena does not occur in particles with a rigid surface. In fact, internal circulation is dependent on the mobility of the surface. Therefore, in this case, the properties of the interface and the effect of surfactants play a significant role.

Any part of the surface of a moving bubble experiences a tangential force proportional to the viscosity of the external medium and to the velocity gradient normal to the surface which induces internal circulation. The circulation pattern is dependent on the fluid particle properties, such as size and shape. Figure 2.8 shows both the internal and external flow pattern for a small and large (highly deformed, skirted) fluid drop (Clift et al., 1978). The air inside the bubble near the interface is swept from the forward stagnation point to the rear by the action of the stress on the interface. At the rear of the bubble the air flowing along the interface is forced into the interior of the bubble (Schechter and Farley, 1963).

In a pure system, internal circulation should always occur, because the surface is completely mobile. In general, the internal circulation reduces with decreasing bubble size and increasing bubble surface rigidity, the latter being enhanced by surfactants. Internal circulation is governed by the velocity, pressure and surface tension gradients in the bubble surface. These factors will be discussed next.

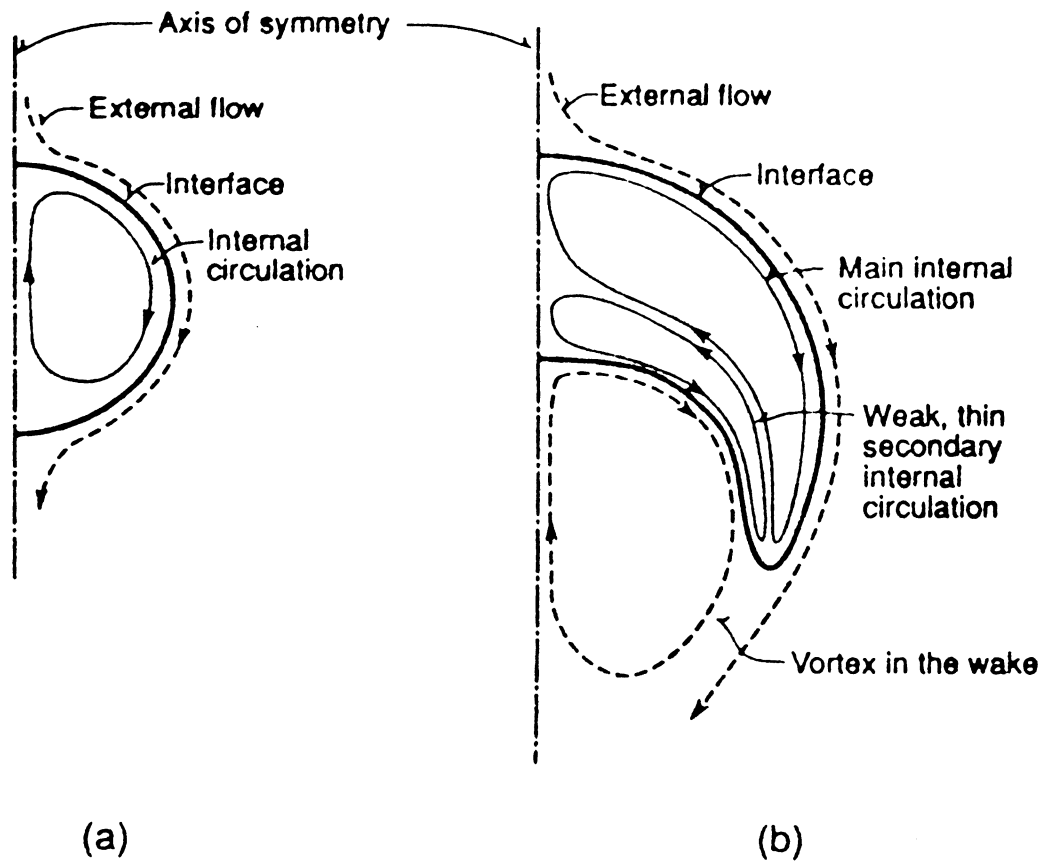


Figure 2.8: Schematic description of internal and external flow patterns (Clift et al., 1978, reprinted with permission); (a) a small liquid drop with negligible distortion, (b) a large, skirted drop.

### 2.7. Bubble Behaviour

Bubble behaviour in the present context refers to size, velocity, shape and path. Figure 2.9 shows the general parameters which determine single bubble behaviour.

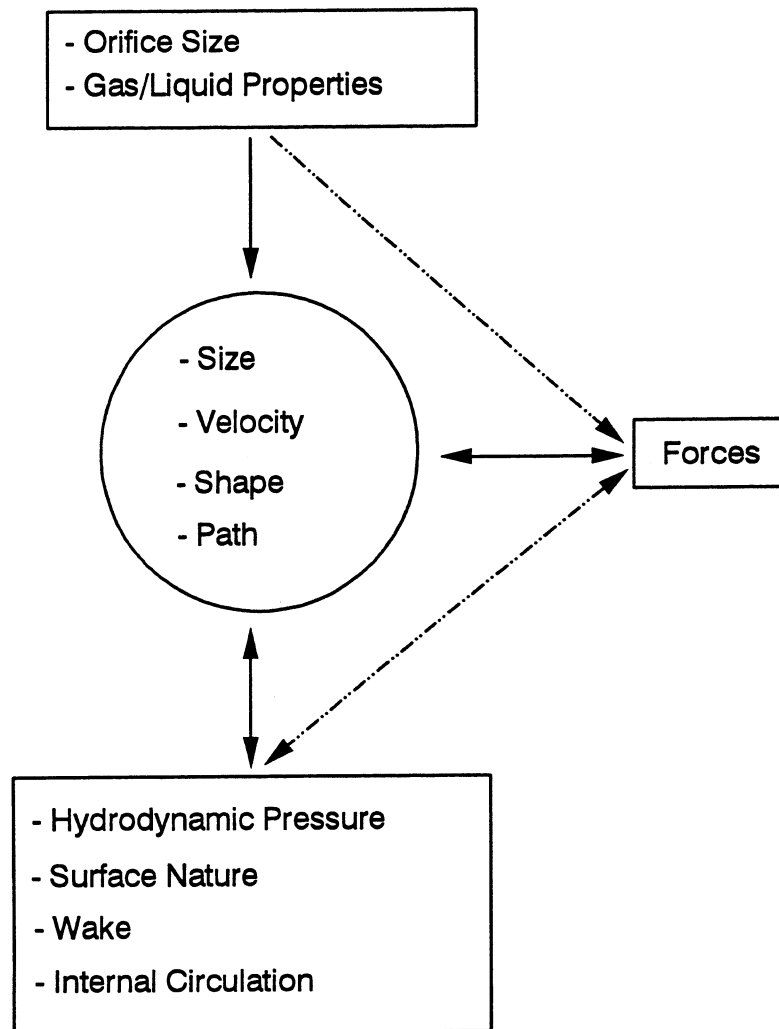


Figure 2.9: General parameters which determine single bubble behaviour.

Single bubble characteristics are related to the orifice size and gas-liquid properties. Examination of these characters can provide an indirect understanding of the forces which are acting on a bubble. Generally, these characters can be explained by the bubble wake structure, interfacial chemistry, dynamic surface pressure and internal circulation. In flotation columns, which can exceed 10 m, the characteristics of rising bubbles become of potential importance.

### 2.7.1. Bubble Size

Bubbles in motion have variable shapes (e.g., spherical and ellipsoidal). In order to describe nonspherical bubbles, the bubble volume equivalent diameter,  $d_e$  (diameter of a sphere having the same volume as the bubble in three dimensions) can be defined:

$$d_e = (h b^2)^{1/3} \quad (2.61)$$

where  $h$  and  $b$  are minor and major axes, respectively. A bubble can be taken as spherical if the minor to major axis ratio lies within 10% of unity (Clift et al., 1978).

#### *Bubble Formation and Bubble Size at the Orifice*

The formation of bubbles at a submerged orifice has been the subject of numerous theoretical and experimental studies and a number of models have been developed to describe the interaction of liquid and gas which occurs during the bubbling process (Davidson et al., 1960a, b ; Davidson and Harrison, 1963; Kumar and Kuloor, 1970; Marmur and Rubin, 1976; Pinczewski, 1981; Geary and Rice, 1991).

Li (1992) summarized the bubble formation theories and models. Generally, gas injector types fall into two categories: those based on the single orifices and those based

on porous media. Most of the models consider gas flow through a single orifice, usually of circular geometry and located at the bottom of a tank of liquid. Bubble formation mechanics at a submerged orifice are dependent strongly on the gas flow properties. Bubble formation models can be divided into spherical and non-spherical ones based on the assumption of the bubble shape. The spherical models can be further classified into constant flow, constant pressure and time dependent flow and pressure models corresponding to different conditions.

In the case of capillary injection (i.e. in present study) where gas flow rate is low, spherical single bubbles form at the orifice under constant flow conditions. According to Tate's law (Blanchard and Syzdek, 1977) which is applicable for spherical bubbles, the bubble volume after formation at a circular orifice can be obtained by a balance of the upward buoyancy force ( $V_b \Delta\rho g$ ) and surface tension force ( $2\pi r_0 \sigma \cos \theta$ ), gives:

$$V_b = \frac{2 \pi r_0 \sigma \cos \theta}{\Delta\rho g} \quad (2.62)$$

and the bubble radius,  $r_b$  is

$$r_b = \left( \frac{3 r_0 \sigma \cos \theta}{2 \Delta\rho g} \right)^{\frac{1}{3}} \quad (2.63)$$

where  $V_b$  is the bubble volume,  $\Delta\rho$ ,  $\sigma$  and  $r_0$  are the density difference between liquid and gas, the uniform and constant surface tension of liquid in contact with air and the glass capillary radius, respectively, and  $\theta$  is the contact angle between liquid and glass (normally assumed to be zero).

*Effect of Hydrostatic Pressure on Bubble Size**- Static Pressure*

In a static fluid, shear and tensile forces are absent, the only forces involved are compressive. Pascal's law indicates that "the pressure in a static fluid is the same in all directions" (Binder, 1973). Consider a particle at rest in a fluid, the total hydrostatic pressure (absolute pressure,  $P_0$ ) on the particle surface is given by

$$P_0 = P_{atm} + \rho_l g h_l \quad (2.64)$$

where  $P_{atm}$  is atmospheric pressure (i.e.  $\approx 10.37$  m H<sub>2</sub>O) and  $h_l$  is the height of liquid over the particle. The term  $\rho_l g h_l$  is called "gauge pressure".

*- Pressure Difference Across a Bubble Surface*

A bubble consists of two spherical surface films very close together, with liquid between. Surface tension makes the film tend to contract, but as the bubble contracts it compresses the inside air, increasing the interior pressure to a point which prevents further contraction (Sears et al., 1977).

Consider a capillary with circular orifice of radius  $r_0$  located at the bottom of a tank filled with liquid and the absolute hydrostatic pressure over that is  $P_0$ . Gas passes through the capillary and forms a meniscus dividing a gas (pressure  $P_c$ ) and liquid (pressure  $P_0$ ). In accordance with the Young-Laplace equation (Soo, 1967; Wallis, 1969; Miller and Meyer, 1984), if  $P_c - P_0 < 2\sigma/r_0$ , the meniscus remains in the capillary; if  $P_c - P_0 > 2\sigma/r_0$ , the meniscus passes up the capillary. When it just begins to protrude into the liquid, the pressure in the incipient bubble is given by

$$P_c - P_0 = \frac{2\sigma}{r_0} \quad (2.65)$$

where  $P_c$  is the pressure in the bubble before expansion. When the bubble begins to expand at the orifice, its radius becomes greater than  $r_0$  and the pressure inside the bubble is obtained by

$$P_i = P_0 + \frac{2\sigma}{r_b} \quad (2.66)$$

The size of a bubble blown slowly from a horizontal circular orifice can be obtained by the balance between the surface tension and buoyancy forces as a function of the capillary radius (Eq. 2.63). When the buoyancy force becomes greater than the surface tension force (due to bubble expansion at the orifice), the bubble leaves the orifice.

A complete treatment of interfacial boundary conditions for static bubbles of different shapes is given by Scriven (1960). The pressure inside the bubble can be approximately found by

$$P_i = P_0 + \sigma \left( \frac{1}{R_1} + \frac{1}{R_2} \right) \quad (2.67)$$

where  $R_1$  and  $R_2$  are the principal radii of the bubble surface.

- *Equation of State (Boyle's Law)*

The volume,  $V$  occupied by a definite mass  $m$  of any substance depends on the pressure,  $P$  to which the substance is subjected, and on its temperature,  $T$ . For every pure substance there is a definite relation between these quantities, called the equation of state which implies an equilibrium state (i.e.,  $P$  and  $T$  are the same at all points). The simplest equation of state (Boyle's law) is that of gas at low pressure. This equation is defined by

$$P V = n R T \quad (2.68)$$

where  $n$  is the number of gas moles,  $T$  is gas temperature in Kelvin. For ideal gas,  $PV/nT$  is constant and  $R$  is called "universal gas constant".

For a fixed number of moles of an ideal gas, the product  $nR$  is constant. Therefore for two states (1 and 2) of the same mass of gas but at different pressure, volume and temperature, we have

$$\frac{P_1 V_1}{T_1} = \frac{P_2 V_2}{T_2} = \text{constant} \quad (2.69)$$

where  $P_1$  and  $P_2$  are absolute pressure. If  $T_1 = T_2$ , then

$$P_1 V_1 = P_2 V_2 = \text{constant} \quad (2.70)$$

Equation 2.63 shows the bubble size at the orifice is not related to the hydrostatic pressure but is a function of the capillary size. Equation 2.66 indicated that the pressure inside a spherical bubble after formation at the orifice is equal to the sum of the absolute hydrostatic pressure ( $P_0$ ) and the surface tension pressure ( $2\sigma/r_b$ ). The latter being almost negligible compared to the hydrostatic pressure. For instance, if the tension,  $\sigma$  (constant and uniform) at the bubble-liquid interface is about 72 dyne/cm and the bubble radius ( $r_b$ ) is 0.1 cm, then  $2\sigma/r_b$  is equal to 1440 dyne/cm<sup>2</sup>, or a pressure of about 1.5 cm H<sub>2</sub>O (compared to atmospheric pressure of approximately 1037 cm H<sub>2</sub>O). Therefore, in the absence of dynamic pressure, it is reasonable to assume that the gas pressure inside a bubble is almost the same as the absolute hydrostatic pressure (i.e.,  $P_i = P_0$ ).

When a bubble starts to move, the pressure inside the bubble during its rise is variable due to the hydrostatic, dynamic and surface tension pressure and bubble shape. The surface tension varies around the bubble due to bubble motion, surfactant concentration or temperature gradients (Linton and Sutherland, 1957; Scriven, 1960; Clift et al., 1978). Indeed, a bubble in a liquid is never truly in equilibrium (Young, 1989) although we will consider it to be so for present purposes. In general, the difference between the total pressure inside and outside of a spherical bubble  $(\Delta P)_{i-o}$  is proportional to the surface tension gradient:

$$(\Delta P)_{i-o} \propto \left( \frac{d\sigma}{d\theta} \right) \quad (2.71)$$

In order to have an appreciation of bubble expansion due only to the hydrostatic pressure, consider that the dynamic and surface tension pressures are negligible (i.e.  $P_i = P_0$ ), and the number of air molecules inside the bubble is constant during its motion. For a spherical bubble 1 mm in diameter at the bottom of a 4 m column under isothermal conditions, solving Eq. 2.70 shows an increase of about 11.5% in diameter at the top.

### 2.7.2. Bubble Shape

The interaction between a rising bubble and the surrounding liquid (or slurry) medium determines the bubble shape and the extent of the disturbance in the surrounding flow field (Fan and Tsuchiya, 1990). Bubbles in motion can be classified by shape as spherical, ellipsoidal and spherical/ellipsoidal cap. Generally, the properties of the flow around the bubble and consequently forces acting on the bubble (i.e. dynamic, viscous, surface tension and inertial forces), control the bubble shape.

When the bubble size is small (e.g.,  $d_b < 1$  mm in water), surface tension forces predominate and exceed dynamic forces and the bubble shape is approximately spherical. In other words, the forces acting on small bubbles are uniform.

With increasing bubble Reynolds number (bubbles of intermediate size), in addition to the surface tension force, the dynamic, viscous and inertial forces have to be taken into account. The dynamic pressure of the flow decreases along the bubble surface from the bubble front to the sides. With increasing bubble size (or  $Re$ ), the dynamic pressure difference between bubble front and bubble sides increases which explains why the bubble flattens (ellipsoidal shape) in the direction of the bubble motion.

In case of large bubbles ( $d_b > 18$  mm, (Clift et al., 1978)), the effect of surface tension and viscosity are negligible but the inertial or buoyancy forces are dominant and the bubble shape is a spherical/ellipsoidal cap. The induced pressure difference between the front and the side of the bubble explains the transition of bubble shape from spherical to ellipsoidal but it is not enough to describe the transition of ellipsoidal to spherical/ellipsoidal cap. One can explain the bubble shape having a sharp edge along the bubble rim (as in a cap) by the effect of the circulating region (wake) behind the bubble which increases with Reynolds number (Bhaga and Weber, 1980, 81; Miyahara et al., 1988). On the other hand, while the overall shape of the bubble gradually flattens, the edges of the bubble become extremely sharp, apparently caused by circulating flow patterns behind the bubble (Fan and Tsuchiya, 1990).

The bubble shape cannot be completely predicted unless all the physical variables are taken into consideration. Based on the Haberman and Morton (1953) suggestion, a dimensional analysis for prediction of bubble shape can be verified based on the acceleration due to gravity, the terminal velocity of bubble rise, the diameter of volume equivalent sphere, the liquid density and viscosity and finally the interfacial tension. These variables appear in three dimensionless numbers: Reynolds, Morton and Eötvös. For bubbles in liquids, it is possible to prepare a general graphical correlation in terms of only these three dimensionless groups (Grace, 1973; Grace et al., 1976). Figure 2.10 shows the shape regimes and bubble shape transition boundaries for bubbles in motion through liquids (Clift et al., 1978).

Generally, a given size of bubble is less flattened when the liquid surface tension is large (low  $We$  or  $Eo$ ) and the liquid viscosity is large (low  $Re$ ). The bubble must be spherical if the surface tension pressure, of order  $\sigma/d_e$ , is much greater than the dynamic pressure, of order  $\rho_1 U_b^2$ , that is,  $We \ll 1$  (Harper, 1972). When the system is contaminated, the surfactant molecules collect at the liquid-bubble interface and the bubble shape cannot be determined by the liquid properties alone. The bubble shape is strongly affected by the interfacial conditions at the gas/liquid interface (Griffith, 1962; Grace, 1973; Grace et al., 1976). By adsorption of the surfactants at the interface, the viscous drag increases (Boussinesq, 1913; Sciven, 1959; Agrawal and Wasa, 1979; Fan and Tsuchiya, 1990). The bubble rise velocity and consequently the inertial force, the Reynolds number and the dynamic pressure difference between bubble front and sides, decrease with increasing viscous drag. Therefore, for a fixed bubble size, the bubble shape is less flattened in the presence of surfactants in a pure liquid (Okazaki, 1963; Clift et al., 1978; Tsuge, 1982; Stone and Leal, 1990).

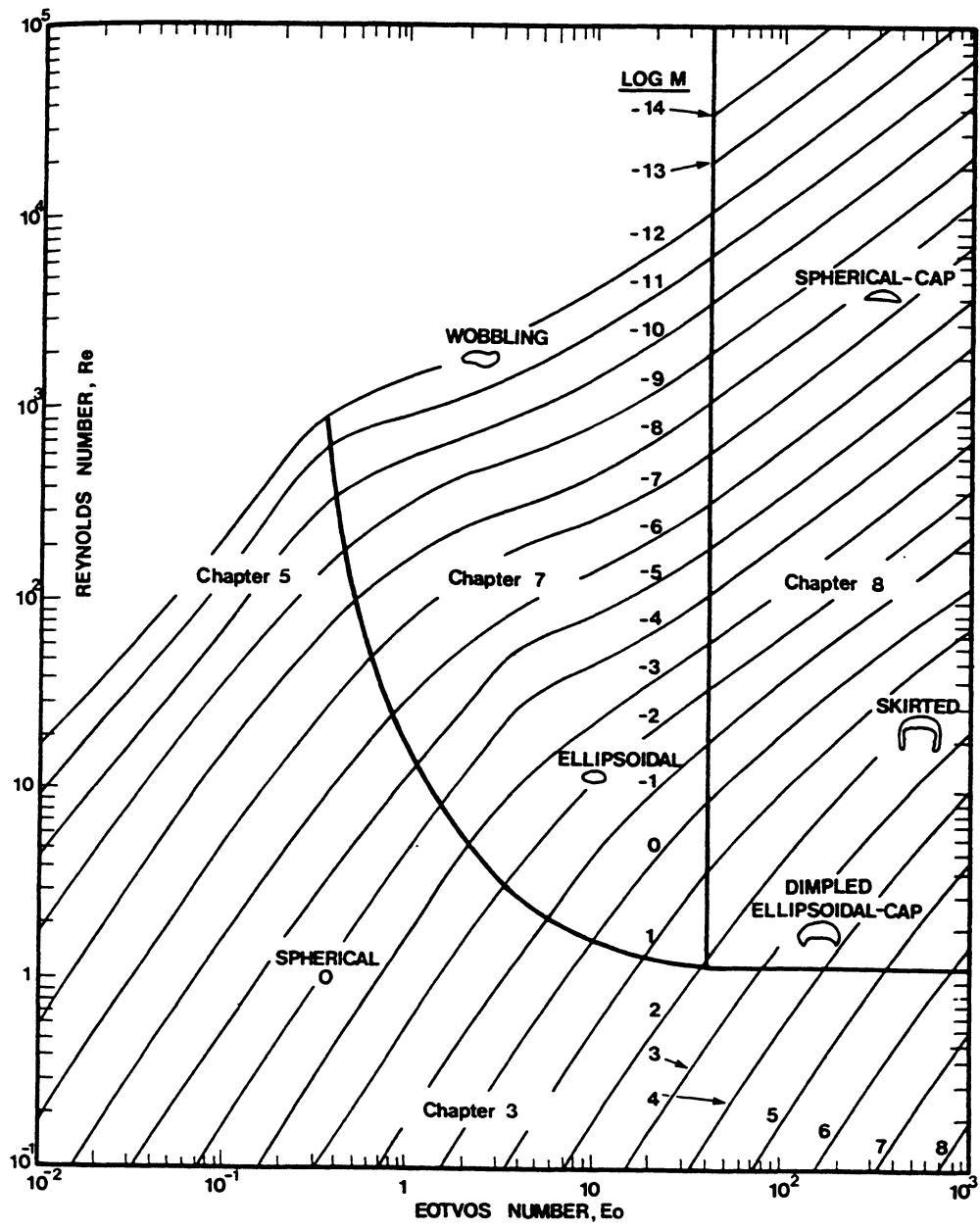


Figure 2.10: Shape regimes for bubbles and drops in unhindered gravitational motion through liquids (Clift et al., 1978, reprinted with permission) ("Chapters" on the figure refers to the chapters in the original reference).

### 2.7.3. Bubble Rise Path

The bubble rise path (defined as the trajectory of the bubble center) and change in orientation (defined as the angle between the bubble major axis and the vertical axis of the system) are strongly dependent on the bubble shape (Fan and Tsuchiya, 1990). Single bubbles rise in a straight line (rectilinear) when the bubble shape is spherical. When the bubble becomes deformed into an ellipsoidal shape, the bubble exhibits zigzag or spiral motion, it also changes its orientation (Tsuge and Hibino, 1977; Fan and Tsuchiya, 1990). As the bubble changes from ellipsoidal to spherical/ellipsoidal cap (at  $Re \approx 5000$  (Miyahara, 1988)), the radius of the spiral or the amplitude of the zigzag decreases and the motion becomes rectilinear, but with rocking.

Saffman, 1956 studied the motion of small bubbles (0.5-4.0 mm in diameter) in water. He suggested that the oscillatory motion is caused by interaction between a periodic oscillation of the wake (onset of vortex shedding from the wake) and instability of the motion near the front of the bubble. He assumed that the flow near the front of the bubble is inviscid and considered the distribution of pressure in the vicinity of the stagnation point. Based on his observations, small bubbles ( $d_b < 1.4$  mm) rise rectilinearly with no oscillations and bubbles with diameter between 1.4 and 2 mm rise in a zigzag path. Bubbles greater than 2 mm in diameter have zigzag or spiral motion dependent on the medium properties.

Hartunian and Sears (1957), investigating the motion of small bubbles moving uniformly in various liquids, believed that the interaction of surface tension and hydrodynamic pressure gave rise to the instabilities in bubble motion. They suggested that there are two distinct criteria for instability: (a) a critical Reynolds number (202) for the impure and somewhat more viscous liquids; (b) a critical Weber number (1.26) for pure, relatively inviscid liquids.

The bubble rise path or fluctuations in the orientation of the bubble can be characterized by the frequency or period of cycle of the motion. As Tsuge and Hibino

(1971) suggested, the frequency decreases from 7.7 to 4 s<sup>-1</sup> as  $d_b$  increases from 2 to 8.5 mm in a contaminated system while in a purified system, the frequency is almost constant, ranging from 6.2 to 8.3 s<sup>-1</sup>. The oscillation frequency ( $f$ ) is usually represented by the dimensionless Strouhal number ( $Sr = f d_b / U_b$ ). Tsuge and Hibino (1971) analyzed their data for both pure and impure systems based on a dimensional analysis including  $Sr$ ,  $Re$ ,  $Mo$  and  $C_D$ . Since  $Re$ ,  $Mo$  and  $C_D$  can be uniquely correlated with  $Ta$ , the Strouhal number can also be presented as a function of  $Ta$  and shows  $Sr$  increases with  $Ta$  (Tsuge and Hibino, 1971). Generally, both the amplitude and frequency of bubble oscillation are related to the bubble size, shape and presence/absence of surfactants.

#### 2.7.4. Bubble Rise Velocity

The prediction of the velocity of a gas bubble in a liquid is a hydrodynamical problem and falls within the more general problem of the flow of fluids past bodies in a fluid stream. In general, bubble velocity is related to the physical properties of the gas and liquid, the fluid flow around the bubble and the interface between the phases. Any change in the bubble size, shape or liquid properties (e.g., presence/absence of surfactants) causes a significant effect on bubble velocity. On the other hand, the bubble behaviour (in general) can be represented by its velocity. Many investigators have studied both theoretically and experimentally the bubble terminal velocity under different conditions (e.g., Peebles and Garbe, 1953; Garner and Hammerton, 1954; Levich, 1962; Moore, 1965; Clift et al., 1978; Zhou, 1992).

Grace (1973) and Grace et al., (1976) presented the correlation for terminal velocity related to the dimensionless groups for both pure and contaminated systems. They also indicated that there is no inherent difference between gas bubbles and liquid drops. Usually, the bubble velocity is measured in one dimension. Fuerstenau and Wayman (1958) suggested that the actual bubble velocity may be somewhat higher than the measurement of vertical velocity indicates, when the motion of a bubble is not

rectilinear.

Experimental terminal velocities from several investigators for air bubbles rising in pure and contaminated water are presented in Fig. 2.11 (Clift et al., 1978). The bubble terminal velocity increases with size up to about 1.4 mm and then decreases because of the effect of bubble shape and wake. Generally, as this figure shows, the bubble velocity decreases when contaminants (surfactants) are present in water. Bubble velocity will be explored in subsequent sections.

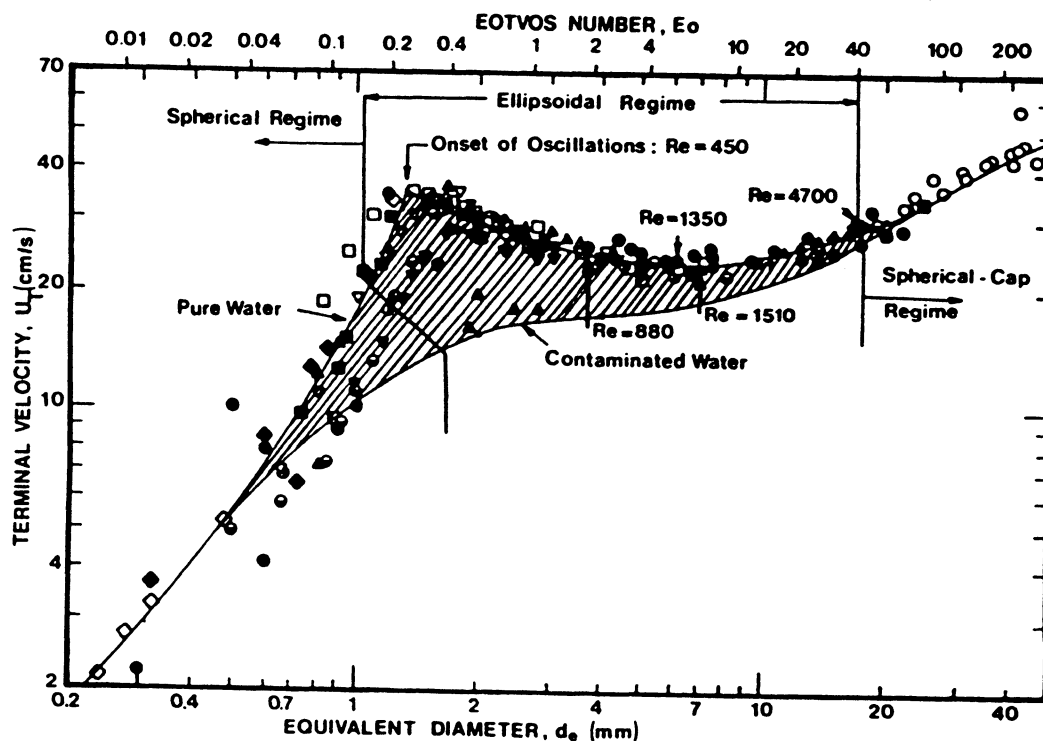


Figure 2.11: Terminal velocity of air bubbles in water reported by several investigators (Clift et al., 1978, reprinted with permission).

### 2.8. Mechanism and Effects of Surfactant Adsorption

Bond and Newton (1928), Garner and Hammerton (1954), Saffman (1956), Fuerstenau and Wayman (1958), Wasserman and Slattery (1969), Anfruns and Kitchener (1977) and Zhou et al. (1992) all showed that the bubble terminal velocity is decreased by surfactant in the system. The surface of a bubble in a pure liquid is mobile but rigidity is imparted by surfactant adsorption. The tangential force at the surface increases with surface rigidity. In distilled water, air bubbles behave as solid spheres when the Reynolds number is less than 40 (even though bubbles remain spherical up to Reynolds number of 400). However, in the presence of a small amount of frother, air bubbles behave as solid objects until the Reynolds number exceeds 130 (Fuerstenau and Wayman, 1958; Anfruns and Kichener, 1976).

Of particular importance is the fact that the drag coefficient of bubbles in pure liquids is considerably smaller than in the impure liquids which dictates high velocity (Hartunian and Sears, 1957).

The behaviour of bubbles in water in the presence or absence of surfactants is dependent on gas-liquid interfacial phenomena. In fact, the surfactants present in even trace quantities assume an important role in determining the hydrodynamic behaviour of bubble-liquid (and bubble-slurry) systems (Schechter and Farley, 1963; Levan and Newman, 1976). The interfacial region between two homogenous phases contains matter in a distinct physical state; matter in the interfacial state exhibits properties different from those in the gaseous or liquid state (Scriven, 1960). From a practical point of view, the properties of the system in the dynamic state are more important than those in equilibrium. In these cases, it is important to study the phenomena associated with the ascent of air bubbles in an aqueous solution of a surfactant (Okazaki, 1963).

The mechanism and the effect of surfactant adsorption, surface tension gradients, surface viscosity and interaction between water and surfactant molecules have been studied for a long time.

### 2.8.1. Time-Dependent Surfactant Adsorption

Ward and Tordai (1946) considered the variation of surface tension of solutions with time and the role of diffusion on this time-effect. The diffusion of a solute to the surface is one cause of the time-dependence of surface tension, another is re-orientation of molecules at the surface, e.g., from flat to standing up or vice versa. Initially a freshly formed surface is practically virgin and every molecule arriving at the surface is likely to find an empty "site" and adsorb. As soon as the concentration in the surface is different from zero, the possibility of back-diffusion from surface to the bulk is introduced. The surface concentration will continue to rise until, at equilibrium, the adsorption/back-diffusion processes are in equilibrium. The overall process is time-dependent and consequently plays a significant role in the time-dependence of surface tension between fluid phases.

Liebermann (1957) studied the effect of diffusivity of air from very small stationary bubbles into undersaturated water on bubble size reduction as a function of time. As he indicates, the theory of the diffusivity for a stationary bubble is known, but, differs considerably for freely rising bubbles. Griffith (1962) suggested that the adsorption of most surfactants is essentially complete after a minute for a stationary drop or bubble.

Aybers and Tapucu (1969a), Bachhuber and Sanford (1974) and Detwiler and Blanchard (1978) showed time-dependent adsorption of impurities and surfactants in water and indicated that the bubble velocity decreased with increasing height (or bubble age). Loglio et al., (1989) compared the gas bubble rising times in a surfactant aqueous solution with respect to those in pure water and showed that the time ratio increases with surfactant concentration. Agrawal and Wasan (1979) summarized the expressions for different controlling mass transport mechanisms such as adsorption-desorption, bulk-diffusion and surface diffusion.

Dynamic surface tension (surface tension versus time) of systems of interest in flotation has been studied by Finch (1971, 73), Finch and Smith (1972), Kulkarni and Somasundaran (1975) and Leja (1982) using the capillary pressure technique.

### 2.8.2. Uniform Surface Tension

Okazaki (1964) studied the effect of surfactant type and concentration on bubble terminal velocity. For a fixed bubble size, the bubble velocity can be altered by a change in the physical properties of the solution which affects the hydrodynamic properties of the solution or by contamination forming an adsorbed film on the bubble surface. Okazaki found that the physical properties of the solution such as density, viscosity and surface tension were almost the same in distilled water and in presence of SDS (sodium dodecyl sulfate). For example, the surface tension of distilled water and a solution of  $10^{-5}$  SDS were both 73.3 dyne/cm. Figure 2.12 shows the results from Okazaki's work for the terminal velocity (average velocity in a 40 cm cylinder) versus bubble size for different SDS concentrations. Terminal velocity decreased with increasing SDS concentration. Thus, bubble velocity retardation results from the effect of surfactant adsorption on the bubble surface and the effect is significant. Levich (1962) indicated that the bubble rise velocity cannot be explained by changes in surface tension since the differences in the surface tension between pure water and surfactant solutions is often small. Okazaki suggested that inhibition of gas circulation and bubble deformation, because of surfactant adsorption on the surface, are possible explanations for the remarkable retardation of the velocity. Okazaki showed that all the static properties of the solution fail to explain the phenomena. Finally, he concluded that the ascending bubble has a surface zone of considerable thickness in which the viscosity of the liquid is not that of the bulk, and there was ample reason to believe that the surface viscosity or flow resistance near the bubble surface was the factor affecting the ascending velocity of bubbles in water.

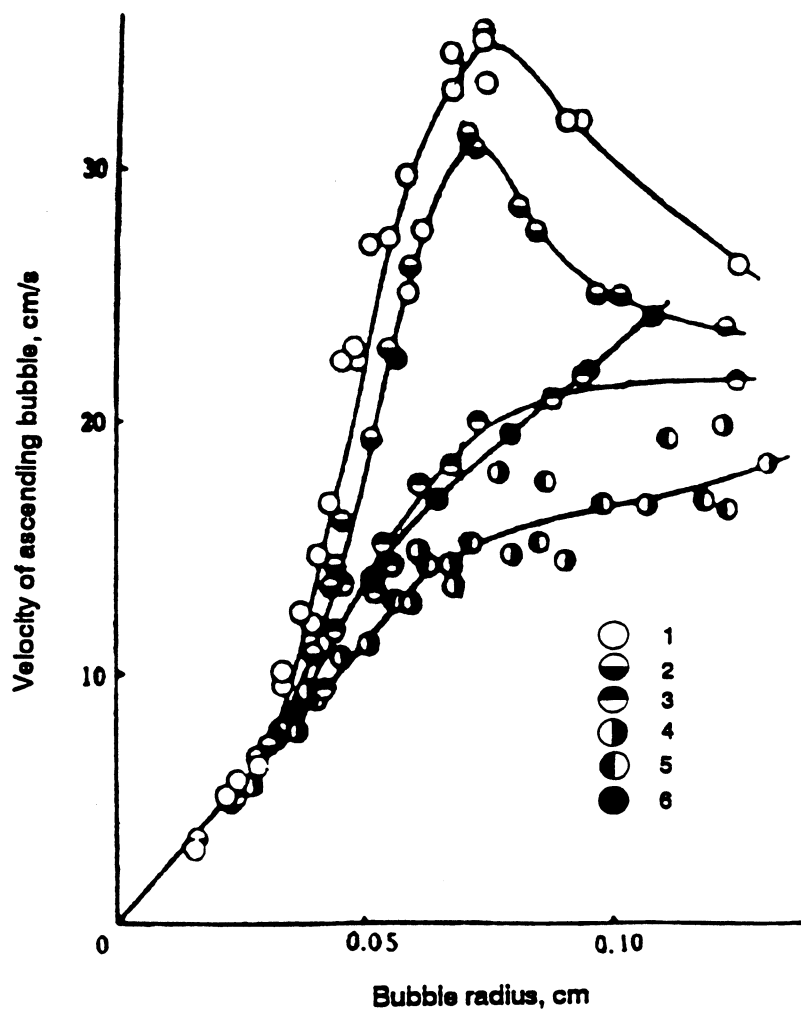


Figure 2.12: Velocity of air bubbles ascending in the aqueous solutions of SDS (Okazaki, 1964);  
(1) distilled water, (2)  $1.0 \times 10^{-6}$  molar SDS,  
(3)  $1.2 \times 10^{-6}$  molar SDS, (4)  $1.0 \times 10^{-6}$  molar SDS,  
(5)  $1.0 \times 10^{-6}$  molar SDS, (6) rigid sphere in distilled water.

Empirical expressions established by Clift et al. (1978), from direct measurement of more than 700 data points also indicate that the surface tension has little effect on the bubble rise velocity. This observation is illustrated in Fig. 2.13, where differences in rise velocities of bubbles at surface tensions of 72 dyne/cm and 50 dyne/cm are found to be negligible (Zhou et al., 1992).

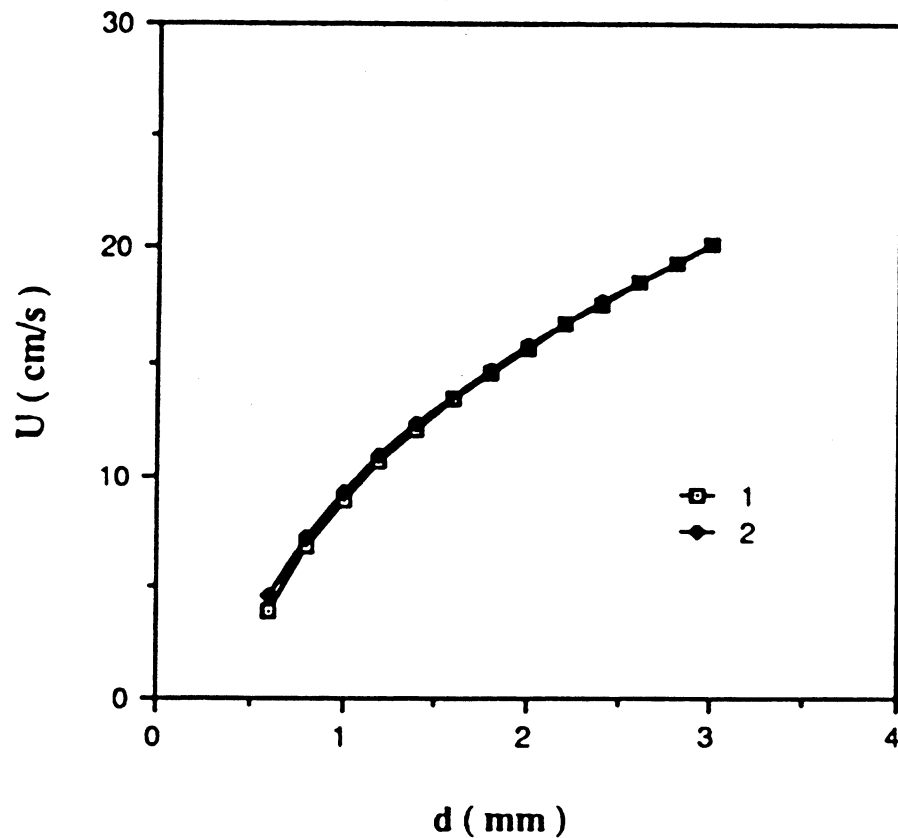


Figure 2.13: Effect of surface tension on bubble rise velocity (Zhou et al., 1991);

(1) surface tension: 72 dyne/cm,

(2) surface tension: 50 dyne/cm.

### 2.8.3. Non-Uniform Surface Tension

#### *Marangoni Effect*

Natural convection due to density differences and Marangoni convection due to an interfacial tension gradient at the free interface of the fluid can form spontaneously in the fluid (Okano et al., 1989; Bergman and Webb, 1990; Gaskell, 1992; Lan and Kou, 1992). For instance, with increasing liquid temperature, density and surface tension of water decrease. Consider a two-dimensional rectangular open container of liquid with a free interface which is heated from one side and cooled from the other. This temperature gradient causes density and interfacial tension gradients in the liquid. The velocity distribution of liquid molecules represents both natural and Marangoni convections. The velocity direction is from the hot (low density and low surface tension) to the cold (high density and high surface tension) sides. In the case of isothermal conditions (in a pure system), there are no convections. The surface tension gradient (even at isothermal conditions) can be produced by non-uniform surfactant distribution at the interface. Lochiel (1965) showed that the surface tension varies from point to point on the interface when surfactant is present in the system. In this case, only Marangoni convection occurs with a circulation flow from low to high surface tension regions at the free interface.

#### *Effect on Bubble Internal Circulation*

The bubble/drop surface rigidity increases and the internal circulation decreases as the surfactants adsorb on the surface. In this case, the change of surface tension with time is an important factor (Garner and Hammerton, 1954).

Linton and Sutherland (1957) showed that internal circulation reduced with adsorption of surfactants on the surface. Any part of the surface of a moving drop

experiences a tangential force  $\tau_0$  proportional to the viscosity of the external medium and to the velocity gradient normal to the surface

$$\tau_0 = \mu_l \left( \frac{\partial u}{\partial n} \right)_{n=0} \quad (2.72)$$

thus inducing internal circulation. On a solid the stress varies from zero at the front of the sphere to a maximum at about  $57^\circ$  and falls to zero behind the equator. The maximum stress is given by

$$\tau_0 = 2.21 U_p^{3/2} \left( \frac{\mu_l \rho_l}{d_p} \right)^{1/2} \quad (2.73)$$

The maximum stress for a particle with velocity 10 cm/s and diameter 2 mm in water is 15.7 dyne/cm<sup>2</sup>. The stress is smaller for a liquid particle (drop) which circulates because the velocity gradient at the surface is less. When calculated from Levich's theory (1949), it is found to be a few dynes/cm<sup>2</sup>. If the drop does not circulate then a force must oppose the tangential force. Such an opposing force cannot arise from a uniform interfacial tension between drop and fluid, so contrary to Hadamard (1911) (see Section 2.9.3), internal circulation should always occur in a pure system.

The surface tension gradient and internal circulation has been studied by Griffith (1962), Oguz and Sadhal (1988) and Stone and Leal (1990). An opposing force to circulation arises if the interfacial tension varies over the surface (surface tension gradient). The mechanism of surfactant adsorption may cause this gradient. Surfactants tend to adsorb at the upstream interface (front) and the flow carries adsorbed molecules towards the rear of the drop (Fig. 2.14). The compressed film at the rear will have a

higher surface pressure and try to spread backwards and so oppose the flow along the surface (Marangoni effect (Loglio et al., 1989; Stone and Leal, 1990)). At the same time surface active material is desorbing at the rear of the drop and adsorbing at the front. If adsorption-desorption is very fast, the surface concentration will be almost constant over the surface so that only a small surface tension gradient is produced. Drops are either: stagnant internally, circulate completely or, circulate partly at the front and are stagnant at the rear (Fig. 2.15).

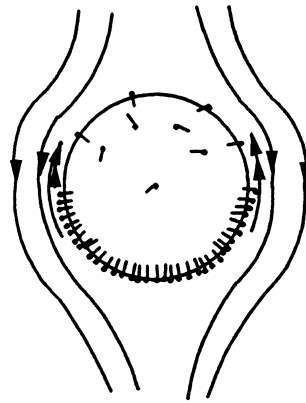


Figure 2.14: The distribution of adsorbed surface active solute on the surface of a rising drop (or Bubble) (Linton, 1957).

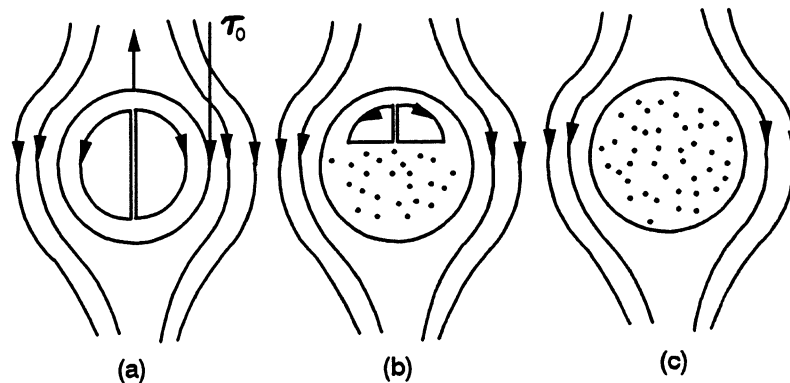


Figure 2.15: The internal circulation of moving drops showing the direction of relative flow (Linton, 1957); (a) circulation, (b) part circulation, (c) stagnant.

The drop initially circulates when first formed and becomes more stagnant with time due to the time-dependence of adsorption. In the presence of non-polar surfactants, the drop tends to either stagnate or partly circulate, but polar surfactants will give it either partial or complete circulation. Some surfactants have been shown to form caps of nearly immobile material on the surface of bubbles (Griffith, 1962). The terminal velocity at small Reynolds numbers has been related to the cap size and to the type and amount of surfactant. The surfactant molecules distribute in such a way as to form an immobile cap over the rear of a bubble (and cause a surface tension gradient) while surface flow remains unimpeded on the forward surface (Griffith, 1962).

The variation of interfacial tension gradients can be assumed to be distributed as (Schechter and Farley, 1963)

$$\sigma = \lambda' - \alpha_1 \cos \theta \quad (2.74)$$

where  $\sigma$  is interfacial tension,  $\lambda'$  is constant and  $\alpha_1$  is the surface tension gradient. In case of small droplets ( $<0.6$  mm) which behave as rigid particles, the interfacial tension gradient ( $\alpha_1$ ) is proportional to  $(U/a)^{1/2}$ , where  $a$  and  $U$  are the droplet radius and velocity, respectively.

For a spherical fluid particle, Levan and Newman (1976) found the following relationship between terminal velocity and surface tension gradient:

$$U_b = \frac{2 g a^2 \Delta\rho}{3 \mu_l} \left( \frac{1 + k}{2 + 3 k} \right) + \frac{1}{\mu_l (4 + 6 k)} \int_0^\pi \sin^2 \theta \frac{d\sigma}{d\theta} d\theta \quad (2.75)$$

This equation reduces to the Hadamard-Rybczynski (1911) equation when the surface tension gradient is zero. When  $k$  ( $\mu_p/\mu_l$ ) (see Section 2.9.3) approaches infinity,

the fluid particle surface is rigid, indicating no internal circulation and this equation becomes the Stokes solution for rigid particles. The surface tension gradient necessary to stop circulation can be derived

$$\frac{d\sigma}{d\theta} = \frac{-a^2 g \Delta\rho}{3} \sin \theta \quad (2.76)$$

### *Temperature Effect*

The motion of bubbles in a vertical temperature gradient was studied experimentally by Young et al., (1959). It was observed that small bubbles in pure liquids could be held stationary or driven downwards by means of a sufficiently strong negative temperature gradient in the vertical direction. This effect is due to the stresses resulting from the thermal variation of surface tension at the bubble surface. It is known that when variations in temperature are maintained on the free surface of a pure liquid, a dynamic steady state is achieved, characterized by a bulk flow in the liquid and at the surface, together with small surface deformation. The nature of this flow is as follows: a local increase in temperature results in a local decrease in surface free energy; a surface temperature distribution therefore is accompanied by a non-uniform tangential stress in the surface, the positive direction of which is opposite to the surface temperature gradient. Their experiments consisted in observing very small bubbles in a cylindrical sample of liquid carried in the gap between the anvils of a machinist's micrometer (Fig. 2.16). The temperatures of the anvils were measured by means of mercury thermometers thrust into copper blocks borne by the anvils. The temperature of the lower block could be raised by increasing the current through a wire wrapped around the lower copper block. Bubble diameters were measured with a travelling microscope. In the experiment, small bubbles were found to collect at the lower (warmer) anvil. As the

temperature gradient was slowly reduced, the larger of these bubbles were observed to detach and slowly rise. A second adjustment of temperature gradient made it possible to poise the bubble essentially motionless midway between the anvils.

Holbrook and LeVan (1983) studied theoretically the effect of nonuniform temperature distribution on surface tension gradient. They also considered the distribution of surfactant concentration through convection and mass transfer processes.

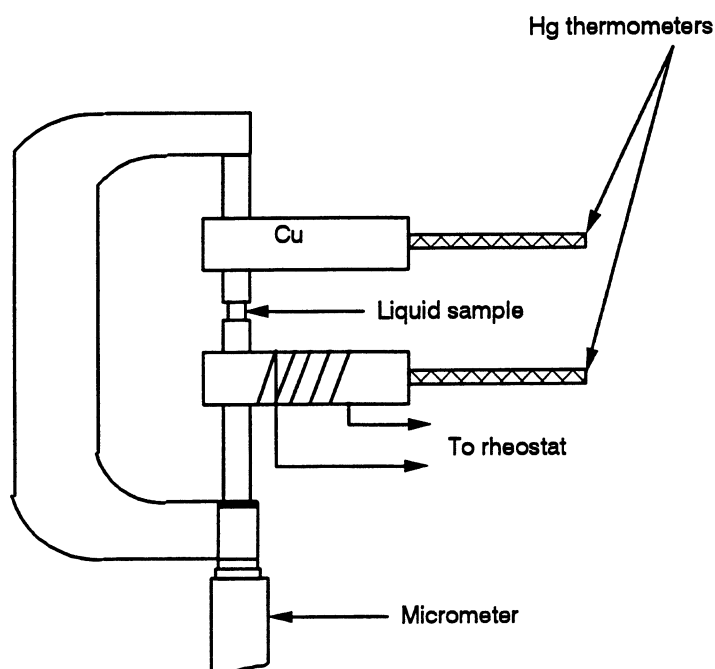


Figure 2.16: Schematic representation of experimental arrangement (Young et al., 1959).

#### 2.8.4. Surface Tension and Surface Viscosity Gradients

The most restrictive condition is constancy of the surface tension, for it requires exceptionally pure fluids (Harper, 1972). So much surface-active materials may be adsorbed that it forms a layer with a measurable surface elasticity or surface viscosity of its own. Harper reviewed these subjects along with the mechanism of surface activity in detail.

Agrawal and Wasan (1979) reviewed the theoretical analyses of Frumkin-Levich (1947) and Saville (1973) which dealt only with surface tension gradients. They extended and modified these theories by incorporating the general momentum balance containing interfacial viscosities which were expressed first by Hadamard-Rybczynski (1911) and Boussinesq (1913). They concluded that the fluid particle terminal velocity is determined by both hydrodynamics and mass transport. They also indicated that: "it is expected that the incorporation of interfacial dilational viscosity and surface tension gradients yields a more accurate description of the motion of bubbles or drops through a quiescent medium".

Levan (1981) explained the creeping motion of a spherical droplet with the interfacial region characterized by an axisymmetric interfacial tension gradient and constant coefficients of surface shear and surface dilational viscosity. Interfacial viscometers have been used to measure the surface shear viscosity. Recently, several methods have been suggested for measuring the surface dilational viscosity (Campanelli, 1987).

Generally, it is well-established that interfacial tension variations and/or interfacial viscosity and elasticity due to surfactants have dramatic qualitative and quantitative effects on free-surface flows (Oguz and Sadhal, 1988; Stone and Leal, 1990).

### 2.8.5. Interaction between Surfactant and Water Molecules

Any molecule or ion with a long enough hydrocarbon chain can affect the shape and terminal velocity of an air bubble in water. The hydrocarbon chain orients into the gaseous phase with the polar head remaining in the water. Water molecules interact with polar groups (through hydrogen bonds) and travel with the bubble and retard the bubble rise. The interaction between surfactant and water molecules increases the drag on the bubble (Fuerstenau and Wayman, 1958; Leja, 1982; King, 1982; Crozier, 1992; Urry, 1995).

Malysa et al., (1988) studied the adsorption of long chain polymers on flow of the colloidal particles. They used nylon spheres with attached threads. Particle velocity decreased with increasing number of attached threads. The effect was significant and for the highest surface coverage (21 threads), the velocity of the covered particle was about 50% lower than that of the bare particle.

Generally, it is quite reasonable to conclude that as mechanisms of retardation of bubble rise in water, surface tension and surface viscosity gradients and interaction between surfactant and water molecules play a significant role. In all three, the structure and concentration of surfactant molecules are important factors.

## 2.9. Theories and Models of Bubble Velocity

### 2.9.1. Single Particle Motion in the Absence of Resistance

Motion may be defined as a continuous change of position. In most motions, different points in a body move along different paths. The complete motion is known if we know how each point in the body moves; here, we consider only a moving point, or a very small body referred to as a particle. Consider a particle falling toward the earth. In the absence of air resistance (drag), all bodies, regardless of their size or

weight, fall with the same acceleration at the same point on the earth's surface, and if the distance covered is small compared to the radius of the earth, the acceleration remains constant throughout the fall (Sears et al., 1977). The relationship between the particle velocity and time is linear ( $U_p = \pm gt + U_m$ ), where  $U_p$  is particle velocity,  $g$  is acceleration due to gravity,  $t$  is time,  $U_m$  is initial velocity and  $\pm$  refers to downward (+) or upward (-) motion.

### 2.9.2. Single Solid Particle Motion in a Viscous Fluid

According to the classical theory, the motion of a particle with diameter  $d_p$  through a viscous fluid (starting from rest) is subjected to three vertical forces: the weight (gravitational force)  $F_w$ , the buoyancy force  $F_B$  and the drag force  $F_D$ . Based on Newton's second law, the equation of motion of a particle in a fluid is

$$F_w - F_B \pm F_D = m \frac{dU}{dt} \quad (2.77)$$

and for a sphere, it can be written as

$$\frac{\pi d_p^3}{6} \rho_p g - \frac{\pi d_p^3}{6} \rho_l g \pm C_D \times \frac{1}{2} \rho_l U^2 \times \frac{\pi d_p^2}{4} = m \frac{dU}{dt} \quad (2.78)$$

At first, when velocity is zero, the drag force is zero and the initial acceleration is positive. The sphere speeds up and, after a while when velocity becomes large enough, the resultant force acting on the sphere becomes zero (the forces acting on the body are in equilibrium and the velocity is maximum). At this moment, acceleration is

zero ( $m \, dU/dt = 0$ ) and from this position, the velocity is constant (terminal velocity,  $U_T$ ). If the sphere velocity in the fluid starts from  $U = U_{in} > U_T$ , the initial acceleration will be negative until it reaches the terminal velocity (Sears et al., 1977). Generally, the terminal velocity of a falling sphere in liquid with density  $\rho_l$  as a function of the drag coefficient ( $C_D$ ) is determined by

$$U_T = \sqrt{\frac{4 \, g \, (\Delta\rho) \, d_p}{3 \, C_D \, \rho_l}} \quad (2.79)$$

and

$$C_D = \frac{4 \, g \, (\Delta\rho) \, d_p}{3 \, \rho_l \, U_T^2} \quad (2.80)$$

where  $\Delta\rho$  is the density difference between particle and fluid phases.

The relationship between the dimensionless drag coefficient and the other dimensionless groups can be defined by (Harper, 1972)

$$C_D = \frac{4}{3} \, Mo \, Re^4 \, We^{-3} \quad (2.81)$$

The drag coefficient can also be expressed as a function of Reynolds number ( $\rho_l U_T d_p / \mu_l$ ) at equilibrium

$$C_D = \frac{4 g \rho_l \Delta \rho d_p^3}{3 \mu_l^2 Re^2} \quad (2.82)$$

and

$$C_D = Re \times \left( \frac{4 g \Delta \rho \mu_l}{3 \rho_l^2 U_T^3} \right) \quad (2.83)$$

In order to determine the particle velocity, it is necessary to know the gravitational and buoyancy forces which are dependent on the physical properties of the particle such as volume and density. The drag force exerted by a liquid on a solid particle is related to the fluid flow properties and boundary layer conditions (e.g., wake structure) and is normally difficult to define.

Total drag is the sum of friction drag (a consequence of liquid viscosity) and form drag (connected to the pressure distribution over the particle surface). In general, the friction drag is predominant when the Reynolds number is low. At intermediate  $Re$ , friction drag and form drag are of the same order of magnitude, whereas at high  $Re$ , form drag predominates.

The drag force is usually presented as a function of the drag coefficient,  $C_D$ . Therefore for a long time, the main objective of theoretical and experimental investigations was to find a formula for the drag coefficient of a sphere that would span a wide range of Reynolds numbers, extending from the Stokes law range at the lower end ( $Re \ll 1$  or  $d_p \leq 50 \mu\text{m}$  in water (Wills, 1988)) to values corresponding to the transition

to turbulent flow (e.g., Newton's law,  $C_D = 0.44$  for  $d_p \geq 5\text{mm}$  in water) at the higher end (Concha and Almendra, 1979; Wills, 1988). These equations can be summarized as

Stokes (1851),  $Re \rightarrow 0$ :

$$C_D = \frac{24}{Re} \quad (2.84)$$

Allen (1990):

$$C_D = 24 Re^{-1} \quad Re \leq 2 \quad (2.85)$$

$$C_D = 18.5 Re^{-0.6} \quad 2 < Re \leq 200$$

Oseen (1910),  $Re \leq 1$ :

$$C_D = \frac{24}{Re} \left( 1 + \frac{3}{16} Re \right) \quad (2.86)$$

Schiller and Naumann (1933),  $Re < 800$ :

$$C_D = \frac{24}{Re} (1 + 0.150 Re^{0.687}) \quad (2.87)$$

Newton,  $Re > 1000$

$$C_D = 0.44 \quad (2.88)$$

Rubey (1933):

$$C_D = \frac{24}{Re} + 2 \quad (2.89)$$

Dallavalle (1943):

$$C_D = \frac{24.4}{Re} + 0.4 \quad (2.90)$$

Dallavalle (1948):

$$C_D = \left( 0.63 + \frac{4.8}{Re^{1/2}} \right)^2 \quad (2.91)$$

Lapple (1951),  $Re < 1000$

$$C_D = 18.5 Re^{-0.6} \quad (2.92)$$

Torobin (1959):

$$C_D = \frac{24}{Re} (1 + 0.197 Re^{0.63} + 0.0026 Re^{1.38}) \quad (2.93)$$

Olson (1961):

$$C_D = \frac{24}{Re} \left( 1 + \frac{3}{16} Re \right)^{1/2} \quad (2.94)$$

Abraham (1970),  $Re \leq 6000$ :

$$C_D = 0.30 \left( 1 + \frac{8.65}{Re^{1/2}} \right)^2 \quad (2.95)$$

Brauer and Sucker (1976):

$$C_D = 0.49 + \frac{24}{Re} + \frac{3.73}{Re^{1/2}} - \frac{4.83 \times 10^{-3} Re^{1/2}}{1 + 3.0 \times 10^{-6} Re^{3/2}} \quad (2.96)$$

Concha and Almendra (1979)  $Re < 10^4$

$$C_D = 0.28 \left( 1 + \frac{9.06}{Re^{1/2}} \right)^2 \quad (2.97)$$

Usually, the authors plot the predictions together with experimental values for the drag coefficient of spheres. Figures 2.17 and 2.18 show the data from  $C_D$  -  $Re$  equations compared to the standard values (Concha and Almendra, 1979). These figures also indicate the proper range of Reynolds number for any equation compared to the standard drag curve. These standard values are based on the combined data of 16 researchers, as given by Lapple and Shepherd (1940).

Solving one of the  $C_D$ - $Re$  prediction equations in concert with Eq. 2.82, the Reynolds number (and  $U_T$ ) of a rigid sphere with known diameter can be determined. If the predicted  $Re$  is in the proper range compared to the standard curve,  $U_T$  is the sphere terminal velocity, otherwise, other  $C_D$ - $Re$  equations should be examined.

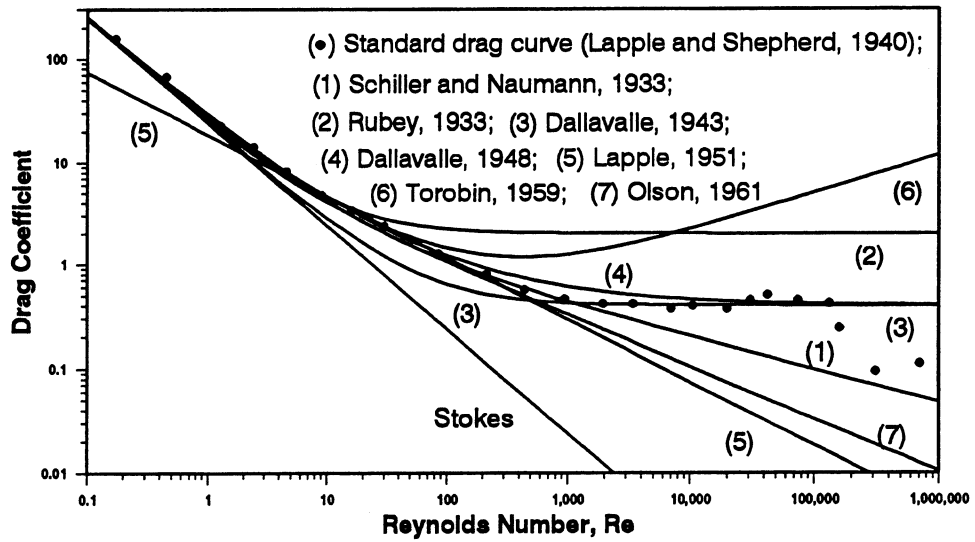


Figure 2.17: Drag Coefficient versus  $Re$  for various empirical formulas (Concha and Almendra, 1979).

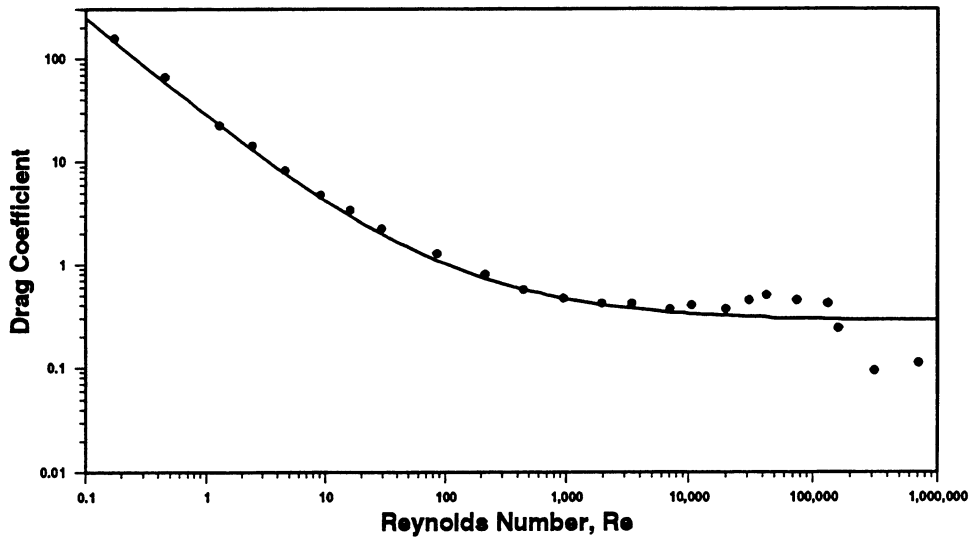


Figure 2.18: Drag Coefficient versus  $Re$ . (line) Concha and Almendra (1979); (•) Standard drag curve (Lapple and Shepherd, 1940).

Several correlations, plots and also dimensionless groups such as the Best number (dimensionless diameter ( $C_D Re^2$ )) and dimensionless velocity ( $Re/C_D$ ) have been used for analysis of spherical and non-spherical particles in motion (Best, 1950; Heywood, 1962; Clift et al., 1978; Concha and Almendra, 1979). Figure 2.19 shows the terminal velocity of solid spheres of various densities as a function of diameter in air and water at 20 °C (Clift et al., 1978).

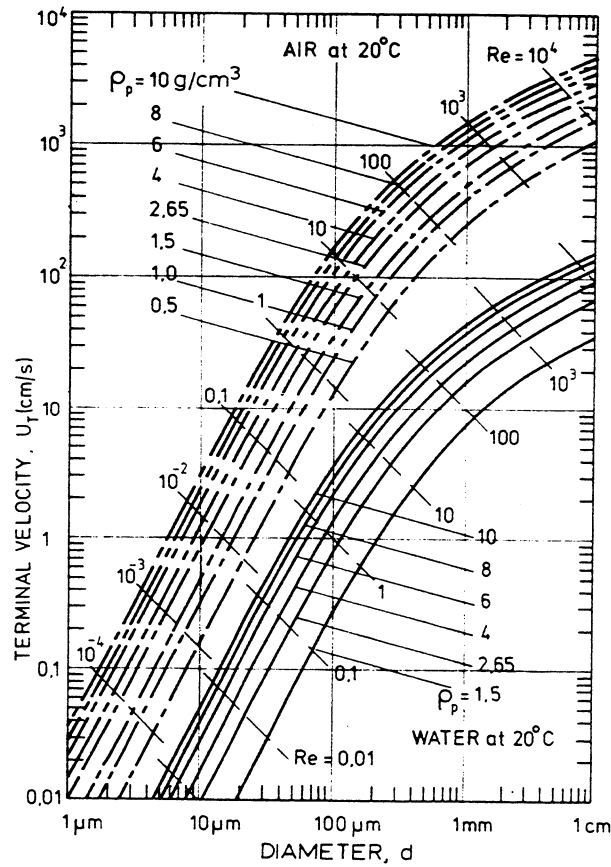


Figure 2.19: Terminal velocities of spheres in air and water at 20 °C (Clift et al., 1978, reprinted with permission).

Nguyen-Van et al. (1994) proposed a method for predicting the terminal settling velocity of a single solid spherical particle in water. They used the dimensionless Archimedes,  $Ar$  ( $3 Re^2 C_D/4$ ) and Lyashchenko,  $Ly$  ( $4 Re/3 C_D$ ) numbers to find the relationship between particle size and terminal velocity. According to their approach, the terminal velocity can be derived by

$$U_T = \frac{d_p^2 \Delta\rho g}{18 \mu_l} \times \left( \frac{1}{1 + \alpha Ar^\beta} \right)^{\frac{1}{3}} \quad (2.98)$$

where,

$$\alpha = 0.0294 \text{ and } \beta = 0.887 \text{ for } 0 \leq Ar \leq 17845$$

$$\alpha = 0.0014 \text{ and } \beta = 1.198 \text{ for } 17845 < Ar \leq 512000$$

By knowing particle diameter and density,  $Ar$  ( $d_p^3 \Delta\rho \rho_1 g / \mu^2$ ) which is not related to  $U_T$  can be calculated. Then, from  $Ar$ ,  $\alpha$  and  $\beta$  and consequently,  $U_T$  can be predicted. This model covers a range of sphere Reynolds number from 0 to 1000.

### 2.9.3. Single Fluid Particle in Motion

#### *Stokes' Law*

The theoretical solution for very slow motion around a solid (rigid) sphere in a pure system was first developed by Stokes (1851). Since, according to the literature (Garner and Hammerton, 1954; Liebermann, 1957; Levich, 1962; Clift et al., 1978; Stone and Leal, 1990), it is known that under the Stokes condition ( $Re \ll 1$ ), fluid particle spheres such as bubbles behave as solid particles, this famous sphere-drag formula is considered in this section.

The total drag ( $F_D$ ) for a particle in motion when the Reynolds number is low can be found by integrating pressure and shear around the particle surface. In general, under Stokes flow conditions, the shear-stress ( $\tau$ ) and pressure ( $P$ ) distribution around a particle are

$$\tau_{r\theta} = \mu_l \left( \frac{1}{r} \frac{\partial U_r}{\partial \theta} + \frac{\partial U_\theta}{\partial r} - \frac{U_\theta}{r} \right) = - \frac{\mu_l U \sin \theta}{r} \left( \frac{3a^3}{2r^3} \right) \quad (2.99)$$

$$P = P_0 - \frac{3 \mu_l a U}{2 r^2} \cos \theta$$

and total drag can be obtained by

$$F_D = - \int_0^\pi \tau_{r\theta} \Big|_{r=a} \sin \theta dA - \int_0^\pi P \Big|_{r=a} \cos \theta dA \quad (2.100)$$

$$dA = 2 \pi a^2 \sin \theta d\theta$$

$$F_D = 4\pi\mu_l U a + 2\pi\mu_l U a = 6\pi\mu_l U a \text{ (or } 3\pi\mu_l U d_p)$$

where  $a$ ,  $d_p$  and  $U$  are sphere radius, diameter and velocity, respectively. This drag force consists of two-thirds viscous force and one-third pressure force. Applying this drag force formula, the particle terminal velocity and drag coefficient in terminal conditions is given by

$$U_T = \frac{g d_p^2 \Delta\rho}{18 \mu_l} \quad (2.101)$$

$$C_D = \frac{24}{Re} \quad (2.102)$$

In principle, the Stokes solution is accurate for  $Re \ll 1$  (e.g.,  $Re \leq 0.1$  (Vennard and Street, 1975)) but agrees with experiment up to about  $Re = 1$  (White, 1991).

#### *Hadamard-Rybczynski Equation*

The Hadamard-Rybczynski (1911) analytical solution indicates that the boundary conditions on the surface of a fluid particle result in a significant change in the velocity of the particle. A spherical fluid particle completely free from surfactants (constant interfacial tension) is considered moving slowly in a liquid. The Reynolds numbers for the outer and inner fluid are small ( $\ll 1$ ). Based on the selected boundary conditions described by Levich (1962), the stream functions and pressure in both phases can be derived by

$$\psi = - \frac{U_0 r^2 \sin^2 \theta}{2} \left( 1 - \frac{a(2+3k)}{2r(1+k)} + \frac{ka^3}{2r^3(1+k)} \right) \quad (2.103)$$

$$\psi_p = - \frac{U_0 r^2 \sin^2 \theta}{4(1+k)} \left( 1 - \frac{r^2}{a^2} \right) \quad (2.104)$$

$$P = P_0 + \left( \mu U_0 a \cos \theta \times \frac{(2 + 3k)}{2r^2(1+k)} \right) \quad (2.105)$$

$$P_p = P_{0p} - \left( \frac{5 \mu_p U_0 r \cos \theta}{a^2(1+k)} \right) \quad (2.106)$$

where  $\psi$  and  $P$  are stream function and pressure distribution, respectively (subscript  $p$  refers to the inner fluid particle),  $k$  is the ratio of fluid particle viscosity to liquid viscosity ( $\mu_p / \mu_l$ ) and  $P_0$  and  $P_{0p}$  are constant. It is also satisfied if  $P_{0p} - P_0 = 2\sigma/a$  (Section 2.7.1, Eq. 2.66).

The total drag coefficient is the sum of three drag components (Clift et al., 1978): form drag (integration of the pressure over the surface of the particle) given by

$$(C_D)_1 = \frac{8}{3 Re} \left( \frac{2 + 3k}{1+k} \right) \quad (2.107)$$

drag due to the normal stress

$$(C_D)_2 = \frac{32}{3 Re (1+k)} \quad (2.108)$$

and from shear stress

$$(C_D)_3 = \frac{16}{Re} \frac{k}{(1+k)} \quad (2.109)$$

where, for the latter  $(C_D)_3$  is equal to zero when  $k = 0$ .

The total drag coefficient and particle terminal velocity in the absence of surfactants can be obtained by

$$C_D = \frac{8}{Re} \left( \frac{2 + 3k}{1 + k} \right) \quad (2.110)$$

$$U_T = \frac{2g a^2 \Delta\rho}{3\mu_l} \left( \frac{1 + k}{2 + 3k} \right) \quad (2.111)$$

The ratio ( $K'$ ) of this terminal velocity to the Stokes equation can be found by

$$K' = \frac{U_T}{(U_T)_{Stokes}} = 3 \times \frac{1 + k}{2 + 3k} \quad (2.112)$$

When  $k \rightarrow \infty$  ( $K' = 1$ ) for a rigid particle, the Hadamard-Rybczynski equation reduces to the Stokes equation ( $U_T = g d_p^2 \nabla\rho / 18\mu_l$ ). When  $k = 0$  ( $K' = 1.5$ ) for a completely mobile particle (e.g., a bubble),  $U_T$  is 50% higher than that of a rigid sphere of the same size and density in the same liquid. In this case, the terminal velocity and drag coefficient can be obtained from

$$U_T = \frac{g d_p^2 \Delta\rho}{12\mu_l} \quad (2.113)$$

$$C_D = \frac{16}{Re} \quad (2.114)$$

This difference between terminal velocities of rigid and mobile spheres is due to the mobility of the interface, the velocity gradients present in the liquid are smaller than those in the case of a solid and this leads to a decrease in the energy dissipated in the liquid (Levich, 1962).

Levich (1962), Wasserman and Slattery (1969) and Clift et al., (1978) compared the Hadamard-Rybczinski theory with experimental data. The results implied that the Hadamard-Rybczinski theory is not applicable under actual conditions.

### *Boussinesq Equation*

Boussinesq (1913) established his model by assuming the existence of a thin layer (interfacial monolayer) with a viscosity higher than the bulk liquid which acts as a viscous membrane near the fluid particle. This viscous skin inhibits the internal circulation. In fact, Boussinesq obtained an exact solution for creeping flow past a fluid particle under the assumption that interfacial behaviour could be described by the Newtonian surface fluid model (Scriven, 1960). The Newtonian surface fluid model expresses the stress in the interface as a linear function of the rate of deformation of the interface and has two parameters in addition to surface tension: surface shear viscosity and surface dilational viscosity (Wasserman and Slattery, 1969). The viscosity of a liquid measured at its interface can be considerably greater than the usual shear viscosity. This surface viscosity does not occur with purely shearing motion, but with surface dilation (or compression) resulting from surface contamination (Liebermann, 1957). The Boussinesq equation can be written as (Clift et al., 1978)

$$U_T = \frac{g d_p^2 \Delta\rho}{6 \mu_l} \left( \frac{1 + k + C_l \mu_l}{2 + 3k + 3C_l \mu_l} \right) \quad (2.115)$$

where  $C$  is equal to the surface dilational viscosity divided by 1.5 times the fluid particle radius. When  $C \rightarrow \infty$  and  $C = 0$ , this equation approaches the Stokes and Hadamard-Rybczynski equations, respectively. The results of Boussinesq's analysis do not appear to be in any better agreement with available experimental data than those of Hadamard-Rybczynski (Levich, 1962). In addition, neither the analysis of Boussinesq nor the theory of Hadamard-Rybczynski considers the possible presence of surfactants (Wasserman and Slattery, 1969).

### *Levich Equation*

Levich (1962) considered boundary layer theory with reference to liquid-gas interfaces and applied it to the computation of the total resisting force ( $F_D$ ) that acts upon a gas bubble rising in a liquid. The application of the boundary-layer theory to a spherical gas bubble led to the following expression for the drag force, terminal bubble velocity and drag coefficient

$$F_D = 6 \pi \mu_l U d_p \quad (2.116)$$

$$U_T = \frac{g d_p^2 \Delta \rho}{36 \mu_l} \quad (2.117)$$

$$C_D = \frac{48}{Re} \quad (2.118)$$

This terminal velocity is claimed to be valid over the range  $1 < Re < 1500$  for spherical bubbles. However, it has been pointed out that experimental verification of model would be difficult because of bubble deformation (Peebles and Garber, 1953).

*Moore's Theory*

Moore (1959, 63, 65) studied the rise of a gas bubble in a viscous liquid at high Reynolds number. He proposed two models for spherical and non-spherical bubbles in the absence of surfactants. He suggested that the drag force on the bubble can be calculated from normal viscous stress of the irrotational flow and the results for drag force, drag coefficient and terminal velocity for spherical bubbles were obtained as

$$F_D = 4 \pi \mu_l U d_p \quad (2.119)$$

$$C_D = \frac{32}{Re} \quad (2.120)$$

$$U_T = \frac{d_p^2 g \Delta \rho}{24 \mu_l} \quad (2.121)$$

Moore developed the drag coefficient for deformable bubbles given by

$$C_D = \frac{48}{Re} G(x) \left( 1 + \frac{H(x)}{Re^{1/2}} \right) \quad (2.122)$$

in which the first term on the right hand side is Levich's original result. The terminal velocity can be obtained by

$$U_T = \frac{d_e^2 g \Delta \rho}{36 \mu_l G(x) \left(1 + \frac{H(x)}{Re^{1/2}}\right)} \quad (2.123)$$

where  $x$  (the ratio of bubble major and minor axes) and functions,  $G(x)$  and  $H(x)$  are given in Table 2.4.

**Table 2.4: Moore's functions for distorted bubbles (Harper, 1972).**

$x$	$G(x)$	$H(x)$	$x$	$G(x)$	$H(x)$
1.0	1.000	-2.211	2.6	4.278	1.499
1.1	1.137	-2.129	2.7	4.565	1.884
1.2	1.283	-2.025	2.8	4.862	2.286
1.3	1.437	-1.899	2.9	5.169	2.684
1.4	1.600	-1.751	3.0	5.487	3.112
1.5	1.772	-1.583	3.1	5.816	3.555
1.6	1.952	-1.394	3.2	6.155	4.013
1.7	2.142	-1.186	3.3	6.505	4.484
1.8	2.341	-0.959	3.4	6.866	4.971
1.9	2.549	-0.714	3.5	7.237	5.472
2.0	2.767	-0.450	3.6	7.620	5.987
2.1	2.994	-0.168	3.7	8.013	6.517
2.2	3.231	0.131	3.8	8.418	7.061
2.3	3.478	0.448	3.9	8.834	7.618
2.4	3.735	0.781	4.0	9.261	8.189
2.5	4.001	1.131			

In general, Moore's theory is valid for  $Re \gg 1$  in pure liquids. Aybers and Tapucu (1969b), Harper (1972) and Jameson (1993) reviewed this theory in detail.

### Mendelson's Theory

Mendelson (1967) proposed an equation based on the wave equation for prediction of terminal velocity. Bubble terminal velocity and drag coefficient can be obtained from

$$U_T = \sqrt{\frac{2 \sigma}{d_e \rho_l} + \frac{g d_e}{2}} \quad (2.124)$$

$$C_D = \frac{8}{3} \left(1 - \frac{1}{We}\right) \quad (2.125)$$

where  $We$  is the Weber number. This theory is defined for bubbles ( $d_e \geq 1.4$  mm or  $Re > 450$ ) in pure water.

Mendelson also explained the characteristic shape of the experimental curve of bubble terminal velocity versus  $d_e$  in pure water (Fig. 2.20). Mendelson's equation covers regions 3 and 4. These characteristics are as follow:

Region 1 ( $d_e < 0.7$  mm): velocity is limited by viscous drag and obeys the Stokes law.

Region 2 ( $0.7 < d_e < 1.4$  mm): as for region 1, the terminal velocity in this region is also limited by viscosity. However due to circulation within the bubble, shear stresses at the interface are reduced and the rise velocity is greater than predicted by Stokes' law.

Region 3 ( $1.4 < d_e < 6$  mm): in this region, the bubbles are no longer spherical and their motion is zigzag. Drag is increased by vortex formation in the wake and terminal velocity can be determined as:  $U_T = 1.35 (2\sigma/d_e \rho_l)^{1/2}$ .

Region 4 ( $d_e > 6$  mm): bubble shape approaches spherical cap and the terminal velocity can be obtained by:  $U_T = 1.02 (g d_e/2)^{1/2}$ .

Lehrer (1976) proposed an equation in order to estimate fluid particle terminal velocity in regions 3 and 4 as:  $U_T = (gd_e \Delta\rho / 2\rho_l + 3\sigma / \rho_l d_e)^{1/2}$ .

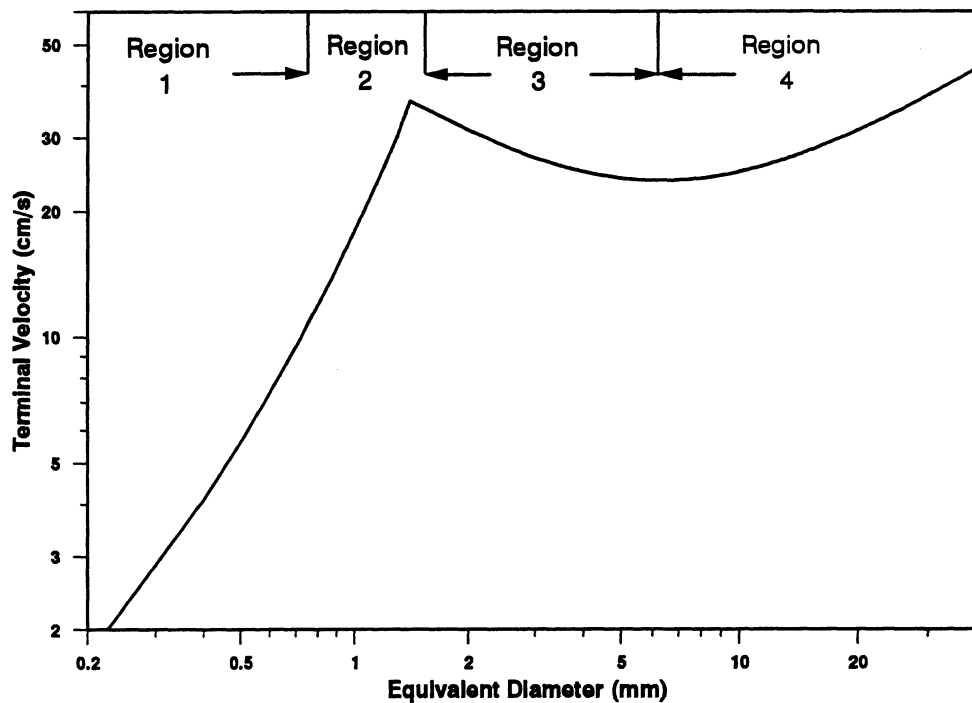


Figure 2.20: Typical curve and regions of the terminal velocity of bubbles (Mendelson, 1967).

*Zhou et al., Model*

The objective of this model (Zhou et al., 1991, 92) was to predict the effect of frothers on bubble rise velocity. This approach assumed changes in the thickness and surface viscosity of the liquid film surrounding the bubble due to frother adsorption. A theoretical expression was developed for the relationship between bubble velocity and size for different kinds of frothers at varied concentrations. In this model, a contamination factor ( $C_c$ ) which is dependent on the frother type and concentration is introduced. The bubble terminal rise velocity decrease is modelled by increasing the contamination factor. Based on this model, when a bubble is formed in a liquid, a thin liquid layer which rises with the bubble as a result of buoyancy also forms. As a result, there is a change in surface viscosity and the net lifting force on the bubble is lower than that where the thickness of the liquid film is zero. In order to account for the effect of this liquid film on the bubble, the virtual mass of the bubble, which can be estimated using different methods, was used (Zhou et al., 1991). The final result was

$$U_T = \frac{g \Delta \rho}{9 \mu_l} \left[ \frac{(1 + 3.36 C_c R_v^2)^{0.5} - 1}{2 C_c R_v} \right]^2 \quad (2.126)$$

where  $R_v$  is radius of a visual bubble (i.e.  $R_v = a$ ).

The contamination factor can be estimated from the following expressions for the three frother types tested:

- pine oil

$$C_c = 110 + 285 [1 - \exp(-0.59 C^{0.5})] \quad (2.127)$$

when ( $0 \leq C \leq 3 \text{ cm}^3 \text{ per } 100 \text{ l}$ )

- Dowfroth 250

$$C_c = 110 + 280 [1 - \exp (- 0.55 C^{0.5})] \quad (2.128)$$

when  $(0 \leq C \leq 3 \text{ cm}^3 \text{ per } 100 \text{ l})$

- MIBC

$$C_c = 110 + 260 [1 - \exp (- 0.11 C)] \quad (2.129)$$

when  $(0 \leq C \leq 6 \text{ cm}^3 \text{ per } 100 \text{ l})$

where  $C$  is frother concentration in the liquid.

From this model, the drag coefficient as a function of contamination factor can be obtained by

$$C_D = \frac{384 \mu_l C_c^4 R_v^5}{\rho_l \frac{g \Delta \rho}{9 \mu_l} [(1 + 3.36 C_c R_v^2)^{0.5} - 1]^4} \quad (2.130)$$

The authors compared these predictions with their experimental results by measuring the average velocity of bubbles in an approx. 90 cm high cylinder at 20 °C.

#### ***Typical Bubble $C_D$ - $Re$ and $U_T$ - $d_c$ Curves***

Figure 2.21 shows the drag coefficient as a function of Reynolds number for air bubbles in water compared with free-rising light particles (Karamanev and Nikolov, 1992), water drops in air and standard drag curve for solid particles (Clift et al., 1978). Also Figure 2.22 represents the theoretical and experimental data and models for terminal velocity of air bubbles in pure and contaminated water.

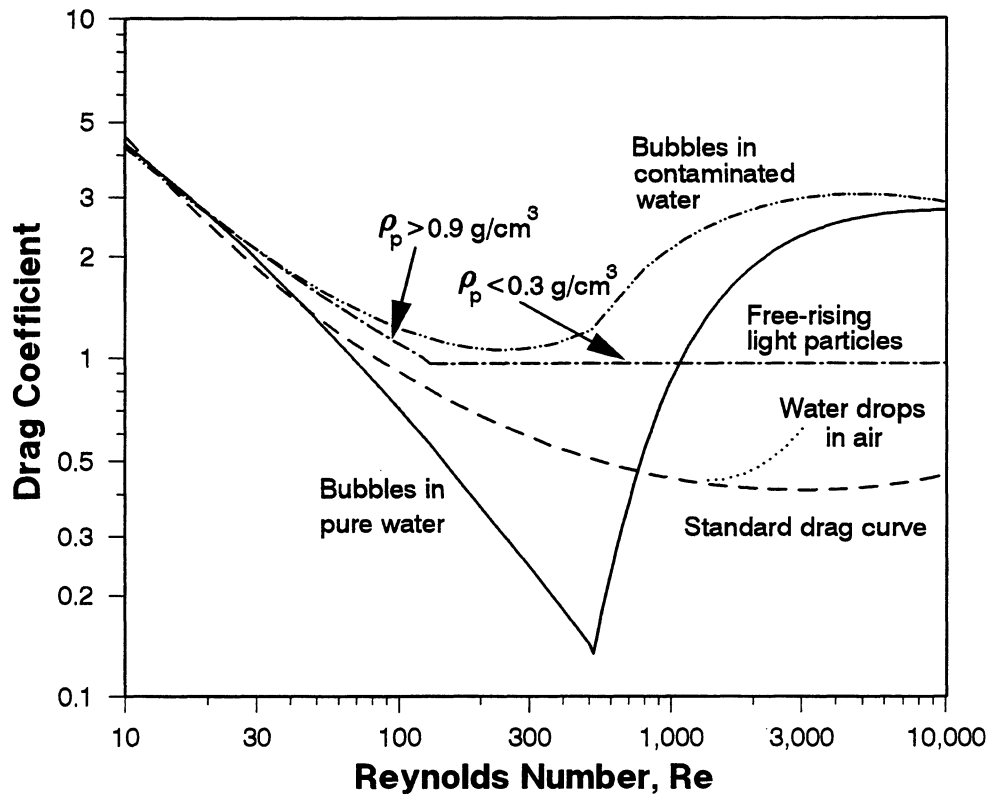


Figure 2.21: Drag coefficient as a function of  $Re$  for water drops in air, air bubbles in water (Clift et al., 1978) and free-rising light particles (Karamanev and Nikolov, 1992), compared with standard drag curve.

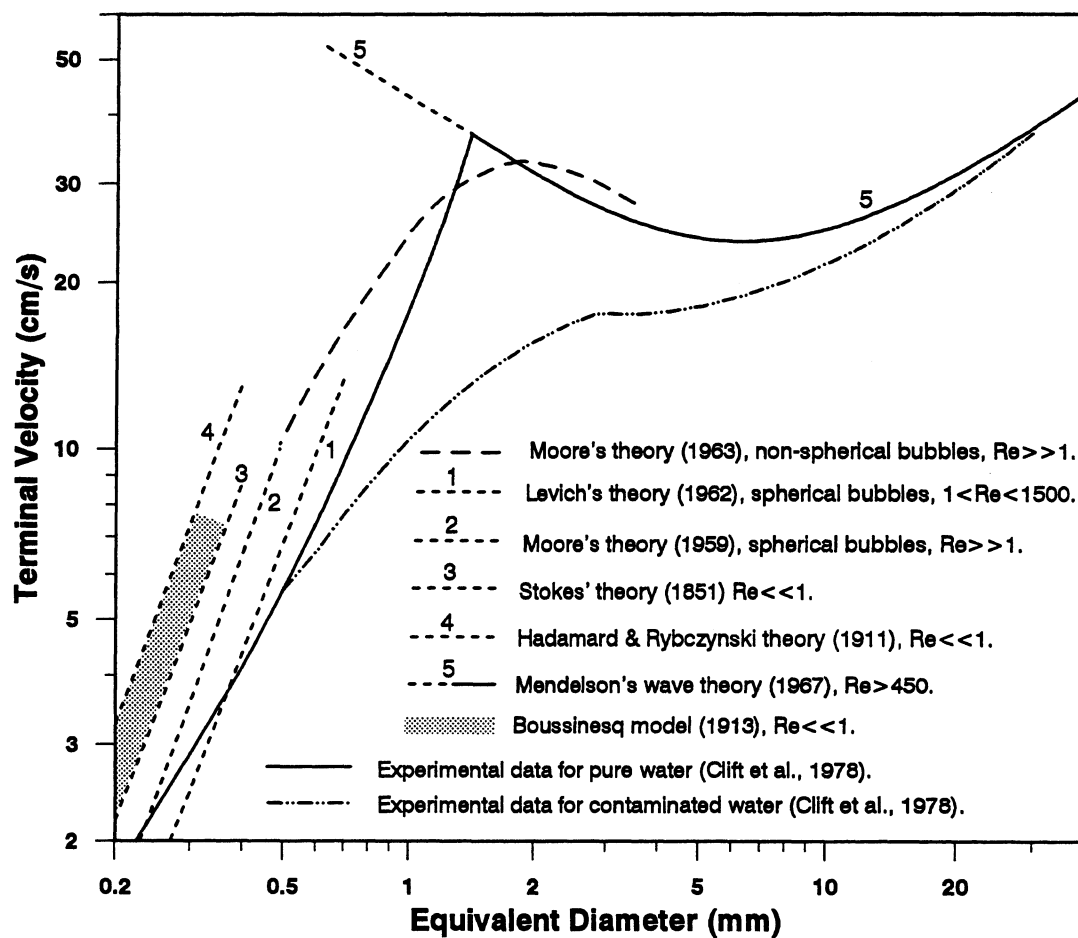


Figure 2.22: Theoretical and experimental data and models for terminal velocity of air bubbles in water.

#### 2.9.4. Bubble Swarms (Drift Flux Model)

The objective of bubble generation in flotation, is to produce relatively small gas bubbles ( $0.5 \text{ mm} < d_b < 3 \text{ mm}$ ) at moderate gas superficial velocities (flow rate/cross-sectional area of column) (1 to 3.0 cm/s).

In a mechanical flotation machine, bubbles are generated by rotating an impeller within baffles. Air is introduced through the impeller to provide good dispersion and sufficient mixing to cause the particle-bubble collisions that are the essential prerequisite to particle-bubble attachment (Kelly and Spottiswood, 1989; Kaya, 1989).

In flotation columns, bubbles are produced by a variety of generation systems or spargers. The size of bubbles produced is determined by the type of generation system, frother type and dosage, and gas rate. Bubble size tends to increase with increasing gas rate (for porous spargers this was described by Dobby and Finch, 1986) and decreases with increasing frother concentration due to prevention of coalescence. When gas is introduced liquid (or slurry) is displaced. The volumetric fraction displaced is called the gas holdup  $\epsilon_g$ . The complement ( $1-\epsilon_g$ ) is the liquid (or slurry) holdup. Gas holdup increases with increasing frother concentration. Gas holdup in the collection zone of flotation columns is usually between 15 and 25 per cent. Gas holdup can be measured in a number of ways such as pressure and conductivity methods. Yianatos et al., (1986), Uribe-Salas et al., (1992) and Gomez et al., (1995) reported that the local gas holdup increased with height in the collection zone.

Masliyah (1979) proposed a general equation for relative solid particle to fluid velocity (or slip velocity) for hindered settling of spherical particles in a multi-species particle system. Based on the Masliyah approach, Yianatos et al., (1988) and Dobby et al., (1988) developed a bubble size estimation technique and introduced an expression for the determination of the slip velocity as a function of gas holdup when  $Re < 500$ . They used the  $C_D$ - $Re$  expression of Schiller and Naumann (1933) for particle motion at terminal conditions (Fig 2.17). According to this approach and from drag coefficient

definition, the terminal velocity of a single bubble ( $\epsilon_g = 0$ ) in a gas-liquid system can be obtained by

$$U_T = \frac{d_b^2 g \Delta\rho}{18 \mu_l (1 + 0.15 Re^{0.687})} \quad (2.131)$$

$$Re = \frac{d_b \rho_l U_T}{\mu_l}$$

The drift flux model offers a mean to correlate gas holdup with the various operating variables. It has been used, for example, in the estimation of bubble size in liquid-gas mixtures, provided some simple parameters are measured or known (Wallis, 1969). In gas-liquid systems (uniform swarms) in which there is a net flow of both phases, the relative or slip velocity,  $U_s$  is defined by

$$U_s = \frac{J_g}{\epsilon_g} + \frac{J_l}{1 - \epsilon_g} \quad (2.132)$$

where  $J_g$  and  $J_l$  are superficial gas and liquid velocities, respectively ( $J_g$  positive upward and  $J_l$  positive downward).

The slip velocity is related to a single bubble terminal velocity and gas holdup. A frequently used relationship is (Xu and Finch, 1990)

$$U_s = U_T (1 - \epsilon_g)^{m-1} \quad (2.133)$$

A method to estimate  $d_b$  was developed from these expressions. The routine is to measure  $U_s$  (by measuring  $J_1$ ,  $J_g$  and  $\varepsilon_g$ ), estimate  $U_T$  from Eq. 2.133 ( $m = 3$ , (Banisi and Finch, 1994)) and iteratively solve for  $d_b$  in Eq. 2.131. This gives a reasonable estimate of mean bubble diameter ( $< 1.5$  mm) in a flotation system as reported by Dobby et al., (1988), Yianatos et al., (1988) and Xu and Finch (1990). As these results show, mean bubble size is related to  $J_g$ ,  $J_1$ ,  $\varepsilon_g$  and frother type and concentration.

### 2.10. Interaction between Bubbles

The interaction between successive bubbles rising in the same vertical path has been studied by Crabtree and Bridgwater (1971), Narayanan et al., (1974), Otake et al., (1977), Bahaga and Weber (1980), Hahn and Slattery (1985), Dekée et al., (1986), Fan and Tsuchiya (1990).

There is a critical distance at which the leading bubble starts to exert a noticeable influence on the following one. This distance is about 3 to 4 times the diameter of the leading bubble. Coalescence can take place when more than about a half of the projected area of the following bubble is overlapping with that of the leading bubble. On the other hand, breakup may occur in the case where overlap is less than about a half of the projected area of the following bubble. Coalescence between bubbles is related to the bubble Reynolds number, vertical distance between bubbles (bubble frequency) and bubble surface properties in terms of surfactants. Tsuchiya et al., (1989) studied the coalescence between bubbles in a chain in liquid-solid fluidized bed. They found that the critical bubble spacing is around 5-7 times the bubble diameter.

The effect of bubble formation frequency on velocity has been studied by Garner and Hammerton (1954) and Marks (1973). For a fixed bubble size, and with increasing frequency, the bubble velocity increases because of the effect of the leading bubble wake on the trailing bubble. At high bubble Reynolds number, this effect is more significant. For example, the effect of frequency up to 20 bubbles/min on bubbles ( $d_b = 6$  mm) in

water is almost negligible, but this frequency has an effect on bubbles of 15 mm diameter (Marks, 1973).

### 2.11. Wall Effects

Data from several sources show that the bubble velocity can be affected by the ratio of bubble diameter to column diameter ( $d_b/D$ ). Generally, the error introduced in the determination of velocity by the wall effect is less than 1% if the column is more than 100 times the diameter of the bubble (Garner and Hammerton, 1954).

Grace (1973) suggested that the wall effects on bubble motion are negligible, when  $d_b/D \leq 0.074$ ,  $d_b/D \leq 0.113$  and  $d_b/D \leq 0.2$ , for the spherical, ellipsoidal and spherical-cap bubbles, respectively.

The magnitude of the wall effect, which is significant when  $d_b > 0.1 D$ , may be determined from a theoretical equation derived by Uno and Kintnerer, 1956 and Collins (1967). Generally, the bubble rise velocity ( $U_c$ ) in a column is lower than the bubble velocity ( $U_{if}$ ) in a liquid of infinite dimensions. The ratio of  $U_c$  to  $U_{if}$  (or  $k_1$ ) can be determined as a function of the ratio of  $d_b$  to  $D$  (or  $k_2$ ) (Wallis, 1969). Shen, 1994 summarized the following corrections for the relationship between  $k_1$  and  $k_2$ : for large inviscid bubbles, Collins (1967) derived

$$k_2 < 0.125 \quad k_1 = 1 \quad (2.134)$$

$$0.125 < k_2 < 0.6 \quad k_1 = 1.13 e^{-k_2} \quad (2.135)$$

$$k_2 > 0.6 \quad k_1 = 0.496 k_2^{-1/2} \quad (2.136)$$

while for bubbles treated as solid spheres in viscous fluids, Ladenburg (1907) derived

$$k_1 = (1 + 2.4 k_2)^{-1} \quad (2.137)$$

and, for fluid spheres with  $\mu_g \ll \mu_l$ , Edgar (1966) obtained

$$k_1 = (1 + 1.6 k_2)^{-1} \quad (2.138)$$

A slug is a bubble that fills the entire cross-section of the column, apart from a narrow annular gap through which water drains. Its rise velocity is given by:  $U_b = 0.35 (g D)^{1/2}$  (Hills and Darton, 1976). This equation applies when  $d_c$  is greater than about one third of  $D$ . When  $k_2$  increases to about 0.6, bubbles behave as slugs and obey the equation

$$k_1 = 0.12 k_2^{-2} \quad (2.139)$$

## CHAPTER 3

### BUBBLE SIZE AND VELOCITY ESTIMATION TECHNIQUES

Several techniques for measuring bubble size and velocity have been proposed based on such properties as "light", "electroresistivity" and "sound". These techniques are usually classified into optical, electroresistivity and ultrasonic categories.

#### 3.1. Optical Techniques

Based on the properties of reflection and refraction of light, the following methods have been used for detection of bubbles.

##### 3.1.1. Optical Fiber Probes

These probes have been widely applied to measure the size and rise velocity of bubbles. The probes can be single fiber or multiple fibers with one as light transmission and the others as detectors of the light penetrating through and being reflected off the bubbles.

##### *Single Fiber Probe*

Ishida and Tanaka (1982) used a single optical fiber method in a three phase fluidized bed (Fig. 3.1). To achieve total reflection, the end of the single fiber of probe C was made conical. The probes diameter was 350  $\mu\text{m}$  and probe C was set 2.9 mm above D. The received light was converted to an electrical signal by a photomultiplier and was recorded. Comparison of probes C and D showed that both probes gave an intense signal for bubbles but that only probe D gave particle signals (Fig. 3.2).

### *Multiple-Fiber Probes*

Bubble properties have been investigated using this technique by Glicksman et al. (1987). They used horizontal and vertical arrays of optical probes (three dimensional probe array) in three-phase fluidized beds. Two different fiber-optic probes were employed. The first fiber-optic probe consisted of two transmitter-detector pairs separated by a vertical distance of 1.9 cm. Each transmitter was separated horizontally from its corresponding detector by a 5 mm gap. A second optical probe was used to measure the width of voids in the three dimensional beds.

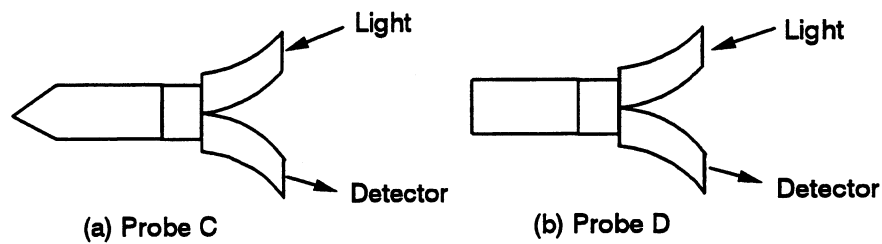


Figure 3.1: Single-fiber probes (Ishida and Tanaka, 1982).

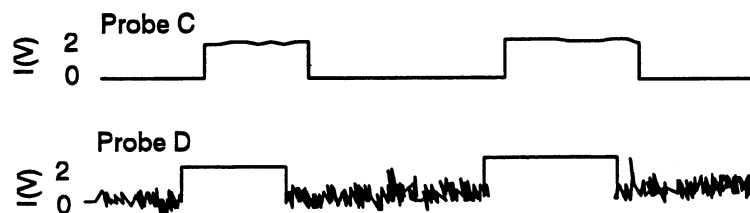


Figure 3.2: Comparison between probe C and D (Ishida and Tanaka, 1982).

### *Optical Detectors Using Capillary Tube*

A method for the measurement of the distribution of bubble sizes within a flotation cell has been described by Randall et al., (1989), O'Connor et al., (1990) and Tucker et al., (1991). The length and velocity of each bubble is measured by a pair of optical detectors in a brass block surrounding a capillary tube through which bubbles are drawn under vacuum (Fig. 3.3). As the bubbles pass the detectors they are monitored as a change in light intensity. The bubbles are then collected in a gas burette so that the total volume of bubbles is known. Up to 4000 bubbles may be collected for the determination of bubble size distribution. O'Connor et al., (1990) used this method for the measurement of the effects of physical and chemical variables on bubble size.

#### **3.1.2. Laser Beam Techniques**

Meernik and Yuen (1988a,b) reported an optical technique developed to determine the size distribution of bubbles in two and three-phase systems. This method involved passing a narrow laser beam through the system (Fig. 3.4) and monitoring the transmitted light intensity. In this case, the light beam diameter should be less than the diameter of the smallest bubbles for which data are desired. By assuming the distance of closest approach between any bubble center and beam axis to be random, a statistical analysis of the data collected yielded size distributions.

An array of three transmitted laser beams has been employed by Sung and Burgess (1987) for bubble detection. A sequence of light pulses was generated by this system when bubbles passed through the array. This sequence was analyzed by high-speed on-line logic to determine the bubble parameters. They used three 2 mW laser tubes in a triangular array and a series of six adjustable mirrors to control the orientation of the beams (Fig. 3.5). Figure 3.6 shows a typical example of the type of pulse sequence produced by the passage of a single bubble after preconditioning by high-

frequency filtering of the photocell output.

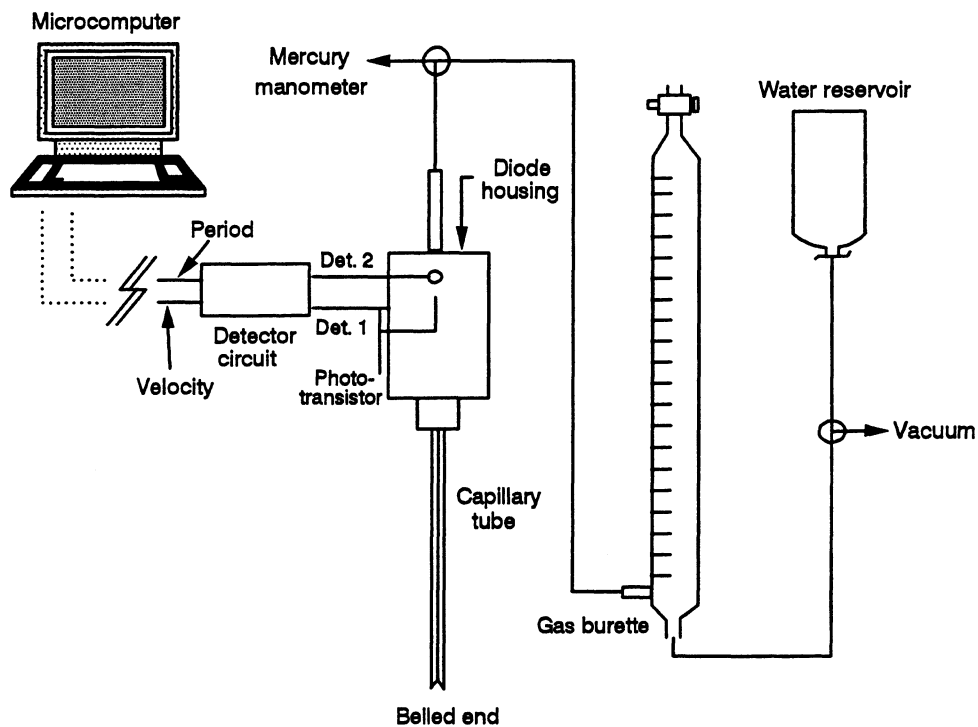


Figure 3.3: Schematic diagram of bubble-sizing apparatus (Randall et. al., 1989).

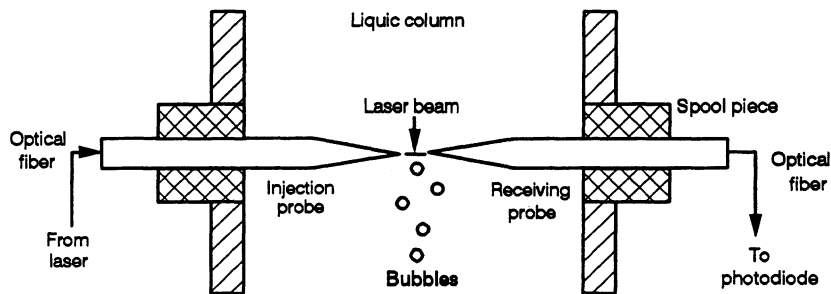


Figure 3.4: Laser beam method (Meernik, 1988).

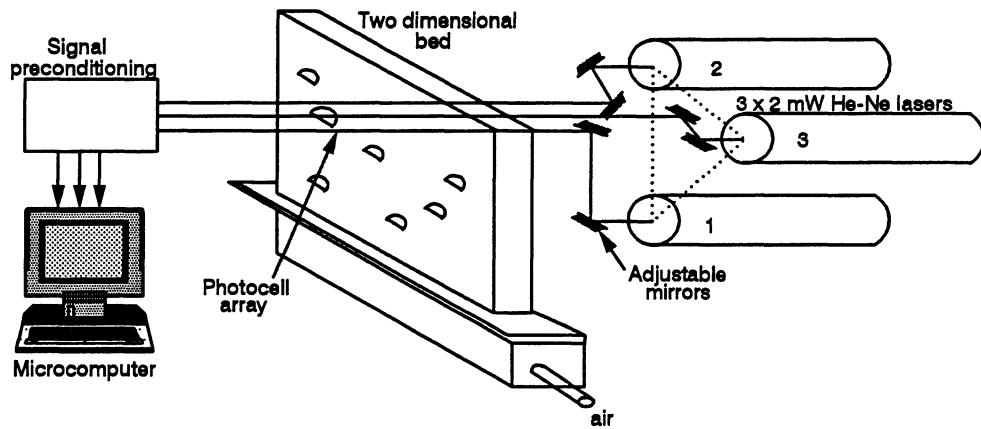


Figure 3.5: Three dimensional laser-beam system (Sung and Burgess, 1987).

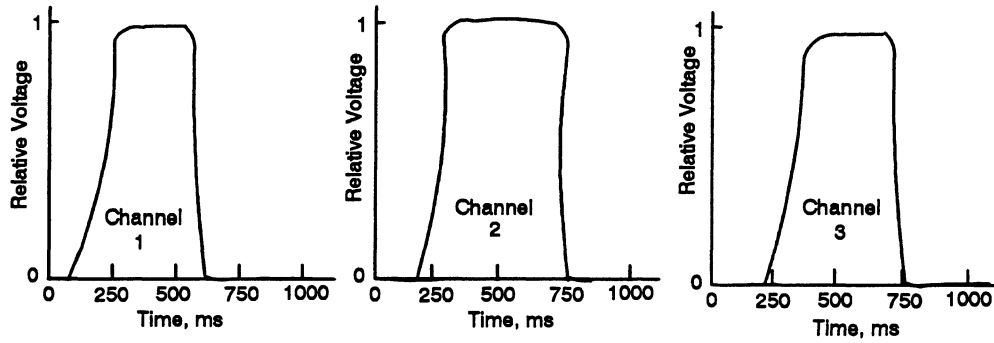


Figure 3.6: Typical pulse sequence (Sung and Burgess, 1987).

### 3.1.3. Photographic Techniques

The most common technique, photography, is used either directly or to calibrate a proposed alternative method (Dobby and Finch, 1987).

Kuehn Walker et al. (1991) used this method with automated image analysis to give mean bubble size and bubble size distribution. They used a special bubble measurement cell, designed to allow regular upward movement of captured bubbles, free from the turbulence within the column (a vacuum system was included). An image was obtained using a camera. To analyze the photographs, a Brinkman image analyzer was used. The image, acquired with a video camera, was transferred to a grey level image on a monitor with a resolution of  $500 \times 400$  pixels.

The rising bubble and its wake have been examined in two-dimensional liquid-solid fluidized beds by Kitano and Fan (1989). They used both optical fiber probe and video camera methods.

Lim et al. (1990a) have developed a method based upon digital image analysis using the video camera. The bubble parameters were investigated in a two-dimensional gas-fluidized bed. The analog signals of the image from the video camera were digitized by a frame grabber (image digitizer). The digitized image was subsequently displayed on the video monitor and the measurements were transferred automatically onto the data worksheet.

High speed cinephotography technique has been used by Saxena et al. (1990) for obtaining bubble properties under different conditions. They used black and white film at a recording speed of 1000 pictures per second. They measured the bubble size distributions for the air-water system as a function of gas velocity.

#### 3.1.4. X-Ray Photography Technique

Single bubble size and velocity in a gas-solid fluidized bed has been measured by Rowe and Matsuno (1971) using an X-ray method. The bed vessel was made of aluminum (because of its transparency to X-rays). The powdered materials used were soda glass Ballotini and crushed quartz. Bubble rise velocity was calculated from the change in vertical position of the bubble center between adjacent frames and from the known film speed.

A gamma-ray-attenuation method was studied by Nassos (1963). This technique employed a radioactive source and a crystal detector. The strength of the attenuated beam passing through the stream is a function of the stream density and, therefore, is related to the void fraction.

#### 3.2. Electroresistivity Techniques

These methods are based on the difference in electrical conductivity between the liquid and the gas phase (Castillejos and Brimacombe, 1987; Igusti-Ngurah, 1989). When the bubble contacts the probe tip, the resistance between the probe and ground will change.

##### 3.2.1. One Element Probe

The resistivity probes used by Herringe and Davis (1974) were stainless steel surgical needles spot welded to an insulated wire housed in a stainless steel support tube and insulated by Araldite epoxy resin, except for the tip. The resistance between the needle and ground indicates the phase surrounding the tip, provided the continuous phase is an electrical conductor.

A microcomputer-aided one-element electroresistivity probe technique has been

developed (Otero and De La Fuente, 1991) to determine simultaneously various parameters which characterize bubbles and drops in flotation and solvent extraction processes, such as: frequency, velocity and diameter (Fig. 3.7). In this case, the rise velocity corresponds to the velocity at which a bubble or drop is pierced by the sensor electrode tip; in other words, transit time and pierced length are the main parameters involved.

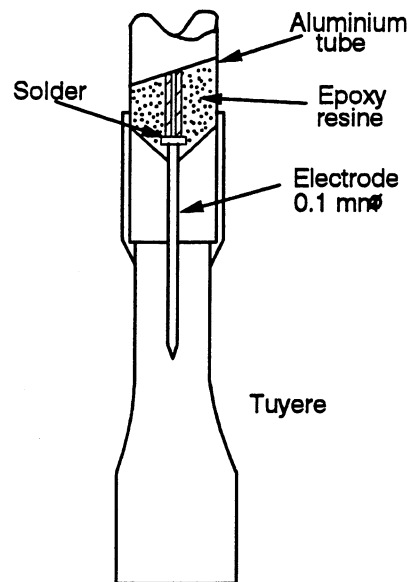


Figure 3.7: Scheme of the sensor probe, one-element (Otero et al., 1991).

### 3.2.2. Two-Element Probe

The two-element electroresistivity probe was studied by Castillejos and Brimacombe (1987). Knowing the vertical distance between two probe tips, then by comparing the signals from channel A and B (Fig. 3.8) the time of bubble travel between these tips can be determined. By this method the bubble velocity and pierced length can be obtained.

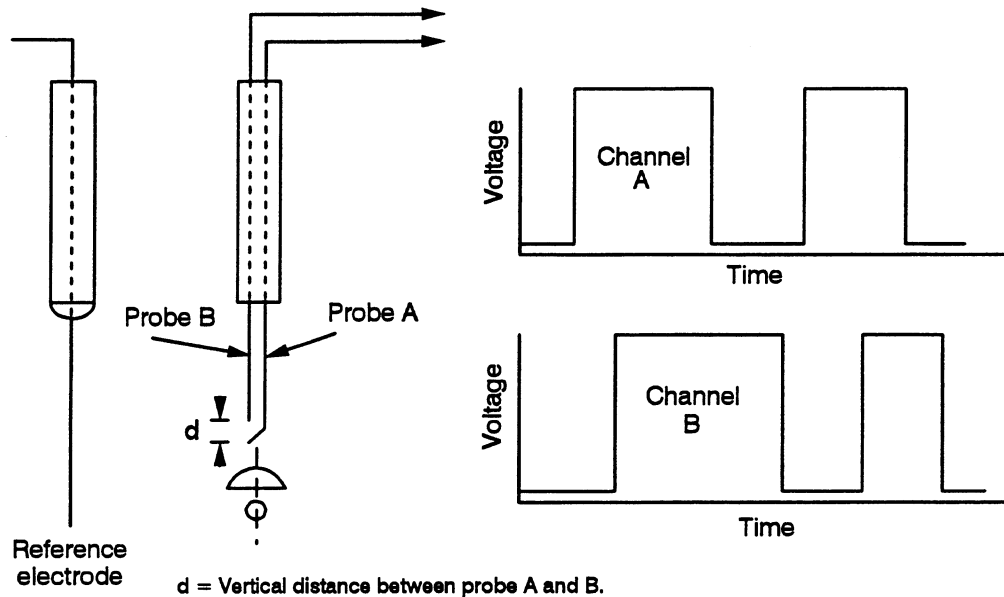


Figure 3.8: Two-element probe (Castillejos, 1986).

### 3.2.3 Multi-Element Probe

A three dimensional resistivity probe with five channels was designed by Burgess and Calderbank (1975) in order to sense the bubble local interface approach angle as well as to measure the bubble size and velocity in three-phase and three dimensional fluidized-beds. This device has been coupled to a high speed digital computer with facilities for rapid, accurate conversion of analog voltage signals to discrete binary numbers and with software to undertake logical decisions consequent to the spatial orientation of the bubble with respect to the probe axis.

### 3.3. Ultrasonic Techniques

It is known that bubbles have a resonance frequency that is inversely proportional to the radius of the bubble. This fact has been exploited for detection and estimation of bubble size by different methods including: resonant scattering, second harmonic generation and double frequency techniques.

The sound of air bubbles at a nozzle was investigated by Strasberg (1956), who showed experimentally that gas bubbles, when entrained in water or other liquids, can generate high sound pressures. Significant sound pressure is associated with volume pulsation of the bubble. Bubbles are excellent sound scatters and have a characteristic resonant frequency dependent on their sizes (Cathignol et al., 1990).

#### 3.3.1. Resonant Scattering Method

A resonant scattering method was studied by Nishi (1972) to detect gas bubbles in blood circulatory systems during hyperbaric decompression. In this case, transducers consisted of two piezo-electric elements mounted at some angle to the direction of the blood flow (Fig. 3.9). A continuous signal was transmitted by one element and reflected back to the other element by particles in the blood. Since these particles are in motion, the frequency of the reflected signal differs from that of the transmitted signal (Doppler effect), the difference being proportional to the velocity of the particles. This method accurately detects bubbles and gives a crude estimate of size. This technique have been used by Commander and Moritz (1989) for estimation of bubble densities (populations) in the surface and subsurface layer of the oceans.

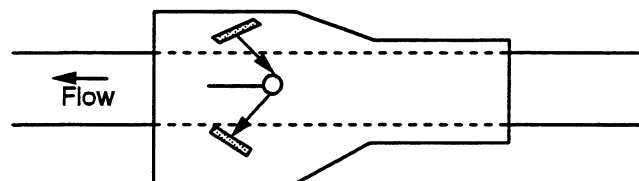


Figure 3.9: Configuration of Doppler blood-flow transducer (Nishi, 1972).

### 3.3.2. Second Harmonic Method

This ultrasonic detection method is based on the non-linear emission of harmonics by bubbles pulsating in an ultrasonic field. A device (Fig. 3.10) has been constructed (Miller, 1981) to detect resonant bubbles in a flowing liquid by monitoring second harmonic responses to a low amplitude, 1.64 MHz, ultrasonic field. This technique is much better (twice the driving frequency and strong harmonic at low amplitudes) than the first-harmonic scattering method for counting resonant bubbles. However, this technique still gives inaccurate size measurements.

### 3.3.3. Double Frequency Technique

The theory established by Doppler in 1842 (the Doppler effect) states that the rate of change in distance between a receiver and a radiation source determines the change in frequency (Graf, 1984). A double frequency technique was studied by Newhouse and Shankar (1984), Chapelon et al. (1985a,b, 1987), Shankar et al. (1986) and Cathignol et al. (1984, 87, 88, 90) for the determination of bubble properties. The double frequency method is efficient for the non-invasive estimation of bubble size distributions (and for the accurate measurement of pressure changes in fluids). In this technique, a "pumping" field of low frequency  $F_2$  and an "image" field of higher frequency  $F_1$  are used (Fig. 3.11). The radiated field then contains the sum and difference of frequencies,  $F_1+F_2$  and  $F_1-F_2$ . These sum and difference of frequencies exhibit a single unambiguous peak as a function of the bubble radius. This method can be used for detection and sizing micro bubbles accurately.

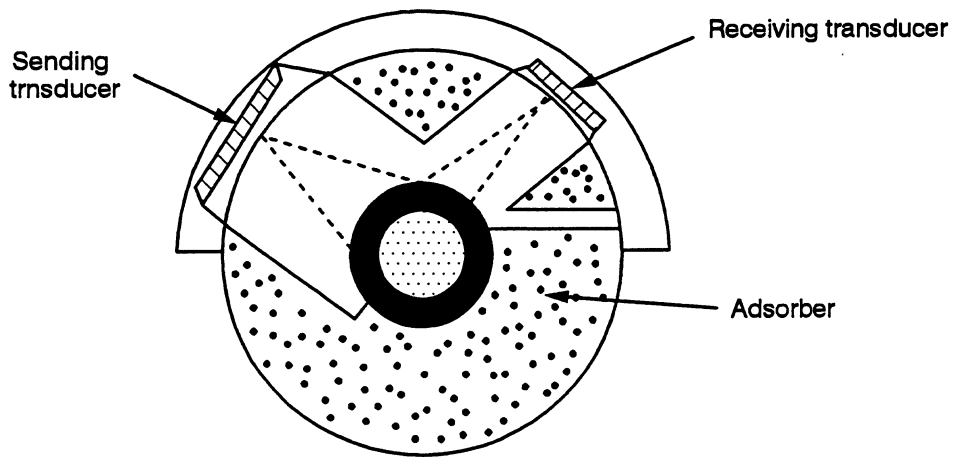


Figure 3.10: Second harmonic technique device (Miller, 1981).

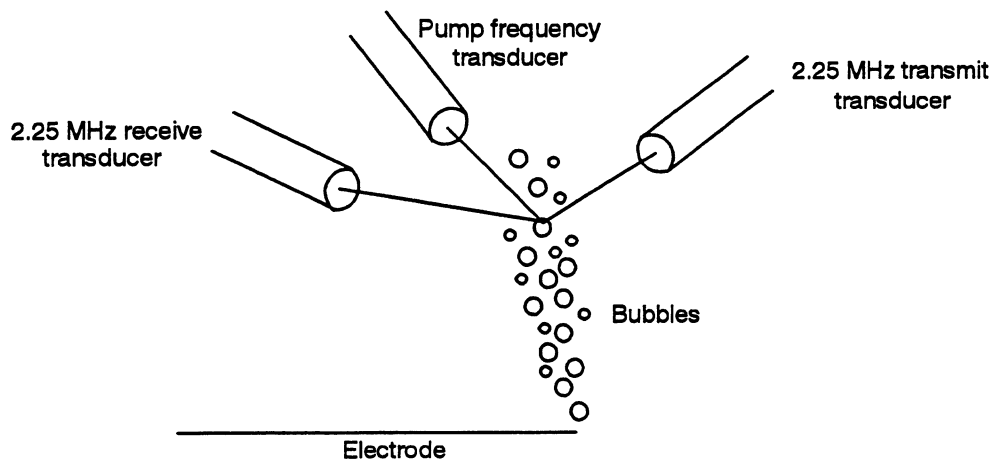


Figure 3.11: The double frequency technique (Chapelon, 1985).

### 3.4. Discussion

In the case of the electroresistivity probe, it is well documented (Nassos, 1963; Burgess and Calderbank, 1975) that a resistivity or capacitance element when struck by a bubble, produces a voltage pulse which is not square due to probe wettability effects. In gas-liquid systems this is due to the finite rate of liquid film thinning at the element tip. The total time taken to signal the change from liquid to gas may amount to a significant fraction of the pulse duration.

In beam (e.g., lasers) intersection techniques, the signal voltage decreases upon intersecting with the bubble from  $v_1$  to  $v_2$ , this difference ( $\Delta v$ ) being proportional to the chord length. After the bubble has passed through the beam, the voltage returns to  $v_1$ , and this time ( $\Delta t = t_2 - t_1$ ) is inversely proportional to the bubble velocity. The beam does not always intersect the bubble at its center, i.e., a chord length smaller than the largest vertical dimension is typically measured (Fukuma and Muroyama, 1987; Clark and Turton, 1988; Lim et al., 1990b). This problem is a disadvantage with these techniques for bubble sizing.

To solve this problem and measure the actual bubble size/velocity, a novel technique was contemplated by the author (Sam, 1993). This method was called "Laser Plane Technique". A laser plane was created by using the set-up in Fig. 3.12. A power supply, an He-Ne laser (10 mW), some cylindrical glass lenses, one detector, an amplifier, some mounts, carriers, post holders and optical rails were used with a 486 computer and high speed data acquisition system written in Quick-BASIC. Preliminary work showed that the laser plane was sensitive to the passage of bubbles and the signals were distinguishable from noise. More work was required to get clean signals and extend the technique for use at different levels in a column. It is apparent that while the method is suited for measuring the size/velocity of bubbles in a chain it cannot be applied for measuring the bubble shape and path.

Photography is a common, direct and relatively accurate technique for predicting all bubble behaviour characteristics. In the present study, we opted for this method since it was also well suited for our specific purpose, measuring the bubble velocity at different positions in the column. The major drawback of this technique is the considerable time and effort required to analyze the film (or video tape).

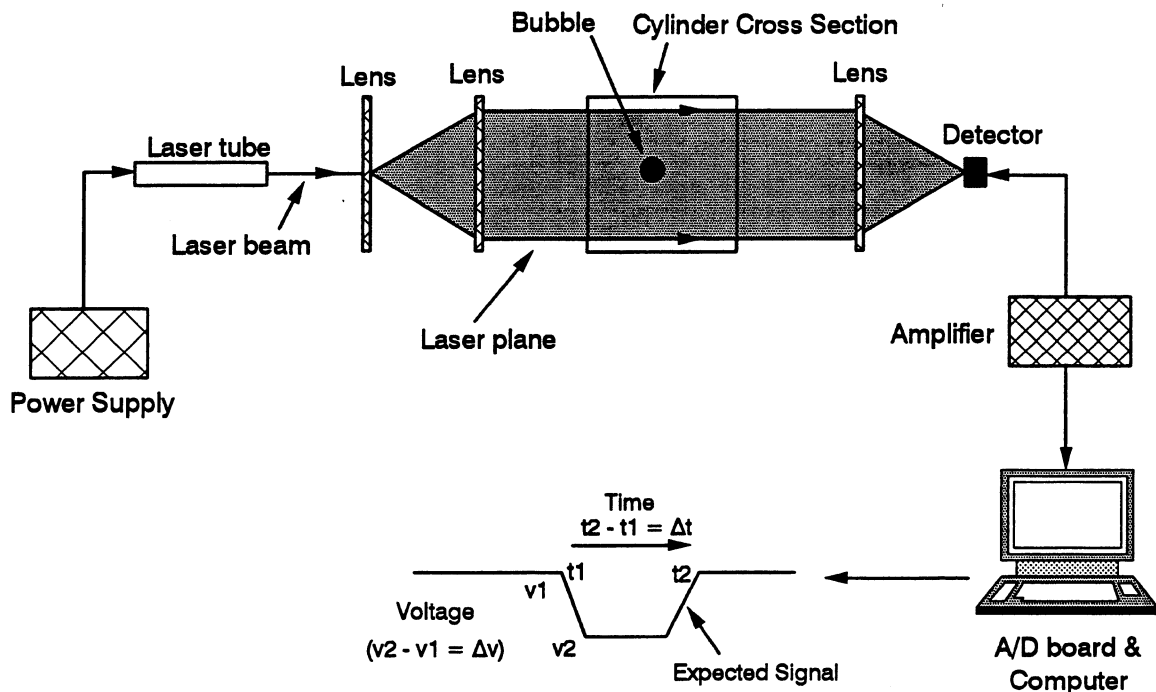


Figure 3.12: Laser plane technique (plan view).

## CHAPTER 4

### EXPERIMENTAL EQUIPMENT AND PROCEDURES

To detect the single bubble characteristics during its rise in a tall column, it was necessary to have an experimental system where the test liquid did not disturb the bubble and the bubble did not disturb the test liquid, and which would provide a photographic record of the bubble motion.

#### 4.1. Column Set-up

A water-jacketed transparent Plexiglas square column ( $10 \times 10 \times 400$  cm) was used (Fig. 4.1). The wall thickness was about 7 mm and the water-jacket was 2 cm wide and completely enclosed the column except for the top and bottom. A square cross-section was chosen to avoid optical distortion. The column was selected large enough ( $d_b/D < 0.03$ ) not to have significant effects on the behaviour of bubbles  $< 3$  mm (see Section 2.11). A fiberglass measuring tape was placed along the central axis of the column to measure the size, local velocity and the oscillation frequency of the bubbles.

#### 4.2. Temperature Control

Bubble behaviour is affected by temperature gradients in the system. In fact the gas-liquid properties such as viscosity, surface tension and density and consequently the fluid flow properties around the bubble are influenced by temperature (see Section 2.8.3). Surfactant adsorption (rate and extent) will also vary with temperature. To measure the temperature along the column, seven thermistors (Omega, OL-710 PP) were installed (Fig. 4.1), three ( $T_0$ ,  $T_1$  and  $T_2$ ) inside the column (for test liquid), three ( $T_3$ ,  $T_4$  and  $T_5$ ) outside (for room temperature) and one ( $T_6$ ) inside the tank (for water in the jacket).

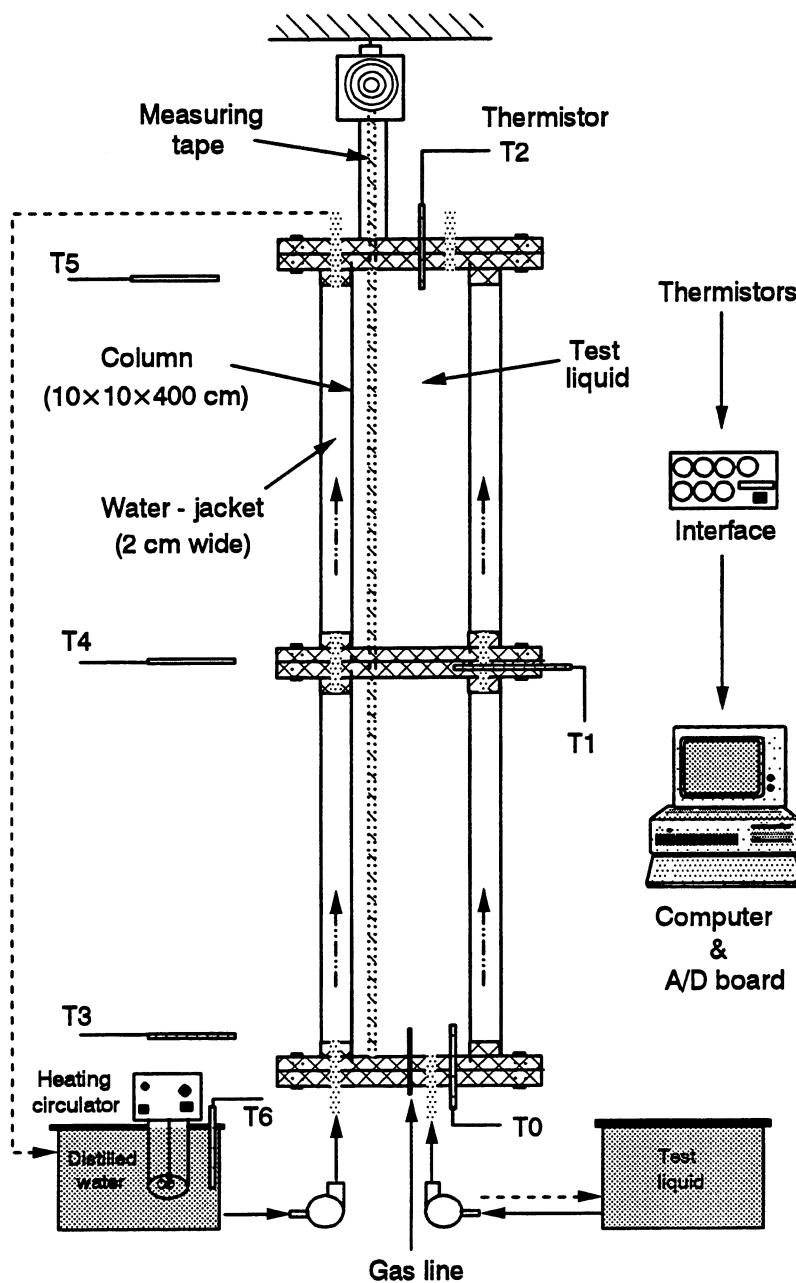


Figure 4.1: Schematic of the column set-up and water temperature control device.

To read and save the temperature data during the experiments, a Quick-BASIC data-acquisition program (Appendix 1) was developed. The hardware included: interface with seven channels (to convert the thermistor output,  $\Omega$  to voltage), a 486 computer (IBM compatible) and a data acquisition board (Omega, CIO-AD16JR). The thermistors, which were linear response probes, were calibrated against an accurate ( $\pm 0.1$  °C) thermometer. Figure 4.2 shows the calibration diagram (temperature versus output voltage) of one of the thermistors ( $T_1$ ).

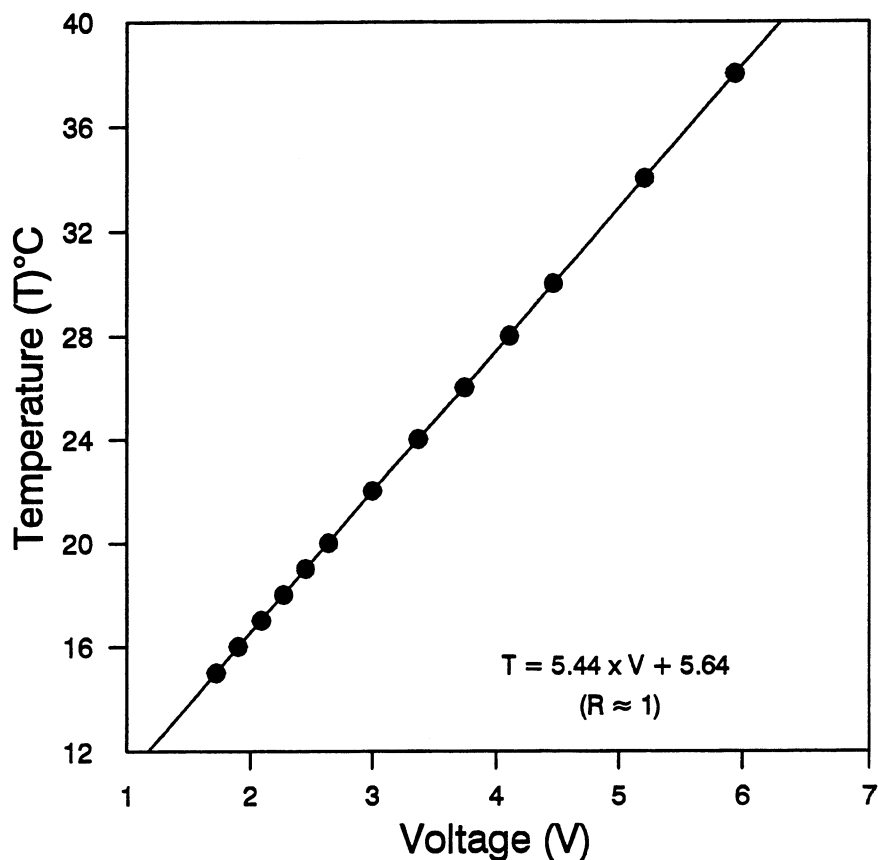


Figure 4.2: Calibration diagram of the thermistor no. 1 for channel no. 1 (as an example).

Figure 4.3 shows the schematic of the water temperature gradients in the column compared to the room temperature for a period of time. As this figure shows, the water temperature gradients inside the column were related to the room temperature which was variable, non-uniform and uncontrollable. To eliminate the effect of temperature variation on bubble behaviour, it was important to provide a uniform and constant temperature in the 4 m column.

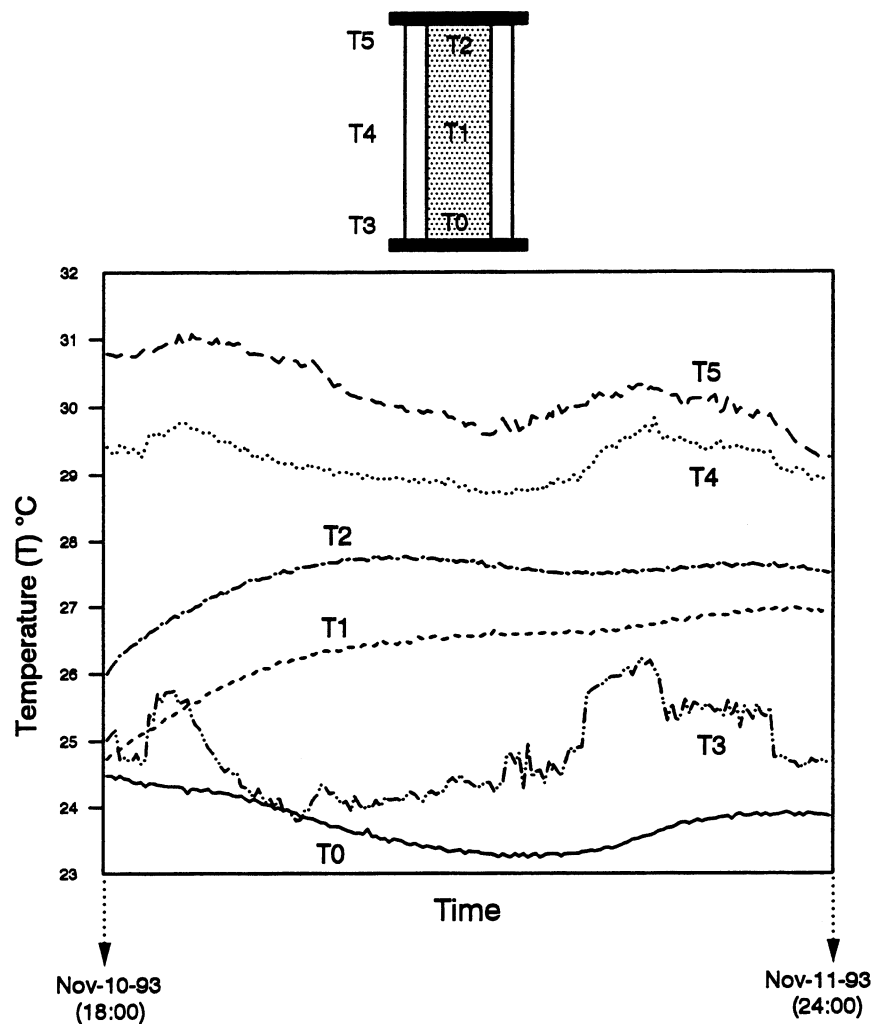


Figure 4.3: Water (in the column) and room temperature at three locations as a function of time (no temperature control).

The test liquid temperature was controlled by water circulation in the jacket. By measuring it over a period of time, it was found that 30 °C was the maximum temperature encountered and thus the easiest to maintain with the available control system. Distilled water (to keep the jacket walls clean) was set at 30°C using a heating circulator in the tank during circulation in the jacket. Figure 4.4 shows the test liquid temperature gradients after starting the circulation over a 24 hour period. The temperature was held constant and uniform at  $30 \pm 0.25$  °C over the length of the column.

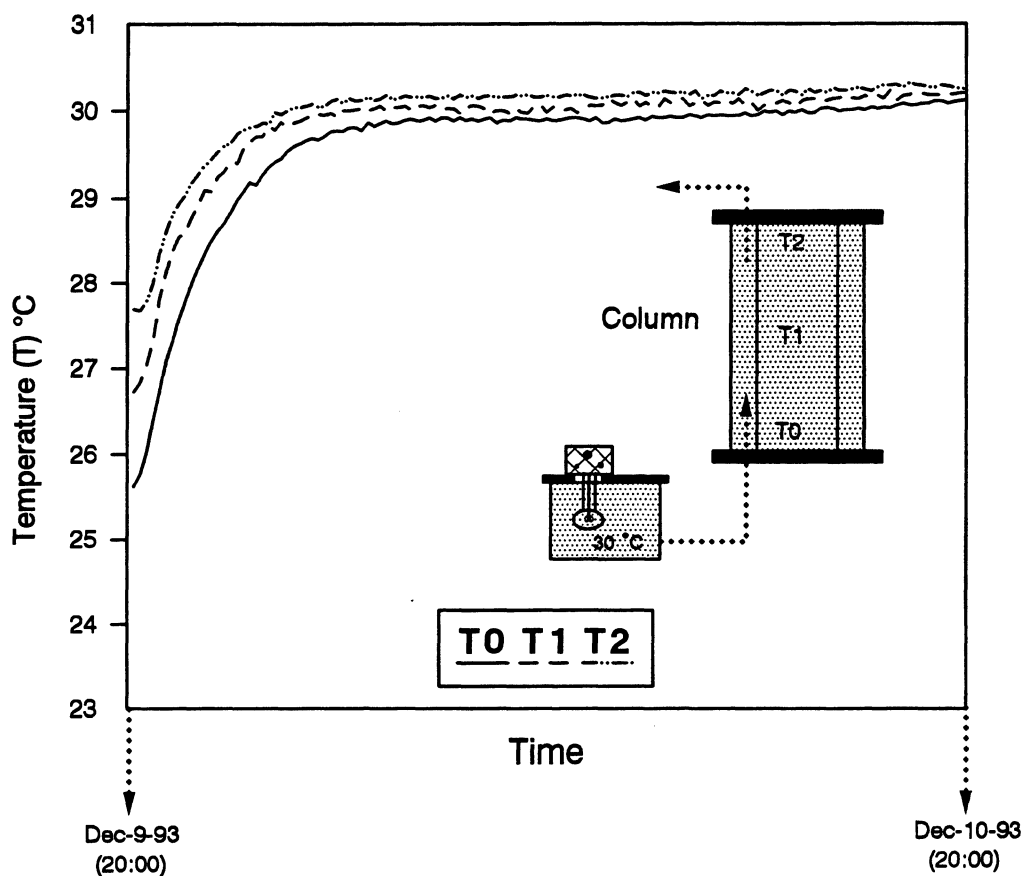


Figure 4.4: Temperature in the column at three locations as a function of time with temperature control at 30 °C. The system gave a constant and uniform temperature.

### 4.3. Gas Line

To produce single bubbles of a size relevant to flotation (0.5-3 mm) and to prevent interaction between bubbles in a chain (see Sections 2.7.1 and 2.10), it was necessary to provide a gas line system capable of giving a low bubble generation frequency. This comprised a compressed air cylinder, stainless steel tubes (1 and 0.12 mm), pressure gauge, micro valve and glass capillary tubes (Fig. 4.5). Four glass capillary tubes with circular orifices and sizes: 17, 70, 203 and 508  $\mu\text{m}$  (each with outside diameter  $\approx$  3 mm and length  $\approx$  15 cm) were used (see Section 5.1.3). The bubble generation frequency (bubbles/min) was adjusted by the micro valve located in the gas line. Bubble frequency was measured from video tape ( $\pm$  1 bubble/min). It was found that for bubble sizes  $<$  3 mm, the effect of bubble generation frequency up to 25 bubbles/min on bubble velocity was negligible (see Section 5.1.1).

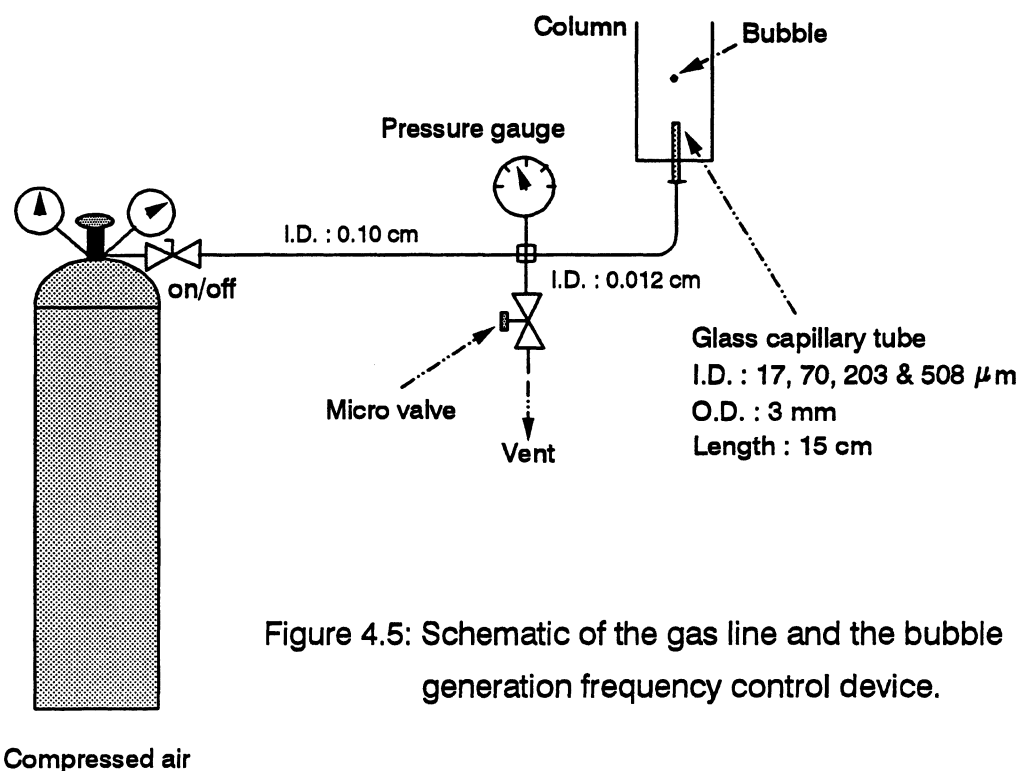


Figure 4.5: Schematic of the gas line and the bubble generation frequency control device.

#### 4.4. Camera Moving Device

A video camera was used to track the single bubble during its rise. In order to follow the bubble from the moment of leaving the orifice to the top of the column, a variable speed motor driving a chain belt over a pulley with a counterweight was used to move the camera (Fig. 4.6). This arrangement is referred to as a "mobile video camera". Limit switches were placed at the bottom and top of the column to stop the movement. Movement was controlled manually through the motor speed controller over a range from zero to 50 cm/s.

A high resolution CCD (Charged Coupled Device) video camera recorder (Sony, Hi8-V801), a video monitor (Sony, PVM-1340) and a color video printer (Sony, CVP-G700) were used to collect the data on bubble velocity and motion, and approximate size and shape.

The video camera included a frame controller, time code generation (hour, minute, second and frame number) and variable shutter speed (up to 1/10,000 of a second). The system recorded 30 frames per second. With a shutter speed of 1/60 of a second (normal shutter speed) the bubble image was elongated. To obtain the actual shape (and size) of the bubble, a shutter speed 1/1000 of a second was used. A stationary camera (Canon, EOS-1000F) was used to determine the bubble size and shape more precisely.

#### 4.5. Procedures

The column was filled with water at an initial temperature between 29 and 30 °C while the water in the jacket was circulating at 30 °C. The water temperature was uniform and constant after about 40 min. The single bubbles were released ( $\leq 25$  bubbles/min) from the orifice of a selected glass capillary tube.

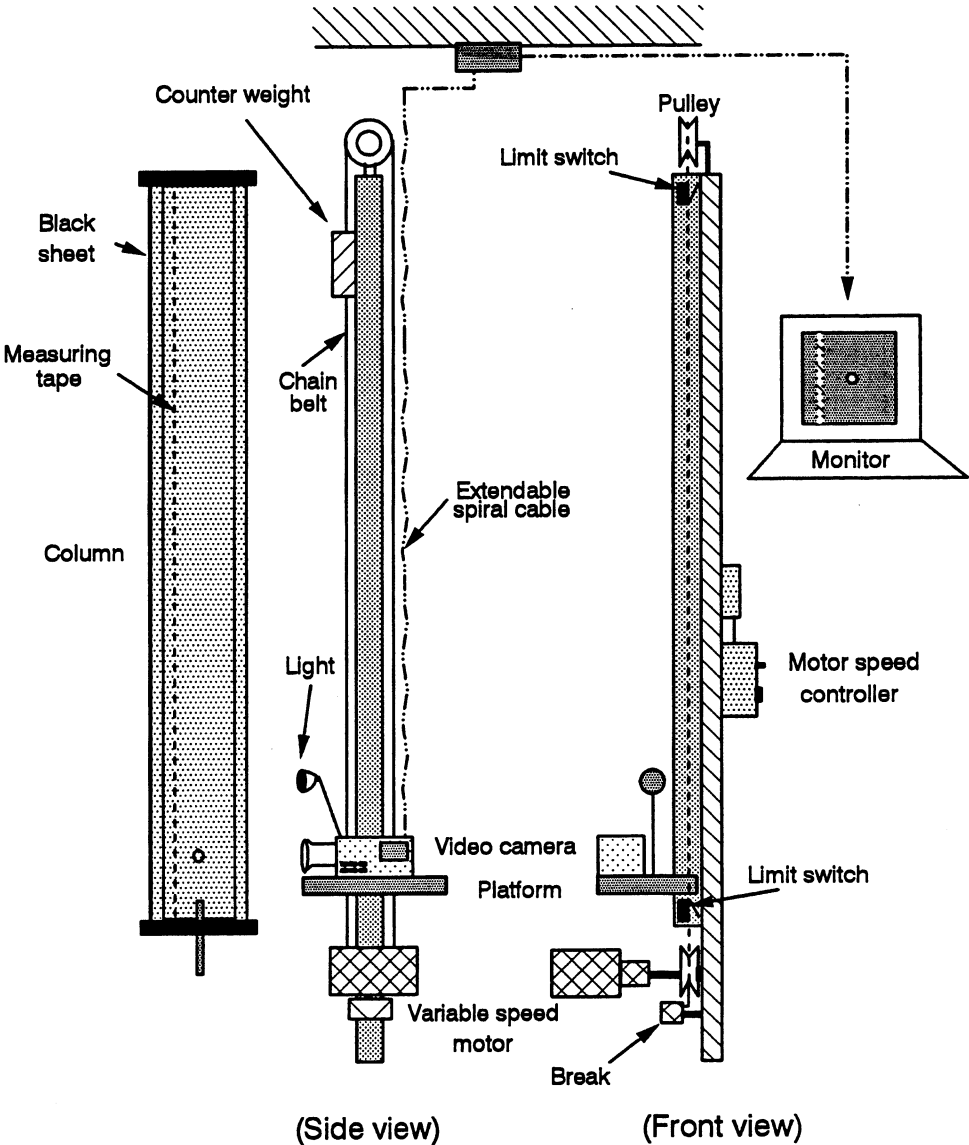


Figure 4.6: Schematic of arrangement for video camera to follow the bubble motion.

It was observed that after first introducing water in the column, a small bubble (e.g., 0.9 mm in diameter) had a rocking motion (variable horizontal distance between bubble and measuring tape during its rise) due to water temperature gradients and turbulence. The bubble motion was quite rectilinear after 40 min and indicates that the water was stagnant.

The experiment was initiated by activating the mobile video camera at the moment the bubble left the orifice. The image was displayed on a monitor continuously and the experimenter adjusted the speed to maintain the image at approximately the center of the field of view. The field of view was about 8 cm and it proved quite easy to follow the bubble during its rise.

After recording, the images were freezed frame by frame on the monitor. The data were obtained from the printed pictures or directly from the screen. The magnification of images on screen was 2.5. Using a piece of transparent graph paper attached on the screen, it was relatively easy to distinguish the position of the bubble center in  $1/5$  of mm on the high resolution monitor screen. Every frame contained a time code and the measuring tape for reference. The horizontal distance between bubble and measuring tape determined the bubble rise path. The vertical displacement moved by a bubble in  $1/30$  of a second (one frame) was determined to calculate the local velocity. This was repeated as a function of distance (time) from the orifice to the top of the column (4 m) to give the "velocity profile". Figure 4.7 shows the method of measuring the local velocity of a single bubble at any time in its motion. The bubble rise path (amplitude and frequency of motion relative to the vertical path) was also determined. In all experiments an audio recording of the test conditions was made which was helpful for later analysis.

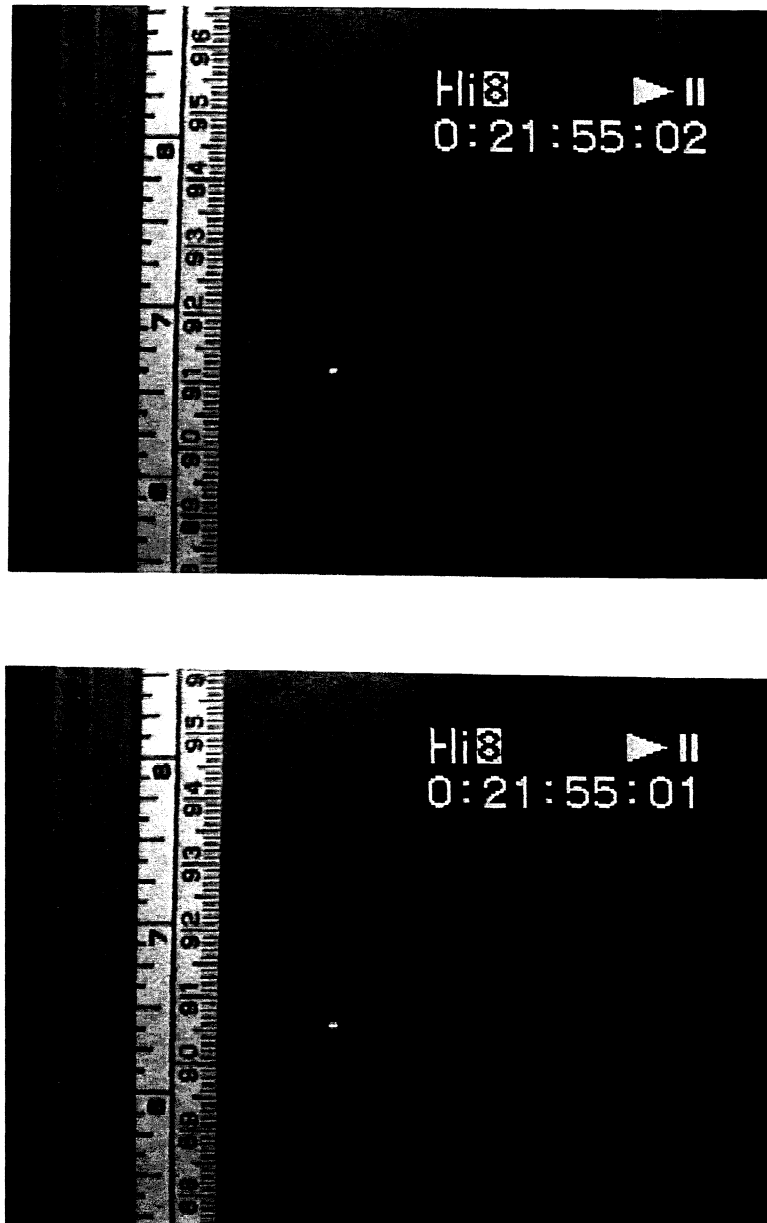


Figure 4.7: Bubble position in consecutive frames ( $1/30$  s): distance moved is measured on measuring tape (0.6 cm), therefore local velocity is 18 cm/s.

## CHAPTER 5

### RESULTS

#### 5.1. Bubble Size, Shape and Path

##### 5.1.1. Effect of Bubble Generation Frequency

Figures 5.1a and b show the effect of bubble generation frequency on bubble velocity at given positions: about 20 and 400 cm above the orifice, respectively. In these experiments two video cameras were located at these positions. Tap water was used at uniform and constant temperature (30 °C). The velocity was determined by measuring the vertical displacement moved by a bubble in 1/3 of a second (10 frames). The maximum error was  $\pm 0.12$  cm/s. The single bubble was defined as the first bubble in the chain of bubbles, i.e., in the absence of any leading bubble. Bubble frequency up to 80 bubbles/min had little effect on velocity: a frequency  $\leq 25$  bubbles/min was selected (also see Section 4.3). In general, operating at a given set of conditions (see Section 4.5), individual bubbles in the chain showed the same behaviour and the vertical distance between consecutive bubbles ( $> 75$  cm) was maintained constant during their rise.

##### 5.1.2. Test Liquid Properties

The water density, viscosity and surface tension (in contact with air) were measured in a thermostated bath, at 30 °C. The water density was  $0.988 \pm 0.002$  g/cm<sup>3</sup> measured using a Pycnometer. The water viscosity was  $0.0085 \pm 0.0003$  g/cm.s measured using an Ubbelohde Viscometer (Fisher Scientific). The measurements indicated that the effect of frother dosage (up to 100 ppm in this study) on water density and viscosity was negligible.

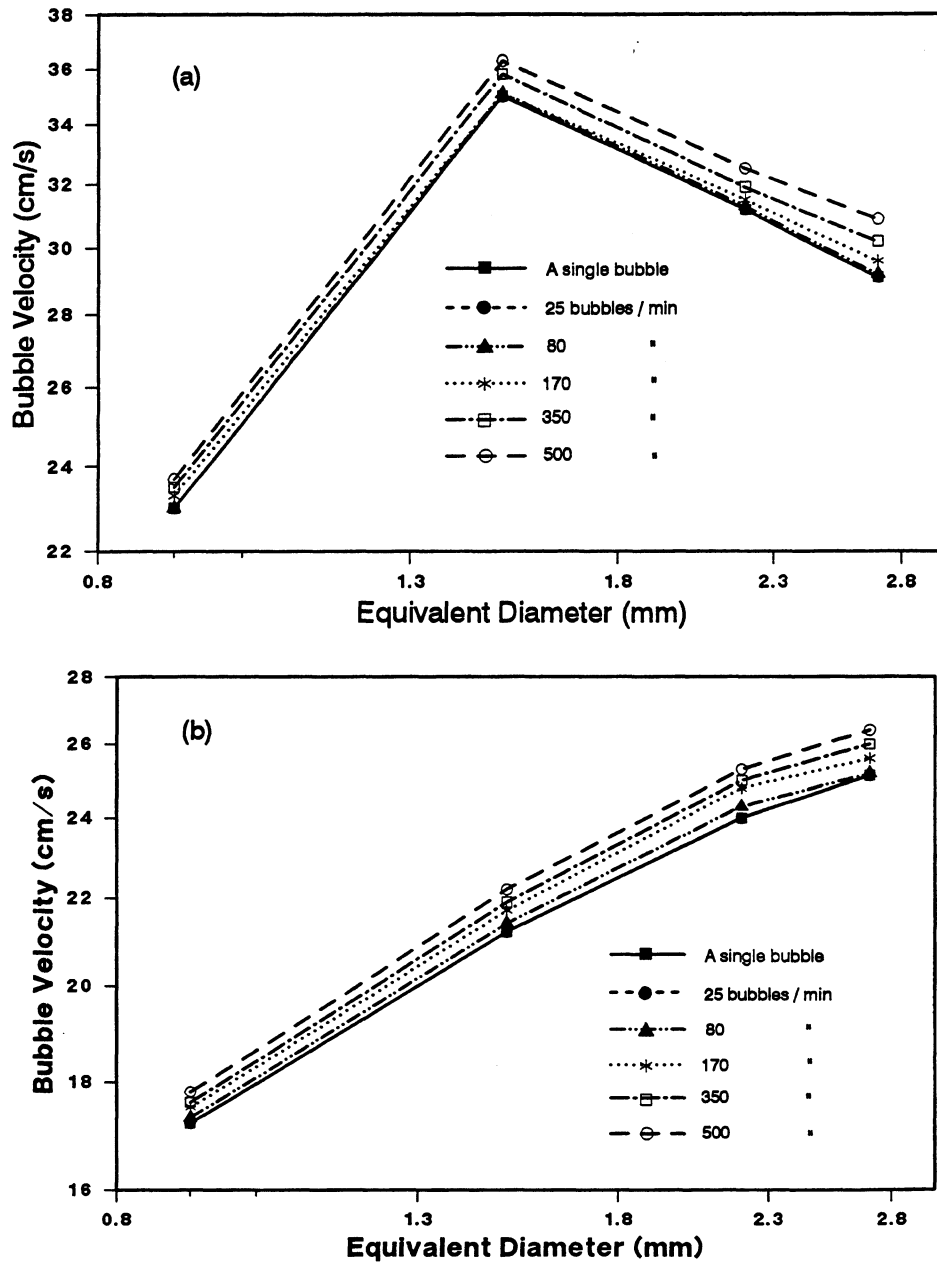


Figure 5.1: The effect of bubble generation frequency on velocity in tap water at locations:  
 (a):  $\approx 20$  cm above the orifice,  
 (b):  $\approx 400$  cm above the orifice.

The effect of three frothers on bubble motion was studied. These frothers were: MIBC (methyl isobutyl carbinol) from Aldrich Chemical, Dowfroth 250 (methoxy polypropylene glycols) from Dow Chemical and pine oil from Matheson Coleman and Bell. The frothers were used as supplied with no further purification.

The surface tension of water was measured for various frother concentrations using a tensiometer (Fisher Autotensiomat 215). Table 5.1 shows the frother specifications (Crozier, 1992; Laskowski, 1993; chemical reagent catalogues) and Figs. 5.2a and b show the measured surface tension of water-frother solutions as a function of concentration at 30 °C. Two micro syringes of 25 and 500  $\mu\text{L}$  were used to add the frother. Also, methanol ( $\text{CH}_3\text{OH}$ ), one collector (potassium ethyl xanthate,  $\text{C}_2\text{H}_5\text{OCS}_2\text{K}$ ) and two modifiers (lime,  $\text{CaO}$  and soda ash,  $\text{Na}_2\text{CO}_3$ ) were used (see Section 2.2). Values for air density = 0.0013  $\text{g}/\text{cm}^3$ , air viscosity = 0 and the acceleration due to gravity = 981  $\text{cm}/\text{s}^2$  were assumed.

**Table 5.1: Frother specifications.**

Frother	General formula	Molecular weight g/mole	HLB*	Density $\text{g}/\text{cm}^3$	Water solubility g/l
MIBC	$\text{C}_6\text{H}_{13}\text{OH}$	102	6.1	0.80	slight ( $\approx 17$ )
Dowfroth 250	$\text{CH}_3-(\text{O}-\text{C}_3\text{H}_6)_4-\text{OH}$	264	7.8	0.98	total
Pine oil	$\text{C}_{10}\text{H}_{17}\text{OH}$	154	5.4	0.92	slight ( $\approx 2$ )

\* Hydrophile-Lipophile Balance (Laskowski, 1993).

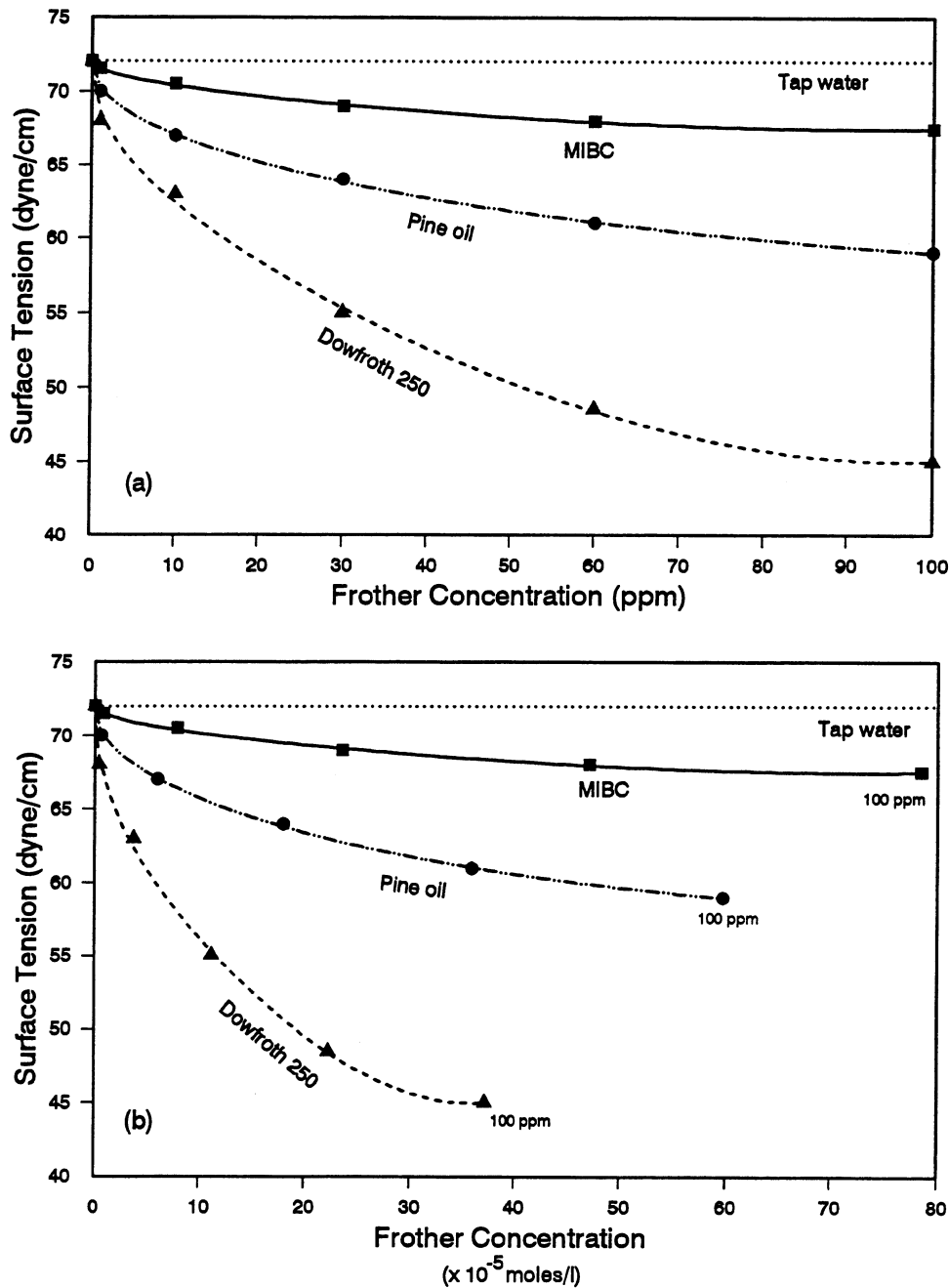


Figure 5.2: Relationship between surface tension of solutions and concentration (a: ppm, b: mole/l) of the three types of frother at 30 °C.

### 5.1.3. Bubble Size and Shape

The bubble axes (major,  $b$  and minor,  $h$ ) were measured using a stationary camera (see Section 4.4). The sphere volume equivalent diameter ( $d_e$ ) was calculated using Eq. 2.61 (see Section 2.7.1). The bubble size was also predicted by Tate's Law from Eq. 2.63 (see Section 2.7.1).

The surface tension of water was measured as 72 dyne/cm (Figs. 5.2a and b). A Scanning Electron Microscope (SEM - JEOL - JSM 840A) was used to measure the diameter of the glass capillary tube orifices. Since the glass tubes were not electrically conductive, they were coated with a very thin layer of Au/Pd, using an Ion Sputtering machine (HUMMER VI) for 10 min. The orifices of the glass tubes were circular. Figure 5.3 shows the inside diameter of the 17  $\mu\text{m}$  glass capillary tube.

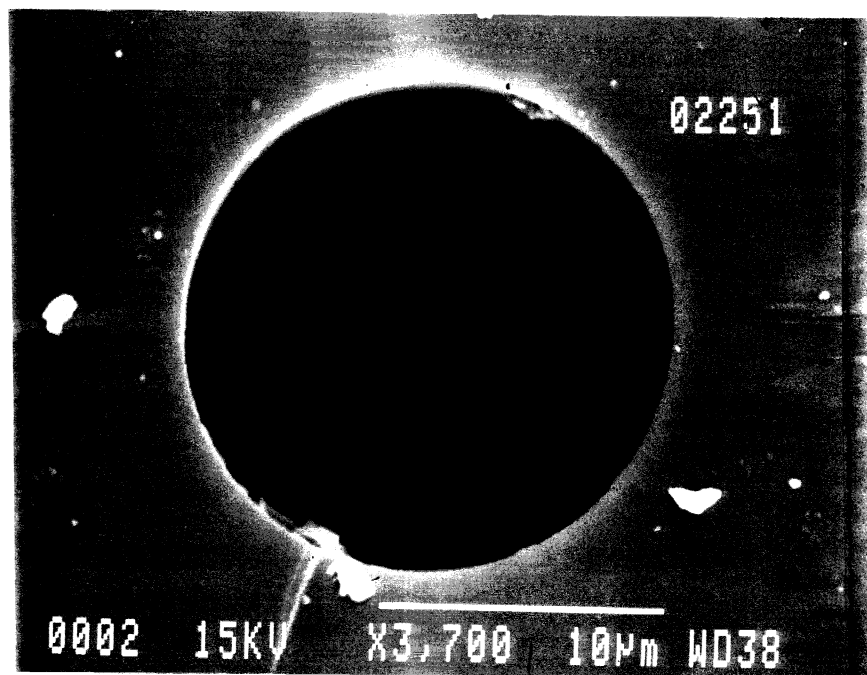


Figure 5.3: Inside diameter of the glass capillary tube (SEM micrograph).

Tables 5.2a and b show the orifice sizes and the bubble sizes measured about 20 and 400 cm above the orifice in tap water and in the presence of frother (30 ppm), respectively. The predicted bubble sizes from Tate's Law are included.

**Table 5.2a: Bubble size measured about 20 and 400 cm above the orifice in tap water and predicted from Tate's Law ( $\pm$  refers to standard deviation).**

Orifice I.D.  $\mu\text{m}$	Bubble size								
	$\approx 20$ cm above the orifice					at top ( $\approx 4\text{m}$ )			
	b mm	h mm	b/h	$d_e$ measured mm	Tate's Law mm	b mm	h mm	b/h	$d_e$ measured mm
$17 \pm .7$	0.9	0.8	1.1	$0.9 \pm .05$	0.9	0.9	0.9	1.0	$0.9 \pm .07$
$70 \pm .8$	1.6	1.2	1.3	$1.5 \pm .05$	1.4	1.6	1.5	1.1	$1.6 \pm .05$
$203 \pm .6$	2.6	1.7	1.5	$2.2 \pm .07$	2.1	2.5	2.1	1.2	$2.3 \pm .06$
$508 \pm .8$	3.4	1.7	2.0	$2.7 \pm .08$	2.8	3.4	2.2	1.5	$2.8 \pm .09$

**Table 5.2b: The equivalent measured results in the presence of Dowfroth 250 (30 ppm).**

Orifice I.D.  $(\mu\text{m})$	Bubble size							
	$\approx 20$ cm above the orifice				at top ( $\approx 4\text{m}$ )			
	b (mm)	h (mm)	b/h	$d_e$ measured (mm)	b (mm)	h (mm)	b/h	$d_e$ measured (mm)
$17 \pm .7$	0.9	0.9	1.0	$0.9 \pm .06$	0.9	0.9	1.0	$0.9 \pm .05$
$70 \pm .8$	1.6	1.4	1.1	$1.5 \pm .07$	1.55	1.5	1.0	$1.5 \pm .06$
$203 \pm .6$	2.3	2.1	1.1	$2.2 \pm .09$	2.35	2.2	1.1	$2.2 \pm .05$
$508 \pm .8$	2.8	2.4	1.2	$2.7 \pm .08$	2.9	2.5	1.2	$2.8 \pm .08$

The bubble shape changed to become more oblate with increasing size (Tables 5.2a and b and also see Section 2.7.2). Figure 5.4 shows the bubble ( $d_c = 2.7$  mm) about 20 cm and 400 cm above the orifice in the absence (A) and presence (B) of frother. For a fixed bubble volume, the bubble was more oblate in the absence of frother and became more spherical as frother dosage was increased. Bubble shape also changed from bottom to top of the column; bubbles which were oblate at the bottom, became less oblate at the top, although this effect was almost negligible in presence of high frother concentration (e.g., 30 ppm).

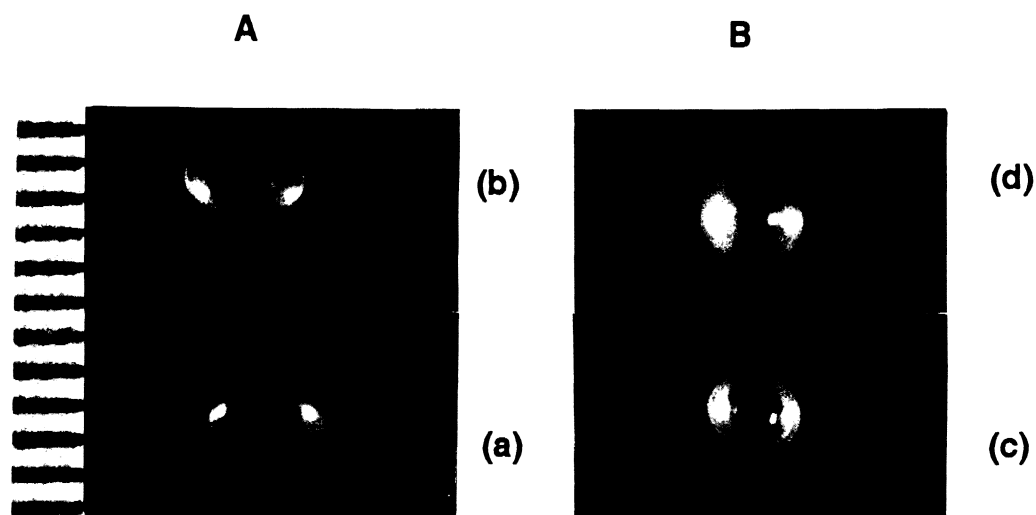


Figure 5.4: Bubble shape in tap water under different conditions and at different positions:

5.4A - Bubble shape in tap water only: (a) 20 cm above the orifice; (b) at top (4m),

5.4B - Bubble shape in presence of 30 ppm Dowfroth 250: (c) 20 cm above the orifice;

(d) at top (4m). Note,  $d_c = 2.7$  mm.

The effect of frother dosage on bubble shape was significant but negligible on bubble size. For a given orifice size and frother dosage at a certain level in the column, bubble volume and shape were indistinguishable for the different frother types. The maximum bubble expansion over 4 m, due to reduced hydrostatic pressure, was about 10% on  $d_e$  (Tables 5.2a and b) which is close to that expected under isothermal conditions (see Section 2.7.1). In general, the orifice diameter was the major parameter effecting  $d_e$ .

#### 5.1.4. Bubble Rise Path

With increasing bubble size, the motion changed from rectilinear to oscillatory (see Section 2.7.3). The type of motion was affected by the presence of frother, oscillation decreasing with increasing frother concentration. Table 5.3 shows the bubble rise path characteristics: amplitude (Y) and frequency (f).

**Table 5.3: Bubble oscillation amplitude and frequency (bubble rise path) in the absence and presence of frother (Dowfroth 250, 30 ppm) about 20 cm and 400 cm above the orifice.**

$d_e$ (mm)	Oscillation amplitude (Y) and frequency (f)							
	Tap water				30 ppm frother			
	$\approx 20$ cm		at top		$\approx 20$ cm		at top	
	Y (cm)	f (s <sup>-1</sup> )	Y (cm)	f (s <sup>-1</sup> )	Y (cm)	f (s <sup>-1</sup> )	Y (cm)	f (s <sup>-1</sup> )
0.9	0	0	0	0	0	0	0	0
1.5	0.6	5.8	0.4	2.5	0	0	0	0
2.2	2.1	6.4	1.5	4.4	0.4	3.4	0.3	3.2
2.7	2.6	6.9	1.9	4.8	0.8	4.0	0.7	3.8

In all cases, during the first stage (see Section 5.2) of bubble rise (acceleration phase), the bubble path was rectilinear. From the bottom to the top, the oscillation amplitude and frequency decreased. This effect was not significant in the presence of high frother concentration (e.g., 30 ppm): for bubbles as large as  $d_b = 2.2$  mm in the presence of frother the path from bottom to top was practically rectilinear ( $Y=0.4$  cm decreasing to  $Y=0.3$  cm).

## 5.2. Axial Bubble Velocity Profiles

### 5.2.1. In the Absence of Surfactant

Figure 5.5 shows the velocity profiles (local velocity versus time) of the four bubble sizes in tap water over the 4 m. The profiles show two stages: the velocity initially increased rapidly to reach a maximum value (acceleration, first stage) and then decreased continuously (deceleration, second stage). Depending on the time selected, the local velocity has a different order with respect to bubble size (see Section 2.7.4). Figure 5.6 shows the velocity profiles of a 1.5 mm bubble in distilled and tap water on different dates. In all cases these two stages were observed in the profiles (even in distilled water, Fig. 5.6) but, the profile shape, particularly the slope of the second stage was variable presumably reflecting differences in water quality. Table 5.4 shows the maximum velocity of the bubbles in water.

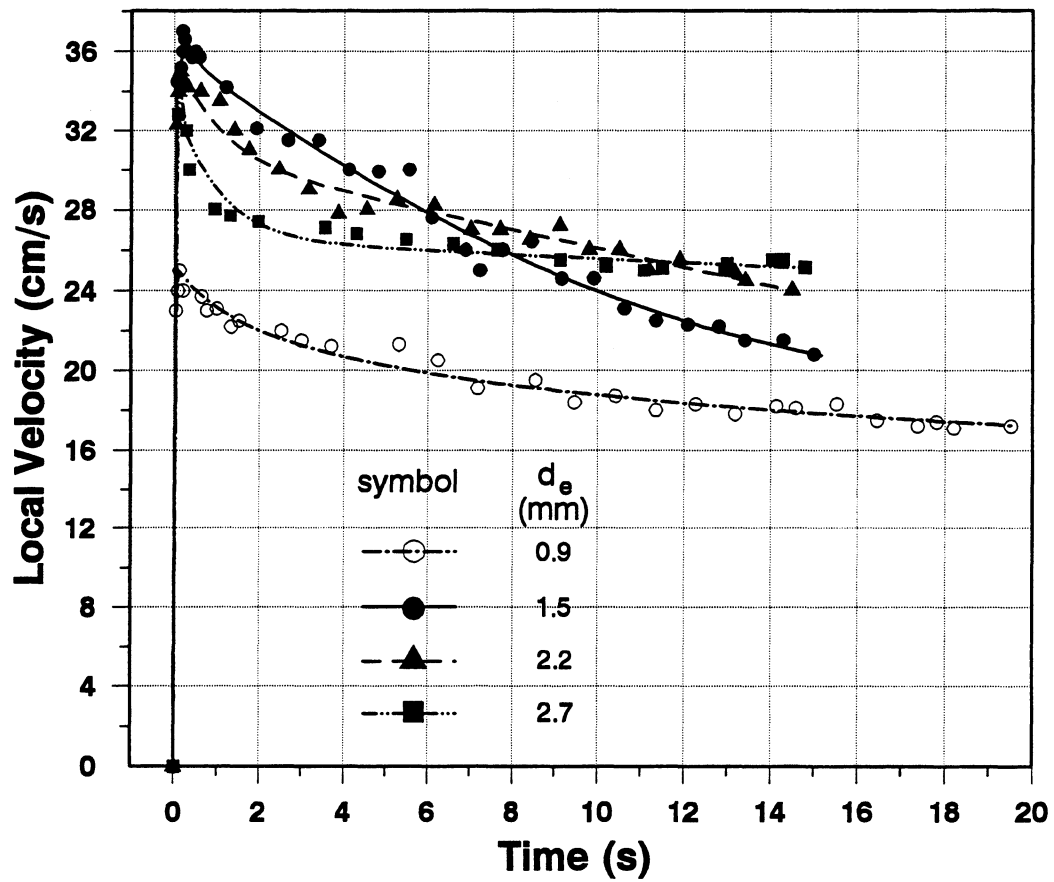


Figure 5.5: Bubble velocity profiles in the same tap water for different bubble sizes (April 94).

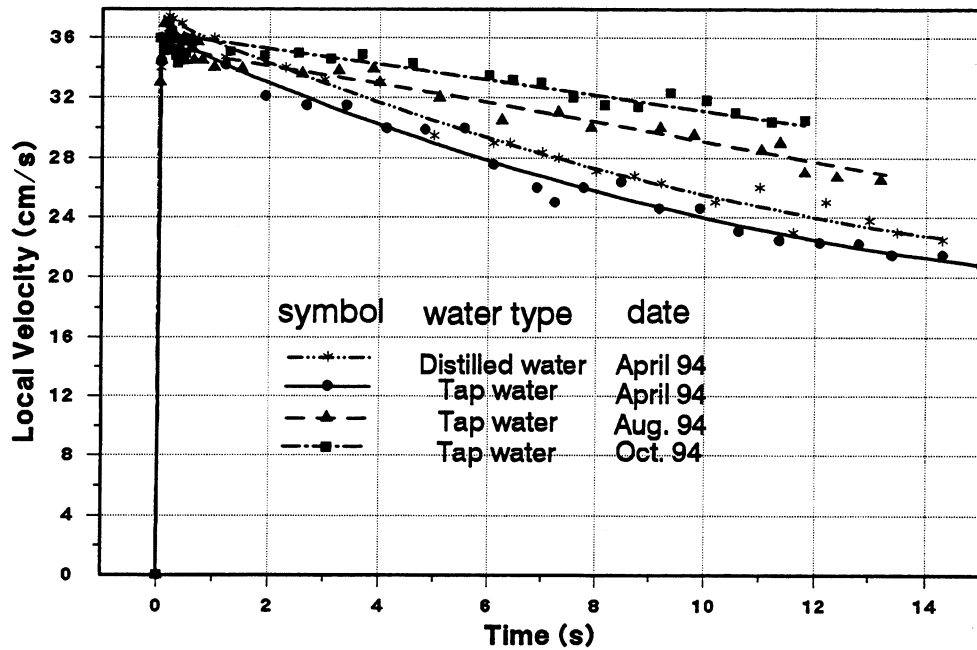


Figure 5.6: Bubble velocity profiles in distilled water and tap water on different dates ( $d_e = 1.5$  mm).

Table 5.4: The maximum velocity of bubbles in tap water.

$d_e$ (mm)	Maximum velocity (cm/s)
0.9	$25.0 \pm 0.4$
1.5	$36.5 \pm 0.5$
2.2	$34.2 \pm 0.6$
2.7	$32.0 \pm 0.5$

### 5.2.2. In the Presence of Frother\*

Figures 5.7-5.10, 5.11-5.14 and 5.15-5.18 show the velocity profiles in the presence of frother: Dowfroth 250, pine oil and MIBC (at various concentrations), respectively, for bubble sizes 0.9, 1.5, 2.2 and 2.7 mm. In general, the profiles show three stages: first, velocity increased rapidly, then decreased and in the third stage, the velocity became almost constant. In all cases with frother the results were highly reproducible, i.e., the quality of the tap water (Fig. 5.6) was not a factor.

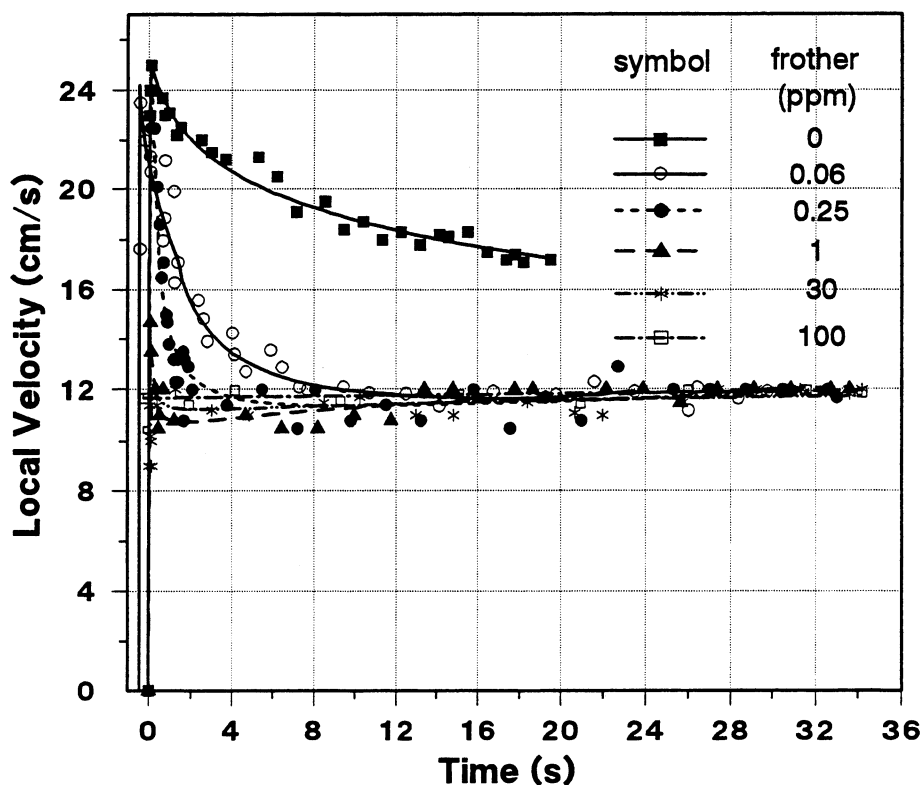


Figure 5.7: Bubble velocity profiles ( $d_b = 0.9$  mm, frother = Dowfroth 250).

\* A version of the Sections 5.2.1 and 5.2.2 is to be published in the International Journal of Mineral Processing (accepted, March 1995).

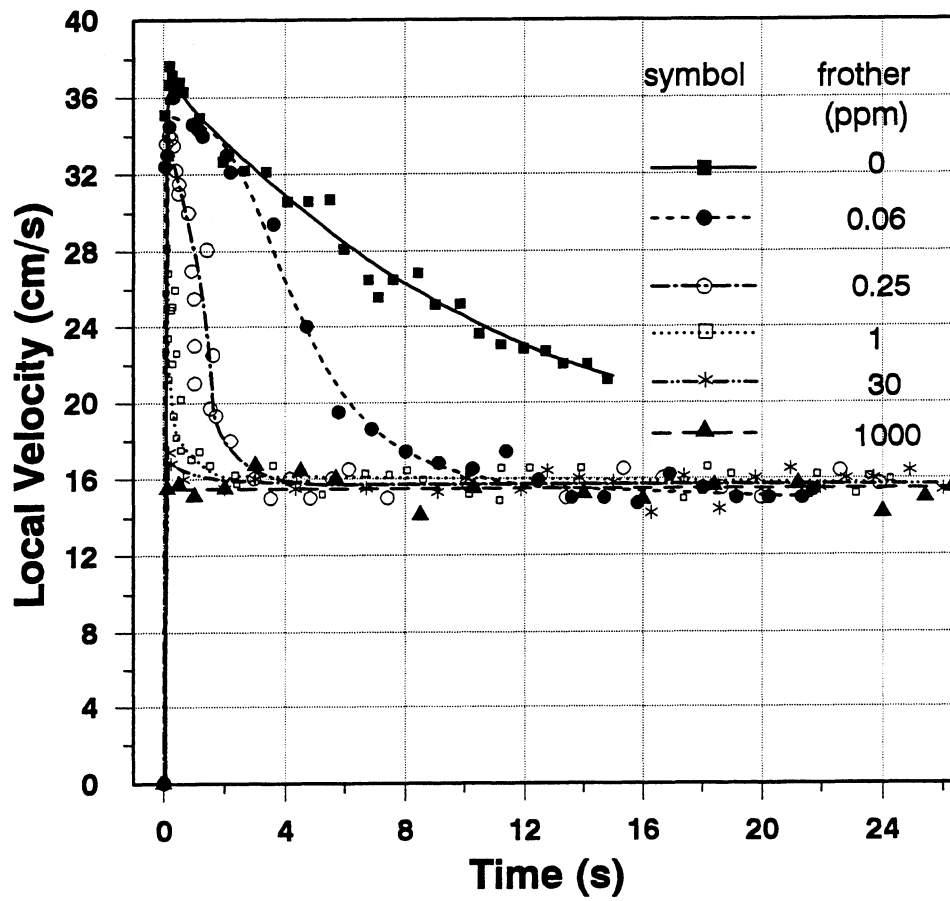


Figure 5.8: Bubble velocity profiles ( $d_e = 1.5$  mm, frother = Dowfroth 250).

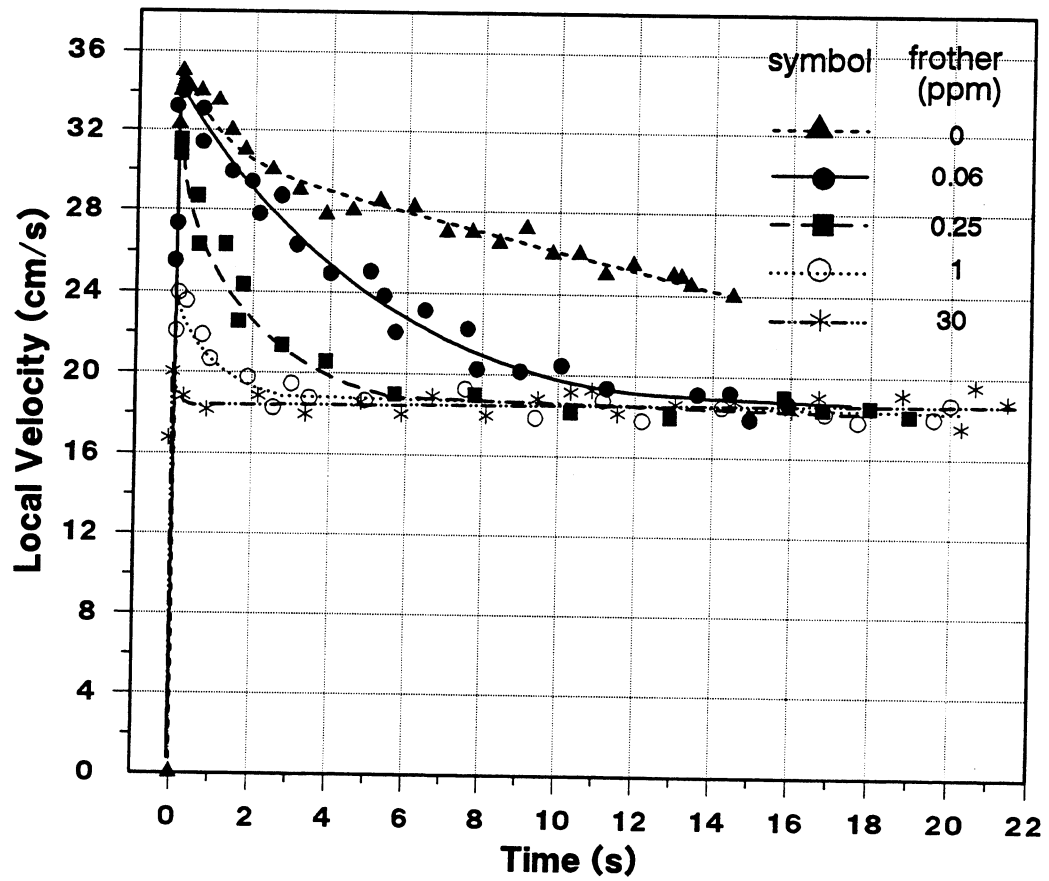


Figure 5.9: Bubble velocity profiles ( $d_e = 2.2$  mm, frother = Dowfroth 250).

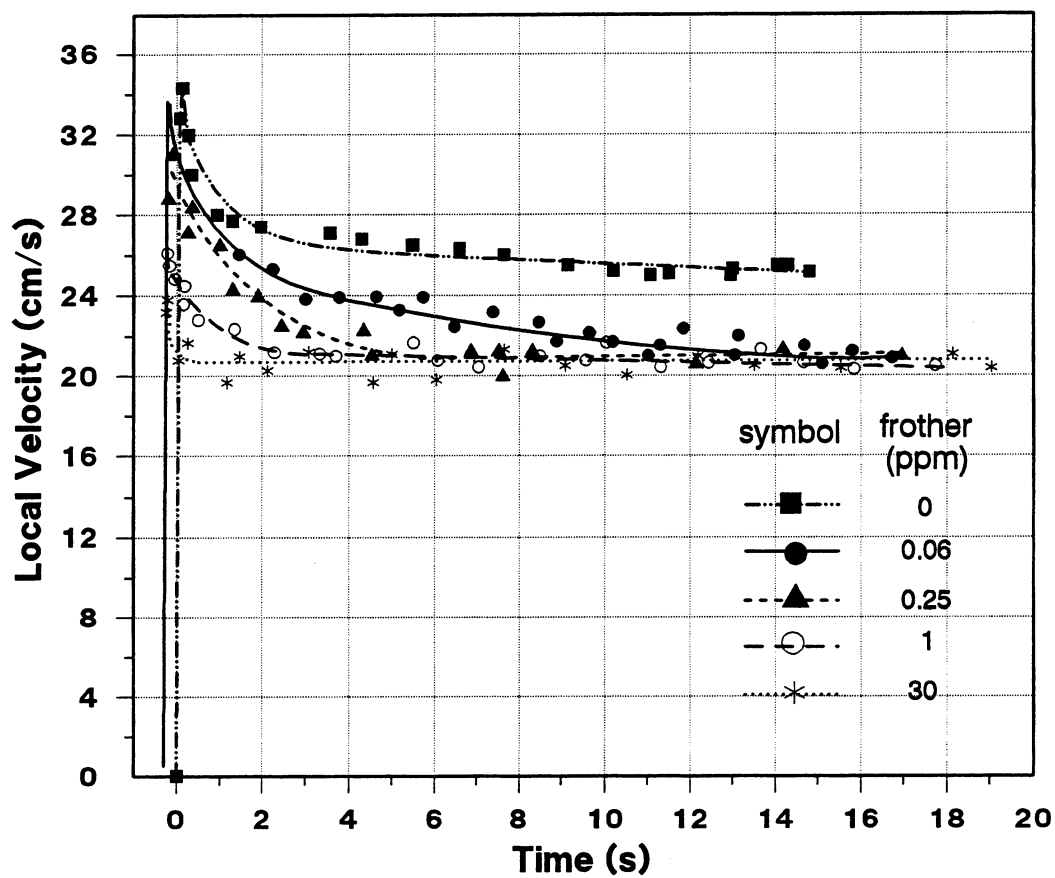


Figure 5.10: Bubble velocity profiles ( $d_b = 2.7$  mm, frother = Dowfroth 250).

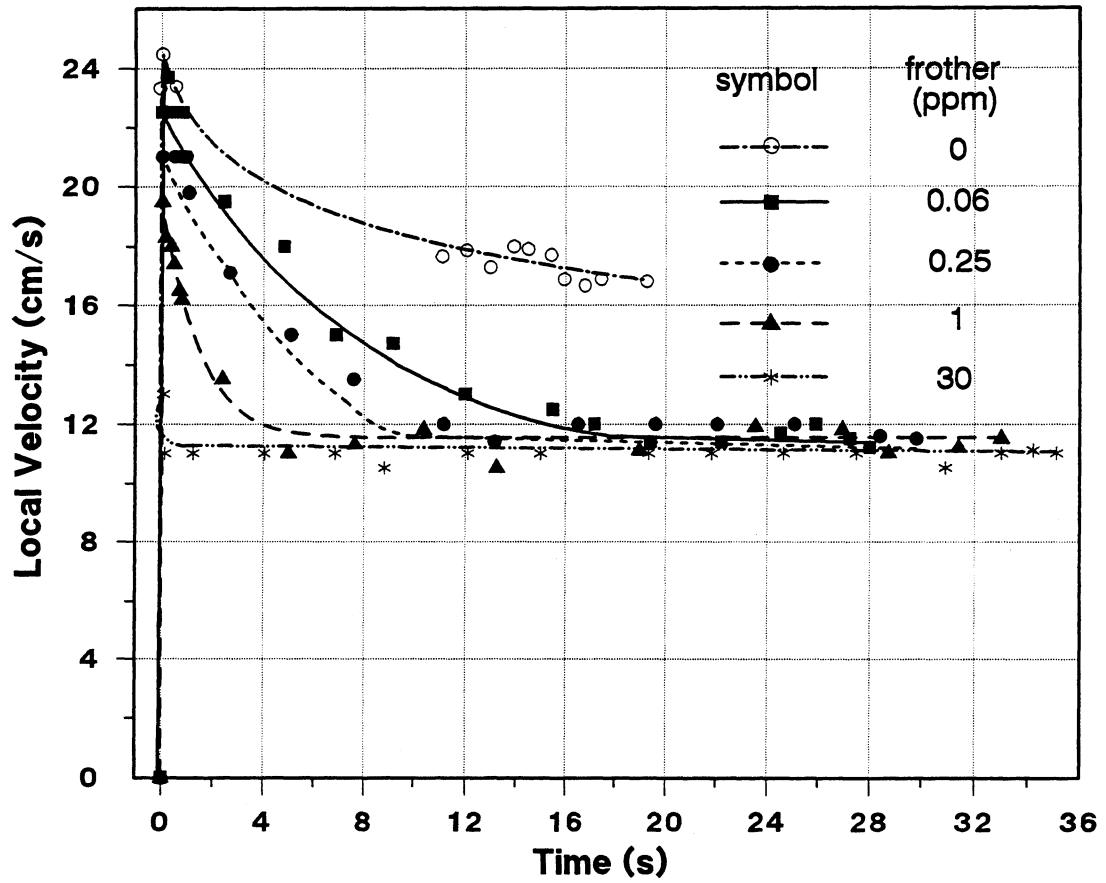


Figure 5.11: Bubble velocity profiles ( $d_e = 0.9$  mm, frother = pine oil).

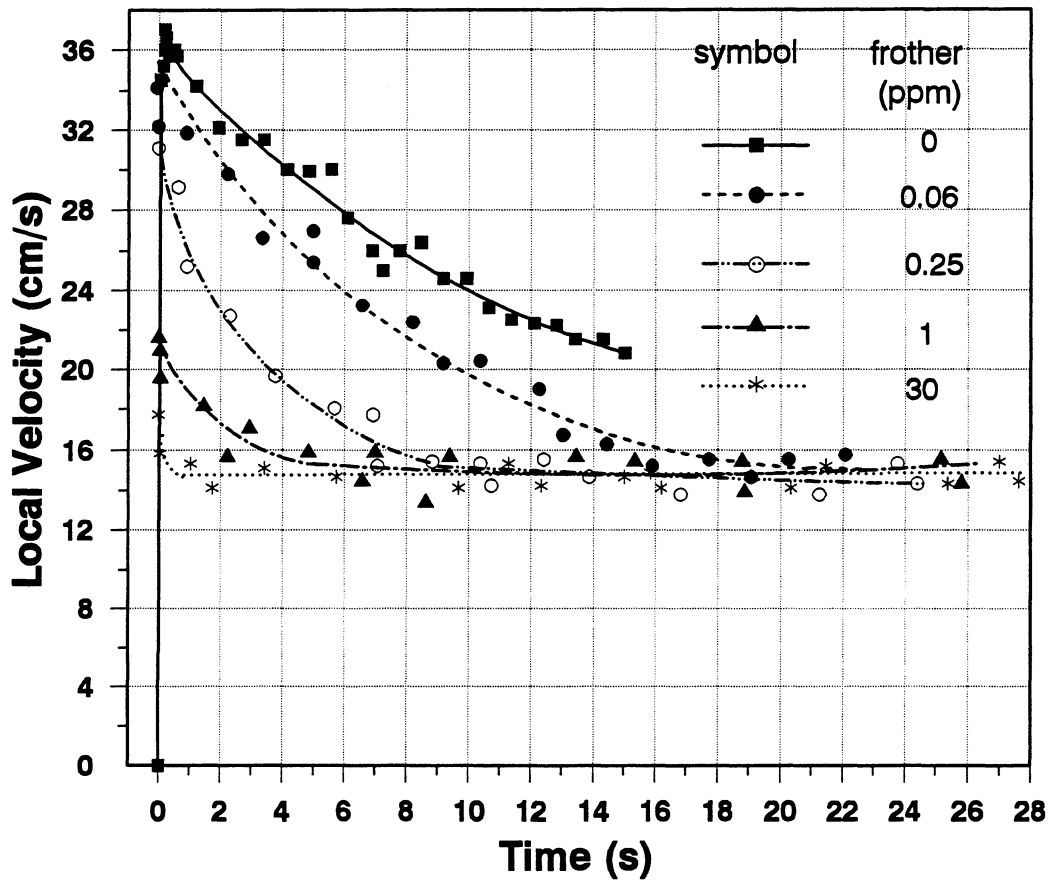


Figure 5.12: Bubble velocity profiles ( $d_e = 1.5$  mm, frother = pine oil).

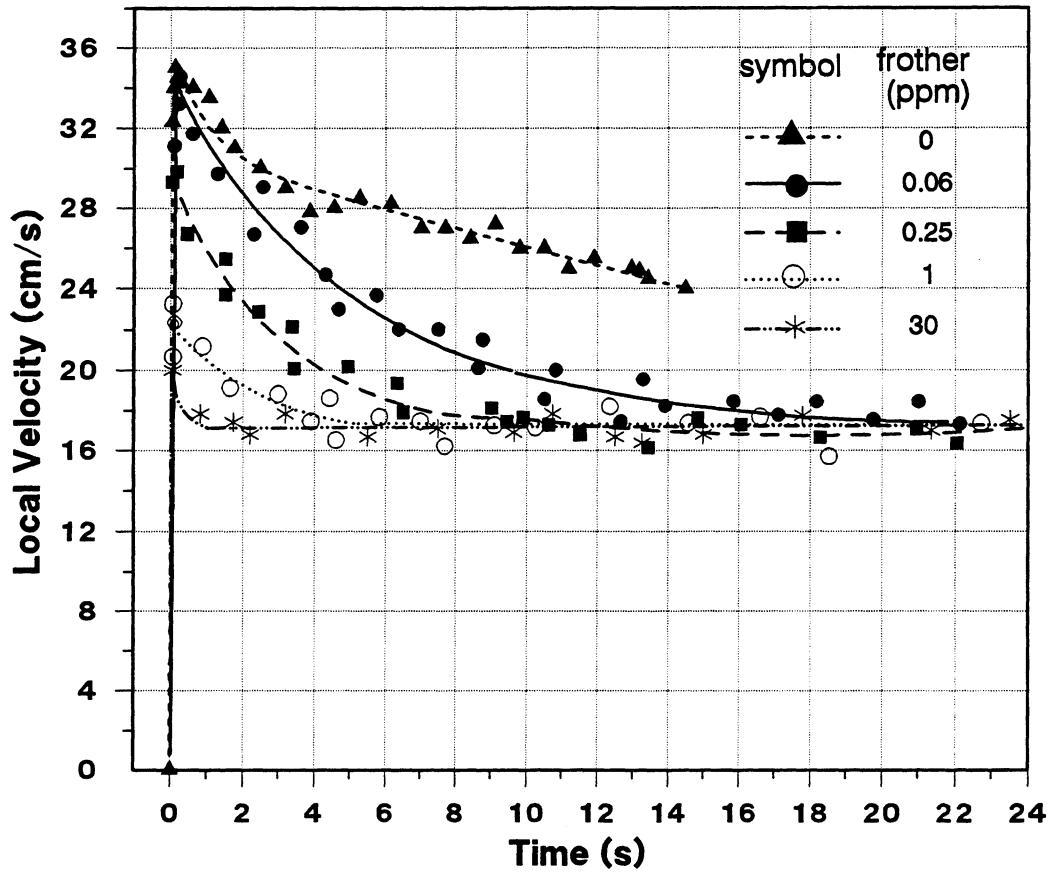


Figure 5.13: Bubble velocity profiles ( $d_e = 2.2$  mm, frother = pine oil).

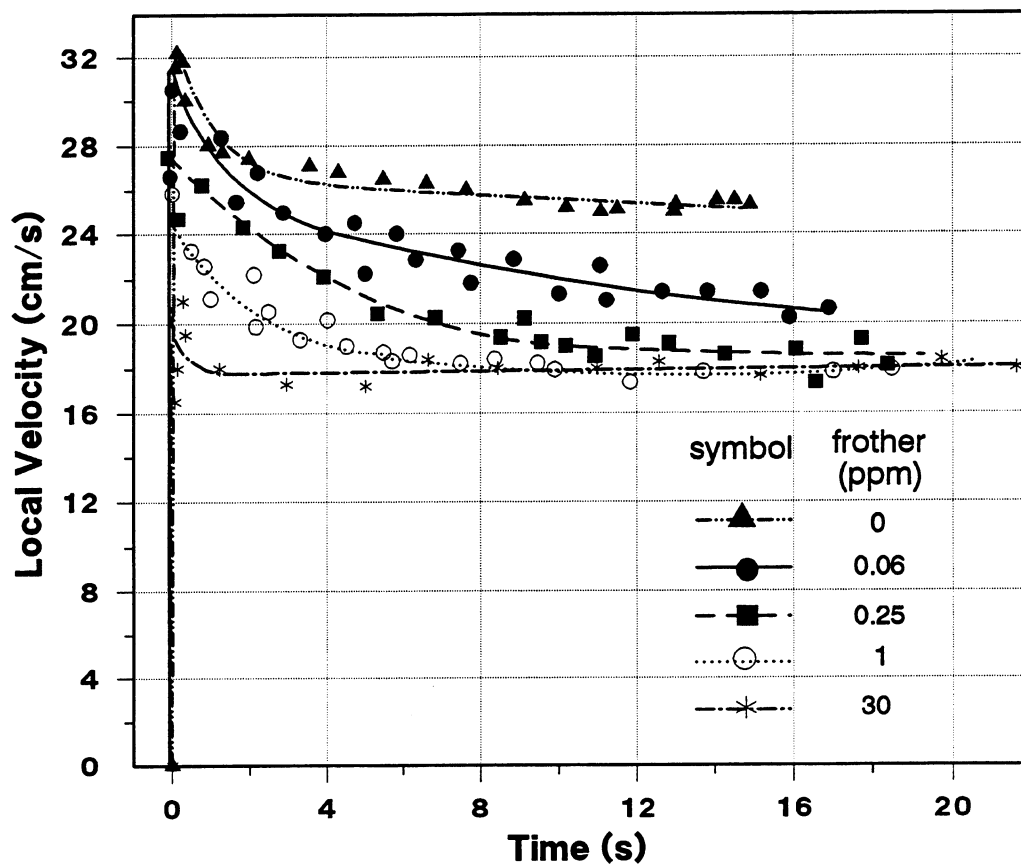


Figure 5.14: Bubble velocity profiles ( $d_e = 2.7$  mm, frother = pine oil).

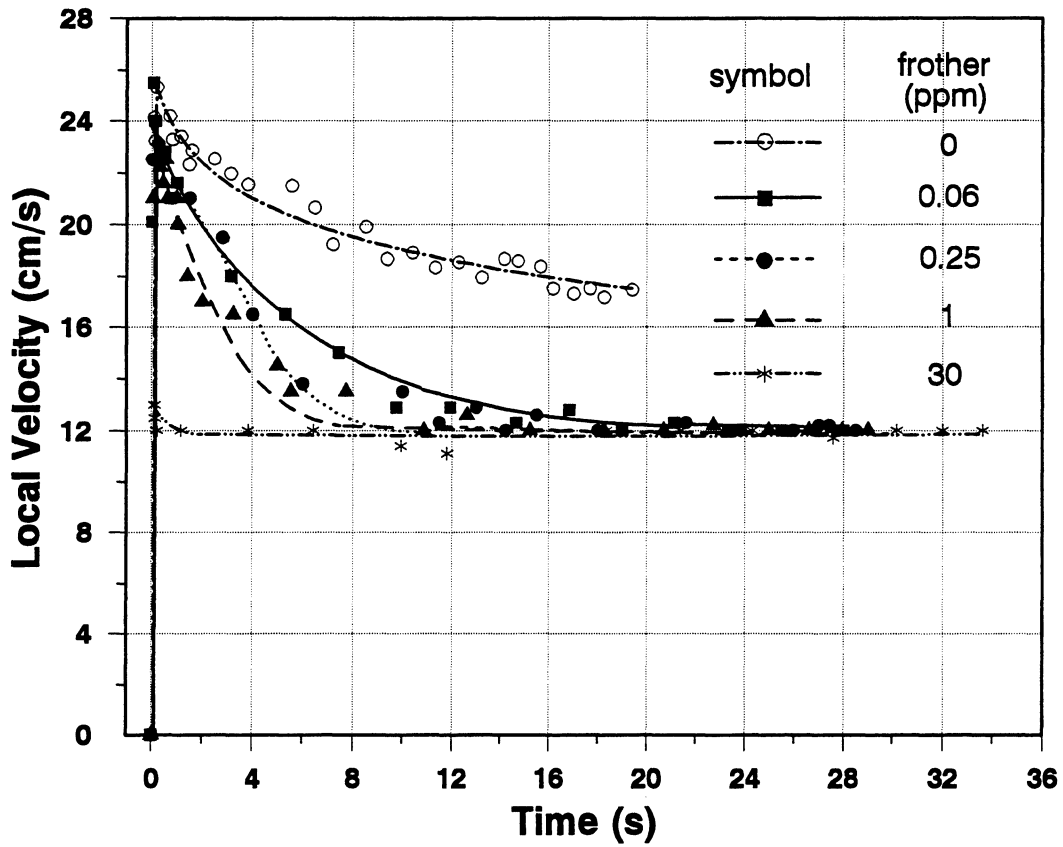


Figure 5.15: Bubble velocity profiles ( $d_e = 0.9$  mm, frother = MIBC).

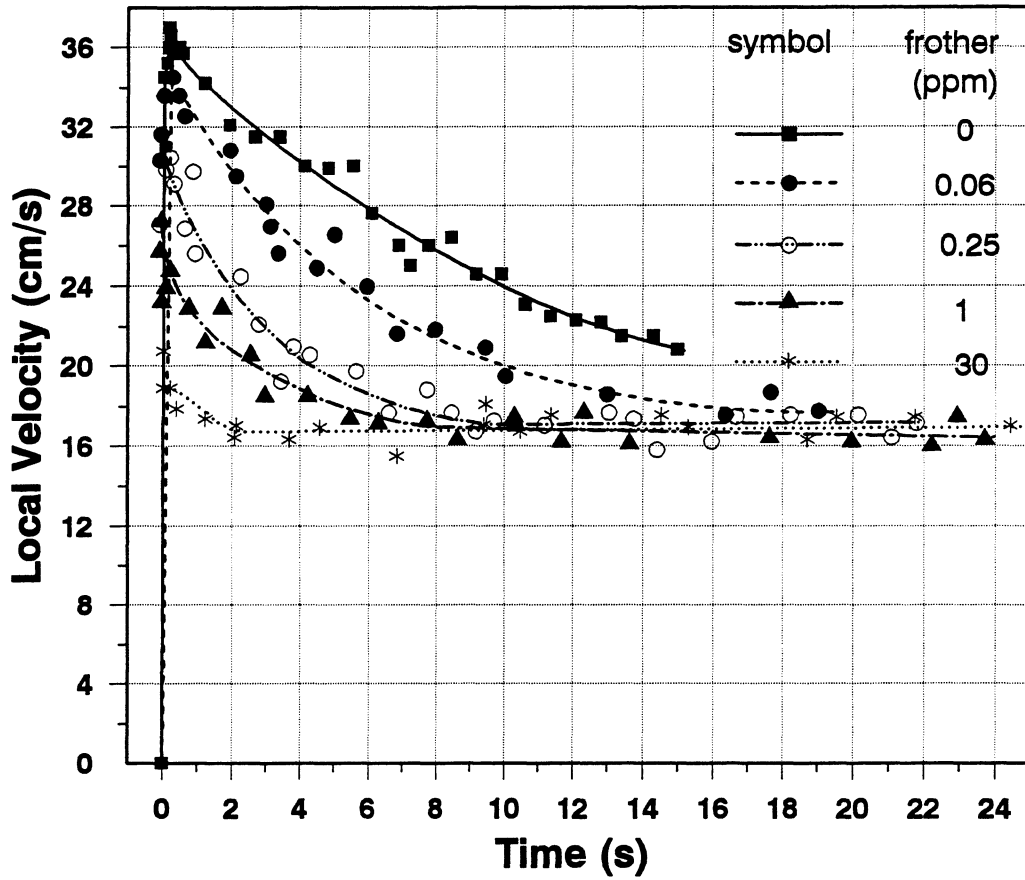


Figure 5.16: Bubble velocity profiles ( $d_e = 1.5$  mm, frother = MIBC).

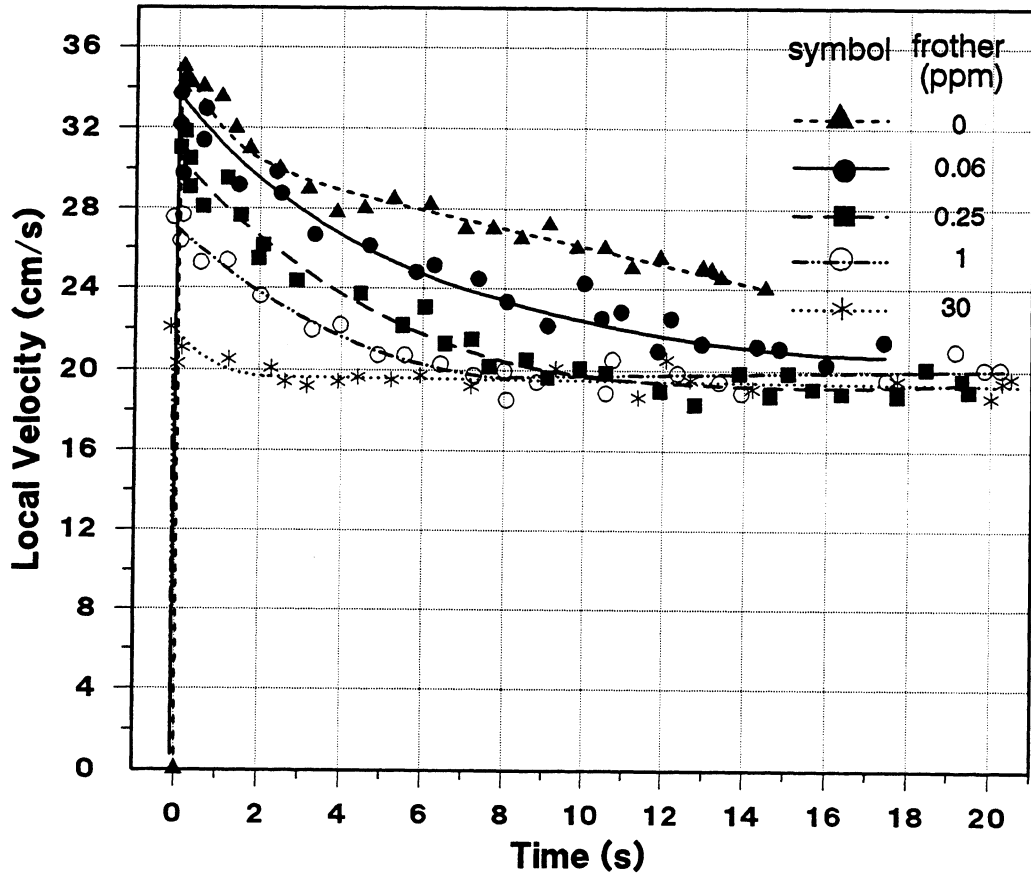


Figure 5.17: Bubble velocity profiles ( $d_e = 2.2$  mm, frother = MIBC).

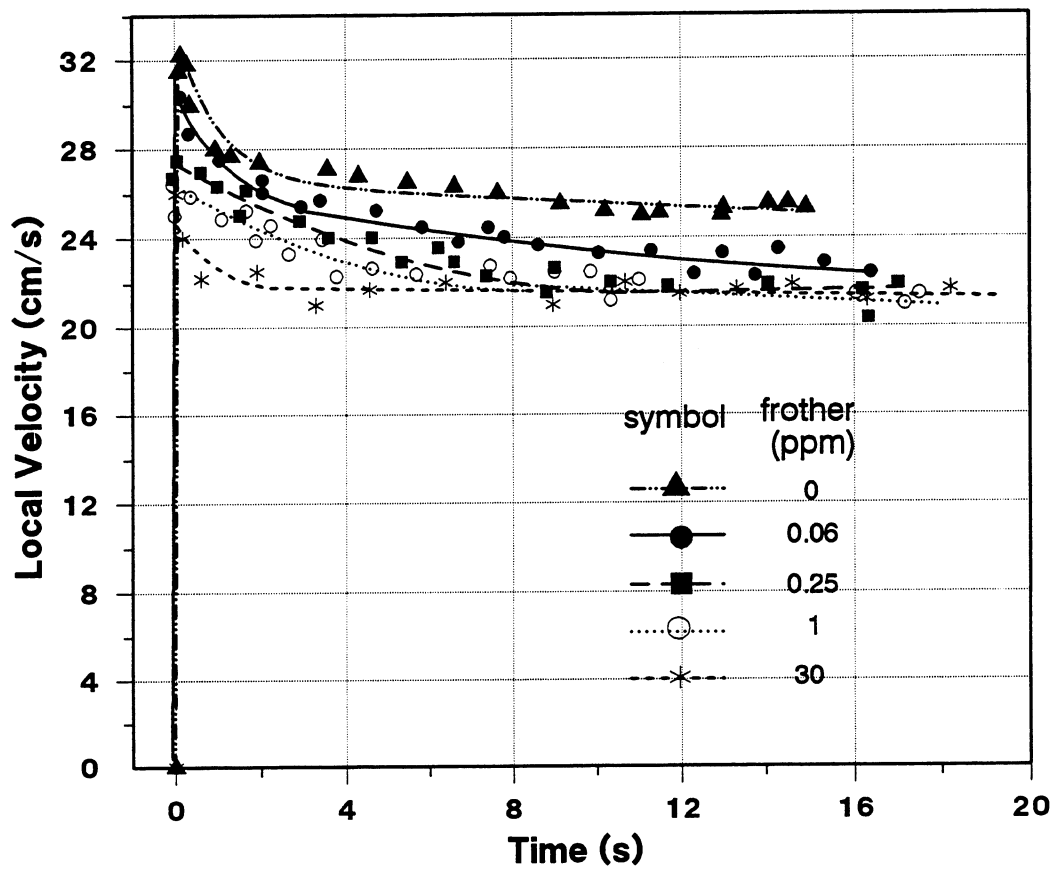


Figure 5.18: Bubble velocity profiles ( $d_e = 2.7$  mm, frother = MIBC).

The results revealed the following features:

a- Bubble velocity decreased on addition of frother (Figs. 5.7-5.18).

b- The pattern of the bubble velocity profile showed three stages (Fig. 5.19): first, a rapid increase to a maximum value; second, a decrease; and third, if there is sufficient time (height), a constant velocity stage. The major velocity profile characteristics were: a maximum velocity ( $U_{max}$ ), an adsorption time,  $t_a$  (referring to time to reach  $dU/dt=0$ , i.e., the third stage which is related to adsorption of surfactant (see later)) and a terminal velocity ( $U_T$ ).

c- The velocity profile was very sensitive to the presence of frother, amounts  $< 1$  ppm having a profound effect (e.g., Fig. 5.8). This appears to be the situation in the case of water only (Figs. 5.5 and 5.6) as the velocity profile was affected by "impurities" in the water, e.g., the "impurity" in tap water in October was more than in April (Fig. 5.6).

d- Stages one and two were dependent on frother concentration and type (Figs. 5.7-5.18) and showed two characteristics, a maximum velocity and a given adsorption time. The maximum velocity ( $U_{max}$ ) and time to reach  $U_{max}$  ( $t_a$ ) were reduced in the presence of frother (Fig. 5.20 shows this clearly). The time required to reach the terminal velocity (or adsorption time) increased with decreasing frother dosage (it was almost zero in presence of high frother concentration (e.g., 30 ppm)) and increasing  $d_c$ . Table 5.5 shows the approximate adsorption time measured for different bubble sizes and frother types at various concentrations. As this table shows, for a certain bubble size and frother dosage, the adsorption time was less with Dowfroth 250 than for pine oil and MIBC ( $(t_a)_{Dowfroth} < (t_a)_{pine\ oil} < (t_a)_{MIBC}$ ).

e- The third stage (constant velocity) was dependent on frother type but not on frother concentration. This velocity is taken as the terminal velocity ( $U_T$ ). Table 5.6 shows the effect of frother type on terminal velocity for various bubble sizes. In the absence of frother (distilled or tap water only) or in presence of low frother concentration (e.g., 0.06 ppm) for large bubbles (e.g.,  $d_c=2.7$  mm), this stage was not reached in the 4 m column.

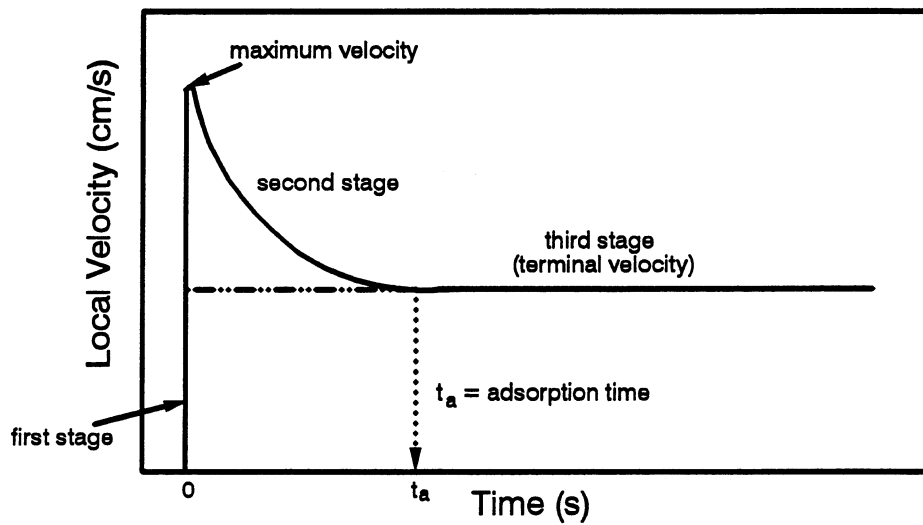


Figure 5.19: Bubble velocity profile characteristics.

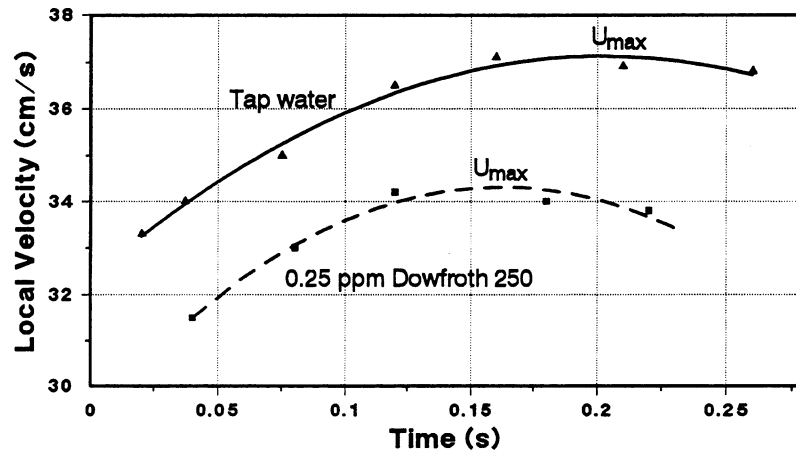


Figure 5.20: First stage of bubble velocity profile ( $d_e = 1.5$  mm).

**Table 5.5: Adsorption time (time to reach terminal velocity) for different bubble sizes and frother types at various concentrations.**

$d_e$ (mm)	ppm	Adsorption time, $t_a$ (s)		
		Dowfroth 250	Pine oil	MIBC
0.9	0.06	10.5	18.0	21.5
	0.25	4.0	8.6	9.1
	1.00	1.9	4.5	7.5
	30.0	0.4	0.8	2.0
1.5	0.06	12.0	21.0	*
	0.25	4.3	9.1	9.6
	1.00	2.3	5.0	7.8
	30.0	0.6	0.9	2.1
2.2	0.06	13.8	21.9	*
	0.25	5.1	9.5	10.1
	1.00	2.9	5.3	8.2
	30.0	0.7	0.9	2.3
2.7	0.06	15.2	*	*
	0.25	5.5	10.1	10.5
	1.00	3.4	5.8	8.4
	30.0	0.8	1.1	2.4

\* terminal velocity was not reached in a 4m column.

**Table 5.6: The effect of frother type on terminal velocity (cm/s).**

Frother type	$d_c$ (mm)			
	0.9	1.5	2.2	2.7
MIBC	$12.0 \pm 0.3$	$16.5 \pm 0.3$	$19.3 \pm 0.3$	$21.7 \pm 0.3$
Dowfroth 250	$11.5 \pm 0.4$	$15.6 \pm 0.5$	$18.2 \pm 0.4$	$20.8 \pm 0.5$
pine oil	$11.0 \pm 0.3$	$14.8 \pm 0.2$	$17.0 \pm 0.3$	$18.0 \pm 0.3$

### 5.2.3. Effect of Methanol

Methanol is the shortest chain alcohol, i.e., it is expected to have little effect compared to the commercial frothers. This was indeed the case. Figure 5.21 shows velocity profiles for bubble size 1.5 mm in presence of methanol at various concentrations. The third stage (terminal velocity) was not observed even in concentration of 1000 ppm.

This shows that "impurities" in tap water must be fairly complex species; the nature of the impurity is important, although in the case of the frothers tested, they are relatively equal when compared to methanol. It would be interesting to check when the effect of hydrocarbon chain length of alcohols approaches the typical frother effect on bubble velocity profile.

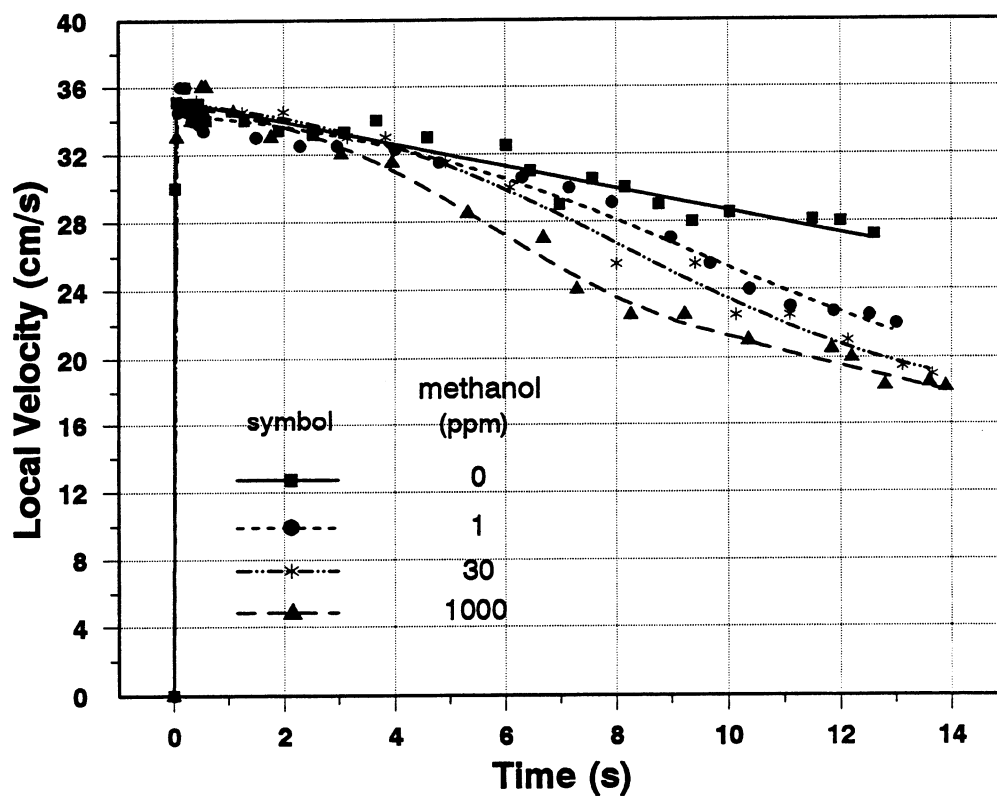


Figure 5.21: Bubble velocity profiles ( $d_b = 1.5$  mm) in presence of methanol.

#### 5.2.4. Effect of Collector

Figure 5.22 shows the effect of potassium ethyl xanthate (collector) on bubble velocity profiles ( $d_e = 1.5$  mm). At high concentration the velocity profile was affected by the collector but terminal velocity was not reached.

This result of little effect compared to that of a frother, was expected as xanthate is known to be surface active for the sulphide mineral/water interface but not for the air/water interface (Leja, 1982). Combinations of collector and frother could be an interesting extension of the current work.

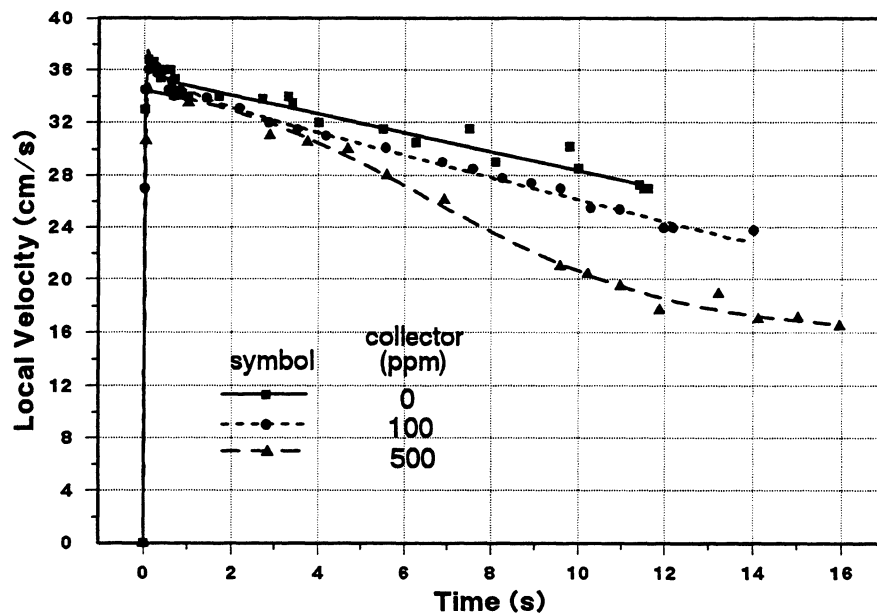


Figure 5.22: Bubble velocity profiles ( $d_e = 1.5$  mm) in presence of collector (potassium ethyl xanthate).

### 5.2.5. Effect of pH

Two types of modifiers (soda ash and lime) were used at pH 10. As Fig. 5.23 shows, the effect of pH on bubble velocity profiles ( $d_e = 1.5$  mm) was almost negligible (the pH of the original tap water was about 7.6).

This work was done in part because several mineral processing plants have started to substitute lime with soda ash. Possible interactions among the pH modifier, collector and frother may be revealed by a bubble velocity profile study.

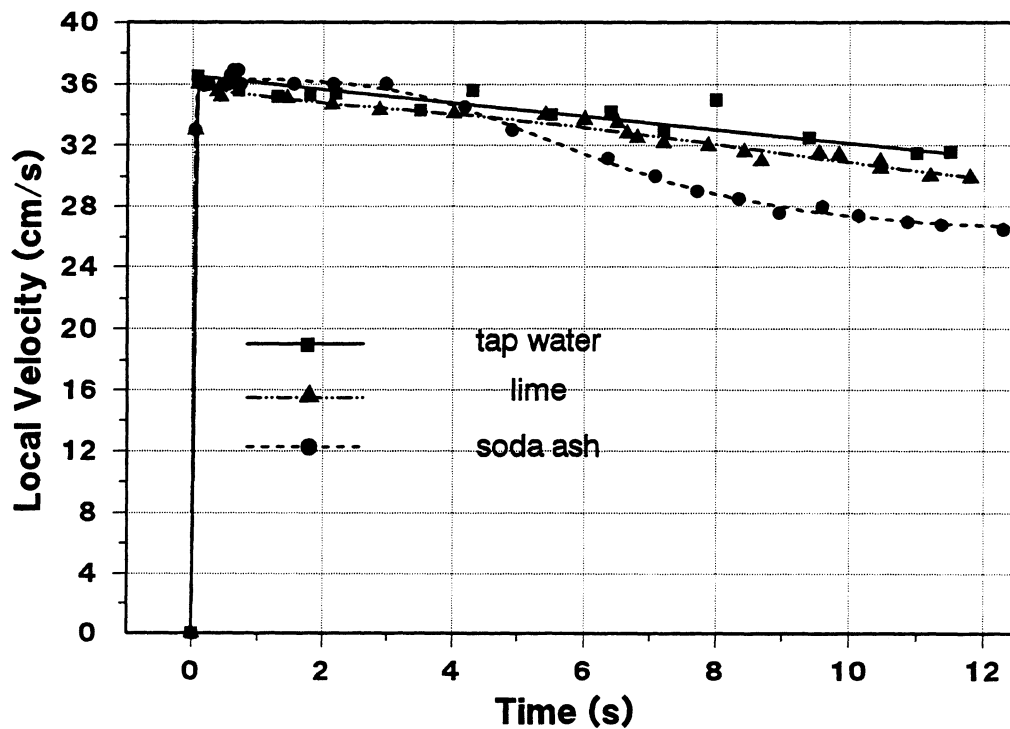


Figure 5.23: Bubble velocity profiles ( $d_e = 1.5$  mm) in presence of modifiers (pH = 10).

### 5.2.6. Effect of Temperature

Figure 5.24 shows the effect of temperature (20 and 40 °C) on bubble velocity profiles ( $d_e = 1.5$  mm) in presence of 0.06 and 0.25 ppm Dowfroth 250. Increasing the temperature increased the maximum velocity but decreased the adsorption time. The effect on terminal velocity was negligible.

This work was done as a starting point to determine whether diffusion or adsorption governs the observed kinetics.

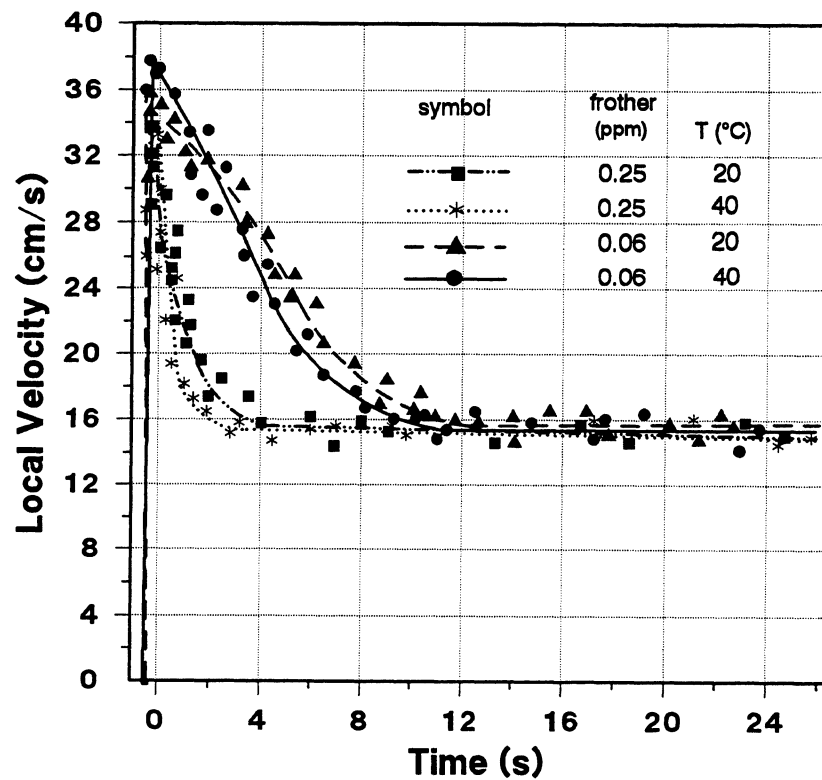


Figure 5.24: Bubble velocity profiles ( $d_e = 1.5$  mm, frother = Dowfroth 250) at 20 and 40 °C.

## CHAPTER 6

### GENERAL DISCUSSION

In the present investigation the effect of the column wall (see Section 2.11), temperature (see Section 4.2) and bubble generation frequency (see Section 5.1.1) on bubble behaviour were negligible and the use a square cross-section column eliminated the optical distortion effect (see Section 4.1). These features, therefore, will not be discussed.

#### 6.1. Bubble Size, Shape and Path

The measured bubble sizes were in good agreement with Tate's law (see Section 5.1). The effect of frother on bubble volume (or  $d_b$ ) was negligible and the maximum bubble expansion observed over 4 m, due to reduced hydrostatic pressure, was about 10% on  $d_b$  which is close to that expected under isothermal conditions.

The frother effect on bubble shape and rise path was significant. For a fixed bubble volume, the bubble was more spherical and path more rectilinear in the presence of frother. It was observed that the bubble shape and path changed from the bottom to the top in the column. Bubbles which were oblate with oscillatory motion at the bottom, became less oblate and their motion less oscillatory at the top. This is due to the time-dependent adsorption of surfactant (or impurities in the case of tap/distilled water) on the bubble surface. In the presence of high frother concentration the bubble shape and path from bottom to top were almost the same which indicates in that case a very short adsorption time.

## 6.2. Axial Bubble Velocity Profile

The bubble velocity profile showed three stages. The principal characteristics, maximum velocity, adsorption time and terminal velocity are discussed in this section.

### 6.2.1. Stage 1, Maximum Velocity

The bubble grows at the orifice until the buoyancy force just exceeds the surface tension force and then it releases (see Section 2.7.1). As the initial velocity is zero (gas injection rate here is sufficiently low to assume this), the drag force is initially zero and consequently the bubble experiences high acceleration (see Section 2.9). Concomitantly, the drag force increases with velocity until it equals the buoyancy force and the bubble reaches its maximum velocity (Figs. 5.5-5.6 and Table 5.4). This occurs over a short time interval (e.g., 0.2s, Fig. 5.20). In a perfectly clean (i.e. contaminant free) liquid, the maximum velocity would also equal the terminal velocity. This is clearly not the case here.

Figure 6.1 shows the experimental data from the literature for bubble terminal velocity as a function of  $d_c$ . The figure includes the present estimates for  $U_T$  in "pure water". This was done by taking the maximum velocity attained (i.e., at the end of stage one in tap water only). The argument is that by the time the maximum velocity is reached the influence of contaminants will be small and thus this maximum velocity is as close as one can get to the velocity the bubble is trying to reach in the clean system. The "maximum" velocity will, therefore, be less than in a perfectly clean system, but taking Moore's theory (Fig. 6.1) (see Section 2.9.3) as being correct for the clean system, the maximum velocity appears to be a good approximation of the terminal velocity in truly contaminant-free water.

### 6.2.2. Stage 2, Adsorption Time

In the second stage, the bubble velocity decreases with time, at a rate dependent on impurity (surfactant) type and concentration. This suggests that the drag coefficient is increasing with time which must reflect time-dependent changes at the bubble surface related to adsorption of surfactant molecules (see Section 2.8). In a truly pure system or in the presence of high surfactant concentration this stage is eliminated (or at least very difficult to detect). The accumulation of surfactant at the bubble surface alters at least two properties, surface rigidity and surface viscosity.

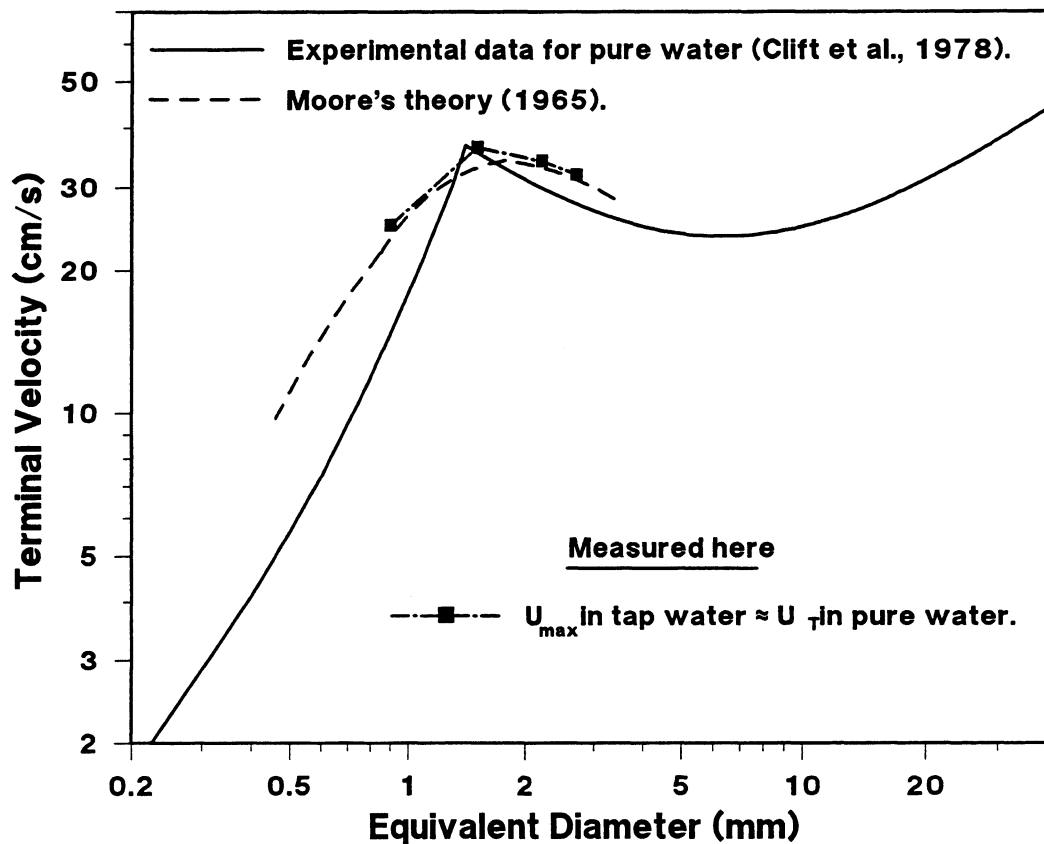


Figure 6.1: Comparison between the present and published data for pure water.

As the surfactant adsorbs, surface tension gradients develop which oppose the surface motion: the surface becomes "rigid" and the internal circulation is reduced. A rigid surface offers more resistance to the flow of water than does a mobile surface, hence the drag coefficient increases.

In addition to surface tension gradients, the surface viscosity tends to increase as surfactant molecules accumulate. One way of interpreting this is to consider the role of the OH groups of the surfactant molecule. The OH groups are oriented towards the water, being hydrophilic (King, 1982). These groups form H-bonds with water molecules and this reduces the ability of the bubble to "shear" or "slip" (Vinogradova, 1994) past the water, i.e., the surface viscosity increases.

These changes in the surface nature due to adsorption of surfactant are well known. What is new here is the revelation of the time required for the changes to occur on bubbles in motion in the presence of typical frothers used in flotation. Surfactant molecules must transport to and orient correctly at the bubble surface and both phenomena require time. Data such as those here may permit identification of the rate limiting step in the adsorption process.

#### *Model of adsorption time based on diffusion*

If it is assumed that only diffusion is controlling the movement of molecules from bulk to the interface, then, a simple diffusion equation can be derived to calculate the adsorption time. Ward and Tordai (1946) showed that:

$$t_d = \frac{\pi \Gamma^2}{4 C^2 D_d} \quad (6.1)$$

where  $C$  is the bulk concentration (mole/cm<sup>3</sup>),  $D_d$  is diffusion coefficient (cm<sup>2</sup>/s) and  $t_d$  is adsorption time (s). To determine the adsorption time, the values of  $\Gamma$  (surface excess

mass or adsorption density, mole/cm<sup>2</sup>) at equilibrium may be obtained independently by application of the Gibbs equation to the observed relationship between the concentration and the equilibrium surface tension. Equation 6.1 will only hold if there is no build-up of molecules in the sub-surface.

The Gibbs adsorption equation for the surface excess (Bikerman, 1958) is given by

$$\Gamma = \frac{C}{RT} \times \left( - \frac{d\sigma}{dC} \right) \quad (6.2)$$

where C, R, T and  $\sigma$  are surfactant concentration (mole/l) universal gas constant (8.314  $\times 10^7$  erg/mole °K), temperature (303 °K) and solution surface tension (dyne/cm), respectively.

The relationship between adsorption density ( $\Gamma$ ) at the gas-liquid interface and frother concentration (for the three frother types) is derived from the measured surface tension-concentration data (see Section 5.1.2 (Fig. 5.2)) and is plotted in Fig. 6.2.

Diffusion coefficient ( $D_a$ ) can be obtained from the empirical correlation of Wilke and Chang (Treybal, 1968) for dilute solutions of nonelectrolyte (see Appendix 2).

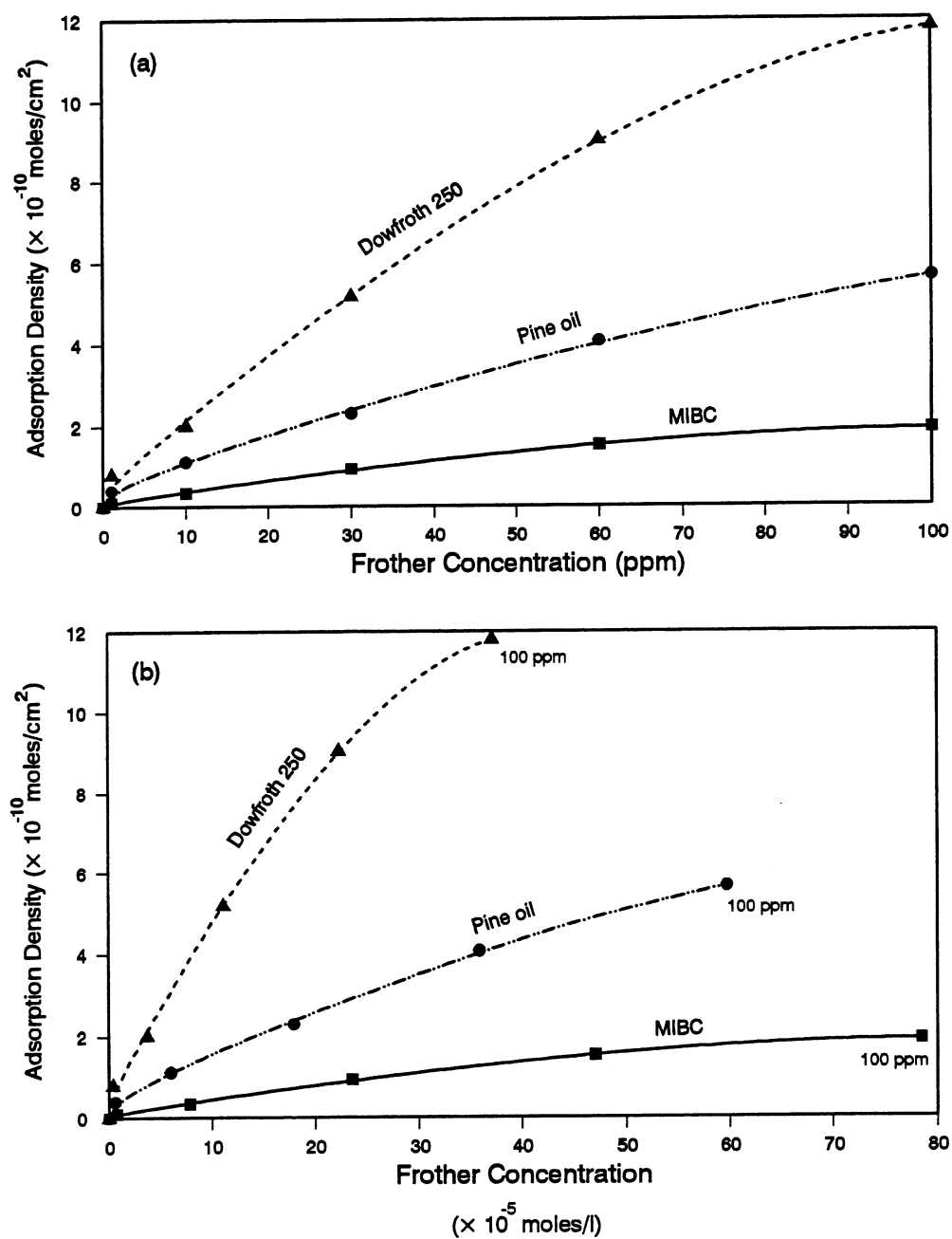


Figure 6.2: Relationship between adsorption density at gas-liquid interface (a: ppm, b: mole/l) and frother concentration at 30 °C using Gibbs' equation.

Table 6.1 shows the bulk concentration,  $C$ , adsorption density,  $\Gamma$  (Eq. 6.2 and Fig. 6.2), diffusion coefficient,  $D_d$  (see Appendix 2) and the adsorption time,  $t_d$  (Eq. 6.1) for various frothers at different concentrations.

**Table 6.1: Adsorption time (Eq. 6.1) for various frothers at different concentrations.**

(Frother)	(C)		$\Gamma$ $\times 10^{-10}$ mole/cm <sup>2</sup>	$(D_d)$ $\times 10^{-6}$ cm <sup>2</sup> /s	$(t_d)$ s
	ppm	$\times 10^{-5}$ mole/l			
Dowfroth 250	0.06	0.022	0.228	5.53	1525.4
	0.25	0.093	0.30	5.53	147.7
	1.00	0.37	0.79	5.53	64.74
	30.00	11.13	5.17	5.53	3.06
Pine oil	0.06	0.036	0.118	7.06	119.52
	0.25	0.15	0.173	7.06	14.79
	1.00	0.597	0.396	7.06	4.89
	30.00	17.92	2.296	7.06	0.18
MIBC	0.06	0.047	0.021	9.00	1.74
	0.25	0.20	0.036	9.00	0.28
	1.00	0.78	0.10	9.00	0.14
	30.00	23.52	0.93	9.00	0.01

The measured adsorption time,  $t_a$ , in the present study (Table 5.5) is not in agreement with the predicted adsorption time ( $t_d$ ) based on diffusion theory. Compared to the measured, the predicted adsorption times are generally too long, are not related to bubble size, and show the incorrect order: (i.e.,  $(t_d)_{\text{Dowfroth}} > (t_d)_{\text{pine oil}} > (t_d)_{\text{MIBC}}$ ) vs Table 5.5:  $(t_a)_{\text{Dowfroth}} < (t_a)_{\text{pine oil}} < (t_a)_{\text{MIBC}}$ . This suggests that the adsorption time for a moving bubble is quite different from a stationary surface (for which the theory was developed), or at least for a moving bubble diffusion is not the only mechanism of

surfactant transport.

*Model of adsorption time considering surface tension gradient*

An approximate expression for the order of magnitude of the characteristic adsorption time by consideration of surface tension gradient can be made as follows:

When the viscous resistance of the surface is assumed to be negligible, the tangential stress at the surface of a sphere (radius  $a$ ) in motion with a mobile interface as a function of surface tension gradient is (Griffith, 1962; Harper, 1972):

$$(\tau_{r\theta})_i - (\tau_{r\theta})_o = \frac{1}{a} \frac{d\sigma}{d\theta} \quad (6.3)$$

where subscripts  $i$  and  $o$  refer to fluid inside and outside the sphere, respectively.

Assuming that the fluid viscosity inside the sphere is negligible compared to the outside fluid viscosity ( $(\tau_{r\theta})_i = 0$ ), then we have

$$\tau_{r\theta} = \mu_l \left[ \frac{1}{r} \frac{\partial U_r}{\partial \theta} + r \frac{\partial}{\partial r} \left( \frac{U_\theta}{r} \right) \right] = \mu_l \left( \frac{1}{r} \frac{\partial U_r}{\partial \theta} + \frac{\partial U_\theta}{\partial r} - \frac{U_\theta}{r} \right) = - \frac{1}{a} \frac{d\sigma}{d\theta} \quad (6.4)$$

If  $r = a$ , the velocity in the  $r$  direction ( $U_r$ ) is equal to zero. Assuming  $d\sigma/d\theta$  is sufficiently large,  $U_\theta$  can decrease to zero, and the order of magnitude argument can be written as:

$$\mu_l a \left( \frac{\partial U_\theta}{\partial r} \right)_{r=a} \approx \frac{d\sigma}{d\theta} \quad (6.5)$$

where the order of magnitude of the velocity derivative is

$$\left(\frac{\partial U_\theta}{\partial r}\right)_{r=a} \approx \frac{U}{a} \quad (6.6)$$

and  $U$  is the sphere velocity. From Eqs. 6.5 and 6.6, the surface tension gradient is

$$\frac{\Delta\sigma}{\Delta\theta} \approx \mu_l U \quad (6.7)$$

If the surface of a sphere at the front stagnation point is free of surfactant, the variation of surface tension over the surface between  $\theta = 0$  and  $\pi$  ( $\Delta\theta$  is of order one) (Savic, 1953; Griffith, 1962; Harper, 1972) is

$$\Delta\sigma \approx \mu_l U \quad (6.8)$$

The Gibbs adsorption equation for the surface excess (Eq. 6.2) is

$$\Gamma = \frac{C}{RT} \times \left(-\frac{d\sigma}{dC}\right) \quad (6.9)$$

where  $C$  is surfactant concentration,  $\text{g/cm}^3$  (in the bulk at interface).

Taking  $\sigma_0$  and  $\sigma$  as the surface tension at 0 and C surfactant concentration, respectively, then from the  $\sigma$ -C relationship,  $\Delta C = C$  and  $\Delta\sigma = \sigma_0 - \sigma = SC$ , where S is the absolute value of the slope of the  $\sigma$ -C curve (when C is very small). Then from Eq. 6.8 we have  $C = \mu_1 U/S$  and from Eq. 6.9 the following can be written

$$\Gamma \approx \frac{\mu_1 U}{R T S} \times \frac{S C}{C} \approx \frac{\mu_1 U}{R T} \quad (6.10)$$

When this amount of surfactant ( $\Gamma$ , mole/cm<sup>2</sup>) has accumulated, surface motion should be correspondingly negligible. Equation 6.10 is not dependent on the slope S. However, it is required that S be positive (when the slope is negative, the material is not a surfactant and does not adsorb at the interface).

Let the rate of mass transfer (per unit area) be  $k_m C_B$  where  $k_m$  (cm/s) is the mass transfer coefficient and  $C_B$  (mole/cm<sup>3</sup>) is the bulk concentration, then  $\Gamma = k_m C_B t_s$ , where  $t_s$  (s) is the characteristic adsorption time. From Eq. 6.10 we have

$$t_s \approx \frac{\mu_1 U}{k_m R T C_B} \quad (6.11)$$

The relationship between two mass transfer dimensionless numbers, Sherwood ( $Sh = k_m d_e / D_d$ ) and Peclet ( $Pe = d_e U / D_d$ ) when  $Re \rightarrow \infty$  is given by Clift et al., (1978)

$$\frac{k_m d_e}{D_d} \approx 1.13 \sqrt{\frac{d_e U}{D_d}} \quad (6.12)$$

From Eq. 6.12,  $k_m$  is

$$k_m \approx 1.13 \sqrt{\frac{U D_d}{d_e}} \quad (6.13)$$

$k_m$  can be substituted in Eq. 6.11 to give

$$t_s \approx \frac{\mu_l}{R T C_B} \times \frac{1}{1.13} \sqrt{\frac{d_e U}{D_d}} \quad (6.14)$$

Knowing the frother concentration in the bulk (mole/cm<sup>3</sup>), sphere velocity (Table 5.6) and diffusion coefficient (Table 6.1),  $t_s$  can be estimated. Table 6.2 shows the calculated  $t_s$  from Eq. 6.14 for frothers at various concentrations. This table shows the calculated  $t_s$  from (Eq. 6.14) is not in agreement with measured data (Table 5.5), being too short.

Table 6.2: The predicted adsorption time,  $t_s$  (Eq. 6.14) for frothers at various concentrations.

$d_c$ (cm)	Frother (ppm)	Dowfroth 250 $t_s$ (s)	Pine oil $t_s$ (s)	MIBC $t_s$ (s)
0.09	0.06	0.575	0.290	0.177
	0.25	0.138	0.069	0.042
	1.00	0.035	0.017	0.010
	30.00	0.0012	0.0006	0.0004
0.15	0.06	0.865	0.434	0.270
	0.25	0.208	0.104	0.064
	1.00	0.052	0.026	0.016
	30.00	0.0017	0.0009	0.0005
0.22	0.06	1.131	0.564	0.352
	0.25	0.271	0.135	0.084
	1.00	0.068	0.033	0.021
	30.00	0.0023	0.0011	0.0007
0.27	0.06	1.340	0.643	0.414
	0.25	0.322	0.154	0.099
	1.00	0.080	0.038	0.024
	30.00	0.003	0.0013	0.0008

*Empirical model for prediction of adsorption time for moving bubbles*

The measured terminal velocity (see Section 5.2), appears to be independent of frother concentration but dependent on frother type. Since the adsorption density of surfactant (Gibbs equation for a stationary interface) on a bubble does depend on solution concentration, the lack of concentration effect suggests that for a moving bubble, above a certain adsorption density the physical properties dictating the drag force (surface rigidity and viscosity) become constant. The other possibility is the adsorption density for a moving bubble is greater than the Gibbs equation suggests.

In this section an empirical model for estimating the adsorption time based on the present observations is introduced. The fundamental assumptions for establishing the model are:

- a- above a certain adsorption density the drag on the bubble becomes constant regardless of the frother concentration. This adsorption density can be greater than that suggested by Gibbs.
- b- a relationship exists between surface excess of a moving bubble and the Gibbs excess for a stationary flat surface.

Introducing the adsorption height ( $h_a$ , cm) as the distance moved by the bubble before terminal velocity is reached (at the end of the second stage, Fig. 6.3), then an estimate of this is

$$h_a = \frac{U_{\max} + U_T}{2} \times t_a \quad (6.15)$$

where  $U_{\max}$  (cm/s) is the maximum bubble velocity in tap water (or  $U_T$  in pure water),

$U_T$  (cm/s) is the terminal velocity in presence of frother and  $t_a$  (s) is the adsorption time (this estimate of "average" velocity  $((U_{max} + U_T)/2)$  is to avoid at this juncture trying to fit the  $U$  vs  $t$  data).

The total volume of water ( $V_a$ ,  $\text{cm}^3$ ) through which a bubble moves before it reaches terminal velocity is, therefore

$$V_a = h_a \times A_a \quad (6.16)$$

where  $A_a$  ( $\pi d_c^2/4$ ) is the bubble projected area ( $\text{cm}^2$ ).

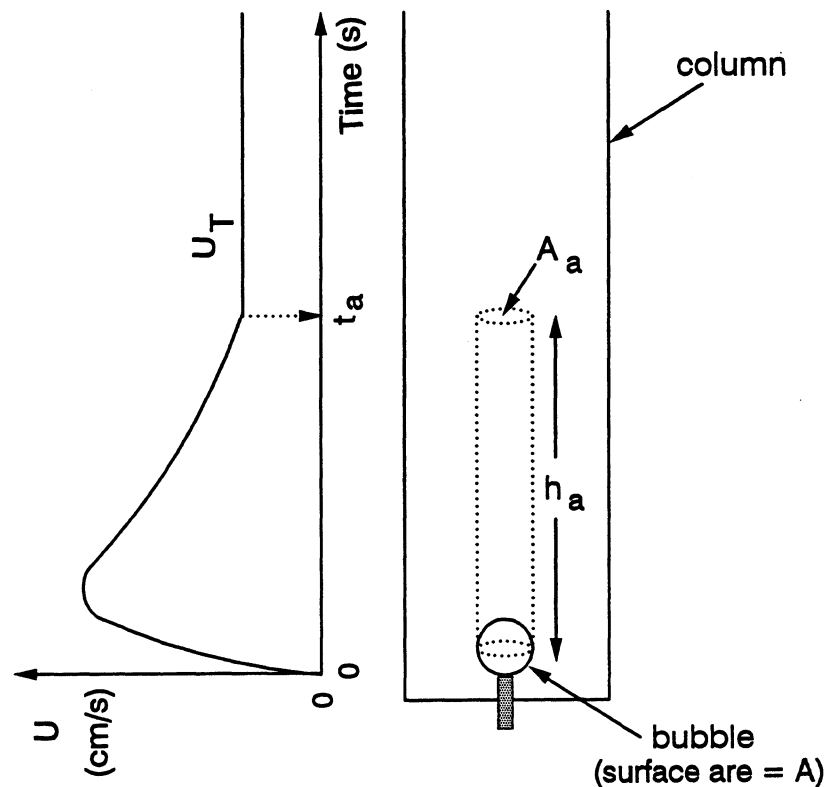


Figure 6.3: Adsorption distance ( $h_a$ ) for a moving bubble.

The total number of frother moles ( $C_t$ ) in  $V_a$  is

$$C_t = C \times V_a \quad (6.17)$$

where  $C$  is bulk frother concentration (mole/cm<sup>3</sup>).

The total number of frother moles per unit bubble surface area ( $C_b$ , mole/cm<sup>2</sup>) is given by

$$C_b = \frac{C_t}{A} \quad (6.18)$$

where  $A$  ( $\pi d_c^2$ ) is the bubble surface area (cm<sup>2</sup>).

The occupied area on a bubble surface by a frother molecule is assumed to be approximately 20 Å<sup>2</sup> (Leja, 1982): this leads to a maximum number of frother moles which can be placed at the unit surface area ( $N$ ), shown in Table 6.3. Table 6.3 also shows the adsorption density ( $\Gamma$ ) from the Gibbs equation and  $C_b$  (Eq. 6.18) (for 1.5 mm bubble). The comparison between these numbers clearly shows that  $C_b > N > \Gamma$  (i.e., the bubble encounters prior to reaching  $U_T$ , more than enough surfactant to completely cover its surface).

**Table 6.3: The numbers  $N$ ,  $\Gamma$  and  $C_b$  ( $d_c = 1.5$  mm).**

Frother (ppm)	N $\times 10^{-10}$ mole/cm <sup>2</sup>	Dowfroth 250		Pine oil		MIBC	
		$\Gamma$ $\times 10^{-10}$ mole/cm <sup>2</sup>	$C_b$ $\times 10^{-10}$ mole/cm <sup>2</sup>	$\Gamma$ $\times 10^{-10}$ mole/cm <sup>2</sup>	$C_b$ $\times 10^{-10}$ mole/cm <sup>2</sup>	$\Gamma$ $\times 10^{-10}$ mole/cm <sup>2</sup>	$C_b$ $\times 10^{-10}$ mole/cm <sup>2</sup>
0.06	8.3	0.23	170	0.12	700	0.02	940
0.25	8.3	0.30	220	0.17	1000	0.03	1600
1.00	8.3	0.79	590	0.40	2400	0.10	4500
30.00	8.3	5.15	3800	2.30	14000	0.93	42000

Now a dimensionless number ( $K_a$ ) is introduced as the ratio of  $C_b$  to  $\Gamma$

$$K_a = \frac{C_b}{\Gamma} \quad (6.19)$$

$K_a$  was calculated for different bubble sizes, frother types and concentrations with known  $U_{\max}$  (Table 5.4),  $U_T$  (Table 5.6),  $t_a$  (Table 5.5),  $C$  and  $\Gamma$  (Fig. 6.2). The average  $K_a$  (for various frother concentrations for a given frother type) was plotted as a function of  $d_e$  (since  $K_a$  is related to  $t_a$  and velocity and both are dependent on the bubble size) for the different frother types (Figure 6.4). The following equation was fitted ( $r^2 = 0.97$ ) namely,

$$K_a = a + b \times d_e^{\frac{1}{2}} \quad (6.20)$$

where  $d_e$  is the bubble volume-equivalent diameter (cm). The coefficients  $a, b$  are presented in Table 6.4.

**Table 6.4: The coefficients for Eq. 6.20.**

Frother	a	b
Dowfroth 250	-41.6	2061.5
Pine oil	38.3	10380.3
MIBC	614.6	81605.6

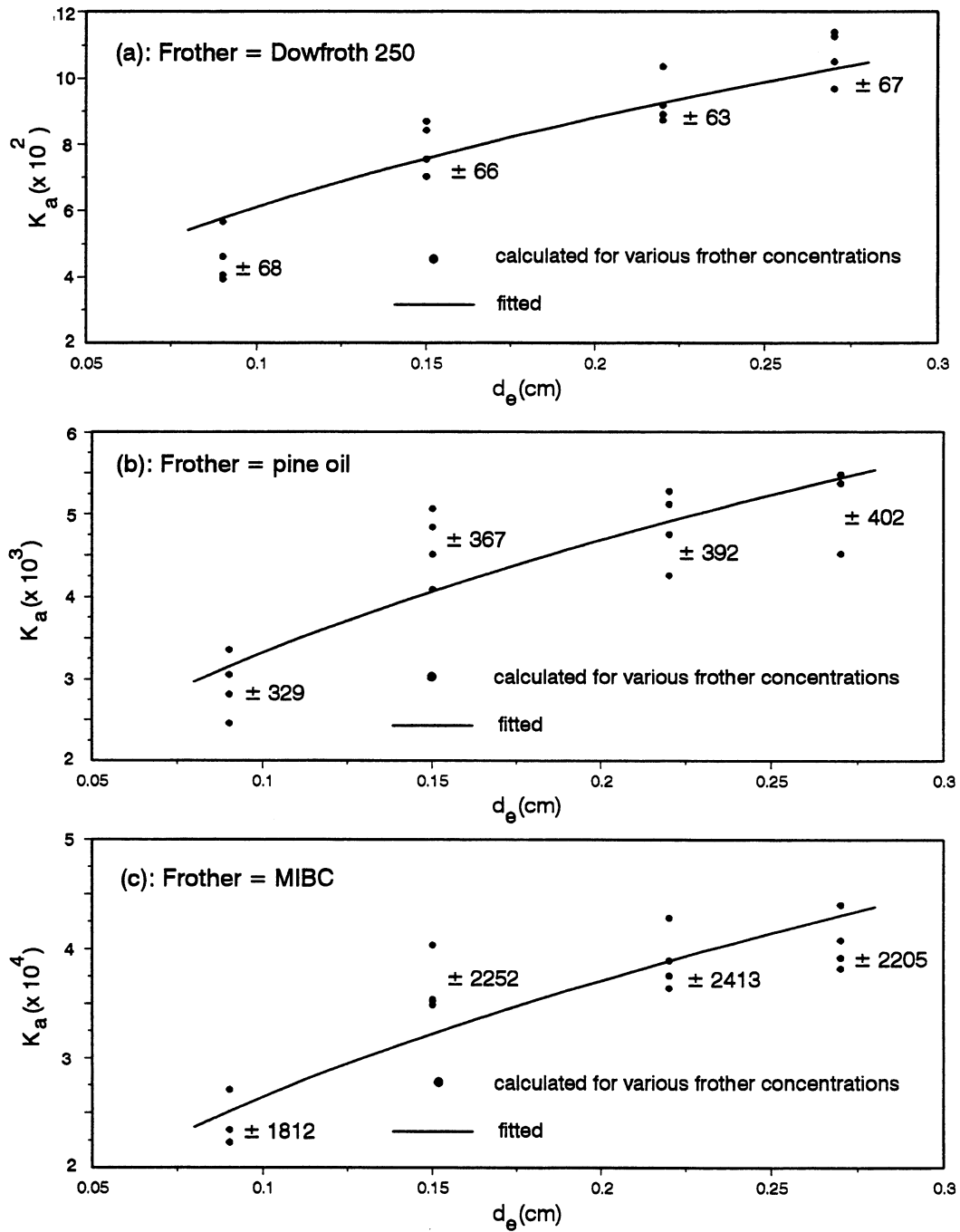


Figure 6.4:  $K_a$  as a function of  $d_e$  for various frothers; a: Dowfroth 250, b: pine oil, c: MIBC ( $\pm$  represents the standard deviation at that point).

From the above,  $t_a$  is

$$t_a = \frac{8 K_a \Gamma}{(U_{\max} + U_T) C} \quad (6.21)$$

Table 6.5 shows the measured (Table 5.5) and predicted (Eq. 6.21) adsorption time for various bubble sizes and frothers.

Table 6.5: Measured ( $t_a^*$ ) and predicted ( $t_a^{**}$ ) adsorption time.

$d_e$ (mm)	Dowfroth 250			Pine oil		MIBC	
	(ppm)	$t_a^*$ (s)	$t_a^{**}$ (s)	$t_a^*$ (s)	$t_a^{**}$ (s)	$t_a^*$ (s)	$t_a^{**}$ (s)
0.9	0.06	10.50	12.3	18.00	21.8	21.5	22.9
	0.25	4.00	4.0	8.60	8.1	9.10	9.7
	1.00	1.90	2.8	4.50	4.9	7.50	7.3
	30.00	0.40	0.6	0.80	0.9	2.00	2.3
1.5	0.06	12.00	10.7	21.00	18.7	***	19.5
	0.25	4.30	3.5	9.10	6.8	9.6	8.1
	1.00	2.30	2.4	5.00	4.0	7.80	6.0
	30.00	0.60	0.5	0.90	0.8	2.10	1.9
2.2	0.06	13.80	12.38	21.90	21.6	***	22.2
	0.25	5.10	3.9	9.50	7.8	10.10	9.22
	1.00	2.90	2.7	5.30	4.6	8.20	6.7
	30.00	0.70	0.6	0.90	0.9	2.30	2.1
2.7	0.06	15.20	13.8	***	24.7	***	24.7
	0.25	5.50	4.4	10.10	8.8	10.50	10.2
	1.00	3.40	3.0	5.80	5.2	8.40	7.4
	30.00	0.80	0.7	1.10	1.0	2.40	2.3

\*\*\* terminal velocity was not reached in a 4m column.

Figure 6.5 shows the measured and predicted adsorption time as a function of frother concentration for various bubble sizes and frothers. The model (Eq. 6.21) was established based on the idea that for a moving bubble (for a given bubble size and frother type), the number of frother molecules ( $N_a$ ) which can be adsorbed at the

interface before reaching the terminal velocity can be greater than that suggested by Gibbs (i.e.,  $\Gamma < N_s \leq N$ ). However, the drag on the bubble at terminal conditions is the same regardless of bulk concentration.

The measured adsorption time for Dowfroth 250 was less than for pine oil or MIBC which can be related to frother molecule properties (e.g., its structure):

a- at a given frother concentration, the surface tension of Dowfroth 250 is less than that of pine oil or MIBC.

b- the molecular weight and HLB (Hydrophile-Lipophile Balance) of Dowfroth 250 are greater than pine oil and MIBC. (The HLB number alone may not be enough to characterize flotation frothers. Increasing molecular weight at roughly the same HLB values makes frothers more powerful (Laskowski, 1989).)

It is to be noted, however, that the properties under static conditions (e.g., surface tension) are not adequate to explain the phenomena associated with moving bubbles. For instance, the present experimental data for adsorption time may be related to the dynamic surface tension for moving bubbles. In addition, the nature of the surface of a bubble in motion in terms of extent of surfactant adsorption appears to differ significantly from a stationary surface.

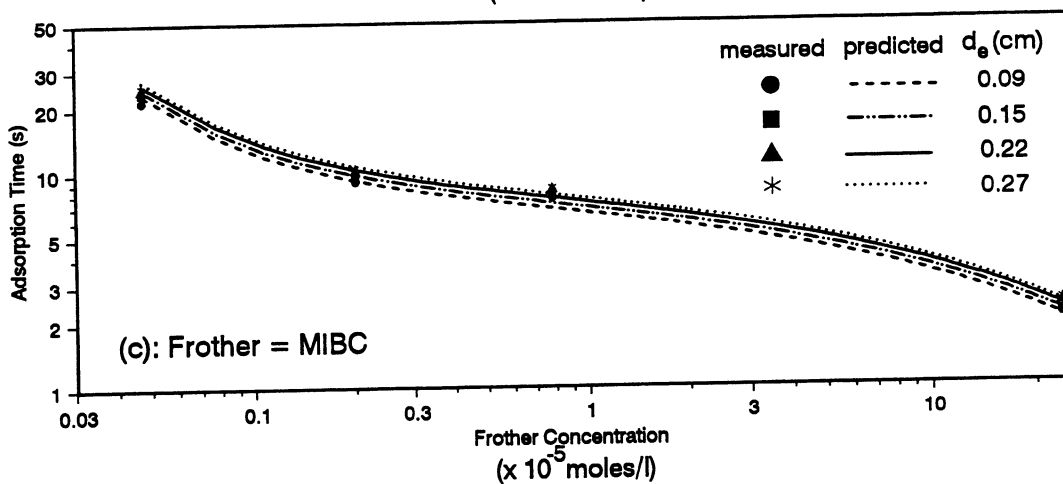
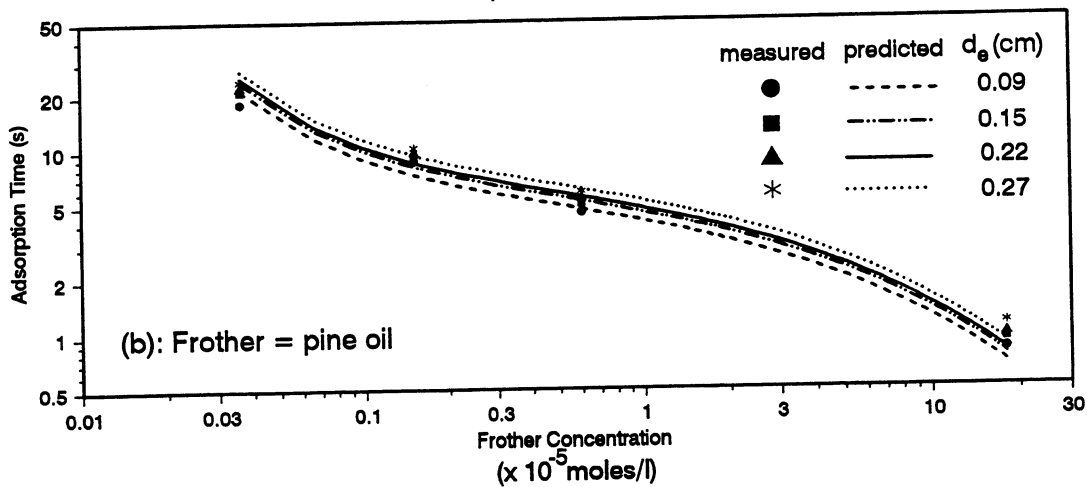
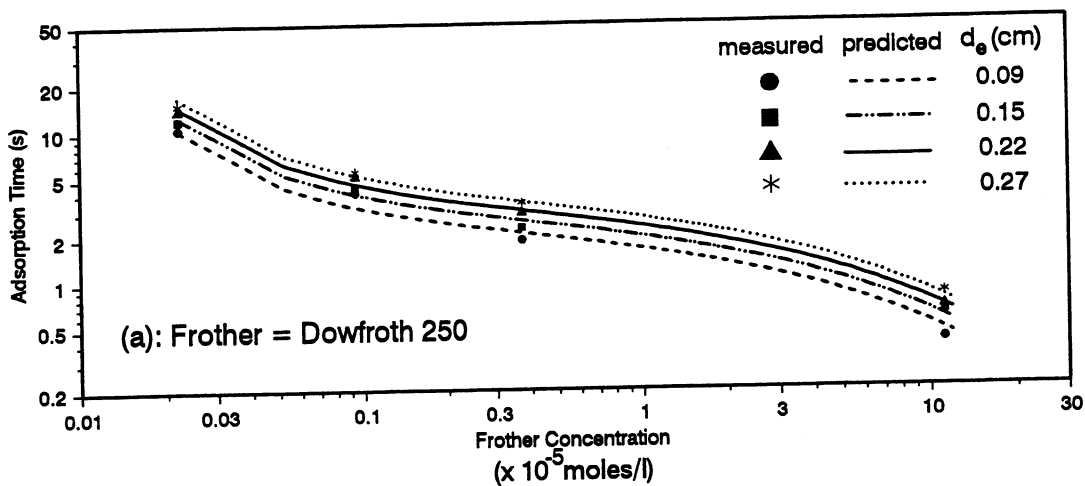


Figure 6.5: Adsorption time versus frother concentration for various  $d_e$ ; a: Dowfroth 250, b: pine oil, c: MIBC (in log-log form).

### 6.2.3. Stage 3, Terminal Velocity

Given sufficient time (i.e., column height), the bubble reaches a terminal velocity,  $U_T$  (Figs. 5.7-5.18). In some situations, the 4 m height of the present set-up is not sufficient: e.g., low frother (or impurity in the case of tap water) concentration or weak surface activity (methanol, xanthate).

There are examples in the literature of terminal velocity for the frothers used here which are different and show a concentration dependence (Fuerstenau and Wayman, 1958; Zhou et al., 1992). This difference can be resolved by considering the effect of stage two. If terminal velocity is measured by timing the bubble passage over a fixed distance (essentially an average velocity) which is the common procedure, then the terminal velocity may depend on the distance selected if a significant change in local velocity (characterized by stage two) occurs. The data of Zhou et al., (1992) were reexamined in this light. Table 6.6 shows that the measured average velocities over 90 cm from the present work agree with those from the empirical correlations developed by Zhou et al., based on experimental data for average velocity in a 90 cm column. This clearly indicates the need to consider the experimental procedure when measuring bubble terminal velocity.

**Table 6.6:** The measured (here) and calculated (Zhou et al., 1992) bubble average velocity over a distance of 90 cm from the orifice ( $d_o = 1.5$  mm).

Frother type	Dosage (ppm)	Average velocity (cm/s)	
		Measured	Zhou et al.
No frother	0	29.0	26.3
Dowfroth 250	0.06	26.4	25.2
	30	16.0	16.1
MIBC	0.06	27.6	26.3
	30	19.9	20.6

The drag force becomes maximum sometime during the second stage and then decreases until it equals the buoyancy force and the bubble reaches the terminal velocity. The terminal velocity appears to be independent of frother concentration but dependent on frother type. This suggests that either, regardless of solution concentration, frother adsorbs to eventually reach the same surface concentration (constant surface rigidity and viscosity), or above a certain surface concentration the drag becomes constant and independent of additional adsorption. The second possibility is more likely as, from the Gibbs adsorption equation, it is known that surface concentration is dependent on solution concentration. The fact that  $U_T$  depends on frother type presumably reflects differences in frother properties (e.g., molecular structure) and in the way the molecules interact with water molecules as the bubble moves through the water. The ratio of hydrophobic (H-C) to hydrophilic (OH) groups governs the extent of interaction with water molecules (Leja, 1982; Laskowski, 1993). An effect of adsorbed molecules on the terminal settling velocity of solid particles has been observed (Malysa et al., 1988) and the mechanism may be similar to that at play here.

Figures 6.6a and b compare the measured bubble terminal velocity with data and models from literature (see Section 2.9.2). The terminal velocity with frother lies close to the "contaminated water" data. The following equation was fitted ( $r^2 = 0.99$ ) to the present data:

$$U_T = (a + b d_e + c d_e^2) \quad (6.22)$$

Table 6.7 presents the coefficients for Eq. 6.22 (for different frothers). Figure 6.7 shows the measured data compared with predicted data from Eq. 6.22.

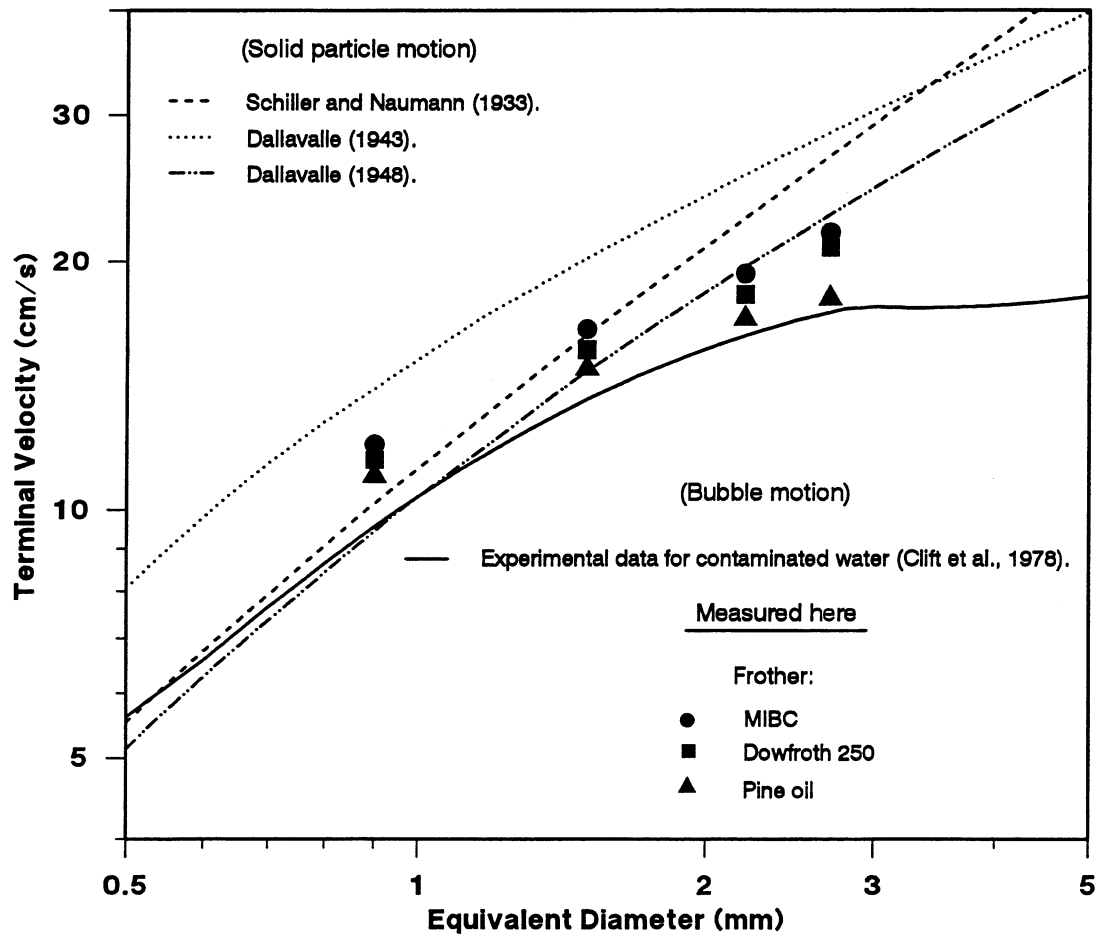


Figure 6.6a: Comparison between the present data on terminal velocity for bubbles in presence of frother and published data for bubbles in contaminated water and solid particles in water.

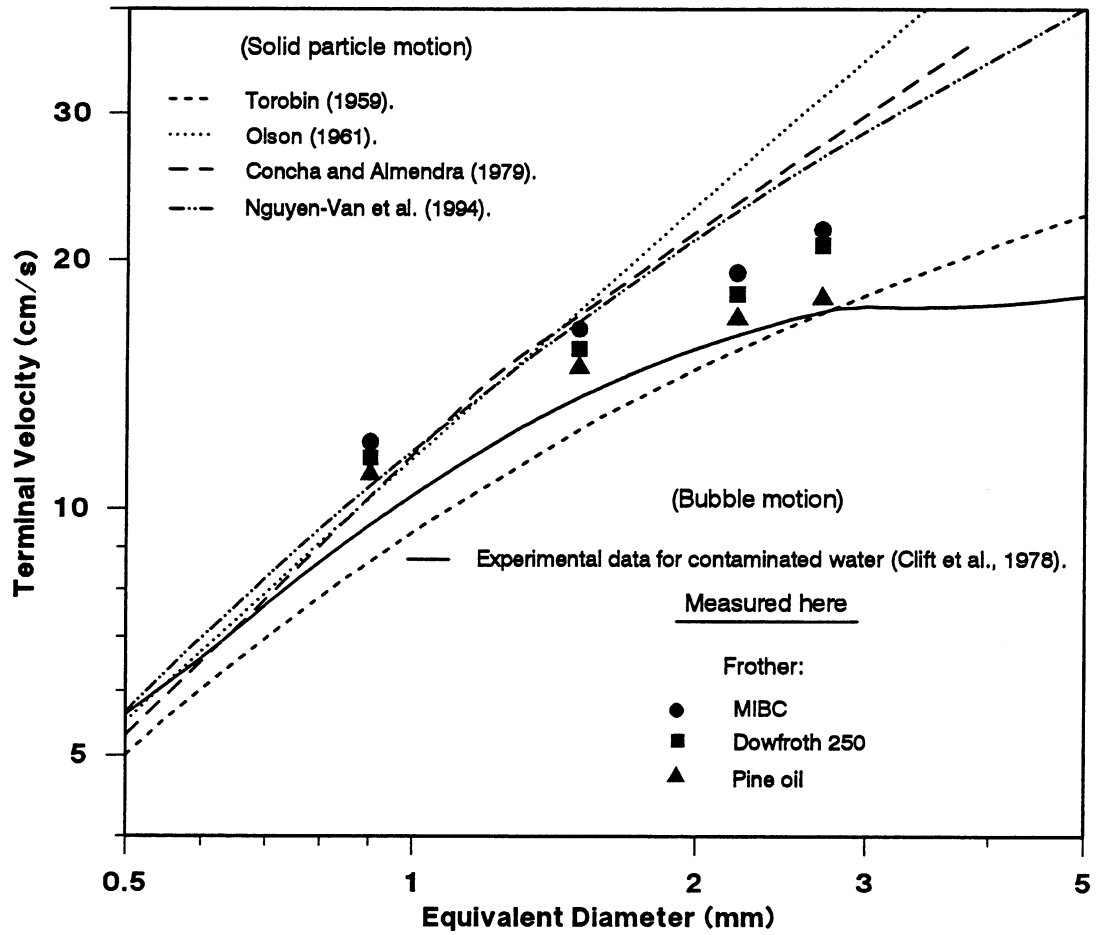


Figure 6.6b: Figure 6.6a continued.

Table 6.7: Coefficients for Eq. 6.22

Frother	a	b	c
MIBC	4.50	95.74	-120.92
Dowfroth 250	5.23	78.40	-79.32
Pine oil	3.27	102.62	-179.10

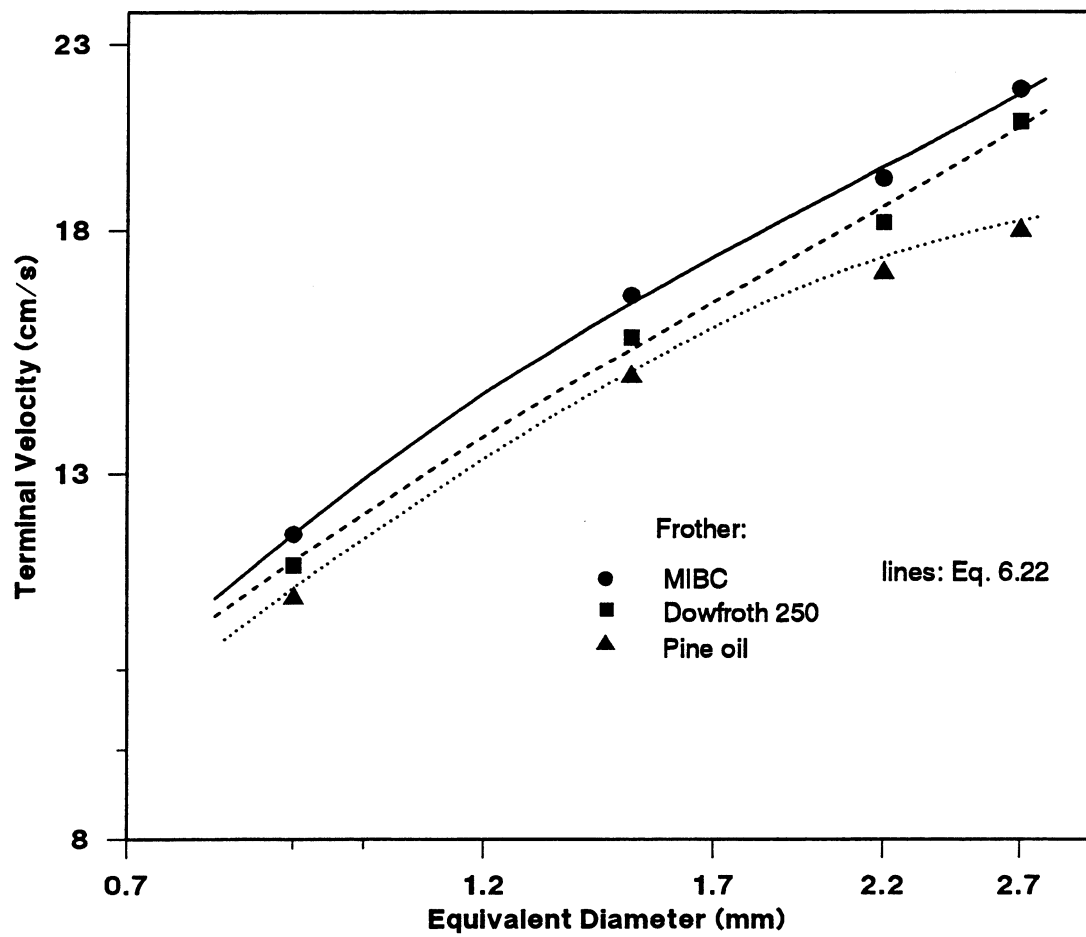


Figure 6.7: Terminal velocity of bubbles in presence of frother.

### 6.3. Significance to Flotation

In flotation, the properties of fresh bubbles, as opposed to aged bubbles, have periodically attracted attention (e.g., Leja, 1982; Detwiler and Blanchard, 1978). One property, surface tension, is known to decrease with time in the presence of surfactants, (so - called dynamic surface tension). For some surfactants the time interval can be long enough for effects related to flotation to be demonstrated (Finch and Smith, 1972). From simple wetting theory, using either Young's (1805) or Zisman's (1964) equation, a high surface tension favours a high contact angle. Since, a fresh bubble exhibits a high surface tension it favours a high contact angle and flotation. In the present case, the extent of surface tension decrease is sufficiently small that this effect probably is not significant. The present experimental data for adsorption time may be related to the dynamic surface tension for a moving bubble. The bubble velocity profile could be a method of studying dynamic surface tension for a moving bubble.

Frother/collector interactions are considered to play a role in flotation. One theory (Leja, 1982) suggests that the adsorbed frother molecules on the bubble are penetrated by adsorbed collector molecules on the particle. This interaction may be revealed by measuring bubble velocity profiles in the presence of both frother and collector; if the profile for a frother was changed in the presence of a collector it may support the penetration model. Xanthate is a good choice of collector in this regard as it is weakly surface active with regard to the bubble surface, as further supported by data here (Fig. 5.22).

Bubble size plays a role in particle collection. One of the application of the drift flux model (see Section 2.9.4) is to estimate bubble size in bubble swarms. Generally, the procedure is first to estimate  $U_T$ , then estimate  $d_b$  from available  $U_T$  vs  $d_b$  relationships (the Schiller and Naumann model is usually used). The present  $U_T$  vs  $d_b$  data permit this procedure to be refined. Taking the average  $U_T$  (for the three frother types), relationship is

$$U_T = \frac{g d_e^2 \Delta\rho}{18 \mu_l (a + b Re + c Re^2 + d Re^3)} \quad (6.23)$$

The coefficients in this equation are:  $a=2.485$ ,  $b=0.0023$ ,  $c=0.000112$  and  $d=-1.09 \times 10^{-7}$ . The  $U_T$  is estimated within  $\pm 1.5$  cm/s (range for the three frothers) giving a range in  $d_b$  of  $\pm 0.1$  mm. (Quoting a range was considered more useful than using a separate expression for the three frothers as recently suggested by Ityokumbul et al. (1995).) Table 6.8 compares the estimated bubble sizes using Eq. 6.23 instead of the Schiller and Naumann equation for data in the literature (Banisi and Finch, 1994). Table 6.8 does not suggest any major improvement using Eq. 6.23, but improvements may be more evident for larger bubbles ( $d_b > 1.5$  mm) as the deviation from the Schiller and Naumann equation for the present data increases (Fig. 6.6a).

Table 6.8: Comparison of bubble size estimation from drift flux model.

Frother* ppm	$J_g$ cm/s	$J_l$ cm/s	$\epsilon_g$ (%)	$d_b$ (mm) (measured)	$d_b$ (mm) (estimated)	
					Banisi and Finch (1994)**	current***
5	1.0	0.91	9.5	1.20	1.14	1.20
10	1.0	0.85	12.9	0.86	0.88	0.89
15	1.0	0.82	15.8	0.77	0.77	0.80
20	1.0	0.85	15.5	0.69	0.78	0.81
25	1.0	0.77	16.2	0.73	0.75	0.78
15	0.5	1.00	12.3	0.62	0.54	0.58
15	0.5	1.00	17.0	0.67	0.64	0.68

\* Dowfroth 250, \*\* using Schiller and Naumann, \*\*\* using Eq. 6.23

The present work was provoked in part by the observation that the increase in gas holdup with height in tall columns was greater than could be accounted for with available drift flux models (Finch, et al., 1995). The larger than expected increase in gas holdup with height could be explained if the bubble did not speed up as much as the pressure - bubble size - velocity relationship predicts. There seems to be some evidence for that possibility here. At relatively low concentrations of frother the bubble actually slows down appreciably (stage two). Typically in flotation, frother concentrations are a few ppm (Klassen, 1963), i.e., concentrations at which, from the results shown here, the bubble can be expected to reach terminal velocity relatively quickly. The question is what is the concentration experienced by a single bubble in a swarm? It could be that in a swarm a bubble encounters a concentration much lower than the nominal concentration and actually does experience a significant stage two component.

## CHAPTER 7

### CONCLUSIONS AND SUGGESTIONS FOR FUTURE WORK

#### 7.1 Conclusions

- 1- Bubble behaviour has been investigated in a 4 m high column for bubbles over a range of interest in flotation (from 0.9 to 2.7 mm volume-equivalent diameter) in the absence and presence of reagents used in flotation (e.g., frothers).

#### *Experimental Equipment*

- 2- The column was selected large enough (cross section: 10 × 10 cm) not to have significant wall effects on the behaviour of the bubbles. A square cross section was chosen to avoid optical distortion.
- 3- The column was water-jacketed and held at a constant and uniform temperature ( $30 \pm 0.25$  °C).
- 4- Controllable gas injection was used to provide a low enough frequency (<25 bubbles/min) to avoid an effect on bubble behaviour.
- 5- In order to follow the bubble from the moment of leaving the orifice to the top of the column, a video camera supported on a track and capable of moving vertically at adjustable speeds was employed.

*Results (Bubble Size, Shape and Motion)*

- 6- It was found that bubble generation frequency up to 80 bubbles/min had little effect on bubble behaviour.
- 7- The measured bubble sizes were in agreement with Tate's law. The bubble expansion over a 4 m rise was about 10% which agreed with the equation of state under isothermal conditions. Frother had a negligible effect on bubble volume-equivalent diameter.
- 8- The bubble shape and motion in the presence of frother changed to become less oblate and oscillatory (both in amplitude and frequency), compared to the system in the absence of frother. The shape and motion changed from the bottom to the top of the column which reflected the effect of accumulation (adsorption) of impurities (in water) or surfactants (frother) with height (or time). This effect was almost negligible in presence of high frother concentration indicating a short adsorption time.

*Results (Axial Bubble Velocity Profiles)*

- 9- Axial single bubble velocity profiles were determined. The effect of flotation reagents such as frother (type and concentration) on velocity profiles was evaluated.
- 10- In general, the velocity profile showed 3 stages: an initial acceleration followed by a deceleration and finally a constant (terminal) velocity. The major velocity profile characteristics were: a maximum velocity, an adsorption time and a terminal velocity. The velocity reduction (in the second stage) reflected the time-

dependent adsorption of impurities or surfactants.

- 11- In the case of water-only, only the first and the second stages were identified which showed that the column height (4m) was not sufficient to reach the terminal velocity (third stage).
- 12- In the case of water-only, the maximum velocity was in good agreement with Moore's theory for bubble terminal velocity in pure water. It is expected that in pure water the terminal velocity is equal to the maximum velocity.
- 13- The velocity profile was very sensitive to frother type and concentration, even amounts  $< 1$  ppm had a large effect.
- 14- For a given bubble size and frother type, the first 2 stages were strongly affected by the amount of frother but the third stage (terminal velocity) was independent of the frother dosage.
- 15- Time-dependence of the velocity was attributed to time-dependent adsorption of surfactant causing increased bubble rigidity and surface viscosity.
- 16- The adsorption time for Dowfroth 250 was less than for pine oil and MIBC which reflects an effect of frother molecule structure.
- 17- According to the present results, the terminal velocity (for a given bubble size and frother type) is not a function of frother concentration. This indicates that: (1) above a certain adsorption density the physical properties dictating the drag force (surface rigidity and viscosity) become constant, (2) since the adsorption density for a stationary interface (Gibbs equation) does depend on solution

concentration, based on the present results, the adsorption density for a moving bubble can be greater than that suggested by Gibbs.

- 18- An empirical model was established to determine the adsorption time. In this model the adsorption density for a moving bubble is allowed to be greater than that calculated from the Gibbs equation.
- 19- Terminal velocity was dependent on frother type. This was attributed to the differences in the frother structure (e.g., hydrophobic/hydrophilic balance of the frother molecules controlling bubble/water interaction).
- 20- The average terminal velocity of bubbles in presence of the three frothers as a function of bubble diameter was used to reexamine the drift flux method for bubble size estimation in swarms. The results were in agreement with the measured bubble sizes from the literature.

## 7.2 Claims for Original Research

- 1- Bubble velocity profiles were measured for three frothers commonly used in flotation.
- 2- Three stages to the profile were identified and related to time-dependent adsorption.
- 3- An empirical model to estimate adsorption time was developed. This model introduces the possibility that adsorption density on a moving bubble can exceed that calculated from the Gibbs equation.
- 4- The experimental results showed that the bubble terminal velocity is not related to the frother concentration but is dependent on frother type.
- 5- An empirical model of terminal velocity vs bubble diameter was introduced.

### 7.3 Suggestions for Future Work

- 1- Measuring the bubble motion directly from the monitor is tough on the eyes and requires a lot of time to analyze the data. A technique is needed to determine the bubble motion automatically.
- 2- Testing surfactants with various structures and molecular weights under different conditions (e.g., temperature) is recommended to investigate the parameters which influence the adsorption time and terminal velocity. The velocity profiles may give enough information to determine theoretically the mechanism of surfactant adsorption on moving interfaces (e.g., bubbles).
- 3- To investigate the effect of frother, collector and pH combinations on velocity profiles.
- 4- The velocity profiles being so sensitive to impurities may open up a new method for studying dynamics of adsorption.

## REFERENCES

- Agrawal, S.K., and Wasan, D.T., 1979, The effect of interfacial viscosities on the motion of drops and bubbles, *Chem. Eng. J.*, **18**, 215-223.
- Ahmed, N., and Jameson, G.J., 1989, Flotation kinetics, *Mineral Processing and Extractive Metallurgy Review*, **5**, 77-99.
- Ahmed, N., and Jameson, G.J., 1985, The effect of bubble size on the rate of flotation of fine particles, *International Journal of Mineral Processing*, **14**, 195-215.
- Anfruns, J.F., and Kitchener, J.A., 1976, The absolute rate of capture of single particles by single bubbles, Published in "Flotation, vol.2", Fuerstenau, M.C., *American Institute of Mining, Metallurgical, and Petroleum Engineers, Inc.*, New York, 625-637.
- Anfruns, J.F., and Kitchener, J.A., 1977, Rate of capture of small particles in flotation, *Trans. Instn. Mining Met.*, **86**, C9-C15.
- Aybers, N.M., and Tapucu, A., 1969a, The motion of gas bubbles rising through stagnant liquid, *Wärme- und Stoffübertragung*, Bd. 2, 118-128.
- Aybers, N.M., and Tapucu, A., 1969b, Studies on the drag and shape of gas bubbles rising through a stagnant liquid, *Wärme- und Stoffübertragung*, Bd. 2, 171-177.
- Bachhuber, C., and Sanford, C., 1974, The rise of small bubbles in water, *Journal of Applied Physics*, **45**, 6, 2567-2569.
- Banisi, S., 1994, On-line phase holdup measurement and analysis in flotation columns, Ph.D. Thesis, McGill University, Montreal, Canada.
- Banisi, S., and Finch, J.A., 1994, Technical note: Reconciliation of bubble size estimation methods using drift flux analysis, *Minerals Engineering*, **7**, 1555-1559.
- Bergman, T.L., Webb, B.W., 1990, Simulation of pure metal melting with buoyancy and surface tension forces in the liquid phase, *Int. J. Mass Transfer*, **33**, 1, 139-149.
- Best, A.C., 1950, Empirical formula for the terminal velocity of the water drops falling through the atmosphere, *Quart. J. Royal Meteor. Soc.*, **76**, 302-311.
- Bhaga, D., Weber, M.E., 1981, Bubbles in viscous liquids: shapes, wakes and velocities, *J. Fluid Mech.*, **105**, 61-85.
- Bhaga, D., and Weber, M.E., 1980, In-line interaction of a pair of bubbles in a viscous liquid, *Chemical Engineering Science*, **35**, 2467-2474.

- Bhaga, D., 1976, Bubbles in viscous: shapes, wakes and velocities, Ph.D. Thesis, *McGill University*, Montreal, Canada.
- Bikerman, J.J., 1958, Surface chemistry, Academic Press, New York.
- Binder, R. C., 1973, Fluid mechanics, *Prentice-Hall*, Englewood Cliffs, N.J.
- Blanchard, D.C., and Syzdek, L.D., 1977, Production of air bubbles of a specified size, *Chemical Engineering Science*, **32**, 1109-1112,
- Bond, W.N., and Newton, D.A., 1928, Bubbles, drops and Stokes' law, *Phil. Mag., Ser. 7*, **5**, 794-800.
- Boussinesq, J., 1913, Vitesse de la chute lente, devenue uniforme, d'une goutte liquide sphérique, dans un fluid visqueux de poids spécifique moindre, *C.R. Acad. Sci.*, **156**, 1124-1130.
- Boutin, P., and Wheeler, D.A., 1967, Column flotation, *Mining World*, **20**, 3, 47-50.
- Burgess, J.M., and Calderbank, P.H., 1975, The measurement of bubble parameters in two-phase dispersions - I: The development of an improved probe technique, *Chemical Engineering Science*, **30**, 743-750.
- Castillejos, A.H., and Brimacombe, J.K., 1987, Measurement of physical characteristics of bubbles in gas-liquid plumes, part I: An important electroresistivity probe technique, *Metallurgical Transaction*, **18B**, 649-658.
- Cathignol, D., Chapelon, J.Y., 1984, Real time Doppler imaging: a new way, *Ultrasonic Symposium Proceedings '84*, IEEE, New York, 703-706.
- Cathignol, D., Chapelon, J.Y., Newhouse, V.L., and Shnakar, P.M., 1990, Bubble sizing with high spatial resolution, *IEEE Transactions on Ultrasonic, Ferroelectrics, and frequency control*, **37**, 1, 30-37.
- Cathignol, D., Trawinski, Z., and Chapelon, J.Y., 1987, Full range pseudorandom Doppler flowmeter using serial processing, *Ultrasonic Symposium Proceedings '87*, IEEE, New York, 889-892.
- Cathignol, D., Chapelon, J.Y., Newhouse, V.L., and Shankar, P.M., 1988, Bubble sizing with high spatial resolution, *Ultrasonic Symposium Proceedings '88*, IEEE, New York, 933-936.
- Chapelon, J.Y., Cathignol, D., Newhouse, V.L., and Shankar, P.M., 1987, A double frequency Doppler technique for bubble size measurement, *Ultrasonic Symposium Proceedings '87*, IEEE, New York, 885-888.

- Chapelon, J.Y., Shankar, P.M., and Newhouse, V.L., 1985a, Ultrasonic measurement of bubble cloud size profiles, *Journal of Acoustical Society of America*, **78**, 1, 196-201.
- Chapelon, J.Y., Shankar, P.M., and Newhouse, V.L., 1985b, Application of the double frequency in bubble sizing and pressure measurements in fluids, in *Acoustical Imaging '85*, Proceeding of the International Symposium, Plenum Press, New York, **14**, 753-755.
- Chhabra, R.P., and De Kee, D., 1992, Transport process in bubbles, drops, and particles, *Hemisphere Publishing Corporation*, pp. 1-41.
- Claridge, P.G., Holmes, G.P., and Redfearn, M.A., 1989, Operation and maintenance in mineral processing plants, Edited by P.G. Claridge, *Harpell's Press Cooperative*, Published for Canadian Mineral Processors division of CIM (as special volume 40), 265-293.
- Clark, N.N., and Turton, R., 1988, Chord length distribution related to bubble size distribution in multiphase flows, *International Journal of Multiphase Flow*, **14**, 4, 413-424.
- Clift, R., Grace, J.R., and Weber, M.E., 1978, Bubbles, drops and particles, *Academic Press*.
- Collins, R., 1967, The effect of a containing cylindrical boundary on the velocity of a large gas bubble in a liquid, *J. Fluid Mech.*, **28**, Part 1, 97-112.
- Commander, K.W., and Morits, E., 1989, Inferring bubble populations in the ocean from acoustic measurements, in *Ocean '89*, International Conference Addressing Methods for Understanding the Global Ocean, **4**, 1181, 1185.
- Concha, F., and Almendra, E.R., 1979, Settling velocities of particulate systems, 1. Settling velocities of individual spherical particles, *Int. J. Mineral Processing*, **5**, 349-367.
- Crabtree, J.R., and Bridgwater, J., 1971, Bubble coalescence in viscous liquids, *Chemical Engineering Science*, **26**, 839-851.
- Crozier, R.D., 1992, Flotation: theory, reagents and ore testing, *Pergamon Press*, pp. 95-100.
- Davidson, J.F., and Harrison, D., 1963, Fluidised particles, *Cambridge, At the University Press*, 20-78.
- Davidson, J.F., and Harrison, D., 1971, Fluidization, *Academic Press*, London and New York.
- Davidson, J.F., and Schüler, O.G., 1960a, Bubble formation at an orifice in a viscous liquid, *Trans. Instn Chem. Engrs*, **38**, 144-154.
- Davidson, J.F., and Schüler, O.G., 1960b, Bubble formation at an orifice in an inviscid liquid, *Trans. Instn Chem. Engrs*, **38**, 335-342.

- Davies, J.T., and Rideal, E.K., 1961, Interfacial phenomena, *Academic Press*, New York.
- Dekée, D., Carreau, P.J., and Mordarski, J., 1986, Bubble velocity and coalescence in viscoelastic liquids, *Chemical Engineering Science*, **41**, 9, 2273-2283.
- Derjaguin, B.V., and Dukhin, S.S., 1961, Theory of flotation of small and medium-size particles, *Transactions Institution of Mining and Metallurgy*, Feb. 61, 221-245.
- Detwiler, A., and Blanchard, D.C., 1978, Aging and bursting bubbles in trace-contaminated water, *Chem. Eng. Sci.*, **33**, 9-13.
- Dobby, G.S., and Finch, J.A., 1986a, Particle collection in columns - Gas rate and bubble size effects, *Canadian Metallurgical Quarterly*, **25**, 1, 9-13.
- Dobby, G.S., and Finch, J.A., 1986b, Flotation column scale-up and modelling,, *CIM Bulletin*, May 86.
- Dobby, G.S., and Finch, J.A., 1987, Particle size dependence in flotation derived from fundamental model of the capture process, *Int. j. Mineral Processing*, **21**, 241-260.
- Dobby, G.S., Yianatos, J.B., and Finch, J.A., 1988, Estimation of bubble diameter in flotation columns from drift flux analysis, *Canadian Metallurgical Quarterly*, **27**, 2, 85-90.
- Dobby, G.S., 1984, A fundamental flotation model and flotation column scale-up, Ph.D. Thesis, McGill University, Montreal, Canada.
- Edgar. C.B.Jr., 1966, AEC Report No. NYO-3114-14 by G.B. Wallis, 19-21.
- Eskinazi, S., 1968, Principles of fluid mechanics, *Allyn and Bacon*, Boston.
- Fan, L.-S., and Tsuchiya, K., 1990, Bubble wake dynamics in liquids and liquid-solid suspensions, *Butterworth-Heinemann*, 17-66.
- Finch, J.A., and Dobby, G.S., 1990, Column flotation, *Pergamon Press*, New York, pp. 37-47.
- Finch, J.A., and Smith, G.W., 1972, Dynamic surface tension of alkaline dodecylamine acetate solutions in oxide flotation, *Trans IMM*, **81**, C213-218.
- Finch, J.A., 1973, The liquid-vapor interface and adhesion in flotation, Ph. D. Thesis, McGill University, Montreal, Canada.
- Finch, J.A., 1971, Interfacial phenomena in cationic magnetite flotation, Master Thesis, McGill University, Montreal, Canada.
- Finch, J.A., 1995, Column flotation: A selected review - Part IV: Novel flotation devices, *Mineral Engineering*, **8**, 6, 587-602.

- Finch, J.A., Uribe-Salas, A., and Xu, M., 1995, Flotation science and engineering, Edited by K.A. Matis, *Marcel Dekker, Inc.*, New York. pp. 291-330.
- Flint, L.R., and Howarth, W.J., 1971, The collision efficiency of small particles with spherical air bubbles, *Chem. Eng. Sci.*, **26**, 1155-1168.
- Foust, A.S., 1980, Principles of unit operations, *Wiley*, New York.
- Frumkin, A., and Levich, V.G., 1947, *Journal of physical Chemistry (USSR)*, **21**, 1183-1204.
- Fuerstenau, D.W., and Wayman, C.H., 1958, Effect of chemical reagents on the motion of single air bubbles in water, *Transaction AIME, June, Mining Engineering*, 694-699.
- Fuerstenau, D.W., 1962, Froth flotation, 50th anniversary volume, *AIME*, New York.
- Fukuma, M., and Muroyama, K., 1987, Properties of bubble swarm in a slurry bubble column, *Journal of Chemical Engineering of Japan*, **20**, 1, 28-33.
- Gahi, R., 1917, History of the flotation process at inspiration, *Trans, AIME.*, **55**, 576-645.
- Garner, F.H., and Hammerton, D., 1954, Circulation inside gas bubbles, *Chem. Eng. Sci.*, **3**, 1, 1-11.
- Gaskell, D.R., 1992, An Introduction to transport phenomena in mineral processing, *Macmillan Publishing Company*, New York.
- Gaudin, A.M., 1957, Flotation, *McGraw-Hill*, New York.
- Geary, N., and Rice, R.G., 1991, Bubble size prediction for rigid and flexible spargers, *AICHE Journal*, **37**, 161-168.
- Glembotskii, V.A., 1963, Quoting concentration of non-metallic minerals by flotation, *Izd. AN SSSR*, 1952.
- Glicksman, L.R., Lord, W.K., and Sakagami, M., 1987, Bubble properties in large-particle fluidized beds, *Chemical Engineering Science*, **42**, 3, 479-491.
- Gomez, C.O., Uribe-Salas, A., Finch, J.A. and Huls, B.J., 1995, Axial gas holdup profiles in the collection zones of flotation columns, *Minerals and Metallurgical Processing*, **12**, 1, 16-23.
- Grace, J.R., Wairegl, T., and Nguyen, T.H., 1976, Shapes and velocities of single drops and bubbles moving freely through immiscible liquids, *Trans. Instn Chem. Engrs*, **54**, 167-173.
- Grace, J.R., 1973, Shapes and velocities of bubbles rising in infinite liquids, *Trans. Instn Chem. Engrs*, **51**, 116-120.

- Graf, R.F., 1984, Modern dictionary of electronics, *Indianapolis*, Ind., USA, H.W. Sams.
- Griffith, R.M., 1962, The effect of surfactants on the terminal velocity of drops and bubbles, *Chem. Eng. Sci.*, **17**, 1057-1070.
- Haberman, W.L., and Morton, R.K., 1953, An experimental investigation of the drag and shape of air bubbles rising in various liquids, Navy Department, The David W. Taylor Model Basin, Report 802.
- Hadamard, J., 1911, Mouvement permanent lent d'une sphère liquide et visqueuse dans une liquide visqueux, *C. R. Acad. Sci.*, **152**, 1735-1738.
- Hahn, P.-S., and Slattery, J.C., 1985, *AIChE Journal*, **31**, 950-955.
- Harkins, W.D., 1952, The physical chemistry of surface films, Chap. 2, *Reinhold*, New York.
- Harper, J.F., 1972, The motion of bubbles and drops through liquids, *Advance Applied Mechanics*, **12**, 59-129.
- Harris, C.C., 1976, Flotation machines, in Flotation-A.M. Gaudin Memorial Volume (M.C. Fuerstenau, ed.) *A.I.M.E.*, N.Y., 753-815.
- Hartunian, R.A., and Sears, W.R., 1957, On the instability of small gas bubbles moving uniformly in various liquids, *J. Fluid Mech.*, **3**, 27-47.
- Herringe, R., and Davis, M.R., 1974, Detection of instantaneous phase changes in gas liquid mixtures, *Journal of Physics E: Scientific Instruments*, **7**, 807-812.
- Heywood, H., 1962, Uniform and nonuniform motion of particles in fluids, in Proceeding of the Symposium on the interaction between Fluids and Particles., *Inst. Chem. Eng.*, London, 1-8.
- Hills, J.H., and Darton, R.C., 1976, The rising velocity of a large bubble in a bubble swarm, *Trans, Instn Chem. Engrs*, **54**, 258-264.
- Holbrook, J., and LeVan, M.D., 1983, Retardation of droplet motion by surfactant. Part 1. Theoretical development and asymptotic solutions, *Chem. Eng. Commun*, **20**, 191-207.
- Igusti-Ngurah, A., 1989, Effect of air bubble size distribution on the flotation rate of complex ore in a froth flotation column, Master Thesis, Department of Materials Engineering, Wollongong University, Australia.
- Ishida, M., and Tanaka, H., 1982, An optical probe to detect both bubbles and suspended particles in a three-phase fluidized bed, *Journal of Chemical Engineering of Japan*, **15**, 5, 389-391.

- Ityokumbul, M.T., Salama, A.I.A., and Al Taweel, A.M., 1995, Estimation of bubble size in flotation columns, *Minerals Engineering*, **8**, 77-89.
- Ives, K.J., 1984, The scientific basic of flotation, *Martinus Nijhoff Publishers*, pp. 53-74.
- Jameson, G.J., and Manlapig, E.V., 1991, Applications of the Jameson cell, in *Column '91* (eds. G.E. Agar, B.J. Huls and D.B. Hyma) MITEC, CIM (CMP), 673-688.
- Jameson, G.J., 1988, A new concept in flotation column design, in *Column Flotation '88* (K.V.S. Sastry, ed.), SME Annual Meeting Phoenix, Arizona, 281-286.
- Jameson, G.J., 1993, Bubbles in motion, *Trans. J. Chem. E.*, **71**, 587-594.
- Jiang, Z.W., and Holtham, P.N., 1986, Theoretical model of collision between particles and bubbles in flotation, *Trans. Instn Min. Metall. (London)*, **95**, C187-194.
- John, J.E.A., and Haberman, J.W.L., 1988, Introduction to fluid mechanics, *Prentice-Hall*, Englewood Cliffs, NJ.
- Karamanev, D.G., and Nikolov, L.N., 1992, Free rising spheres do not obey Newton's law for free settling, *AIChE Journal*, **38**, 11, 1843-1846.
- Kaya, M., 1989, Froth washing in mechanical flotation cells, Master Thesis, McGill University, Montreal, Canada.
- Kelly, E.G., and Spottiswood, D.J., 1989, *John Wiley and Sons*, Australia.
- King, R.P., 1982, Principles of flotation, South African, *Institute of Mining and Metallurgy*, Johannesburg.
- King, R.P., 1982, Principles of Flotation, *South African Institute of Mining and Metallurgy Monograph Series*, pp. 31-71 and 237-250.
- Kitano, K., and Fan, L.-S., 1987, Near-wake structure of a single gas bubble in a two dimensional liquid-solid fluidized bed: Solids holdup, *Chemical Engineering of Japan*, **1**, 1, 45-50.
- Klassen, V.I., and Mokrousov, V.A., 1963, An introduction to the theory of flotation, *Butterworths*, London, pp. 39-62.
- Kojima, E., Akehata, T.A., and Shirai, T., 1968, Rising velocity and shape of single air bubbles in highly viscous liquids, *J. Chemical Engineering of Japan*, **1**, 1, 45-50.
- Kreischer, B.E., Moritomi, H., and Fan, L.-S., 1990, Wake solids holdup characteristics behind a single bubble in a three-dimensional liquid-solid fluidized bed, *Int. J. Multiphase Flow*, **16**, 2, 187-200.

- Kuehn, Walker, L.A., Cienski, T., and Reynolds, V., 1991, Air sparging evaluation method, *International Conference on Column Flotation (Column 91)*, Sudbury, Ont. Canada, **1**, 321-340.
- Kumar, R., and Kuloor, N.R., 1970, *Adv. Chem. Engng*, **8**, (Edited by Drew, T.B. et al.), Academic Press.
- Lan, C.W., and Kou, S., 1992, Heat transfer and fluid flow in flotation-zone crystal growth with a mostly covered melt surface, *Int. Heat Mass Transfer*, **35**, **2**, 433-442.
- Lapple, C.E., and Shepherd, C.B., 1940, Calculation of particle trajectories. *Ind. Eng. Chem.*, **32**: 605.
- Laskowski, J.S., 1989, Frothing in flotation, *Gordon and Breach Science Publishers*, New York, pp. 225-239.
- Laskowski, J.S., 1993, Frothers and flotation froth, *MINERAL PROCESSING AND EXTRACTIVE METALLURGY REVIEW*, **12**, 61-89.
- Lehrer, I.H., 1976, A Rational terminal velocity equation for bubbles and drops at intermediate and high Reynolds number, *J. Chemical Engineering of Japan*, **9**, **3**, 237-240.
- Leja, J., 1982, Surface chemistry of froth flotation, *Plenum Press*, pp. 75-76 and 597-600.
- LeVan, M.D., 1981, Motion of a droplet with Newtonian interface, *Journal of Colloid and Interface Science*, **83**, **1**, 11-17.
- LeVan, M.D., and Newman, J., 1976, The effect of surfactant on the terminal and interfacial velocities of a bubble or drop, *AIChE J.*, **22**, **4**, 695-701.
- Levich, V.G., 1962, Physicochemical Hydrodynamics, *Prentice-Hall*, Englewood Cliffs, New Jersey.
- Li, R.-Q., 1992, Hydrodynamic instabilities of cylindrical interfaces, Ph.D. thesis, McGill University, Canada.
- Liebermann, L., 1957, Air bubbles in water, *Journal of Applied Physics*, **28**, 205-211.
- Lim, K.S., Agarwal, P.K., and O'Neill, B.K., 1990a, Measurement and modeling of bubble parameters in a two-dimensional gas-fluidized bed using image analysis, *Powder Technology*, **60**, 159-171.
- Lim, K.S., and Agarwal, 1990b, Conversion of pierced lengths measured at a probe to bubble size measures: an assessment of the geometrical probability approach and bubble shape models, *Powder Technology*, **63**, 205-219.

- Linton, M., and Sutherland, K.L., 1957, Dynamic surface forces, drop circulation and liquid-liquid mass transfer, *Second international congress on surface activity*, Butterworth, London, 1, 494-501.
- Lochiel, A.C., 1965, The influence of surfactants on mass transfer around spheres, *Can. J. Chem. Eng.*, **43**, 40-44.
- Loglio, G., Innocenti, N.D., Tesi, U., and Cini, R., 1989, Rising of gas bubbles in an aqueous medium in presence of surfactants, *Il Nuovo Cimento*, **12**, 3, 289-304.
- Malysa, K., Masliyah, J.H., Neale, G., and van de Ven, T.G.M., 1988, Settling velocity of a polymer coated particle. Model experiments and theory, *Materials Science Forum*, **25-26**, 401-404.
- Mark, C.H., 1973, Measurements of the terminal velocity of bubbles rising in a chain, *J. Fluid Engineering*, **March 73**, 17-22
- Marmur, A., and Rubin, E., 1976, A theoretical model for bubble formation at an orifice submerged in an inviscid liquid, *Chemical Engineering Science*, **31**, 453-463.
- Masliyah, J.H., 1979, Hindered settling in a multi-species particle system, *Chemical Engineering Science*, **34**, 1166-1168.
- Massey, B.S., 1983, *Mechanics of fluids*, Wokingham, Berkshire, England: Van Nostrand Reinhold (UK).
- Matis, K.A., and Mavros, P., 1991, Recovery of metals by ion flotation from dilute aqueous solutions, *Separation and Purification Methods*, **20**, 1, 1-48.
- Mecklenburg, M.M., 1991, Hydrodynamic study of a downwards concurrent bubble column, Master Thesis, McGill University, Montreal, Canada.
- Meernik, P.R. and Yuen, M.C., 1988a, An optical method for determining bubble size distribution - part I: Theory, *Journal of Fluids Engineering, Transactions of ASME*, **110**, 325-331.
- Meernik, P.R. and Yuen, M.C., 1988b, An optical method for determining bubble size distribution - part II: Application to bubble size measurement in a three-phase fluidized bed, *Journal of Fluids Engineering, Transactions of ASME*, **110**, 332-338.
- Mendelson, H.D., 1967, The prediction of bubble terminal velocities from wave theory, *AIChE J.*, **13**, 250-252.
- Miller, D.L., 1981, Ultrasonic detection of resonant cavitation bubbles in a flow tube by their second-harmonic emissions, *Ultrasonics*, **19**, 217-224.

- Miller, T.E., and Meyer, W.C., 1984, Measurement of dynamic surface tension, reprinted from: *American Laboratory*, Feb. 84.
- Miyahara, T., Tsuchiya, K., and Fan, L.-S., 1988, Wake properties of a single gas bubble in a three-dimensional liquid-solid fluidized bed, *Int. J. Multiphase Flow*, **14**, 6, 749-763.
- Moore, D.W., 1959, The rise of a gas bubble in a viscous liquid, *J. Fluid Mech.*, **6**, 113-130.
- Moore, D.W., 1965, The velocity of rise of distorted gas bubbles in a liquid of small viscosity, *J. Fluid Mech.*, **23**, 749-766.
- Moore, D.W., 1963, The boundary layer on a spherical gas bubble, *J. Fluid Mech.*, **16**, 161-176.
- Narayanan, S., Goossens, L.H.J., and Kossen, N.W.F., 1974, Coalescence of two bubbles rising in line at low Reynolds numbers, *Chem. Eng. Sci.*, **29**, 2071-2082.
- Nassos, G.P., 1963, Development of an electrical resistivity probe for void-fraction measurement in air-water flow, *ANL-6738, Engineering and Equipment (TID-4500, 22nd Ed.)*, AEC Research and Development Report, Illinois, USA.
- Newhouse, V.L., and Shankar, P.M., 1984, Bubble size measurements using the nonlinear mixing of two frequencies, *Journal of Acoustical Society of America*, **75**, 5, 1473-1477.
- Nguyen-Van, A., Schulze, H.J., and Kmet, S., 1994, A simple algorithm for the calculation of the terminal velocity of a single solid sphere in water, *Int. J. Miner. Process.*, **41**, 305-310.
- Nishi, R.Y., 1972, Ultrasonic detection of bubbles with Doppler flow transducers, *Ultrasonics*, **10**, 173-179.
- O'Connor, C.T., Randall, E.W., and Goodall, C.M., 1990, Measurement of the effects of physical and chemical variables on bubble size, *International Journal of Mineral Processing*, **28**, 139-149.
- Oguz, H.N., and Sadhal, S.S., 1988, Effects of soluble and insoluble surfactants on the motion of drops, *J. Fluid Mech.*, **194**, 563-579.
- Okano, Y., Itoh, M., and Hirata, A., 1989, Natural and Marangoni convections in a two dimensional rectangular open boat, *J. Chemical Engineering of Japan*, **22**, 3, 275-281.
- Okazaki, S., 1964, The velocity of ascending air bubbles in aqueous solutions of a surface active substance and the life of the bubble on the same solution, *Bull. Chem. Soc. Japan.*, **37**, 144-150.
- Otake, T., Tone, S., Nakao, K., and Mitsuhashi, T., 1977, Coalescence and breakup of bubbles in liquids, *Chemical Engineering Science*, **32**, 327-383.

- Otero, A., De La Fuente, I., 1991, Development of a sensor for on-line control and characterization of bubbles and drops in flotation cells and mixer settler units, *Mineral Processing and Process Control*, Edited by Dobby, G.S., Argyropoulos, S.A., and Rao, S.R., 501-516.
- Peebles, F.N., and Garber, H.J., 1953, Studies on the motion of gas bubbles in liquids, *Chemical Engineering Progress*, **49**, 88-97.
- Pinczewski, W.V., 1981, The formation and growth of bubbles at a submerged orifice, *Chemical Engineering Science*, **36**, 405-411.
- Pnueli, D., and Gutfinger, C., 1992, Fluid mechanics, *Cambridge University*, Cambridge, New York.
- Potter, M.C., and Foss, J.F., 1982, Fluid mechanics, *Great Lakes Press*, Michigan.
- Randall, E.W., Goodall, C.M., Fairlamb, P.M., Dold, P.L., and O'Connor, C.T., 1989, Method for Measuring the sizes of bubbles in two-and three-phase systems, *Journal of Physics E: Scientific Instruments*, **22**, 827-833.
- Reay, D., and Ratcliff, G.A., 1975, Experimental testing of the hydrodynamic collision model of fine particle flotation, *Can. J. Chem. Eng.*, **53**, 481-486.
- Reay, D., and Ratcliff, G.A., 1973, Removal of fine particles from water by dispersed air flotation: effect of bubble size and particle size on collection efficiency, *Can. J. Chem. Eng.*, **51**, 178-185.
- Rickard, T.A., and Ralston, O.C., 1917, Flotation, *Mining and Scientific Press*, San Francisco.
- Rowe, P.N., and Matsuno, R., 1971, Single bubbles injected into a gas fluidized bed and observed by X-Rays, *Chemical Engineering Science*, **26**, 923-935.
- Rybczynski, W., 1911, On the translatory motion of a fluid sphere in a viscous medium (in German). *Bull. Int. Acad. Pol. Sci. Math. Natur., Ser. A*, 40-46.
- Saffman, P.G., 1956, On the rise of small air bubbles in water, *J. Fluid Mech.*, **1**, 249-275.
- Savic, P., 1953, Natl. Res. Counc. Can., Rep. No. MT-22.
- Saville, D.A., 1973, The effect of interfacial tension gradients on the motion of drops and bubbles, *Chem. Eng. J.*, **5**, 251.
- Saxena, A.C., Rao, N.S., and Saxena, S.C., 1990, Bubble size distribution in bubble columns, *Canadian Journal of Chemical Engineering*, **68**, 159-161.
- Schechter, R.S., and Farley, R.W., 1963, *Can. J. Chem. Eng.*, **41**, 103-107.

- Schiller, Von L., and Naumann, A., 1933, Über die grundlegenden Berechnungen bei der Schwerkraftaufbereitung, *Zettschrift DEs Vereines Deutscher Ingenieure (Z. Ver. dt Ing.)*, **77**, 12, 318-320.
- Schulze, H.J., 1984, Physico-chemical elementary processes in flotation, *ELSEVIER*, New York.
- Schulze, H.J., Radoev, B., Geidel, Th., Stechemesser, H., and Töpfer, E., 1989, Investigations of the collision process between particles and gas bubbles in flotation - A Theoretical anakysis, *International Journal of Mineral Processing*, **27**, 263-278.
- Schulze, H.J., 1989, Hydrodynamics of bubble-mineral particle collisions, *Mineral Processing and Extractive Metallurgy Review*, **5**, 43-76.
- Scriven, L.E., 1960, Dynamics of a fluid interface, *Chem. Eng. Sci.*, **12**, 98-108.
- Sears, F.W., Zemansky, M.W., and Young H.D., 1977, University physics, *Addison-Wesley Publishing Company*.
- Shan, G., 1994, Bubble swarm velocities in a flotation column, Ph.D. Thesis, McGill University, Montreal, Canada.
- Shankar, P.M., chapelon, J.Y., and Newhouse, V.L., 1986, Fluid pressure measurement using bubble insonified by two frequencies, *Ultrasonic*, **24**, 333-336.
- Soo, S. L., 1967, Fluid dynamics of multiphase, *Blaisdell Pub. Co.*, Waltham, Mass.
- Stokes, G.G., 1851, On the effect of the internal friction of fluids on the motion of pendulums, *Transactions of the Cambridge Philosophical Society*, **9**, 8-106.
- Stone, H.A., and Leal, L.G., 1990, The effect of surfactant on drop deformation and breakup, *J. Fluid Mech.*, **220**, 161-186.
- Strasberg, M., 1956, Gas bubbles as source of sound in liquids, *Journal of the Acoustical Society of America*, **28**, 1, 20-26.
- Sung, J.S., and Burgess, J.M., 1987, A laser-based method for bubble parameter measurement in two-dimensional fluidized beds, *Powder Technology*, **49**, 165-175.
- Sutherland, K.L., and Wark, I.W., 1955, Principles of flotation, *Aust. Inst. Min. Metall.*, Melbourne.
- Szatkowski, M., Freyberger, w.L., 1988, The effect of bubble size distribution on selectivity of iron ore flotation, *International Journal of Mineral Processing*, **23**, 213-227.
- Treybal, R. E., 1967, Mass transport operations, *McGraw-Hill*, New York.

- Tsuchiya, K., Miyahara, T., and Fan, L.-S., 1989, Visualization of bubbles-wake interactions for a stream of bubbles in a two-dimensional liquid-solid fluidized bed, *Int. J. Multiphase Flow*, **15**, 1, 35-49.
- Tsuchiya, K., and Fan, L.-S., 1988, Near wake structure of a single gas bubble in a two-dimensional liquid-solid fluidized bed: Vortex shedding and wake size variation, *Chem. Eng. Sci.* **43**, 1167-1181.
- Tsuge, H., and Hibino, S.-I., 1977, The onset conditions of oscillatory motion of single gas bubbles rising in various liquids, *J. Chem. Eng. Japan*, **10**, 66-68.
- Tucker, J.P., Franzidis, J.-P. and O'Connor, C.T., 1991, The effect of physical and chemical parameters on bubble size distribution in a Cominco air sparging test ring, *International Conference on Column Flotation (Column 91)*, Sudbury, Ont. Canada, **1**, 289-302.
- Tyurnikova, V.I., and Naumov, M.E., 1981, *Technology Limited*, England.
- Uribe-Salas, A., Gomez, C.O., Finch, J.A., and Hulls, B., 1992, Axial gas holdup profiles in flotation columns, *24 Canadian Chemical Engineering Conference, Toronto - Ontario, Canada*, 519-520.
- Uribe-Salas, A., 1991, Process measurements in flotation columns using electrical conductivity, Ph.D. Thesis, McGill University, Montreal, Canada.
- Urry, D.W., 1995, Elastic biomolecular machines, *Scientific American*, Jan. 95.
- Vennard, J.K., and Street, R.L., 1975, Fluid flow about immersed objects, *John Wiley and Sons Inc*, 645-671.
- Vinogradova, O. I., 1994, On the attachment of hydrophobic particles to a bubble on their collision, *Colloids and Surfaces A: Physicochemical and Engineering Aspects*, **82**, 247-254.
- Wallis, G.B., 1969, One-dimensional two-phase flow, *McGraw-Hill*, New York.
- Ward, A.F.H., and Tordai, L., 1946, Time-dependence of boundary tensions of solutions I. The role of diffusion in time-effects, *J. Chem. Physics*, **14**, 453-461.
- Wasserman, M.L., and Slattery, J.C., 1969, Creeping flow past a fluid globule when trace of surfactant is present. *AIChE J.*, **15**, 4, 533-547.
- Weber, M.E., and Bhaga, D., 1982, Fluid drift caused by a rising bubble, *Chemical Engineering Science*, **37**, 113-116.
- Weber, M.E., and Paddock, D., 1983, Interceptional and gravitational collision efficiencies for single collectors at intermediate Reynolds numbers, *J. Coll. Int. Sci.*, **94**, 2, 328-335.

- Wheeler, D.A., 1966, Big flotation column mill tested, *E & MJ*, **167**, 11, 98-99.
- White, F.M., 1991, Viscous fluid flow, New York: *McGraw - Hill*, 173-184.
- Wills, B.A., 1988, Mineral processing technology, *Pergamon Press*, 457-595.
- Xu, M., and Finch, J.A., 1990, Simplification of bubble size estimation in a bubble swarm, *Journal of Colloid and Interface Science*, **140**, 296-299.
- Xu, M., and Finch, J.A., 1988, Bubble diameter estimation in a mechanically agitated flotation machine, *Mineral and Metallurgical Processing*, Feb. 88, 43-44.
- Xu, M., 1991, Radial gas holdup profile and mixing in the collection zone of flotation columns, Ph. D. Thesis, McGill University, Montreal, Canada.
- Yang, D.C., 1988, New packed column flotation system, in *Column flotation '88* (K.V.S. Sastry), SME Annual Meeting Phoenix, Arizona, 257-266.
- Yianatos, J.B., Finch, J.A., and Laplante, A.R., 1986, Holdup profile and bubble distribution of flotation column froths, *Canadian Metallurgical Quarterly*, **25**, 1, 23-29.
- Yianatos, J.B., Finch, J.A., Dobby, G.S., and Xu, M., 1988, Bubble size estimation in a bubble swarm, *Journal of Colloid Interface Science*, **126**, 1, 37-44.
- Yoon, R.H., Luttrell, H.H., 1989, The effect of bubble size on fine particle flotation, *Mineral Processing and Extractive Metallurgy Review*, **5**, 101-122.
- Young, F.R., 1989, Cavitation, *McGraw-Hill Book Company*, pp. 8-37.
- Young, N.O., Goldstein, J.S., and Block, M., 1959, The motion of bubbles in a vertical temperature gradient, *J. of Fluid Mechanics*, **6**, 350-356.
- Young, T., 1805, *Phil. Trans. Roy. Soc.*, pp. 85.
- Yu, S., 1985, Particle collection in a flotation column, Master Thesis, McGill University, Canada.
- Zhou, Z.A., Egiebor, N.O., and Plitt, L.R., 1992, Frother effects on single bubble motion in a water column, 1992, *Canadian Metallurgical Quarterly*, **31**, 1, 11-16.
- Zhou, Z.A., Egiebor, N.O., and Plitt, L.R., 1991, Effect of frothers on bubble rise velocity in a flotation column - 1. Single bubble system, *Column 91*, **1**, 249-261.
- Zisman, W.A., 1964, Contact angle, wettability and adhesion, Chap. 1, Washington, D.C., *Am. Chem. Soc.* (Adv. in Chem. Ser. No. 43.).

## APPENDIX 1

## COMPUTER DATA ACQUISITION PROGRAM

The following data acquisition program was used for temperature measurements. The program was compiled using QuickBASIC 4.0 under DOS system.

```

*****
'*   Data Acquisition Program (QuickBASIC 4.0)
'*           Abbas Sam
'*           McGill University
*****
,

DIM D%(8), DIO%(16)
DIM DAT%(3000), CHAN%(3000) 'INTEGER ARRAYS FOR A/D DATA AND CHANNEL TAGS
DIM ch0%(3000), ch1%(3000), ch2%(3000), ch3%(3000)
DIM setch%(10)
COMMON SHARED D%(), DIO%(), DAT%(), CHAN%()
DECLARE SUB CIO16 (MD%, BYVAL DUMMY%, F%)

'$DYNAMIC
DIM RAWDAT%(6000)
'$STATIC

*****
SCREEN 0, 0, 0
CLS
KEY OFF
WIDTH 80

B% = 768                'Base address

MD% = 0: FLAG% = 0
DIO%(0) = B%
DIO%(1) = 3
DIO%(2) = 1
CALL CIO16(MD%, VARPTR(DIO%(0)), FLAG%)

GOTO RANGE
ACQUISITION:
    MD% = 3
    CALL CIO16(MD%, VARPTR(DIO%(0)), FLAG%)           'do A/D conversions
    ydata = DIO%(0)
    RETURN

DSPLY:
    SCREEN 1
    IF y = 0 AND BIPOLAR = 1 THEN y = 100 - ydata * 78 / 2048: GOTO SKIP

```

```
IF y = 0 AND BIPOLAR = 0 THEN y = 100 - (ydata - 2048) * 78 / 2048: GOTO SKIP
X = X + 1
IF BIPOLAR = 1 THEN y = 100 - ydata * 78 / 2048
IF BIPOLAR = 0 THEN y = 100 - (ydata - 2048) * 78 / 2048
IF X < 52 OR X >= 300 THEN LINE (51, 179)-(51, 21), 0: X = 52
DSPLY1:
LINE (X, 179)-(X, 21), 0
DOT = DOT + 1: IF DOT = 5 THEN DOT = 1
LINE (X - 1, yp)-(X - 1, y), DOT
LINE (X, 182)-(X, 185)
LINE (X - 1, 182)-(X - 1, 185), 0
SKIP:
yp = y
RETURN

menu:
SCREEN 0
WIDTH 80
CLS
SCREEN 0
LOCATE 12, 25
PRINT "(I)nput Select"
LOCATE 13, 25
PRINT "(P)lot"
LOCATE 14, 25
PRINT "(C)hange Range"
LOCATE 15, 25
PRINT "(D)ata Acquisition"
LOCATE 16, 25
PRINT "(E)xit"

CHECK1:
A$ = INKEY$: IF A$ = "" THEN GOTO CHECK1
IF A$ = "i" OR A$ = "I" THEN GOTO INSELECT
IF A$ = "p" OR A$ = "P" THEN GOTO PLOT
IF A$ = "E" OR A$ = "e" THEN END
IF A$ = "c" OR A$ = "C" THEN GOTO RANGE
IF A$ = "d" OR A$ = "D" THEN GOTO DATAC
GOTO CHECK1

INSELECT:
CLS
LOCATE 10, 10
PRINT "SELECT AN INPUT CHANNEL 0 - 7"
```

## CHECK2:

```
A$ = INKEY$: IF A$ = "" THEN GOTO CHECK2
ch% = VAL(A$)
PRINT ch%
IF ch% < 0 OR ch% > 7 THEN GOTO INSELECT
GOTO menu
```

## PLOT:

```
IF ch% < 0 OR ch% > 15 THEN ch% = 0
MD% = 1: DIO%(0) = ch%: DIO%(1) = ch%
CALL CIO16(MD%, VARPTR(DIO%(0)), FLAG%)
GOTO USER1
```

## OUTSELECT:

```
source$ = "USER IN"
GOTO menu
```

## USER1:

```
GOSUB SCREENPREP
```

## USER1LOOP:

```
A$ = INKEY$: IF A$ = "M" OR A$ = "m" THEN GOTO menu
GOSUB ACQUISITION
GOSUB DSPLY
GOTO USER1LOOP
```

## SCREENPREP:

```
SCREEN 1
CLS
y = 0
DOT = 1
back = 0
LINE (50, 180)-(50, 20)
LINE (301, 180)-(301, 20)
LINE (50, 180)-(301, 180)
LINE (50, 20)-(301, 20)
LOCATE 1, 10
PRINT "CIO-AD16"
LOCATE 1, 1
PRINT "VOLTS"
LOCATE 2, 22
PRINT "INPUT IS CH"; ch%
LOCATE 1, 22
PRINT "SOURCE IS "; source$
LOCATE 2, 10: PRINT "(M)ENU"
fs1 = FS
FOR i = 3 TO 24 STEP 2
LOCATE i, 1
PRINT USING "###.#"; fs1
LOCATE i, 6
```

```
PRINT "-"
fs1 = fs1 - decr
NEXT i
RETURN
```

```
RANGE:
CLS
SCREEN 0
BIPOLAR = 0
LOCATE 10, 20
PRINT "1 - 0 to +1.25 volt"
LOCATE 11, 20
PRINT "2 - 0 to +2.5 volt"
LOCATE 12, 20
PRINT "3 - 0 to +5 volt"
LOCATE 13, 20
PRINT "4 - 0 to +10 volt"
LOCATE 14, 20
PRINT "5 - -.625 to +.625 volt"
LOCATE 15, 20
PRINT "6 - -1.25 to +1.25 volt"
LOCATE 16, 20
PRINT "7 - -2.5 to +2.5 volt"
LOCATE 17, 20
PRINT "8 - -5 to +5 volt"
LOCATE 18, 20
PRINT "9 - -10 to +10 volt"
range1:
LOCATE 5, 15
INPUT "Please enter the range"; RANGE
rang = RANGE
IF RANGE = 1 THEN RANGE$ = "0 to +1.25 volt": gaincode% = 7
IF RANGE = 2 THEN RANGE$ = "0 to +2.5 volt": gaincode% = 6
IF RANGE = 3 THEN RANGE$ = "0 to +5 volt": gaincode% = 5
IF RANGE = 4 THEN RANGE$ = "0 to +10 volt": gaincode% = 4
IF RANGE = 5 THEN RANGE$ = "-.625 to +.625 volt": gaincode% = 3
IF RANGE = 6 THEN RANGE$ = "-1.25 to +1.25 volt": gaincode% = 2
IF RANGE = 7 THEN RANGE$ = "-2.5 to +2.5 volt": gaincode% = 1
IF RANGE = 8 THEN RANGE$ = "-5 to +5 volt": gaincode% = 0
IF RANGE = 9 THEN RANGE$ = "-10 to +10 volt": gaincode% = 8
IF RANGE < 1 OR RANGE > 9 THEN PRINT "Invalid entry. Please try again.": GOTO range1
IF RANGE > 4 THEN BIPOLAR = 1
IF rang = 1 THEN BIPOLAR = 0: FS = 1.25: decr = .125
IF rang = 2 THEN BIPOLAR = 0: FS = 2.5: decr = .25
IF rang = 3 THEN BIPOLAR = 0: FS = 5: decr = .5
IF rang = 4 THEN BIPOLAR = 0: FS = 10: decr = 1
IF rang = 5 THEN BIPOLAR = 1: FS = .625: decr = .125
IF rang = 6 THEN BIPOLAR = 1: FS = 1.25: decr = .25
IF rang = 7 THEN BIPOLAR = 1: FS = 2.5: decr = .5
```

```

IF rang = 8 THEN BIPOLAR = 1: FS = 5: decr = 1
IF rang = 9 THEN BIPOLAR = 1: FS = 10: decr = 2
OUT B% + 11, gaincode%
GOTO menu

```

```

CHANNEL:
CLS
LOCATE 5, 5
COLOR 15
INPUT "Enter your channel configuration 8 or 16"; CHANNELS
IF CHANNELS <> 8 AND CHANNELS <> 16 THEN PRINT "Invalid entry. Please try again.":
GOTO CHANNEL
CLS
RETURN

```

```

DATAC:
GOSUB SETUP

```

```

***** INITIALIZE *****

```

```

D%(0) = BA%                'CIO16 BASE I/O ADDRESS
D%(1) = INTLVL%            'INTERRUPT LEVEL
D%(2) = DMALVL%            'DMA LEVEL
MD% = 0
F% = 0
CALL CIO16(MD%, VARPTR(D%(0)), F%)
IF F% <> 0 THEN PRINT "MODE 0 ERROR # "; F%: STOP

```

```

***** CHANGE GAIN *****
      OUT BA% + 11, gaincode%

```

```

***** COUNTER SETUP *****

```

```

' SAMPLE RATE = 1,000,000 (D%(0) * D%(1)) JUMPER IN X1 POSITION

D%(0) = 25
D%(1) = 1000 / D%(0) * 1000 / FREQ
MD% = 17                'DETERMINE CLOCK RATE
CALL CIO16(MD%, VARPTR(D%(0)), F%)
IF F% <> 0 THEN PRINT "ERROR IN SETTING TIMER RATE. ERROR # "; F%: STOP

```

```

***** CHANNEL SELECTION *****

```

```

CLS

'MODE 1 IS USED TO SET CHANNEL INFORMATION
D%(0) = LOLIM%

```

```
D%(1) = UPLIM%
MD% = 1
CALL CIO16(MD%, VARPTR(D%(0)), F%)
IF F% <> 0 THEN PRINT "ERROR IN SETTING CHANNEL LIMITS # "; F%: STOP
```

```
'*****'
```

```
SAMPLES = FREQ * TI + (UPLIM% - LOLIM% + 1)
IF SAMPLES > 3000 THEN SAMPLES = 3000
```

```
CLS
LOCATE 10, 15
PRINT "HIT ANY KEY TO BEGIN COLLECTING DATA"
DO:
A$ = INKEY$
LOOP WHILE A$ = ""
```

```
LOCATE 10, 15
PRINT "PLEASE BE PATIENT, DATA IS BEING COLLECTED"
```

```
'***** DMA MODE 6 SETUP *****'
```

```
ACQUIRE:
D%(0) = SAMPLES          'TOTAL # OF CONVERSIONS
D%(1) = VARSEG(RAWDAT%(0)) 'QUICK BASIC SETS DATA SEGMENT
D%(2) = 1                '1 = INTERNAL TIMER
D%(3) = 0                '0 = ONE PASS OF 'N' CONVERSIONS
'                        1 = CONTINUOUS SCANNING OF 'N' CONVERSIONS
MD% = 6                  'DMA DRIVEN A/D CONVERSIONS
CALL CIO16(MD%, VARPTR(D%(0)), F%)
IF F% <> 0 THEN PRINT "ERROR IN DMA MODE = "; F%: STOP
```

```
'SET CONVNUM VARIABLE FOR USE IN LOOP LATER
CONVNUM = D%(0)          '# OF CONVERSIONS DONE BY MODE 6
```

```
'***** CHECK CONVERSION STATUS USING MODE 8 *****'
```

```
DO:
MD% = 8
CALL CIO16(MD%, VARPTR(D%(0)), F%)
LOOP WHILE D%(1) > 0
```

```
CLS
LOCATE 6, 15
PRINT "COLLECTION COMPLETED !"
LOCATE 8, 15
PRINT "SAVING DATD IN :", F$
PRINT " "
```

```
PRINT "***** NOW DATA ON SCREEN *****"
PRINT " "
```

```
'***** MODE 9 SETUP *****'
```

```
D%(0) = CONVNUM           ' # OF CONVERSIONS TO RETRIEVE
D%(1) = VARSEG(RAWDAT%(0)) ' DATA SEGMENT WHERE ARRAY IS
D%(2) = 0                 ' BEGIN WITH FIRST CONVERSION
D%(3) = VARPTR(DAT%(0))   ' DATA SEG. OF DAT%(*) ARRAY
D%(4) = VARPTR(CHAN%(0))  ' DATA SEG. OF CHAN%(*) ARRAY
MD% = 9
CALL CIO16(MD%, VARPTR(D%(0)), F%)
IF F% <> 0 THEN PRINT "MODE 9 TRANSFER ERROR # "; F%: STOP
```

```
'***** PUT DATA TO ARRAY *****'
```

```
j = 0
FOR i = 0 TO SAMPLES

  IF CHAN%(i) = 0 THEN ch0%(j) = DAT%(i)
  IF CHAN%(i) = 1 THEN ch1%(j) = DAT%(i)
  IF CHAN%(i) = 2 THEN ch2%(j) = DAT%(i)
  IF CHAN%(i) = 3 THEN ch3%(j) = DAT%(i)
```

```
  j = INT(i / (UPLIM% - LOLIM% + 1))
  IF j < 0 THEN j = 0
NEXT i
```

```
'***** DUMP DATA TO FILE *****'
```

```
OPEN F$ FOR OUTPUT AS #1
T# = 0
TDIFF# = 1 / FREQ * (UPLIM% - LOLIM% + 1)
IF BIPOLAR = 0 THEN AA = 4096
IF BIPOLAR = 1 THEN AA = 2048
```

```
title$ = "Time(s) "
IF setch%(0) = 1 THEN title$ = title$ + "CH0  "
IF setch%(1) = 1 THEN title$ = title$ + "CH1  "
IF setch%(2) = 1 THEN title$ = title$ + "CH2  "
IF setch%(3) = 1 THEN title$ = title$ + "CH3  "
'PRINT #1, title$
```

```
'PRINT #1, " "
```

```
D$ = STR$(T)
```

```
' Calibration Equations:
```

```
temp0 = 0
temp1 = 0
```

```

temp2 = 0
FOR i = 0 TO (j - 2)

    volt0 = ch0%(i) / AA * FS
    volt0 = 5.30# * volt0 + 6.87#
    volt1 = ch1%(i) / AA * FS
    volt1 = 5.44# * volt1 + 5.64#
    volt2 = ch2%(i) / AA * FS
    volt2 = 5.26# * volt2 + 7.35#
    volt3 = ch3%(i) / AA * FS

    volt0 = INT(volt0 * 100) / 100
    temp0 = temp0 + volt0
    volt1 = INT(volt1 * 100) / 100
    temp1 = temp1 + volt1
    volt2 = INT(volt2 * 100) / 100
    temp2 = temp2 + volt2
    volt3 = INT(volt3 * 100) / 100

    IF setch%(0) = 1 THEN D$ = D$ + " " + STR$(volt0)
    IF setch%(1) = 1 THEN D$ = D$ + " " + STR$(volt1)
    IF setch%(2) = 1 THEN D$ = D$ + " " + STR$(volt2)
    IF setch%(3) = 1 THEN D$ = D$ + " " + STR$(volt3)
    PRINT #1, D$
    PRINT D$
    T# = T# + TDIFF#
    TT! = INT(T# * 1000) / 1000
    D$ = STR$(TT!)

NEXT i
PRINT #1, " "
temp0 = temp0 / (j - 1)
temp0 = INT(temp0 * 100) / 100
temp1 = temp1 / (j - 1)
temp1 = INT(temp1 * 100) / 100
temp2 = temp2 / (j - 1)
temp2 = INT(temp2 * 100) / 100
PRINT #1, "Avg. T0 [ch. zero] (bottom) = "; temp0; " C'"
PRINT #1, "Avg. T1 [ch. one] (middle) = "; temp1; " C'"
PRINT #1, "Avg. T2 [ch. two] (top) = "; temp2; " C'"
PRINT #1, "THE FILE NAME IS :", F$
PRINT #1, "      DATE :           "; DATE$
PRINT #1, "      TIME :           "; TIME$
PRINT " "
PRINT "Avg. T0 [ch. zero] (bottom) = "; temp0; " C'"
PRINT "Avg. T1 [ch. one] (middle) = "; temp1; " C'"
PRINT "Avg. T2 [ch. two] (top) = "; temp2; " C'"
PRINT " "

```

```
PRINT " "  
LOCATE 23, 15  
PRINT "THE FILE NAME IS :", F$  
PRINT "      DATE :           "; DATE$  
PRINT "      TIME :           "; TIME$
```

```
CLOSE #1  
PRINT " "  
LOCATE 24, 15  
PRINT "HIT ANY KEY TO QUIT"  
DO:  
A$ = INKEY$  
LOOP WHILE A$ = ""
```

GOTO menu

```
***** SET UP SCREEN *****
```

SETUP:

```
CLS  
BA% = &H300  
DMALVL% = 1  
INTLVL% = 5  
POLARITY% = 1
```

```
LOCATE 7, 10  
PRINT "PLEASE INPUT THE NAME OF THE OUTPUT FILE, (DEFAULT IS DATA.PRN):";  
LOCATE 8, 10  
INPUT F$  
IF F$ = "" THEN F$ = "DATA.PRN"
```

```
LOCATE 10, 10  
PRINT "PLEASE INPUT THE FIRST CHANNEL, (0,1,2 or 3) :";  
INPUT LOLIM%  
LOCATE 12, 10  
PRINT "PLEASE INPUT THE LAST CHANNEL, (0,1,2 or 3) :";  
INPUT UPLIM%
```

```
IF LOLIM% < 0 THEN LOLIM% = 0  
IF UPLIM% > 3 THEN UPLIM% = 3
```

```
IF LOLIM% = 0 THEN setch%(0) = 1  
IF LOLIM% <= 1 THEN setch%(1) = 1  
IF LOLIM% <= 2 THEN setch%(2) = 1  
IF LOLIM% <= 3 THEN setch%(3) = 1
```

```
LOCATE 14, 10  
PRINT "PLEASE INPUT THE NUMBER OF SAMPLES PER SECOND, (< 20000) : ";  
LOCATE 16, 10
```

```
INPUT FREQ
FREQ = FREQ * (UPLIM% - LOLIM% + 1)
IF FREQ < 1 THEN FREQ = 10
IF FREQ > 20000 THEN FREQ = 20000

LOCATE 18, 10
PRINT "PLEASE INPUT THE TOTAL SAMPLING TIME, (SECONDS) :";
INPUT TI
bub = TI * FREQ * (UPLIM% - LOLIM% + 1)
IF bub > 3000 THEN TI = 3000 / FREQ
RETURN
```

## APPENDIX 2

## CALCULATION OF THE DIFFUSION COEFFICIENT

Diffusion coefficient ( $D_d$ ) can be obtained from the empirical correlation of Wilke and Chang (Treybal, 1968):

$$D_d = \frac{7.4 (10^{-8}) (\Phi M_w)^{0.5} T}{\mu v_A^{0.6}}$$

where

$\Phi$ , association factor for solvent (2.6 for water as solvent)

$M_w$ , molecular weight of solvent (18.02 g/mole for water)

T, temperature (30 °C = 303 °K)

$\mu$ , dilute solution viscosity (may be taken as that for water = 0.85 centipoise at 30 °C)

$v_A$ , total atomic volume of solute

for Dowfroth 250 =  $13 \times 14.8 + 28 \times 3.7 + 5 \times 7.4 = 333 \text{ cm}^3/\text{g mole}$

for pine oil =  $10 \times 14.8 + 18 \times 3.7 + 1 \times 7.4 = 222 \text{ cm}^3/\text{g mole}$

for MIBC =  $6 \times 14.8 + 14 \times 3.7 + 1 \times 7.4 = 148 \text{ cm}^3/\text{g mole}$

Thus, the estimated diffusion coefficient ( $D_d$ ):

for Dowfroth 250 =  $5.53 \times 10^{-6} \text{ cm}^2/\text{s}$

for pine oil =  $7.06 \times 10^{-6} \text{ cm}^2/\text{s}$

for MIBC =  $9.00 \times 10^{-6} \text{ cm}^2/\text{s}$